Forschungszentrum Jülich

Institut für Festkörperforschung

Scientific Report 1998/99

Scientific Report 1998 / 1999

Introduction

The annual Scientific Report of the Institute for Solid State Research of the Research Centre Jülich will from now on be published in English. The report will then be available to the international scientific community and will replace the 'IFF-Bulletin', that previously was issued by the IFF semi-annually. The Scientific Report includes therefore the information that was previously covered in the Bulletin.

This report has been prepared mainly to inform the external Scientific Advisory Board which visits the IFF yearly to advise and criticise on the work of the institute and to report on this work to the Governing Board of the Jülich Research Centre.

The report is intended to complement the formal presentations by staff members by introducing the Scientific Advisory Board to additional selected themes addressed and results obtained in the institute. Selection of a cross section of work is inevitable in view of the more than 200 publications generated by IFF members in 1998.

Nevertheless, we believe that the report gives an accurate picture of our work, and a picture that we hope will interest friends and colleagues around the world. We would of course be happy to learn of questions, feedback, support and criticism on the report, and indeed on all matters pertaining to the work programme of the institute.

All large scientific institutions are today more than ever required to justify their existence, even of institutions like IFF that continually rejuvenate themselves and remain at the scientific cutting edge, whilst taking care to avoid merely 'following trends'. In what respect(s) does the Institute serve the tax-payer? Perhaps I may comment on this by quoting some lines of Friedrich Nietzsche's:

> **... Die Wissenschaft aber kennt keine Rücksichten auf letzte Zwecke, ebensowenig als die Natur sie kennt: sondern wie diese gelegentlich Dinge von der höchsten Zweckmäßigkeit zustande bringt, ohne sie gewollt zu haben, so wird auch die echte Wissenschaft, *als die Nachahmung der Natur in Begriffen,* den Nutzen und die Wohlfahrt der Menschen gelegentlich, ja vielfach fördern und das Zweckmäßige erreichen - aber ebenfalls, *ohne es gewollt zu haben. ...***

> **.... No less than nature itself, science recognizes no end purpose: rather, as nature inadvertently creates things of the greatest utility, so also will genuine science, *the abstraction of nature*, occasionally, abundantly, satisfy the needs and welfare of people and so deserve the etiquette of 'useful' - but similarly, *without intending it to be so*.**

G. Eilenberger

Managing Director 1999

Contents

1. Management and Structure

Institutes:

Prof. G. Eilenberger,

Insitute 'Theory I'

(IFF Managing Director for 1999)

Prof. K. Kehr (interim),

Institute 'Theory II'

Prof. H. Mueller-Krumbhaar,

Institute 'Theory III'

Prof. Th. Brückel,

Institute 'Scattering Methods'

Prof. D. Richter,

Institute 'Neutron Scattering'

Prof. H. Wenzl,

Institute 'Materials Development'

Prof. R. Waser,

Institute 'Electroceramic Materials'

(To be appointed)

Insitute 'Soft Matter'

Prof. K. Urban,

Institute 'Microstructural Research'

Prof. W. Eberhardt,

Institute 'Electronic Properties'

Special Group:

'Materials under high doses of radiation'.

Prof. H. Ullmaier

Central Facilities:

'Electronics Laboratory'

Dr. G. Durcansky

'Numerical Methods and Data Processing'

Prof. G. Eilenberger

'Accelerator'

Dl. R. Hoelzle,

'Construction'

H. Feilbach

'Workshop'

K.Hirtz

'Administration'

H.Geisler

(Permanent Deputy of the Managing Director)

2. Overview

The Institute for Solid State Research (IFF) pursues research on condensed materials in the solid or liquid state. With the study of the properties of materials in bulk as a foundation, work in the IFF covers inhomogeneous systems and systems with reduced dimensionality and the rich phenomena associated with such systems. Particular emphasis is placed on clusters, surfaces, thin films and membranes. The overall approach, in the theoretical as well as the experimental groups, can be characterized in terms of three strategic components:

- Method Oriented Research: Development of new methods and the improvement of existing methods, both in the experimental and the theoretical/numerical sectors.

- Phenomena Oriented Research: The search for, discovery of and research on, an explanation for general phenomena and behaviour in condensed matter systems, including the mathematical and physical concepts and structure underlying this behaviour.

- Materials Oriented Research: The investigation of specific materials or classes of materials with a view to gaining an understanding of their special properties and, where appropriate, exploring their potential for practical application.

The general physical basis for all these components is provided by statistical physics and by quantum mechanics, which describe on a microscopic scale the behaviour and the reaction to external influences of electrons and atoms, the building blocks whose aggregation and cooperation is responsible for the formation of condensed phases. Investigating the manner in which this occurs and the relations between the various building blocks and the condensed phases to which they give rise, subsumes the current thrust of theoretical and experimental work in the IFF.

At the same time, past work on special materials and methods of preparation has spawned an increasing experimental effort in the development of systems and components that show promise of outstanding characteristics. In turn, this development has led to participation of the theoretical institutes and Working Group, which employ modern methodologies in order to describe and understand the often extraordinarily complex behaviour of these new systems.

In pursuing a research strategy oriented towards the future, the IFF has extended its sphere of activity substantially by founding Institutes focused on Ceramic Materials and on Scattering Methods. This establishes new areas in the Department with strong potential for the future, and extends and builds on the core activities. Similarly, the research sector 'Soft Materials' has been strengthened via the founding of a new Institute with this focus, by the choice of a Director of the institute Theory II whose research focuses on this area, by coordinating work in other institutes to impact on soft materials research and by providing wide-ranging and attractive possibilities for cooperation within the Jülich Research Centre in general.

The following specific foci of work in the IFF are symptomatic of the nature and purpose of a Helmholtz-Research-Centre:

- Contributing to the construction and running of new experimental equipment and measuring facilities for international sources of neutron and synchrotron radiation. In

addition to the Jülich Research Reactor 'DIDO', the following facilities are currently in use: BESSY, HASYLAB, ESRF, neutron sources in Argonne, Berlin, Brookhaven, Gaithersburg, Grenoble, Munich, Riso, Saclay and Appleton.

- Using the Jülich Computer Centre, mainly for theoretical investigation and large-scale numerical simulations.
- Subject matter requiring especially high levels of investment and/or the continuity of a highly qualified team of staff (in most cases in the context of national and international cooperative projects and services). Examples are: the centre for high-resolution electron-microscopy, the maintenance of particle accelerators, the electro-ceramic laboratory, the crystal growth facility, superconductor technology, the development of specialized numerical procedures and programs.

Over the long term, the research effort of the IFF has achieved a broad-based and internationally recognized status. Special technical excellence was achieved in the following areas: electron-microscopy, electron-spectroscopy, high-temperature superconductivity for information technology, growth of compound semiconductor crystals, magnetic thin film systems, cluster-physics, electron-theory, dynamical features of phase-transitions, quasi-crystals and polymer-physics.

The foundation for the focal areas of research in the IFF mentioned above and the position of the IFF in the international community as a valued partner for cooperation is its strong position in basic research. The IFF carries out basic research in areas where interesting developments having potential for the future occur, especially where this provides the underpinnings of more applied research projects.

Genuine innovation (as distinct from continuous development) occurs typically as a by-product of curiosity-driven research. An excellent example is the discovery in the IFF in 1988 by Prof. Peter Grünberg of the so-called 'giant magnetoresistance effect'. This has in the intervening years evolved into a highly active branch of solid state physics and is the basis for several attractive applications in magnetic sensors, for example as read-heads for magnetic discs and as control sensors for moving parts. The contribution of Prof. Grünberg in opening up this area of applied research was recognized by the Bundespräsident via the award of the 1998 'German Future Prize for Technology and Innovation'. The license revenue from the patents which were taken out as a result of this work represent the largest contribution to the total patent revenue of the Research Centre Jülich devolving from a single application!

Together with the ISI and the IGV, the IFF participates in Jülich's program 'Basic Research in Information Technology' (PGI). In this context, with its strong basic research infrastructure as foundation, the IFF has in recent years extended its facilities for technical-development and component-design substantially. For example, the PGI-Program has led to the incorporation within the framework of the 'HGF-Strategic-Fund Scheme' of the programs 'Superconductors for the Communications Technology of the Future' and 'Microtechnological High-Performance Components - Micro-inductors'. In addition, the IFF has demonstrated the synergy between sophisticated basic research and applied research of direct relevance to industry in the areas 'Growth of Compound Semiconductor Crystals' and 'Superconducting SQUID-systems and High-frequency Components'.

The scientific work of the IFF has generated in 1998 256 publications, 7 patents and 13 patent applications. IFF scientists gave 328 seminars at universities, institutes, conferences and workshops of which 201 were invited. In addition, IFF staff carried out 36 courses or

educational seminars at universities. 28 staff members are represented in the formal lecture schedules of teaching institutions.

The traditional IFF-Spring School was held in 1998 with topic 'Physics of Nanostructures' and attracted 300 participants.

In 1998, 11 students working at the IFF were awarded their Diplom (M.Sc. equivalent) and 21 received their Doctorates (Ph. D. equivalent). In total during 1998, 20 students were working at the IFF on a Diplom program and 52 on a Doctoral program.

In the past few years, the IFF has significantly increased its role as contractor to large companies (e.g. Bosch, Siemens, Daimler/Chrysler, Thompson, Philips) and contract work has become the main focus of some groups. This is especially the case in connection with attracting large-scale national (German) and international external funding for specific projects. Under the auspices of the Technology Transfer Bureau of the Jülich Research Centre, the IFF rents equipment to companies that have established themselves in the Jülich Technology Centre. The IFF has also designed and built pilot equipment for companies, focusing on areas where a cooperative effort within the respective industry could not be achieved (e.g. vertical Bridgman-Process for GaAs), and has developed and sold to a number of research institutions duplicates of equipment developed locally (e.g. SQUID Measuring Systems; sputtering apparatus for superconductors and oxides).

Amongst the most important roles of a large Research Centre is to make its facilities and equipment available to universities and other research institutions for work that may or may not bear a simple relation to the scientific programs that are being pursued by the Centre. In this regard, the Jülich Research Centre with its exemplary infrastructure under the auspices of the individual institutes that constitute the IFF, offers the following highly utilized capabilities:

- Access of the international research community to the neutron scattering facility FRJ2
- Use of the Jülich Center for High-resolution Microscopy
- Short-term availability of beam time on the Cyclotron and Tandetron for guest scientists in the context of the program 'Verbundforschung' financed by the Federal Ministry of Education and Researcch (BMBF)
- Maintenance and further development of the apparatus JUSIFA at HASYLAB, assistance with experiments conducted by guests

Personal Honours, Awards, and Distinctions

Markus Breidenich (Dipl-Phys) was awarded the Spingorum-Medal of the Technical-University of Aachen for his masters thesis.

Prof. Thomas. Brückel was appointed to the Scientific Board of the Laue-Langevin Institute (ILL Grenoble). Together with Prof. Mikeska (University of Hannover). Prof. Brückel was voted as 'Representative' on the BMFT-Joint-Project 'Space and time correlations in magnetic materials'.

In June 1998, Prof. Wolfgang Eberhardt was appointed to serve for three years as a member of the Scientific Advisory committee (SAC) of the Advanced Light Source (ALS) at Lawrence Berkeley Laboratory (LBL), Berkeley, California, USA.

Prof. Peter Grünberg received the 1998 German 'Future-Prize for Technology and Innovation'.

In May 1998, Dr. John Harris was awarded an 'Honorary Doctor of Technology' degree by Chalmers Technical University, Gothenburg, Sweden.

Dr. Detlef Hohl completed successfully his 'Habilitation' at the Technical University of Aachen with thesis title 'Computational Theory of High-density Hydrogen'.

In November 1998, Dr. R. Kläsges received in recognition of his dissertation the Ernst-Eckhard-Koch Prize awarded by the 'Support Group of the Berlin Electron-Storage-Ring'.

Prof. Heiner Mueller-Krumbhaar was voted as Representative of the Working Group 'School Physics' of the North-Rhine-Westphalian Conference of University Physics Departments.

Prof. Dieter Richter was appointed to the Research Commission of the Paul Scherrer Institute.

Prof. Dieter Richter was offered a Chair of Experimental Physics by the Technical University of Munich.

Ms Claudia Schlebusch received the Young Scientist Award of the European Materials Research Society for the best paper presented to the E-MRS '98 Symposium in Strasbourg, France.

Dr. Günter Schütz completed successfully his 'Habilitation' at the Mathematics and Science Faculty of the Rheinische Friedrich-Wilhelms-University in Bonn with thesis title 'Integrable Stochastic Many-body Systems'.

Dr. Karsten Wildberger was awarded the Borchers-Medal of the Technical-University of Aachen for his doctoral thesis.

Dr. Walther Zimmermann received and accepted the offer of a professor position at the University of the Saarland, Saarbrücken.

Titles of selected publications

- **Institute Theory I**

  1. **Electronic structure of correlated magnetic metals**
     A. I. Lichtenstein

  2. **Theory of Sum Frequency Generation from Metal Surfaces**
     A. Liebsch

  3. **Model Study of Brittle Fracture of Polymers**
     B. N. J. Persson

- **Institute Theory II**

  1. **Steady state selection in driven diffusive systems with open boundaries**
     G. M. Schütz, V. Popkov

  2. **Ordering phenomena of star polymer solutions approaching the Θ state**
     C. N. Likos, H. Löwen[1]
     [1]Universität Düsseldorf

  3. **Freezing and glass transition in finite systems**
     Z. T. Nemeth, H. Löwen[1]
     [1]Universität Düsseldorf

  4. **Models for slow energetic relaxation processes**
     K. W. Kehr, K. P. N. Murthy[1]
     [1]IGCAR, Kalpakkam, Indien

- **Institute Theory III**

  1. **Direct Exchange and Interaction of 3*d* impurities on the (001) Surface of Iron**
     B. Nonas, K. Wildberger, R. Zeller, P. H. Dederichs

  2. **A Parallelized *ab initio* Molecular Dynamics Code for the Investigation of Atomistic Growth Process**
     R. Berger, S. Blügel, A. Antons, Wi. Kromen, K. Schroeder

  3. **Multifractal structure of eigenstates in the Anderson model with long-range off-diagonal disorder**
     D. A. Parshin[1], H. R. Schober
     [1]Technical State University, 195251 St. Petersburg, Russia

  4. **Partial draining of a tethered polymer in flow**
     Diego Kienle[1], Roland Rzehak[1], Walter Zimmermann[1, 2]
     [1]IFF Theorie III und Forum Modellierung
     [2]Theoretische Physik, Universität des Saarlandes, D-66041 Saarbrücken

  5. **Dynamics of Viscoelastic Flow in Ion Tracks Penetrating Glassy Materials**
     H. Trinkhaus, H. R. Schober

6. **Creep Motion of a Solidification Front in a Two-Dimensional Binary Alloy**
   X. Feng, E. A. Brener, D. E. Temkin, Y. Saito

7. **Surface Instabilities in Cracks**
   Efim A. Brener, V. I. Marchenko

- ## Institute Scattering Methods

  1. **Resonant Inelastic X-Ray Scattering of EuO, EuS, and $Eu_3Fe_5O_{12}$**
     Wolfgang A. Caliebe

  2. **Nanostructrual Characterization of Hydrogen Diluted a-SiGe: H Alloys by Anomalous Small-Angle X-ray Scattering Studies**
     G. Goerigk

  3. **Competing magnetic interactions in Gadolinium-Europium-Sulfide mixed crystals**
     D. Hupfeld, W. A. Caliebe, Th. Brückel

  4. **Interface and magnetic characterization of Fe/ρ-Mn/ Fe sandwich structures using scattering methods**
     E. Kentzinger, U. Rücker, W. Caliebe, G. Goerigk, F. Werges, B. Alefeld, C. Fermon[*]
     [*]DRECAM/ SPEC, CEA Saclay, 91191 Gif sur Yvette cedex, France

  5. **Wide-angle neutron scattering with polarization analysis-structural investigations of Polyalkylmethacrylat polymer glasses**
     W. Schweika

- ## Institute Neutron Scattering

  1. **Crossover from rouse Dynamics to Local Bond Relaxation**
     A. Arbe, M. Monkenbusch, J. Colmenero, D. Richter

  2. **Microscopic Dynamics of a confined glass-forming liquid**
     Reiner Zorn, Lutz Hartmann[*], Dieter Richter, Friedrich Kremer[*], Bernhard Frick[+]
     [*]Universität Leipzig
     [+]Institut Laue Langevin, Grenoble/Frankreich

  3. **Isotropic Lifshitz Critical Behavior in a Mixture of a Homopolymer Blend and Diblock Copolymer**
     Dietmar Schwahn, Kell Mortensen[*], Heinrich Frielinghaus[*], Kristoffer Almadal[*]
     [*]Risø National Laboratory, DK -4000 Roskilde, Denmark

  4. **Constrained dynamics of ordered star polymer solutions: determination of the microscopic confinement size using NSE**
     G. Ehlers[1], P. Schleger[1]
     [1]ILL, Grenoble

  5. **Amphiphilic block copolymers: Micellarization and Emulsification Properties**

L. Willner, A. Poppe, J. Allgaier, D. Richter, B. Jakobs[1], T. Scottmann[1], R. Strey[1]
[1]Universität Köln

6. **Probing a Second Order Phase Transition in a Perovskite by Rotational Tunnelling Spectroscopy**
M. Prager, H. Grimm, P. Schiebel

7. **Design studies of the phase space transforming backscattering spectrometer for the FRM II**
O. Kirstein, H. Grimm, M. Prager

- **Institute Materials Development**

    1. **GaAs crystal growth and defect studies**
    K. Sonnenberg

    2. **Injection of protons into inert gases using a high-temperature proton conductor**
    T. Schober, J. Friedrich, D. Triefenbach

    3. **J. Hauck, K. Bickmann, R. Fischer, K. Mika**
    Ordered bcc alloys
    J. Hauck, K. Bickmann, R. Fischer, K. Mika

- **Institute of Electroceramic Materials**

    1. **Colossal Magnetoresistance (CMR) in acceptor doped Lanthanum Manganites**
    R. R. Arons[1], U. Hasenkox[3], C. Osthöver[2], Ch. Sauer[2]
    [1]Institut für Elektrokeramische Materialien
    [2]Institut für Elektronische Eigenschaften
    [3]Institut für Werkstoffe der Elektrotechnik II, RWTH Aachen

    2. **The nature of perovskites of ABO_3-type at elevated temperatures**
    K. Szot[1], W. Speier[2], J. Herion[3], A. Mück[3]
    [1]Institute for Electroceramic Materials
    [2]Institute of Chemistry and Dynamics of the Geosphere
    [3]Institute of Thin Film and Ion Technology

    3. **Ba-zirconate: an old high temperature proton conductor revisited**
    H. G. Bohn, T. Schober, J. Friedrich, D. Triefenbach

    4. **Melting experiments on the proton conducting oxide BCN18 using microwave heating**
    M. Barton, P. Meuffels, R. R. Arons

- **Institute Microstructure Research**

    1. **Cryogenic dielectric resonators for future microwave communication**
    I. S. Ghosh[3], D. Schemion[1], S. Schornstein[2], M. Winter[1], N. Klein[1]
    [1]Institut fü Mikrostrukturforschung

[2] presently employed at Softlab. Köln
[3] presently employed at Philips Research Center, Aachen

2. **Operation of HTS dc-SQUID Sensors in High Magnetic Fields**
   M. I. Faley[1], U. Poppe[1], K. Urban[1], E. Zimmermann[2], W. Glaas[2], H. Halling[2], H.-J. Krause[3], M. Bick[3], D. N. Paulson[4], T. Starr[4], R. L. Fagaly[4]
   [1] Institut für Festkörperforschung, FZ-Jülich GmbH, D-52425 Jülich, Germany
   [2] Zentrallabor für Elektronik, FZ-Jülich GmbH, D-52425 Jülich, Germany
   [3] Institut für Schicht- und Ionentechnik, FZ-Jülich GmbH, D-52425 Jülich, Germany
   [4] Tristan Technologies inc., San Diego, CA 92121 USA

3. **Formation of As precipitates in Be doped non-stoichiometric GaAs and their influence on the electrical properties**
   M. Luysberg, K. Thul

4. **A novel type of dislocation in an Al-Pd-Mn quasicrystal approximant**
   H. Klein, M. Feuerbacher, P. Schall

5. **Observation of the atomic structure of a $\sum=3$ {111} twin boundary junction in a $BaTiO_3$ thin film by phase-retrieval electron microscopy**
   C. L. Jia[1], R. Rosenfeld[1], A. Thust[1], K. Urban[1]
   [1] Institut für Festkörperforschung, FZ-Jülich GmbH, D-52425 Jülich, Germany

- **Institute Electronic Properties**

  1. **Electronic structure and magnetism of 1-D nanostructures**
     A. Dallmeyer[1], R. Kläsges[1], C. Carbone[1], W. Eberhardt[1], C. Pampuch[2], O. Rader[2], W. Gudat[2], P. Gambardella[3], K. Kern[3]
     [1] Institut für Festkörperforschung, FZ-Jülich GmbH, D-52425 Jülich, Germany
     [2] BESSY GmbH, Lentzeallee 100, D-14195 Berlin
     [3] Institut de Physique Expérimentale, EPF-Lausanne, CH-1015 Lausanne

  2. **The influence of NiO and CoO outerlayers on the GMR effect**
     F. Voges, P. Grünberg, R. Schreiber

  3. **Tunnelling Magnetoresitance Structures with Barries Produced by UV Oxidation**
     P. Rottländer, H. de Gronckel, P. Grünberg

  4. **Photoelectron Spectroscopy of La_2O_n: Experiment and Theory**
     R. Klingeler, M. Neeb, P. S. Bechthold

  5. **Improved charge generation efficiency of an organic photoreceptor material by C_{60}**
     J. Morenzin, C. Schlebusch, B. Kessler

  6. **Electronic Structure of Single Wall Carbon Nanutubes in Buckypaper**
     Annette Karl[1], Stefan Eisebitt[1,2], Ingo Wirth[2], Gunther Kann[2]
     [1] RIXS Work
     [2] STM Work

7. **Femtosecond multi-photon photoemission of small Pt_n-cluster anions**
   Niko Pontius, Paul S. Bechthold, Matthias Neeb, Wolfgang Eberhardt, Jürgen Lauer, Heinz Pfeifer

8. **Excited state dynamics of an organic photoconductor**
   C. Schlebusch, S. Link, A. Scholl, B. Kessler, W. Eberhardt

9. **Electric Field Induced Changes in STM Images of Metal Surfaces**
   S. Heinze, X. Nie, M. Weinert, S. Blügel

- **Special Group: Materials subject to high radiation doses**

   1. **Dimensional changes of α- and β-SiC after helium implantation and thermal annealing**
      P. Jung[1], J. Chen[1], H. Klein[1]
      [1]Sondergruppe Werkstoffe unter hoher Bestrahlungsbelastung

Institute Theory I: General Overview

Research Areas

The main focus in the Institute is on gaining an understanding of electronic structure and atomic-scale processes and, wherever realistically possible, performing quantitative calculations. The term 'quantitative' is used here to draw a distinction to the other important 'qualitative' aspect of theory, which considers characteristic elements of physical reality in the abstract and represents these using the simplest possible theoretical or numerical representation. The individual themes that constitute this area of activity will be described in more detail below.

Another research area of the Institute, the theory of non-linear systems, has been transferred to the 'Modelling Forum', where Dr Lustfeld, co-opted as a member of the Forum for the the period 1997-99, is applying his know-how to environmental problems. This, together with activities of the Forum Members Dr. Baumgärtner (Theory II) and Dr. Zimmerman (Theory III, now the University of Saarbrücken) and doctoral students of the Forum, constitutes a purely theoretical, multi-institutional approach to interdisciplinary tasks. This activity will retain its support from theory in the future.

The research area of Prof. Eisenriegler - 'Geometric Effects in Complex Fluids' - bears a close relationship to the theory of soft-matter, though it remains a separate activity. The work studies the forces that operate between geometric objects - walls, spheres (colloids) and cylinders having dimensions in the mesoscopic range - which arise as a result of thermodynamic effects in the surrounding fluid. Examples are critical fluid mixtures and dilute polymer solutions. The methods employed in these studies include analytical, field-theoretical approaches as well as numerical simulations in collaboration with Dr. Bringer, who contributed methodologies and programmes. In addition, Dr. Bringer has established a close collaboration with the experimental Institute of Prof. Lengeler, RWTH Aachen, with regard to the quantum-mechanical treatment of interference effects in semiconductor-nanostructures.

For a given collection of nuclei, the structure and properties of the resulting atomic assemblies are determined in the last analysis by the electrons. Thus the main focus of the Institute's work programme, referred to above, in fact includes the entire physics of condensed materials! A choice of relevant problems in this area, which is addressed by a virtual army of theorists worldwide, is made according to the following aspects:

- current issues of a methodological or thematic nature,
- the expertise of staff members,
- the availability of computer programme-packages that have evolved over many years (and so can be compared to moderately expensive experimental equipment),
- special capabilities of the Jülich computer facility,
- status of competition and possibilities for collaboration, local, national and international.

In this sense, a central feature is the ongoing development and application of current density-functional/ab initio molecular dynamics programmes, especially in conjunction with the powerful computational facility in ZAM. Work in this area has been performed by Dr. Jones, Dr. Lichtenstein, Dr. Ballone, Dr. Kaschner and Ms Montanari (student). An example of work in this research area can be found below.

The computer programmes run currently on the T3E. On-going development includes the testing of new, non-local approximations for the exchange-correlation energy functional. Such approximations are essentially empirical and not the result of ab initio theory. This leads to systematic deviations with respect to measured values and with values calculated for small systems by more reliable, but much more resource intensive quantum methods. Combining accuracy with ease of computation will remain a challenge into the future. The focus of applications has been to atomic clusters, especially those with light atoms (organic molecules, carbon-aggregates, systems containing water), which require 'hard' pseudopotentials and so represent difficult numerical problems. Other applications include energy surfaces and phonons in glasses.

A further area of research concerns the interaction of electrons and electromagnetic fields in bulk materials (Prof. Sturm) and on sufaces (Dr. Liebsch). In the former case, new results constitute a consistent calculation of the dielectric function ε (k, w). In the latter, the focus is on the calculation of linear and non-linear optical response on clean and adsorbate covered surfaces, an area of especially active research for spectroscopy and diagnostics at surfaces. An example of work in this area can be found below.

An important research topic in the Institute is the atomic theory of friction and the related issue of crack propagation in polymers. This work is summarized below as an example of the general area of research. Over the past four years, Dr. Persson has pioneered work in this area (much of which is summarized in his 1997 monograph on this topic). This remains an area whose development is just breaking out of infancy, and has broad-based ramifications and many open questions.

External Funding and Collaborative Projects

- Dr. Liebsch was awarded a grant from the EU to conduct a collaboration with South-American Universities over the period 1996-98. The grant covered Dr. Liebsch's travel and local expenses.
- Dr. Hohl received financial support in the form of a BAT IIa position from the DFG (German Research Association) to assist pursuit of a research programme on 'Computersimulations in Materials Research'. This was used to finance the position of Dr. Kaschner up to May 1998.
- Between 1994 and 1999, Dr. Persson was granted support by the DFG to cover annual 3-month guest visits to IFF by Prof. Volokitin, University of Samara, Russia.
- As a participant on a 5-year BMBF(German Research Ministry)-supported German-Israeli Cooperative Project, Dr. Persson receives from 1998 annual funding of 50,000 DM to cover guest visits and travel expenses.
- As a contributor in a collaboration between institutes from Jülich, Mainz and Heidelberg, Dr. Jones received for the years 1996-98 from the MaTech Programme of the BMBF funding of in total 1,141,000DM. These funds were used in part to finance the positions of Dr. Lichtenstein and Ms Montanari. An extension of this funding will be applied for as soon as the next round of applications is announced.
- Within the framework of the German-Chinese Exchange Programme, funding for a month's visit to the Zhejiang University, Hangzhou was made available to Prof. Eilenberger.

- Under the auspices of the German-Hungarian Exchange Programme, Dr. Lustfeld was awarded funding during the period 1996-98 for Hungarian guests. The funding covered visits up to 100 days annually. Unfortunately, this funding was not extended.

Oustanding Results (brief reports)

- The behavior of mesoscopic particles dissolved in a dilute solution of long, flexible, and nonadsorbing polymer chains is studied by field-theoretic methods. For spherical and cylindrical particles the solvation free energy for immersing a single particle in the solution is calculated explicitly. For the effective interactions between a small sphere and a wall, between a thin rod and a wall, and between two small spheres quantitative results are presented. A systematic approach for studying effective many-body interactions is provided.

- The MD/MF method in conjunction with all-electron DF calculations were applied succesfully to a series of molecules. Examples are: a) Calculations for bisphenol-A-polycarbnate-oligomer crystals. The agreement with the measured structure is very good. b) Structural trends and trends in the vibration frequencies of polycarbonate molecules and their fragments led to a detailed picture of the energy surface of the polycarbonates. c) Cluster calculations showed unexpected geometrie - as is usually the case. Work on carbon clusters with 4 - 32 atoms showed structures that were previously not anticipated, and gave a satisfying picture of structural changes with increasing cluster-size.

- Optimized structures and energies for several isomers of glyzin and alanin were calculated systematically using the LDA and three different gradient corrections. The results were compared with those obtained via considerably more expensive Hartree-Fock calculations. The agreement was generally good except for the isomers where intra-molecular hydrogen bonds occur. The use of gradient corrections improved the agreement considerably leaving only small deviations (of approximately 40meV in the relative energies). Correspondingly, gradient corrections are necessary for a better description of hydrogen bonds. In addition, the energy changes accompanying torsional changes around bond directions could be determined.

G.Eilenberger

Personnel 1998/99

a) Staff Members

Dr. A Bringer	Problems of electron correlation and the spectroscopy of mesoscopic systems.
Prof. G. Eilenberger, Institute Director	Theory of non-linear systems.
Prof. E. Eisenriegler	Geometric effects in complex fluids.
Mrs. Ch. Hake	Secretary
Dr. J. Harris	Practical Applications of computational and informational

methods to materials research.

Dr. R. O. Jones	Structure and Dynamics of clusters and amorphous and liquid systems Project: Chemistry-Laboratory Computer
Dr. A. Liebsch	Linear and non-linear response and electronic structure of surfaces and adsorbate layers.
Dr. H. Lustfeld	Theory of non-linear systems and its applications.
Dr. B.N.J. Persson	Electronic response at surfaces, atomic friction, adsorbate modes, crack propagation.
Prof. K. Sturm	Electronic response; dielectric properties of metals and semiconductors.

b) Guests 1998

Dr. P. Ballone (MPIF)	Development and Applications of the DF/MD Method.
Drs. J. Bene, Z. Kaufman (German-Hungarian Exchange Programme)	Theory of non-linear systems.
Prof. K.H. Fischer (retired)	Vortices in d-wave and high-T_c superconductors.
Dr. R. Kaschner (DFG)	DF-calculations for peptides.
Dr. A. Lichtenstein (MaTech, BMBF)	Simulation methods for complex materials.
Prof. A. Volokitin (GUS, DFG)	Adsorbates at surfaces.

c) Doctoral students

Ms S. Bierman (Uni. Köln)	Applications of supersymmetry to the Coulomb problem.
Ms B. Montanari (Uni. Köln; graduated)	Energy surfaces for polymercomponents.

Electronic structure of correlated magnetic metals

A. I. Lichtenstein

Institut für Festkörperforschung, Institut Theorie I

The correlation effects in the electronic structure of magnetic crystals have been investigated. We generalized the fluctuation exchange approximation to the spin-polarized multi-band case in the local dynamical mean-field scheme. The calculation for ferromagnetic iron shows that the quasiparticle description of the bands near the Fermi level is reasonable, while the states beyond approximately 1 eV range are strongly damped, as in the photoemission experiments.

The description of correlation effects in the electronic structure of magnetic metals is still far from being a definite picture and continues to attract interest (see, e.g., [1]). Despite of the many investigations, the situation is still unclear both theoretically and experimentally. From the theoretical point of view, different approaches such as the second-order perturbation theory [1], the three-body Faddeev scheme and the t-matrix approximation, were used. Unfortunately, the conditions of applicability of these schemes are not clear. Recently we investigated different approximations to the LDA-based correlated electronic structure with a local self-energy [2], and argued that for moderately strong correlations one of the most efficient approaches would be the fluctuation-exchange (FLEX) approximation of Bickers and Scalapino [3].

The consideration of the full non-local FLEX self-energy $\Sigma_{mm'}(\mathbf{k}, \omega)$ in the framework of realistic multi-band calculations is faced with significant computational difficulties. On the other hand, the best local approximation which corresponds to the so called dynamical mean field theory (DMFT) [4] appeared to be very effective for the calculations of strongly correlated systems. Therefore we combine the FLEX approximation with the DMFT scheme for LDA-based multiband calculations. In this respect we take into account only on-site Coulomb interactions, which remains a matrix in orbital indices:
$$U = <mm'|V_{ee}|m''m'''>.$$

The resulting LDA-DMFT calculation consists of self-consistent solution for the following set of equations:

$$(\mathcal{G}^{-1})^{\sigma}_{mm'}(i\omega_n) = (G^{-1})^{\sigma}_{mm'}(i\omega_n) + \Sigma^{\sigma}_{mm'}(i\omega_n)$$

$$G_{mm'}(i\omega_n) = \sum_{\mathbf{k}}[i\omega_n + \mu - H_{LDA}(\mathbf{k}) - \Sigma(i\omega)]^{-1}_{mm'}$$

where the self-energy in spin-polarize FLEX approximation is the functional of the bath Green function $\mathcal{G}$:

$$\Sigma^{\sigma}_{mm'}(\tau) = \sum_{m''m'''\sigma'} W^{\sigma\sigma'}_{mm'',m'''m'}(\tau)\mathcal{G}^{\sigma'}_{m''m'''}(\tau)$$
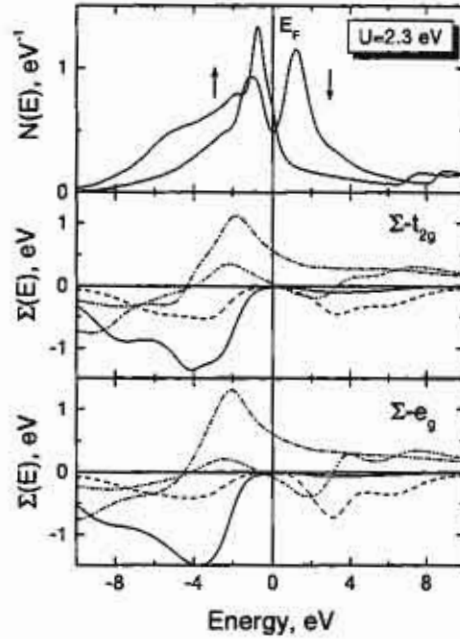

FIG. 1. Total spin-polarized density of states and d-part of self-energy for iron with U=2.3 eV and J=0.9 eV for the temperature T=750 K. Two different self-energies for t_{2g} and e_g d-states in the cubic crystal field symmetry are presented and four different curves corresponds to the imaginary part with spin-up (full line) and spin-down (dashed line) as well as the real part with spin-up (dashed-dot line) and spin-down (dashed-double-dot line).

The finite temperature FLEX equations has a "local form" in the Matsubara frequency ($i\omega_n$) or in the imaginary time (τ) space (where $\omega_n = (2n+1)\pi T$, $n = 0, \pm 1, ...$) and it is very efficient to use the fast-Fourier transforms (FFT) technic. The effective potential $W^{\sigma\sigma'}_{mm'',m'''m'}$ contains contributions from the Hartree-Fock interaction, as well as from the particle-hole and particle-particle fluctuations. Due to coupling of the spin and charge fluctuations corresponding potential has the matrix form in the spin-space:

$$W^{\sigma\sigma'}(i\omega_n) = \begin{bmatrix} W^{\uparrow\uparrow}(i\omega_n) & W^{\uparrow\downarrow}(i\omega_n) \\ W^{\downarrow\uparrow}(i\omega_n) & W^{\downarrow\downarrow}(i\omega_n) \end{bmatrix}$$

Note that the standard LSDA-method did not have such a matrix form of the effective exchange potential and could have a problem to describe magnetic crystals. The transverse part of the spin-polarized FLEX potential, for example, has the following matrix form in the orbital space:

$$W^{\uparrow\downarrow}(i\omega_n) = U * \chi^{\uparrow\downarrow}(i\omega_n) * U,$$

and the RPA-like effective susceptibility matrix:

$$\chi^{\uparrow\downarrow}(i\omega_n) = \left[1 - U * \chi_0^{\uparrow\downarrow}(i\omega_n) \right]^{-1} * \chi_0^{\uparrow\downarrow}(i\omega_n)$$

related to bare transverse susceptibility :

$$\chi_{0mm',m''m'''}^{\uparrow\downarrow}(\tau) = -\mathcal{G}_{m'm''}^{\uparrow}(\tau)\mathcal{G}_{m'''m'}^{\downarrow}(-\tau).$$

We have started from the spin-polarized LSDA band structure of ferromagnetic iron within the TB-LMTO method [5] in the minimal s, p, d- basis set and used numerical orthogonalization to find the H_{LDA} part of the Hamiltonian. In the quasiatomic approximation the full U-matrix for the d-shell is determined by three parameters U, J and δJ [2]. Note that the value of intra-atomic (Hund) exchange interaction J is not sensitive to the screening and approximately equals to 0.9 eV. For the most important parameter U, which defines the Coulomb matrix , we use the value $U = 2.3$ eV [1]. To calculate the spectral functions $A_\sigma(\mathbf{k}, E) = -\frac{1}{\pi}Tr_L G_\sigma(\mathbf{k}, E)$ and the density of states as their sum over the Brillouin zone we first made analytical continuation for the matrix self-energy from Matsubara frequencies to the real energy axis using the Pade approximation, and then numerically inverted the Green-function matrix for each k-point. In the self-consistent solution of the DMFT equations we used about thousand Matsubara frequencies and the FFT-scheme with the energy cut-off at 100 eV. The sum over irreducible Brillouin zone have been made with about hundred k-points for SCF-iterations and with few thousand k-points for the final total density of states.

Figure 1 shows the total density of states and the self-energy for t_{2g} and e_g states for ferromagnetic iron. The value of the total magnetic moment is weakly dependent on U and is of the order of 2 μ_B for this temperature. Energy dependence of the self-energy shows characteristic features of moderately correlated systems. At low energies $|E| < 1$ eV we see a typical Fermi-liquid behavior $\text{Im}\Sigma(E) \sim -E^2$, $\partial\text{Re}\Sigma(E)/\partial E < 0$. At the same time, for the states beyond this interval within the d-bands the damping is rather large ($\text{Im}\Sigma$ is of the order of 1 eV) and these states corresponds to the ill-defined quasiparticles, especially for occupied states.
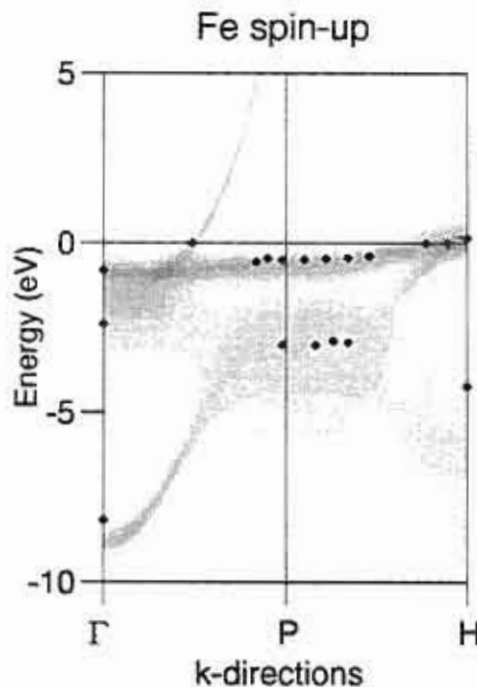

FIG. 2. Spectral function of ferromagnetic iron for spin-up and the two k-directions in the Brillouin zone compare with the experimental angle resolved photoemission and de Haas - van Alphen (at the $E_F=0$) points (from Ref. 1).

Figure 2 present the *full* spectral density $A_\sigma(\mathbf{k}, E)$ including both coherent and incoherent parts as a function of k and E. We see that the maxima of the spectral density (dark regions) coincide with the experimentally obtained band structure. However, for occupied spin-up states at about -3 eV the distribution of the spectral density is rather broad and the description of this states in terms of the quasiparticle dispersion is problematic. This is in a good quantitative agreement with the experimental data on angle-resolved spin-polarized photoemission [6] where the broad non-dispersive second peak in the spin-up spectral function located at around -3 eV.

[1] M.M. Steiner, R.C. Albers, and L.J. Sham, Phys. Rev. B 45, 13272 (1992).

[2] A.I. Lichtenstein and M.I. Katsnelson, Phys. Rev. B 57, 6884 (1998).

[3] N.E. Bickers and D.J. Scalapino, Ann. Phys. (N.Y.) 193, 206 (1989).

[4] A. Georges, G. Kotliar, W. Krauth, and M. Rozenberg, Rev. Mod. Phys. 68, 13 (1996).

[5] O.K. Andersen, Phys. Rev. B 12 , 3060 (1975).

[6] E. Kisker, K. Schroeder, T. Gudat, and M. Campagna, Phys. Rev. B 31, 329 (1985).

Theory of Sum Frequency Generation from Metal Surfaces

A. Liebsch

Institut für Festkörperforschung, Institut Theorie I

The time-dependent density functional approach is used to evaluate the optical sum frequency generation from metal surfaces. Attention is focussed on the magnitude and frequency variation of the element $\chi_{zzz}(\omega_1, \omega_2)$. Four types of surfaces are investigated: simple metals, alkali metal overlayers, noble metals, and charged metal surfaces. Differences and similarities with respect to second harmonic generation are pointed out.

During recent years infrared–visible sum frequency generation has developed into a versatile tool for the study of interfaces. While in linear optics the interface contribution to the total signal is several orders of magnitude weaker than that of the bulk, selection rules ensure that nearly all of the signal in second-order optical methods such as sum frequency generation (SFG) and second harmonic generation (SHG) originates in the vicinity of interfaces. Typically, the infrared laser in SFG is tuned to the frequency of a vibrational mode of molecules at the interface and the visible pump beam gives rise to a nonresonant background signal due to the optical nonlinearity of the metal surface. For example, at metal-electrolyte interfaces, this nonresonant contribution depends sensitively on the electrode potential and reflects the net charge and chemical state of the surface. Until now, SFG has been studied only within phenomenological models. Here, we use the microscopic time-dependent local density approximation (TDLDA) which has proven to be remarkably successful for the description of many phenomena involving linear and nonlinear electronic excitations at metal surfaces [1].

In the present work we focus on the nonlinear response induced by the normal components of electric fields, in particular, the important element $\chi_{zzz}(\omega_1, \omega_2)$ represented by the dimensionless coefficient $a(\omega_1, \omega_2) \sim \int dz \, z \, n_2(z, \omega_1, \omega_2)$, where n_2 is the nonlinear induced density obtained from the self-consistent second-order response equation [2].

Fig. 1 shows the SFG spectrum of a semi-infinite metal with the conduction electron density of Ag. The two spectral peaks are associated with the threshold excitation ($\omega_1 \approx \Phi$, where Φ is the work function) and the multipole surface plasmon ($\omega_1 \approx \omega_m \approx 0.8\omega_p$). Similar features are seen in the linear optical response of metal surfaces and in SHG spectra [3], except that in the latter case these peaks occur at $2\omega \approx \Phi$ and $2\omega \approx \omega_m$. Accordingly, the near-adiabatic region in infrared-visible SFG is much wider than in SHG. Another point which distinguishes infrared-visible SFG from SHG is the occurrence of double-resonances. Whenever the visible incident wave generates a surface collective excitation, the output beam satisfies the same resonance condition as

long as $\omega_2 \ll \omega_1$, i.e., $\omega_3 \approx \omega_1$. Thus, SFG spectral peaks are far more pronounced than in SHG.
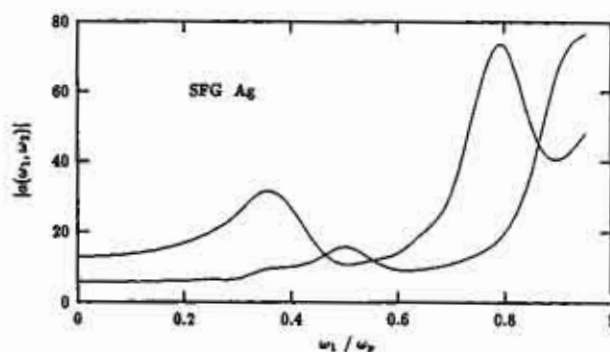

FIG. 1. Optical SFG spectra $|a(\omega_1, \omega_2)|$ for semi-infinite jellium ($r_s = 3$) (lower curve) and Ag ($V_0 = 3$ eV) (upper curve) as a function of ω_1 with $\omega_2 = 0.1$ eV. The low-frequency peaks correspond to the threshold excitation, the high-frequency peaks to the multipole surface plasmon. $\omega_p = 9$ eV is the free-electron bulk plasma frequency.

Many experimental SFG studies are carried out on noble metal surfaces. It is therefore important to investigate the influence of the occupied d bands on the nonlinear response of the conduction electrons. One of the principal consequences is the larger work function of noble metals compared to the equivalent jellium systems. A simple way of treating the s-d interaction is to introduce an average pseudopotential V_0 which enhances the surface barrier. In the case of Ag, $V_0 \approx 3$ eV yields $\Phi = 4.7$ eV in agreement with the experimental value for Ag(111). Fig. 1 illustrates the effect of this pseudopotential on the SFG spectrum of Ag. Compared to jellium, the magnitude of $a(\omega_1, \omega_2)$ at low frequencies is considerably reduced as a result of the stiffer s electron density profile. Naturally, the threshold peak is shifted upwards by the same amount as the work function. The stiffening of the density profile causes in addition a blue shift of the multipole surface plasmon: The double resonance at $\omega_1 \approx \omega_m$ shifts from 7.2 eV to higher than 8.5 eV.

As shown in Fig. 2 for two monolayers of Cs chemisorbed on Ag, very large values of a can be obtained if the visible input and the output frequency are tuned to the intrinsic collective modes of the adsorbate. In the present case, there are two such modes corresponding to the alkali metal multipole surface plasmon and the bulk-like overlayer slab mode. These double peak spectra were recently confirmed via photoyield measurements for Na and K layers adsorbed on Al [4]. Assuming a bare substrate a parameter of the order of 5 to 10, the results shown suggest enhancements of the SFG efficiency of more than 10^6.
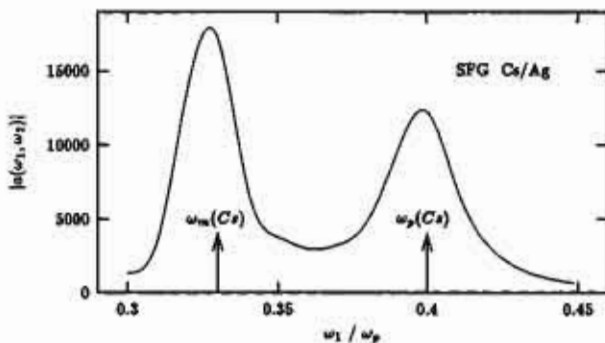

FIG. 2. SFG spectrum $|a(\omega_1, \omega_2)|$ for two Cs layers on jellium as a function of ω_1 with $\omega_2 = 0.1$ eV. The lower peak corresponds to the Cs multipole surface plasmon, the upper peak to the bulk-like Cs overlayer plasmon. $\omega_p = 9$ eV is the substrate bulk plasma frequency.

One of the main applications of infrared-visible SFG is the study of metal–electrolyte interfaces. Although important information can be derived from the vibrational frequencies of adsorbed species, the peak intensity and line shape are greatly influenced by the nonresonant metallic background and its variation with the electric potential. If we limit ourselves to the case of weak bonding between metal and adsorbed molecules, the main effect of the applied potential is to induce positive or negative surface charges. Fig. 3 shows a comparison of the SFG spectrum of neutral Ag with those for positive and negative Ag surfaces. Positive charging causes a stiffening of the density profile and an increase of the effective surface barrier. The magnitude of $a(\omega_1, \omega_2)$ therefore decreases and the frequencies of the threshold excitation and multipole surface plasmon are blue shifted. The opposite effect occurs for negative charging. The lowering of the barrier height in this case is responsible for the pronounced spectral feature near $0.2\omega_p$.
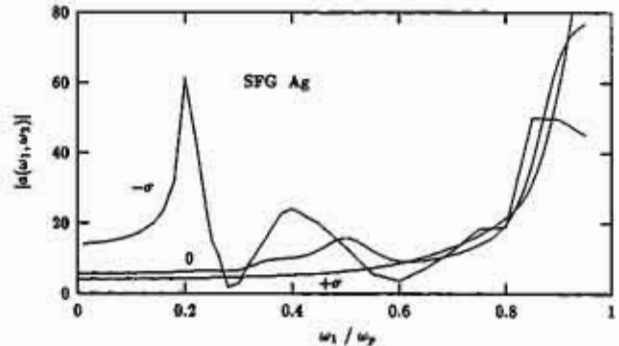

FIG. 3. SFG spectra $|a(\omega_1, \omega_2)|$ for semi-infinite Ag ($V_0 = 3$ eV) as a function of ω_1 with $\omega_2 = 0.1$ eV. Solid curve: neutral surface; dashed curves: charged surfaces with $\sigma = \pm 0.001$ a.u. The lower peaks correspond to the threshold excitation, the upper peaks to the multipole surface plasmon. $\omega_p = 9$ eV is the free-electron bulk plasma frequency.

In summary, previous TDLDA calculations of SHG from metal surfaces were generalized to the case of SFG. Although there are similarities between SFG and SHG spectra, several important differences should be noted. First, the near-adiabatic range employed in many experimental studies is much wider in SFG than in SHG. Second, strong double resonances occur in infrared-visible SFG when the visible and output frequencies are tuned to the multipole surface plasmon. In the case of alkali metal overlayers, this effect leads to the enhancement of the nonlinear efficiency by up to 10^6. On the other hand, occupied d bands in the noble metals tend to strongly reduce the perpendicular surface polarizability owing to larger work functions and stiffer density profiles. The same mechanism gives rise to a blue shift of spectral features. Finally, we have shown that the net surface charge has a pronounced influence on the magnitude and frequency dependence of the nonresonant background observed in SFG studies of metal–electrolyte interfaces.

[1] A. Liebsch, *Electronic Excitations at Metal Surfaces* (Plenum, New York, 1997).
[2] A. Liebsch, Phys. Rev. B, to be published.
[3] A. Liebsch, Phys. Rev. Lett. 61, 1233 (1988); A. Liebsch and W.L. Schaich, Phys. Rev. B 40, 5401 (1989).
[4] S.R. Barman, K. Horn, P. Häberle, H. Ishida, and A. Liebsch, Phys. Rev. B 57, 6662 (1998). B.O. Kim, E.W. Plummer, and A. Liebsch, submitted to Phys. Rev. B.

Model Study of Brittle Fracture of Polymers

B.N.J. Persson

Institut für Festkörperforschung, Institut Theorie I

I present a model study of brittle fracture of polymers. I show that the relation $v = v(F)$ between the crack-tip velocity v and the driving force F exhibit discontinuous transitions and hysteresis. For short polymers, at the onset of crack-propagation the polymer chains separate by pulling out the molecular chains, while a discontinuous transition to a new state of rapid crack motion occur at higher driving force, where the polymer chains break.

The theory of fracture is of central importance in the design of engineering structures. The traditional approach to brittle fracture is to study continuum models. However, in continuum models the stress at the crack tip in an ideally brittle material (no plasticity) is singular (the stress varies as $\sim r^{-1/2}$ with the distance r from the crack tip). Since breaking individual bonds at the crack tip is the fundamental crack-growth mechanism in brittle fracture, it is not clear how accurate a continuum description of brittle fracture is.

The transition from a stationary to a moving crack, as a function of the applied driving force, occurs continuously in continuum models[1]. In atomistic models with strong short-ranged bonds (Fig. 1a) the transition is discontinuous and exhibit hysteresis as a function of the driving force[1,2]. This difference is caused by the absence of important inertia effects in continuum models[1]. Thus, in "simple" brittle solids such as silicon, at zero temperature a crack is either pinned or it propagates with high speed (of order the sound velocity). The situation may be different for polymers (Fig. 1b). Here it may be possible (even at zero temperature) for "slow" crack motion to occur by pulling out the molecular chains. During the pull out of a chain the interaction force between the separating solid surfaces *gradually* decreases and this leads to much weaker inertia effects, i.e., the rapid "snapping" which occurs when strong short-ranged atomic bonds are broken is strongly reduced when the fracture instead occurs by pulling out the molecular chains (see below). However, at large applied stress the polymer chains break, and a discontinuous transition to a new state of rapid crack motion takes place. The latter transition is similar to those found in "simple" brittle materials such as silicon, and is the result of inertia effects.

I have studied the fracture of polymers, using a very simple model where the polymer chains are treated as chains of n "atoms" connected by harmonic springs which, however, break if the elongation of a spring exceeds a fixed value[3]. Fig. 2 shows the relation between the (steady state) crack-tip velocity v (in units of the sound velocity c) and the displacement l (see Fig. 1c),

divided by the number of atoms n in the polymer, for three different length of the polymers, (a) $n = 40$, (b) $n = 30$ and (c) $n = 20$. Note that the *onset of crack motion is continuous and occurs by pulling out the chains*. When the applied force is large enough, a transition to "fast" crack-tip motion takes place (upper vertical dotted line) where the chains break. When the applied force is lowered, the return to "slow" crack-motion [or, in case (a), to a stationary crack] occurs at lower applied force than at the onset of fast crack motion. For very short polymer chains, $n < 10$, the onset of crack motion is discontinuous.

The *fracture energy* E_{el} is equal to the elastic energy (per unit length) stored in the "solid" far to the right of the crack, i.e., $E_{el} \sim El^2/2$ (where E is the elastic modulus). Far to the left of the crack-tip there is no elastic energy stored in the solid so that E_{el} is the *energy dissipated during the crack propagation* [it will end up in the form of surface energy and heat energy (lattice waves)]. Studies of brittle fracture of atomic lattices of the type shown in Fig. 1a show that the fracture energies at the onset of brittle fracture typically are $\sim 10 - 30\%$ higher than the free energies associated with the created surfaces[2]. On the other hand, the model studied above for brittle fracture of polymers predicts fracture energies which are much larger than the surface energy. For example, for the $n = 40$ "atom" polymer the fracture energy at the onset of crack motion is ~ 20 times higher than the energy necessary to break a bond in the chain. For longer chains the difference is even bigger. It is clear that for polymers most of the fracture energy is derived from the complex rate dependent processes associated with the stretching, pull out and breaking of the polymer chains at the crack tip. This is in accordense with experimental data for brittle polymers such as Plexiglas where the fracture energies may be ~ 1000 times higher than the corresponding surface energies.

The theory presented above is in good qualitative agreement with experiments. Thus the calculations show a much slower increase in the speed of the crack tip with increasing driving force than is predicted by either continuum models or by simple atomistic models of the form

shown in Fig. 1a. This is in qualitative agreement with the experimental data for crack propagation in Plexiglas. Secondly, slow crack motion has been observed in Plexiglas at "low" driving force. However, since the experiments have been performed at nonzero temperatures, pull out of the polymer chains at the crack tip is likely to be facilitated by thermally activated processes which are not included in the calculation above.

[1] B.N.J. Persson, J. Phys. C, in press.
[2] D. Holland and M. Marder, Phys. Rev. Lett. **80** 746 (1998).
[3] B.N.J. Persson, Phys. Rev. Lett. **81** 3439 (1998); J. Chem. Phys., submitted.
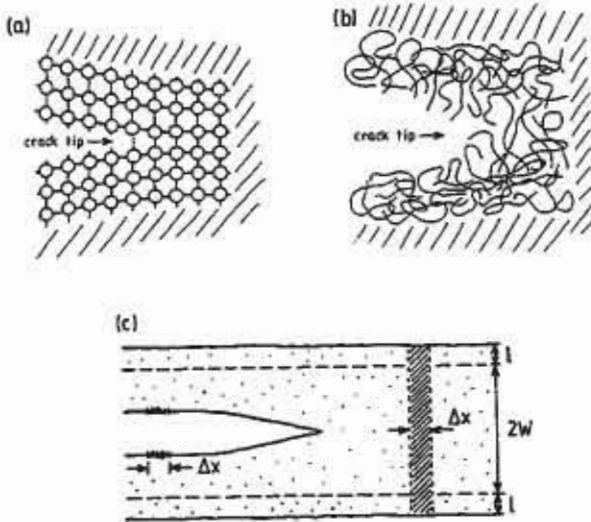
FIG. 1. A crack in (a) a brittle atomic crystal, e.g., silicon, and (b) a brittle polymer. In (a) the crack propagation occur via breaking the atom-atom bonds at the crack-tip. In (b) the crack propagation occur by pulling out polymer chains or by breaking the polymer chains. (c) An infinite plate with a semi-infinite crack. The top and bottom surfaces are clamped and displaced by the distance l. If l is large enough, the crack moves to the right with the velocity v.
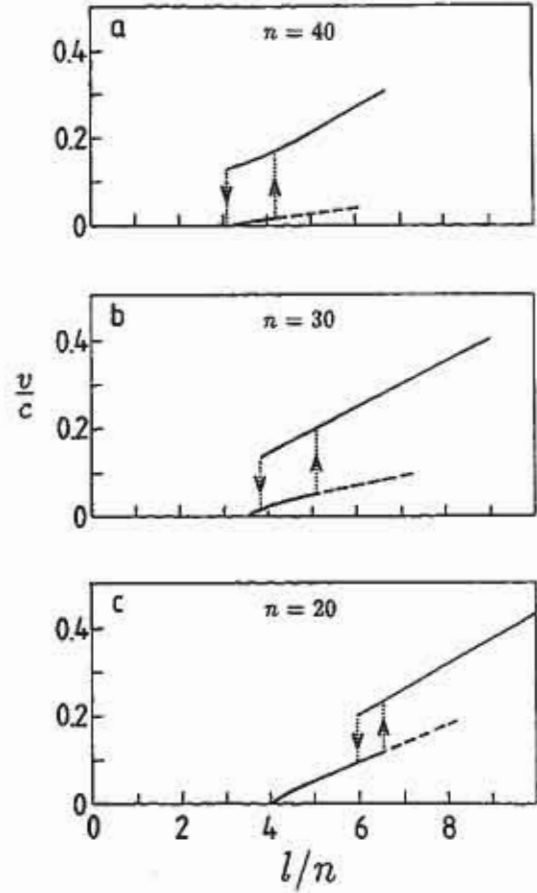

FIG. 2. The relation between the crack-tip velocity v (in units of the sound velocity c) and the displacement l (which is proportional to the driving force) divided by the number of atoms n in the polymer, for three different length of the polymers, (a) $n = 40$, (b) $n = 30$ and (c) $n = 20$.

18

Institute Theory II: Overview.

The Institute Theory II of the IFF is in a transitional phase. Following a prolonged period of interim administration the Institute will acquire a new leader, Dr. G. Gompper (MPI-KG Teltow), who will assume the Directorship in March 1999. Dr. Gompper's main research interests are in the field of soft matter theory, especially microemulsions. It is therefore to be expected that in the future the activities of the Institute will be focussed on these and related topics.

Traditionally, the research activities of Institute Theory II members have been centred on the investigation of the structure and dynamics of soft- and solid-matter. These activities have contributed to the R&D programmes `Cooperative Phenomena in Condensed Matter' and `Polymers, Membranes and Complex Fluids' of the Jülich Research Centre. The work has used numerical techniques to a considerable extent, but has also involved analytic methods wherever this is practical.

One major activity in recent years was the investigation of transport and relaxation processes of particles in disordered media with and without lattice translational invariance. Energetic relaxation processes have been studied in simple hopping models with the aim of elucidating the nature of slow dynamical processes that are observed in glass-forming substances. Further, motional processes as probed by two-dimensional magnetic resonance are being studied in different models of polymer melts. Research into transport and relaxation processes of particles in condensed matter will be reduced considerably on the retirement of Prof. K. Kehr this summer.

Another important activity in Theory II is the study of non-equilibrium behaviour of strongly interacting many-body systems. Major progress has been made in this field in recent years through the development of abstract analytical methods. This progress is documented in the habilitation thesis of Dr. G. Schütz, who has made essential contributions to this field. The abstract methods developed for these many-body systems enable a variety of applications including the treatment of soft-matter. Examples are the relaxation and mobility of long entangled polymers under various external conditions eg. in gel electrophoresis. The development of lattice-gas models for semi-flexible polymers is planned for the future.

Biophysical problems are studied by Dr. A. Baumgärtner. He is currently a member of the `Modelling Forum' and his research activities are tied to the R&D programme of the Forum.

A guest group under the scientific leadership of Prof H. Löwen (University of Duesseldorf) formed part of the Institute Theory II from November 1995 until December 1998. The work of this group focussed on the statistical mechanics of colloidal suspensions and the methods employed included liquid-state integral equations and density-functional theory as well as computer simulations. Examples for recently investigated problems are i) the stability of colloidal quasicrystals ii) the structure of star-polymer solutions and iii) the dynamics of confined systems in two- and three-dimensions. In its three years existence, Prof. Löwen's group contributed greatly to the activities of Institute Theory II in the field of soft-matter during this period of transition.

MEMBERS of THEORY II

(a) Staff members

Baumgärtner, A. Dr.	Statistical mechanics of proteins and membranes Member of Forum Modellierung
Kehr, K. Prof.	Diffusion and relaxation in disordered systems Acting head of institute
Paffen, H.	Secretary
Schütz, G. Dr.	Reptation models

(b) Guests

Denton, A. Dr.	Phase transitions in colloids (until June 98)
Likos, C.N. Dr.	Star polymers
Nemeth, Z. Dr.	Colloids in confined geometries
Popkov, V. Dr.	Reptation models (April - May 98; from Sep. 98)

(c) Graduate students

Ambaye, H.	Frequency-dependent mobility (PhD; Köln)
Krenzlin, M.	Spin relaxation models (PhD; Köln)
Lin, J.-H.	Membrane polymers (PhD; Duisburg)
Mussawisade, K.	Diffusion in disordered structures (PhD; Köln)

Steady state selection in driven diffusive systems with open boundaries

G.M. Schütz, V. Popkov

Institut für Festkörperforschung, Institut Theorie II

We develop a theory of boundary-induced phase transitions which describes the selection of steady states in one-dimensional driven diffusive systems with open boundaries. First- and second order nonequilibrium phase transitions emerge as the result of an interplay between shocks and the drift of density fluctuations.

F&E-Nr.: 23.30.0

A recurrent problem in the investigation of many-body systems far from equilibrium is posed by the coupling of a driven particle system with locally conserved particle number to external reservoirs with which the system can exchange particles at its boundaries. Important examples in which the dynamic degrees of freedom reduce to effectively one dimension include systems as diverse as traffic flow (where the 'particles' represent cars on a road segment between two junctions where cars enter and leave the road), the kinetics of protein synthesis by ribosomes (attaching to one end of a m-RNA, moving along the RNA-chain and finally being released at the other end), and more traditionally studied processes such as ionic or molecular diffusion in narrow channels (e.g. in zeolites) which are open to particle exchange with reservoirs.

In the presence of a driving force along the direction of motion a particle current through the system will be maintained and hence the system will always remain in an nonequilibrium stationary state characterized by some bulk density and the corresponding particle current. This naturally leads to the question of steady-state selection, i.e. the question which stationary bulk density the system will assume as a function of the boundary densities or boundary rates of injection and absorption respectively. Usually such systems exhibit a nonlinear current-density relation and the occurrence of shocks which mark a sudden increase of the local particle density from a left value ρ^- to a right value ρ^+. Since in low dimensions mean field approaches tend to be unreliable this non-trivial collective behaviour requires a careful investigation of the basic mechanisms that determine the selection of the current-carrying steady state.

We shall consider here one-component systems which have a family of bulk stationary states characterized by the particle density ρ. In this context the problem of steady-state selection was first addressed in general terms by Krug [1] who on the basis of mean-field stability arguments postulated a maximal-current principle for the specific case where the density ρ^+ at the right boundary to which particles are driven is kept at zero. Viewing the bulk density as order parameter, an intriguing consequence of this result is the occurrence of second-order boundary-induced phase transitions which have no analogues in 1-D equilibrium systems. These predictions were verified numerically using a standard model of nonequilibrium statistical mechanics known as the totally asymmetric exclusion process (TASEP). In its sim-

plest variant the TASEP is a driven lattice gas where each particle moves to the right with unit rate (and exponential waiting-time distribution) if the neighbouring site is empty. Otherwise the move is rejected. The 'particles' may play the part of cars on a road, ribosomes on a m-RNA, ions in a channel etc. The bulk stationary states of the TASEP are uncorrelated and hence the current-density relation is given by $j = \rho(1-\rho)$, with a estigated in driven diffusive systems modelled by a driven lattice gas with hard-core repulsion. At $\rho = 1$ no hopping can take place and hence the current vanishes. Two maxima can arise as the result of sufficiently strong repulsion between nearest neighbour particles as opposed to the pure on-site repulsion of the usual TASEP which leads to a single maximum (Fig. 1).

At first sight one might not expect such a little change in the interaction radius of the particles to affect the phase diagram. However, the theory of Kolomeisky et al. [4] – even though valid only for systems with a single
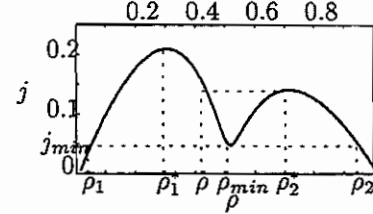

FIG. 1. Exact current-density relation of a TASEP with repulsive nearest-neighbour interaction.

maximum in the current – indicates that the local minimum in the current-density relation leads to a qualitative change in the nature of the shocks and their interplay with density fluctuations. Indeed, the full phase diagram (Fig. 2) consists of seven distinct phases, including two maximal current phases with bulk densities corresponding to the respective maxima of the current and the minimal current phase. To remain in these phases which are characterized by a divergent boundary correlation length no fine-tuning of parameters is required.
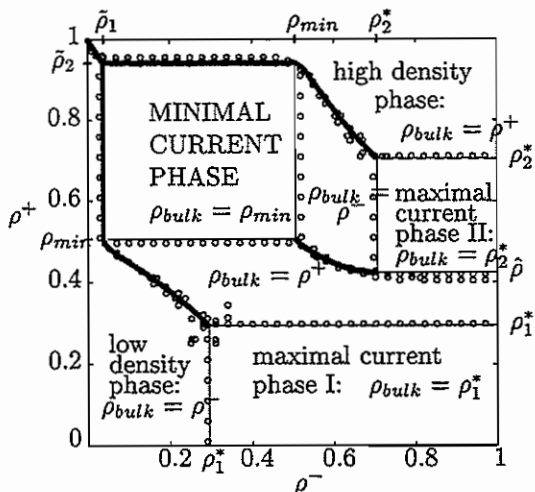
FIG. 2. Exact phase diagram as a function of the boundary densities $\rho^-, (\rho^+)$. Full (bold) lines indicate phase transitions of second (first) order. Circles show the results of Monte-Carlo simulations of an exclusion process.

In the absence of detailed balance stationary behaviour cannot be understood in terms of a free energy, but has to be derived from the system dynamics. The interplay of the collective velocity

$$v_c = j'(\rho) \tag{1}$$

which describes the center-of-mass motion of a local perturbation of the stationary state and the shock velocity

$$v_s = \frac{j^+ - j^-}{\rho^+ - \rho^-} \tag{2}$$

explains the phase diagram of driven diffusive systems with a single maximum in the current density relation [4]. The case of two maxima can be treated by further introducing the concepts of coalescence and branching of shocks [6]. A single shock with a large density difference $\rho^+ - \rho^-$ may be understood as being composed of subsequent smaller shocks with narrow plateaus at each level of density. In the usual asymmetric exclusion process these shocks travel with different relative speeds such that they coalesce and form a 'bound state' equivalent to a single shock. In the present situation, however, the minimum in the current-density relation causes that depending on $\rho^\pm$ a single shock may branch into two distinct shocks, moving away from each other. This mechanism – in conjunction with the motion of the shock front and the drift of perturbations – allows one to calculate all phase transition lines and the order of the phase transition from the macroscopic current-density relation of the system (Fig. 2). A shock may be seen as a 'domain wall' separating two *stationary* regimes of density $\rho^\pm$ respectively. At first order transitions a domain wall changes the sign of its velocity, thus leading to a discontinuous change of the bulk density by leaving the bulk of the system at ρ^- for positive shock velocity and at ρ^+ for negative velocity

respectively. Second order transitions occur when overfeeding occurs as a result of the change of the direction of the collective velocity. Monte Carlo simulations confirm the validity of this extended theory of boundary-induced phase transitions.

We conclude that the interplay of density fluctuations and shock diffusion, coalescence and branching resp. provide an essentially complete understanding of the steady state selection of one-component driven diffusive systems with short-range bulk correlations. A surprising phenomenon in systems with (at least) two maxima in the current-density relation is the occurrence of the self-organized minimal-current phase. Since little reference is made to the precise nature of the dynamics we argue that the phase diagram is generic and hence knowledge of the experimentally accessible macroscopic current-density relation of a given physical system is sufficient to calculate the exact nonequilibrium phase transition lines which determine the density of the bulk stationary state.

[1] J. Krug, Phys. Rev. Lett. **67**, 1882 (1991)
[2] G. Schütz and E. Domany, J. Stat. Phys. **72**, 277 (1993)
[3] G. Schütz, Phys. Rev. E **47**, 4265 (1993)
[4] A.B. Kolomeisky, G.M. Schütz, E.B. Kolomeisky and J.P. Straley, J. Phys. A **31**, 6911 (1998)
[5] J.T. MacDonald and J.H. Gibbs, Biopolymers **7**, 707 (1969)
[6] V. Popkov and G.M. Schütz, submitted (1999).

Ordering phenomena of star polymer solutions approaching the Θ state

C.N. Likos, H. Löwen[1]
Institut für Festkörperforschung, Institut Theorie II
[1] *Universität Düsseldorf*

The liquid-state ordering phenomena of a semidilute polybutadiene 64-arm solution were investigated by small-angle neutron scattering (SANS). We used a Θ-like solvent, modifying its quality by changing the temperature. The experimental data were described theoretically by using an effective pair potential between star polymers.
F&E-Nr.: 23.30.0

Star polymers consist of f polymeric arms attached to a common center which is negligibly small in comparison to the overall size of the molecule [1]. Because of their peculiar architecture, they can be viewed as hybrids between polymers and colloidal particles. Therefore, the study of their static and dynamical properties is of great interest as it provides a natural bridge between these two areas of soft-matter physics. Some of the relevant questions are the influence of the degree of polymerization N and of the arm number f as well as the quality of the solvent in the conformation of a *single* star and, most importantly, on the macroscopic behavior of a concentrated solution of star polymers.

In previous work [2], a colloidal description of star polymer solutions in a good solvent was introduced. There, an entropic effective pair potential between stars was proposed, which yielded good agreement with experimental data regarding (a) the variation of the star size with concentration and (b) the total scattering intensity for a whole series of concentrations. Here, we focus on the effect of the solvent quality on the pair interaction by considering a series of solutions at *fixed* polymer concentration but at different temperatures, which are gradually increasing from the Θ temperature of the solution. The latter is defined as the temperature at which the self-avoidance of the chains is exactly compensated by the polymer-solvent interactions, in such a way that the *macroscopic* behavior of the polymers is identical to the one which corresponds to non self-avoiding chains. Hence, by working in the neighborhood of the Θ temperature, we are dealing effectively with chains having weak self-avoidance.

This work was carried out in collaboration with the Institute 'Neutron Scattering' at the IFF. A semidilute polybutadiene 64-arm star polymer solution was prepared, using 1,4-dioxane as solvent. The latter is a Θ solvent for the stars at temperature 31.5 °C. The solvent quality was modified by varying the temperature in the range between 40 °C and 80 °C. Small-angle neutron scattering (SANS) yielded the total scattering intensity curves which were subsequently described theoretically.

In low concentrations, star-star correlations are absent and the scattering intensity is determined solely by the form factor of a *single* star, $P(Q)$. In order to parametrize $P(Q)$ over a large Q-range we invoked the scattering cross section from polymeric mass fractals, developed by

Beaucage [3]. In its simplest form, this form factor contains two contributions:

$$V_W P(Q) = V_W \exp(-Q^2 R_G^2/3)$$
$$+ B \left(\frac{[\mathrm{erf}(1.06\, Q R_G/\sqrt{6})]^3}{Q} \right)^{d_f}, \qquad (1)$$

where V_W is the molar volume, R_G is the radius of gyration of the stars, d_f is the dimension of the polymeric mass fractal and B is an additional prefactor which we use as a free fit parameter. The results of the fits are shown in Fig. 1. Excellent agreement is obtained between experiment and the functional form given by Eq. (1).
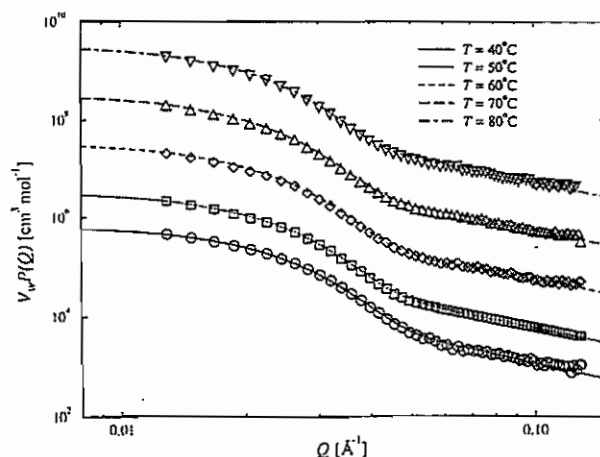

FIG. 1. *Form factors of the star at 40 °C, 50 °C, 60 °C, 70 °C and 80 °C. The solid lines represent the fits according to the Beaucage model. For clarity, the data have been multiplied by constants: 50 °C: 5, 60 °C: 50, 70 °C: 500, 80 °C: 5000.*

At higher concentrations, interstar correlations become important and the form of the effective pair interactions between stars plays a crucial role in determining these correlations. The effect of the solvent quality on the effective pair interaction between stars was manifested by the fact that the pair potential suitable for solutions in a good solvent [2] turned out to be *inappropriate* for the

description of the SANS data in the neighborhood of the Θ point. Instead, it was found that one has to employ a different pair potential, which results from a Derjaguin approximation on the corresponding interaction between two flat plates with polymer brushes grafted on them under conditions of weak self-avoidance [4,5]. This pair potential reads as:

$$\beta V(r) = \begin{cases} \infty & r < 2a; \\ U_0 \, g(y) & 2a < r < 2(a+L); \\ 0 & 2(a+L) < r, \end{cases} \quad (2)$$

where

$$g(y) = -\ln y - \frac{9}{5}(1-y) + \frac{1}{3}(1-y^3) - \frac{1}{30}(1-y^6). \quad (3)$$

Here, r is the center-to-center distance between the stars, β is the inverse temperature, a is the size of the star core, i.e., the part of the star where the chains are completely stretched and L is the length of the flexible polymer layer beyond the core. Moreover, $y = (r-2a)/(2L)$ and the prefactor U_0 is given by

$$U_0 = \frac{\pi^2 L^3 f}{48 N l^2 a}, \quad (4)$$

where N is the number of monomers per chain.

We determined all parameters entering the above expressions directly from the experimental data. The size a of the core can be determined from scaling theory and the overall size $a + L$ of the star is calculated from the experimentally known second virial coefficient of the solution. Using now this pair potential, *without* any free fit parameters, we obtain the theoretical fits of the SANS-data shown in Fig. 2 below. The good agreement between theory and experiment demonstrates that the above pair potential provides for a colloidal description of star polymers in conditions of weak self-avoidance [6].
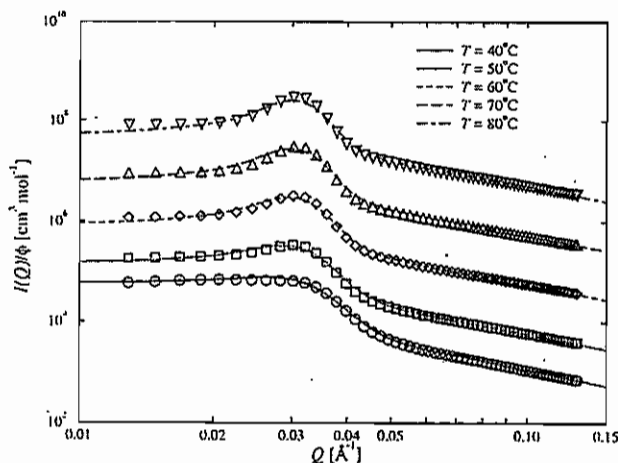
[1] G. S. Grest, L. J. Fetters, J. S. Huang, and D. Richter, Adv. Chem. Phys. **XCIV**, 67 (1996)
[2] C. N. Likos, H. Löwen, M. Watzlawek, B. Abbas, O. Jucknischke, J. Allgaier, and D. Richter, Phys. Rev. Lett. **80**, 4450 (1998)
[3] G. Beaucage, J. Appl. Cryst. **28**, 717 (1995); *ibid.* **29**, 134 (1996)
[4] S. T. Milner, T. A. Witten, and M. E. Cates, Macromolecules **21**, 2610 (1988)
[5] J. Mewis, W. J. Frith, T. A. Strivens, and W. B. Russel, AIChE J. **35**, 415 (1989)
[6] C. N. Likos, H. Löwen, A. Poppe, L. Willner, J. Roovers, B. Cubitt, and D. Richter, Phys. Rev. E **58**, 6299 (1998)

FIG. 2. *Theoretical (curves) vs experimental (points) total scattering intensities for stars in the vicinity of the Θ point. For clarity, the data have been multiplied by constants: 50 °C: 5, 60 °C: 50, 70 °C: 500, 80 °C: 5000.*

Freezing and glass transition in finite systems

Z.T. Nemeth, H. Löwen[1]
Institut für Festkörperforschung, Institut Theorie II
[1] *Universität Düsseldorf*

Dynamical and static properties of $N = 13-4000$ hard spheres in spherical cavities with smooth and rough walls have been calculated by molecular dynamics computer simulations. We use a dynamical criterion to distinguish between fluid- and solid-like states. The associated crossover densities show a strong dependence both on the system size and on the surface roughness. For large N, these crossover densities tend to the *bulk glass transition* density for rough walls and to the *bulk crystallization* density for smooth walls. The crossover densities for finite N are found to be significantly smaller than the corresponding bulk densities. A detailed examination of the layer-resolved radial- and tangential mean-square displacements reveals qualitatively different dynamics for smooth and rough cavities.

F&E-Nr.: 23.30.0

Understanding phase transitions and dynamical features of confined fluids is important for several branches of condensed matter physics. Although a large number of experimental work has been done on this field during the past decade [1], showing the manifold complexity of the problem, a general microscopic picture behind is still missing. The measurement of dynamical features of complicated organic molecules (salol, pentylene glycol, etc.) in porous materials is confronted with serious difficulties such as: the dubious determination of the density within the pores, the missing knowledge of effective interparticle and particle-wall interactions etc. The experimental results are sometimes inconclusive even regarding elementary questions such as, for example, the shift of the glass transition temperature compared to the bulk [2].

We study simple model systems of hard spheres confined in spherical cavities using Molecular Dynamics simulations to understand basic structural and dynamical characteristics induced by different geometrical confinements. For that purpose, we consider spherical cavities both with smooth and with rough walls. For the wall-particle interaction we assume an excluded volume form and we include surface roughness explicitly. This enables us to compare the dynamics directly with that in a smooth cavity. Our model system contains $N = 13-4000$ hard spheres of diameter σ interacting via the usual hard sphere pair potential $V_{HS}(\vec{r})$. In the case of a smooth wall, the spheres interact with the cavity wall via a hard wall potential:

$$V^{ext}(\vec{r}) = \begin{cases} 0 & r \leq R - \sigma/2 \\ \infty & r > R - \sigma/2 \end{cases}$$

where R stands for the cavity radius and $r = |\vec{r}|$ is the distance of the particle from the origin of the coordinate frame, which is taken to be the cavity center. Cavities with rough walls have been built from N_f fixed "boundary" hard spheres of the same diameter σ. In this case,

the external potential can be written as:

$$V^{ext}(\vec{r}) = \sum_{i=1}^{N_f} V_{HS}(\vec{r} - \vec{r}_i^{(f)}),$$

where the $\vec{r}_i^{(f)}$ $(i = 1, ..., N_f)$ denote the position of the fixed wall particles. To study the structure we have calculated the radial density profile $\rho(r)$:

$$\rho(r) = \langle \frac{1}{4\pi r^2} \sum_{i=1}^{N} \delta(r - \vec{r}_i) \rangle.$$

In order to explore dynamical features, which provide a sensitive diagnostic tool to locate freezing and glass transitions we have determined the averaged root mean-square displacement Δ after N_c collisions per particle:

$$\Delta(N_c) = (\frac{1}{N} \langle \sum_{i=1}^{N} |\vec{r}_i(0) - \vec{r}_i(t_c)|^2 \rangle)^{1/2}$$

and its radial and tangential components in several concentric shells around the cavity center. Here, t_c is the time after N_c collisions per particle. We have systematically increased the packing fraction of the system and checked how the structure and the dynamics is affected by such an increase. In particular, we are interested in locating the freezing transition and/or the glass transition in the finite system. Since a thermodynamic limit is lacking in a finite system, the usual definition of a phase transition breaks down. But the dynamics does change rapidly around the transition. These feature carries over nicely to a finite system, defining a crossover behavior. In detail, we have used the following dynamical criterion: If the averaged root-mean square displacement Δ is $\sigma/2$ after $N_c \equiv 500$ collisions per particle, then the associated packing fraction is called *crossover packing fraction* η. Although somewhat arbitrary, this criterion reproduces the bulk hard sphere freezing transition.

The results of the simulations demonstrate transparently the importance of the shape of the confinement.

The difference between smooth and rough walls is striking: for rough walls the radial mobility is significantly higher than that for smooth walls. A cavity wall which is smooth on the typical length scale of the particles induces a strong layering and prefers a crystalline layer. Therefore, the dynamics becomes slow close to the bulk crystallization density. On the other hand, a disordered rough cavity wall prevents crystallization and prefers a glassy layer. For this reason the dynamics is faster for the rough case than for the smooth case. Furthermore, we have detected a clear shift of the freezing and glass transition (see Fig. 1) compared to the bulk: the crossover packings *decrease* with decreasing system size, similar to a two-dimensional system of hard disks in spherical cavities [4].

As far as a comparison with actual experiments in pores is concerned, several caveats are in order: first, our model system of hard spheres exhibits a clear freezing transition at densities which are smaller than the glass transition density. For real molecules this may be quite different. Also, we fixed the total angular momentum to be zero here. Such zero-modes can be actually important in real smooth cavities and may accelerate the dynamics considerably for smooth cavities. The best realization for our model will be for colloids confined in structured cavities. In the present work, the length scale of the wall roughness was comparable to that of the particles. More general studies including different topographically and energetically caused roughnesses are important to understand the dynamics of confined fluids and the mesoscopic nature of friction.
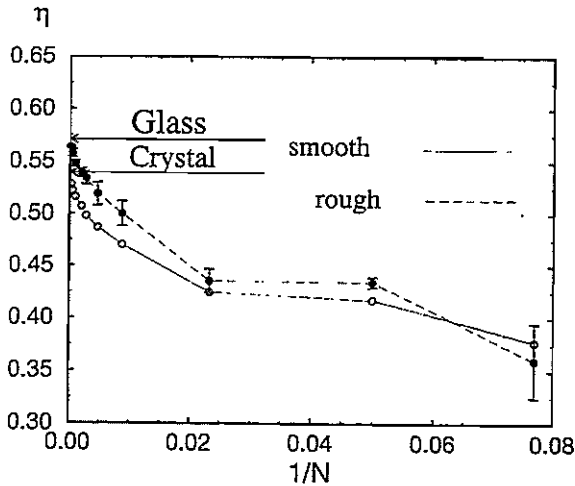

FIG. 1. *Crossover packing fractions η versus $1/N$ for smooth walls (open circles) and rough walls (full circles). Data are given for: $N = 13$, 21, 43, 114, 214, 360, 496, 1048, 2093 and 4000. For smooth walls the statistical errors are smaller than the symbol size; in the case of rough walls the bars show the standard deviation of the transition packing fractions obtained from different rough cavities. The lines between the symbols are a guide to the eye. The packing fractions of the bulk freezing and glass transition are indicated by arrows.*

[1] See, e.g., *Molecular Dynamics in Restricted Geometries*, edited by J. Klafter and J. M. Drake (Wiley, New York, 1989) and references therein.
[2] M. Arndt, R. Stannarius, H. Groothues, E. Hempel, and F. Kremer, Phys. Rev. Lett. **79**, 2077 (1997); M. Arndt, R. Stannarius, W. Gorbatschow, and F. Kremer, Phys. Rev. E **54**, 5377 (1996); W. Gorbatschow, M. Arndt, R. Stannarius, and F. Kremer, Europhys. Lett. **35**, 719 (1996)
[3] Z. T. Németh and H. Löwen, submitted to Phys. Rev. E (1998)
[4] Z. T. Németh and H. Löwen, J. Phys.: Condens. Matter **10**, 6189 (1998)

In conclusion, we have demonstrated that the dynamics in cavities depends sensitively on the surface roughness. A cavity wall which is smooth on the typical length scale of the particles induces a strong layering and prefers, at least in our hard sphere model, a crystalline layer. Therefore the dynamics becomes slow close to the bulk crystallization density. On the other hand, a disordered, rough cavity wall prevents crystallization and prefers a glassy layer. Therefore, the dynamics is faster for the rough case than for the smooth case.

Models for slow energetic relaxation processes

K.W.Kehr and K.P.N. Murthy[1]

Institut für Festkörperforschung,Institut Theorie II

[1]*IGCAR, Kalpakkam, Indien*

Energetic relaxation processes of particles that perform random walk in energy space are studied for the Gaussian density of site energies. Slow energetic relaxation processes are observed at low temperatures: a logarithmic dependence on time at intermediate times is followed by a stretched-eponential (Kohlrausch-Wattts-Williams) behavior.

F&E-Nr.: 23.30.0

The microscopic origin of the slowing down of relaxation processes in glass-forming liquids when they are cooled below the crystallization temperature is still not well understood. Many different experimental and theoretical efforts have been undertaken to elucidate these processes. Because of the difficulty and complexity of the problem, also simplified and sometimes rather abstract models are investigated that exhibit slowing down of relaxation processes, including complete freezing of dynamical processes at a critical temperature. It should be emphasized that these models are not intended to represent real glasses. Nonetheless, these simplified models can show similar behavior as observed in real liquids near the glass transition temperature.

One pertinent model has been introduced long ago to describe transient transport in amorphous semiconductors [1]. Charge carriers are excited at the surface of an amorphous substance and drawn through the sample by an electric field. The charge carriers can be trapped in localized trapping centers of various energetic depths. Depending on the energy distribution of the trapping centers ('density of states', DOS) and the temperature, the dwell time of the charge carriers in the traps can vary over many orders of magnitude. The multiple-trapping model which is based on these ideas gives an adequate description of the experiments. For an exponential DOS, which is a good approximation for amorphous semiconductors, the mean dwell time in the traps diverges below a certain critical temperature, i.e. a dynamical freezing process occurs. The temperature is related to the width E_c of the exponential energy distribution by $k_B T_c = E_c$.

Recently attention has been directed on the energetic relaxation of charge carriers in these systems, which may be probed by optical techniques. In the case of an exponential distribution of energetic states, no equilibrium energy exists for single particles below the freezing temperature mentioned above. The energetic relaxation for unidirectional motion processes can be described as a random walk in energy space [2]. It is possible to formulate a master equation for the random walk of the particle in energy space with transition rates that depend on the energetic depth of the trapping states as given by the Arrhenius law. The master equation is explicitly solved in the Laplace domain and the solution is transformed into the time domain either analytically (exponential DOS) or by an efficient inversion routine (other DOS) [3].

For the exponential DOS and temperatures below T_c, the explicit solution for the energetic relaxation is

$$< E(t) >= - k_B T[\ln(\Gamma_0 t) + const] \qquad (1)$$

where Γ_0 is the prefactor in the Arrhenius law and $\Gamma_0 t >> 1$. The logarithmic dependence on time shows that the energetic relaxation continues indefinitely in time, and no equilibrium state is reached. The model also shows aging [2,4]: The time-dependent energy-energy correlation function $< E(t_w)E(t_w + t) >$ function does not only depend on the time difference t, as it is characteristic for an equilibrium system. Rather it depends on the ratio of t over the waiting time t_w until the first determination of the energy .

We studied the energetic relaxation of particles in the random energy model for the case of a Gaussian density of states [4]. Gaussian densities of states are relevant for many organic substances. Actually, a half-sided Gaussian was used with E_c the energy where the DOS is $1/e$ of the value at $E = 0$, as sketched in Fig.1.
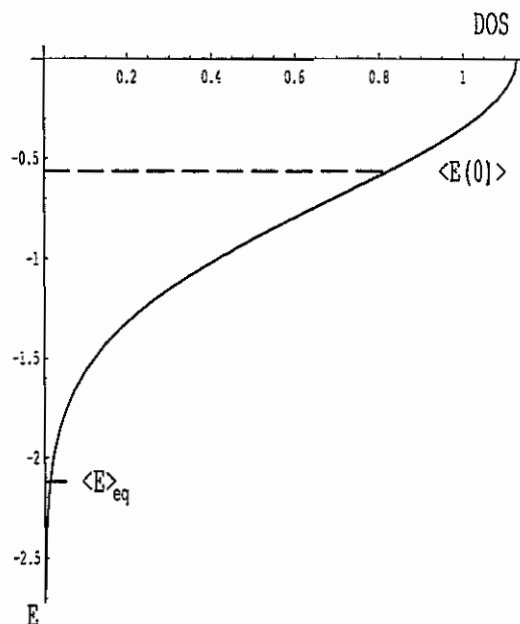

FIG. 1. Gaussian density of trapping states. A half-sided Gaussian of width $\sigma = 1/\sqrt{2}$, corresponding to $E_c = 1$, is shown. The mean value $< E(0) >$ at $t = 0$ (dashed) and the equilibrium energy for $k_B T/E_c = 0.2357$ are indicated.

For this density of states, an equilibrium energy exists which is located at

$$\frac{< E >_{eq}}{E_c} \approx -\frac{E_c}{2k_B T} \qquad (2)$$

at low temperatures. The equilibrium energy for one of the temperatures used later is indicated in the figure.
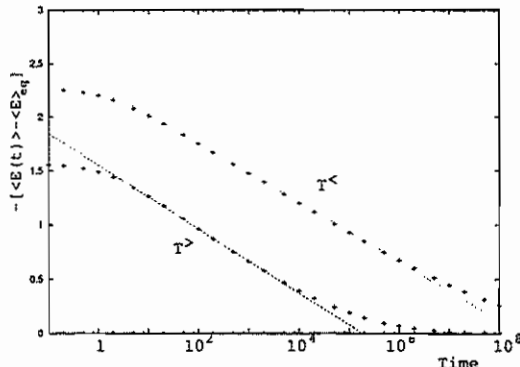

FIG. 2. Energetic relaxation: Shown is $-[< E(t) > - < E >_{eq}]$ as a function of time in a semilogarithmic representation. Time is given in units of inverse transition rates. Points: Numerical Laplace inversion of solution of master equation for $k_B T/E_c = 0.2357$ (lower curve) and $k_B T/E_c = 0.1768$ (upper curve). The straight lines are guides to the eye.

The behavior of the energy relaxation as a function of time turned out to be quite interesting at low temperatures. At time $t = 0$, particles start with random energies according to the DOS, with the mean value $< E(0) > = -E_c/\sqrt{\pi}$. After an initial decay of the energy, there is a regime where the energy decreases logarithmically in time, see Fig.2. This regime is followed by an extended regime where the final relaxation to the equilibrium value occurs in form of the Kohlrausch-Watts-Williams (KWW) law,

$$\frac{< E(t) > - < E >_{eq}}{< E(0) > - < E >_{eq}} = \exp[-(\frac{t}{\tau})^{\beta}], \qquad (3)$$

as shown in Fig.3. The KWW exponent that corresponds to the two straight lines in the figure is $\beta = 0.118$, i.e., it is rather small.

A partial qualitative explanation is as follows: For low temperatures the thermal equilibrium energy as given in Eq.(2) is located in the narrow tail of the Gaussian DOS, cf. Fig.1., and hence not easily accessed. Note that for the lower temperature used, $k_B T/E_c = 0.1768$, the density of states at the corresponding equilibrium temperature is only 3.785×10^{-4}. For intermediate times the particle apparently experiences similar states as for the exponential density of states. A quantitative explanation of the KWW behavior is still missing. We have verified that for a rectangular density of states, where no

low-lying energy states exist, the energetic relaxation is nearly exactly exponential. We point out that the model with a Gaussian DOS does not have a transition to a state with complete freezing of the diffusion process. The transition to the low-temperature behavior with very slow relaxation appears gradually with decreasing temperature. In summary we have found that very slow relaxation processes can occur in a system where an equilibrium state exists which, however, is difficult to be reached in view of the low density of available states at the relevant energy.
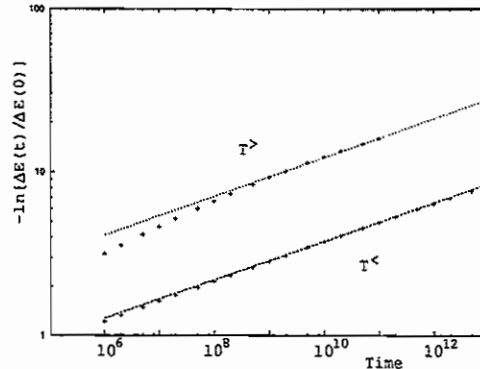

FIG. 3. Energetic relaxation: Shown is the negative logarithm of the left-hand side of Eq.(3) as a function of time in a doubly logarithmic representation. Points: Numerical Laplace inversion of solution of master equation for $k_B T/E_c = 0.2357$ (upper curve) and $k_B T/E_c = 0.1768$ (lower curve). The straight lines are guides to the eye.

[1] For a review, see H. Scher, M.F. Shlesinger, and J.T. Bendler, Phys.Today 44 (1), 26 (1991)

[2] C. Monthus and J.P. Bouchaud, J.Phys.A 29, 3847 (1996)

[3] G. Honig and U. Hirdes, J.Comp.Appl.Math. 10, 113 (1982)

[4] K.W. Kehr and K.P.N. Murthy, to be published.

Institute Theory III: General Overview

The institute *Theory III* investigates the mechanisms of the formation of structures and their consequences in condensed matter. The research starts from electronic properties which define the shortest length and time scales, but it keeps the macroscopic consequences in mind. The analytical and numerical investigations are in many ways closely connected with experimental studies performed in other groups of IFF, but also with activities in other institutes of the Research Center Jülich.

Central points of interest for the research in *Theory III* are in the field of electronic structure of solids (F&E-Nr. 23.20.0). Materials classes under considerations are metals and semiconductors specifically with respect to their importance for information technology (F&E-Nr. 23.42.0). A second mainstream is formed by cooperative phenomena in condensed matter (F&E-Nr. 23.15.0). Questions here aim at dynamics of structure and pattern formation and the statistical mechanics of order and disorder processes. Specific activities in the field of complex fluids (F&E-Nr. 23.30.0) are concerned with structure and dynamics of soft matter. The research of *Theory III* employs all analytical and numerical techniques applicable to many-body problems in condensed matter. In addition the development of new methodological concepts and numerical procedures is part of our research interest. The development of parallel program code adapted to massively parallel computers has received special attention in recent years.

The explanation of the microstructure and dynamics of real solids requires the understanding of the electronic properties. One of the most important methods for the calculation of electronic structure of real solids is the density functional theory in connection with appropriate numerical procedures. While in recent years bulk properties of metals and semiconductors have been a central interest of our research a main concern now is directed towards the understanding of surface and interface properties.

Atoms of 3d-transition metals adsorbed on the 001 surface of iron have been investigated with detailed ab-initio studies by KKR-Greenfunction techniques. Different configurations of impurities adsorbed at the surfaces have been calculated with respect to direct exchange and interaction processes. These first principles results are in good agreement with experimental studies by scanning tunneling microscopy for chromium adsorbed on iron surfaces, performed by the NIST-group, which gives confidence in the predictive power and numerical accuracy of these calculations.

Macroscopic structures are formed by growth processes. The surface of a growing crystal plays a critical role in a solidification process. The study of kinetic properties of surfaces starting from the electronic structure of the material requires an enormous amount of computing time. For this reason massively parallel computers are appropriate tools for the calculation of these phenomena. A parallelized ab-initio computer code combining norm-conserving pseudo-potential calculations with molecular dynamics simulations for the molecular motion has been developed. The materials under consideration are important for information technology: semiconductors like silicon, germanium, galliumarsenide, etc.. Detailed studies of the speed-up of this computation on vector and parallel computers have been performed. The developed computer code will be a sound basis for future investigations of adsorption and surface transport of the semiconductor materials.

The properties of glasses represent a point of interest since several years. In our previous studies the effective interaction between the molecules have been assumed to be of relatively short range. In addition to these direct interatomic interactions indirect long range forces originating for example from electric or elastic dipols may significantly change the systems collective behavior. We therefore have studied a model system with frozen-in disorder where the elements of the medium interact with dipolar forces. As a basic result it was found that the eigenstates of the corresponding Anderson model develop a multifractal structure. The results also give interesting contributions to the theory of large random matrices, where drastic differences are found compared to the Wigner-Dyson random matrix theory.

Ion tracks in glassy materials have been studied also since a few years with remarkable success. In the past year a viscoelastic theory has been formulated to capture the various time scales in this problem from a unified point of view. The solutions of this viscoelastic field equations reproduce all characteristic features of the observed deformation phenomena when energetic heavy ions are penetrating into glassy materials.

Particular long range interactions between atoms or molecules are introduced by the motion of the molecules in a flow-field. The investigation of tethered polymers in flow has started about two years ago. It has now become possible to include into the calculation the feedback effect of all segments of the molecule onto the other segments via the flow. It turned out, that these feedback effects are crucial to understand the behavior of large molecules in a hydrodynamic environment. This extends the previous linear viscoelastic theory for Non-Newtonian fluids towards the incorporation of nonlinear effects. (This interesting field of research will not be continued in *Theory III* since the responsible scientist Prof. W. Zimmermann has accepted a professor position at university Saarbrücken.)

An old problem in the field of order-disorder transitions is the question of pinning and depinning of an advancing front over a background of randomly frozen impurities. A particularly characteristic example of such a process is the high speed phase transition (solidification) of an alloy after laser-induced surface melting. In a combination of analytical methods and numerical large scale Monte-Carlo simulations new insights into this problem have been gained. A central result is the quantitative confirmation of a scaling hypothesis for the dependence of the growth rate upon interaction energies, concentration and strength of impurities, temperature and driving force.

The increasing possibility of realistic calculations of materials properties from first principles has again increased the interest in collective properties of solid surfaces. A technologically very important and theoretically highly challenging problem is the formation and propagation of cracks in solids. A new theory has combined previous concepts on crack formation and surface deformations. It was found that cracks will be susceptible to surface instabilities which may eventually be responsible for directional instabilities during crack propagation.

H. Müller-Krumbhaar

STAFF

THEORIE III

a. Staff members

Brener, E.	Kinetics of phase transformations	23.15.0
Dederichs, P.H.	Electronic properties, interfaces and layered systems	23.20.0
Müller-Krumbhaar, H.	Non-linear dynamics of dissipative systems, correlated fermions	23.15.0
Oubenkhir, S.	Secretary	
Schober, H.	Statics and dynamics of glasses, defects and phonons	23.15.0
Schroeder, K.	Electronic and atomic structure of defects in semiconductors	23.42.0
Trinkaus, H.	Dissipative structure formation, reaction-diffusion problems	23.15.0,23.80.5
Zeller, R.	Electronic structure and magnetic properties of metals	23.20.0

b.
c. Visitors

Caprion, D.	Dynamics of selen-glass
Dattagupta, S. (IND)	Incoherent tunneling
Korhonen, T. (FIN)	Lattice relaxations around defects in metals
Kudrnovsky, J. (CZ)	Interlayer coupling in magnetic layered systems
Marchenko, V. (GUS)	Elastic effects during phase transformations
Mavropoulos, F.	Hyperfine fields on surfaces
Misbah, C. (F)	Solidification processes, non-linear dynamics
Papanikolaou, N. (GR)	Ab-initio calculations of forces and lattice relaxations
Overhof, H.	Defects and impurities in semiconductors
Spettmann, R.	Metals on semiconductor surfaces, Schottky-barriers
Stefanou, N.	Adsorption of atoms at surfaces

d.
e. *PhD and Diploma Students (University = RWTH Aachen)*

Alaga-Bogdanovic, M.	Phase field calculations of surface-wetting
Antons, A.	Ab-initio calculations on surface reconstruction
Bellini, V. (I)	Electron structure of magnetic layered systems
Berger, R.	Polar surfaces of III-V-semiconductors

Feng, X.	Structure formation under fluctuations
Gutheim, F.	Cluster growth on surfaces
Hartmann, M.	Collective effects of cracks and dislocations
Höhler, H.	Defects in semiconductors
Kienle, D.	Transport coefficients in polymer solutions
Kluge, M.	Binary metallic glasses
Kromen, Wi.	Point defects and interfaces in Nitride-semiconductors
Nonas, B.	Fully relativistic band structure methods
Rzehak, R.	Polymer dynamics and hydrodynamic flow
Settels, A.	Electronic structure of point defects in semiconductors
Spatschek, R.	Collective effects of cracks in solids
Temkin, D. (GUS)	Impurity effects during solidification

Direct Exchange and Interaction of $3d$ impurities on the (001) Surface of Iron

B. Nonas, K. Wildberger, R. Zeller and P.H. Dederichs

Theorie III

We made a detailed ab–initio study of direct exchange and interaction processes of $3d$ atoms on the Fe(001) surface. The calculations are based on local density functional theory and apply a KKR–Green function method for impurities on surfaces. For practically all $3d$ transition metal impurities on Fe(001) we found a strong tendency for a direct exchange mechanism into the first surface layer. The early $3d$ impurities V, Cr and Mn strongly repel each other on neighboring positions within the first layer, while Ni and Cu atoms show a moderate repulsion. The ab–initio results are in good agreement with STM studies for Cr/Fe(001) by the NIST group and present valuable predictions for all $3d$/Fe(001) systems.

Fe/Cr(001) layers represent a model system for studying interlayer coupling and giant magnetoresistance. While originally the Fe/Cr interface was thought to be particularly smooth, recent experiments have shown that at the interface strong intermixing occurs. For instance, in an STM study of the NIST group [1] the growth and alloying of Chromium on the Fe(001) surface has been investigated. The authors find that under layer–by–layer growth condition substantial intermixing occurs at the Fe/Cr interface. For instance, adsorbed Cr atoms are directly incorporated into the first Fe-layer and also interdiffusion into deeper layers is observed. Further statistical analysis of the data yields direct information about the interactions of Cr atoms in the surface layer; e.g., the absence of nearest neighbor (nn) dimer pairs shows a strong repulsion between neighboring Cr atoms.

Motivated by these STM results for Cr on Fe(001) we made an ab–initio study of the alloying process for $3d$ impurities on the Fe(001) surface, concentrating on the energetic properties in the dilute limit. In particular we considered the elemental processes sketched in Fig. 1 and asked the following specific questions: Is it for an impurity adatom (Fig. 1a) energetically favorable to exchange with an Fe surface atom ("direct" exchange, Fig. 1b), and is the resulting complex (b) stable or likely to dissociate ("complete" exchange, Fig. 1c), so that effectively a migrating $3d$ adatom (a) is replaced by a migrating Fe adatom as in (c)? Do two $3d$ impurities in the first layer cluster as in (d) or are distant configurations (e) more stable? Our results are in excellent agreement with the STM results for Cr/Fe(001) [1] and predict the behavior of other 3d/Fe(001) systems. More details and further results can be found in [2].

The calculations were based on density functional theory in the local density approximation and applied a KKR–Green function method for impurities on surfaces. The atomic potentials as well as the potentials in the vacuum region were approximated by spherically symmetric ASA–potentials. However the "full" charge density including all non–spherical terms was evaluated and used in the calculation of the total energies. We started from the selfconsistently calculated Green function of the ideal surface which served as the unperturbed reference system. To describe the impurity or the impurity dimer on the surface we considerd a cluster of perturbed ASA–potentials which included the potentials of the impurities and the perturbed potentials of several neighbor shells. The total energy of the perturbed system was evaluated as the energy difference with respect to the reference system by applying Lloyds formula. In this way all single particle contributions were summed up in whole space.
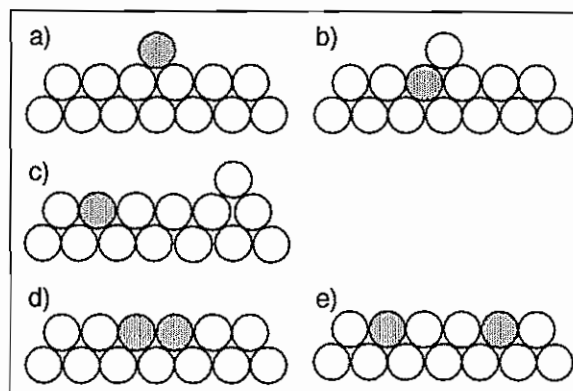

FIG. 1. Schematic representation of different configurations of $3d$ impurities (shaded) at the surface: (a) $3d$ adatom, (b) the direct–exchange complex consisting of a $3d$ surface atom and a neighboring Fe adatom, (c) the complete–exchange complex with a "free" Fe adatom, (d) two $3d$ surface atoms at nn sites in the first layer and (e) two non–interacting $3d$ surface atoms.

Our calculations of the total energy difference between the configurations (a) and (b) in Fig. 1 give a lower energy of the system when a transition metal adatom of the middle of the 3d-series is exchanged with an iron surface atom ("direct exchange" in Fig. 2). This direct exchange implies the replacement of an Fe-Fe bond by an Impurity-Fe bond and leads to a net energy loss for atoms at the beginning and end of the transition row, which makes the process unfavourable for these cases. How-

ever, the energy of the exchanged configuration might be further lowered by diffusion of the exchanged Fe-adatom on the surface, thus replacing the Impurity-Fe bond by the more stable Fe-Fe bond. This is what we found in our calculations, where the comparison of energies for the latter configuration [Fig. 1(c)] and of the impurity adatom [Fig. 1(a)] leads in nearly all cases to a substantial lower energy for the incorporated impurities ("complete exchange" in Fig. 2). The energy gain of the complete exchange process is especially large for Cr and Mn and thus agrees with STM-observations for Cr-atoms on the Fe(001) surface in the dilute limit, where all Cr atoms were found to be incorporated into the surface layer. Our calculations show a strong contribution of the magnetic energy to the calculated exchange energies, which is particularly important for Mn [2].
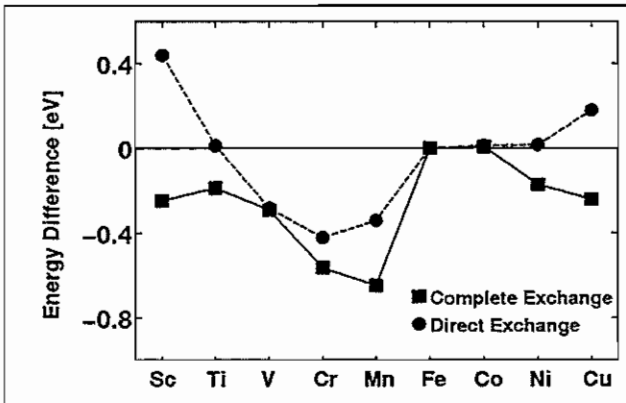
FIG. 2. The differences in total energy for the exchange process. The *direct-exchange* energy is the total energy difference between the exchange complex of Fig. 1(b) and the 3d adatom of Fig. 1(a). The *complete-exchange* energy includes the dissociation energy of the complex and represents the total energy difference between the configurations 1(c) and 1(a).

We considered also the interaction of two 3d surface atoms by calculating the interaction energies on nearest neighbor (NN) sites in the surface (Fig. 3). The interaction energies are defined as the total energy difference between the dimer complex and two isolated impurities at infinite separation. Thus by construction a negative energy means attraction and a positive energy repulsion between the two atoms. For the single surface impurities the preferred magnetic states are [3]: ferromagnetic coupling ($\uparrow$) to the substrate for Fe, Co and Ni and antiferromagnetic coupling ($\downarrow$) for Ti, V, Cr and Mn; the Mn and Fe impurities may also align in the respective other (metastable) configuration. The pairs considered here, are either in the antiferromagnetic configuration ($\downarrow\downarrow$) with both impurities coupling ferromagnetically to each other, but antiferromagnetically to the substrate or in the ferromagnetic one ($\uparrow\uparrow$). The last one is the most stable configuration for Fe, Co and Ni nn-pairs, while the

antiferromagnetic configuration is found for Ti-, V-, Cr- and Mn-pairs. The interaction energies for these surface dimers on nn sites are shown in Fig. 3.
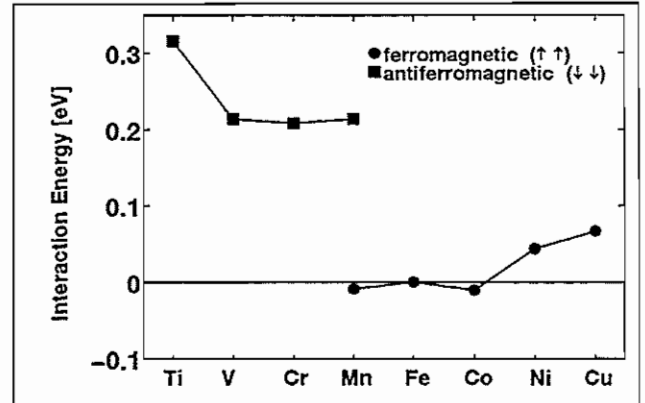

FIG. 3. Interaction energies of 3d impurities on the nearest neighbor sites in the surface layer of Fe(001). The energies are given in eV with positive energies referring to repulsive interactions.

The most important result is here, that the interaction for the nn dimers of Ti, V, Cr and Mn is strongly repulsive with a magnitude of about 0.2 eV, while the interaction for the nn dimers of Co, Ni and Cu is relatively weak, being slightly attractive for Co and repulsive for Ni and Cu. The repulsion of the ($\downarrow\downarrow$) configurations is a consequence of frustration: the two atoms would like to couple antiparallel to each other, which can however not be realized due to the strong antiferromagnetic coupling of each atom to the substrate moments. Our calculations for NNN surface dimers show a reduced interaction of the impurities, repulsive for Cr and Ni and attractive for V and Mn. Our results are in very good agreement with the STM studies for the growth process of Cr on the Fe(001) surface [1]. In the statistical analysis of these data, no nn Cr pairs are found, while the probability for the formation of Cr dimers on nnn sites is reduced by 0.4 ± 0.2 as compared to a random distribution, which would occur in the non-interacting case. From our calculations we obtain a reduction by a factor of 0.01 for the nn Cr dimers and a reduction by 0.6 for the nnn dimers which agrees with the STM results within the statistical errors.

[1] A. Davies, J. Stroscio, D.T. Pierce, and R.J. Celotta, Phys. Rev. Lett. 76, 4175 (1996).
[2] B. Nonas, K. Wildberger, R. Zeller and P.H. Dederichs, Phys. Rev. Lett. 80, 4575 (1998).
[3] B. Nonas, K. Wildberger, R. Zeller, and P.H. Dederichs, J. Magn. Magn. Mat. 165, 137 (1997).

A Parallelized *ab initio* Molecular Dynamics Code for the Investigation of Atomistic Growth Processes

R. Berger, S. Blügel, A. Antons, Wi. Kromen, K. Schroeder
Theorie III

We developed a parallelized *ab initio* molecular dynamics code for materials properties and processes based on the local density approximation to the density functional theory, with separable, norm-conserving pseudopotentials and a plane-wave representation of the wavefunctions and applied it to the calculation of reaction rates of adatoms (Si, Ge, Sn, As) on As-terminated Si(111). We discuss parallelization strategies and speed-ups. We found the program computing in parallel on 64 Cray T3E processing elements is 10 times faster than on a single Cray T90 processor.

The design of new quantum materials relies to a large extent on manipulating and controlling the growth of small structures on the nanometer scale. Examples are strained Ge/Si heterostructures, nanowires or hut clusters. In many cases self-organization of nano-scale structures, i.e. quantum dots, is observed to occur over macroscopic scales for length (> 100 nm) and time (seconds or minutes). For a realistic modeling of such growth phenomena, the relevant microscopic growth conditions such as the presence or absence of surface defects, impurities, steps or reconstructions and the possible reactions of deposited atoms have to be identified.

It is our goal to provide a thorough understanding of the atomistic processes occuring at surfaces during growth. We carry out *ab initio* calculations of the electronic structure, the total energy and forces on atoms in order to find equilibrium configurations, dynamical properties and reaction rates on an atomic scale (length scale of chemical bonds ~ 0.1 nm and time scale of atomic vibrations $\sim 10^{-12}$ sec), which are relevant to explain and describe the microscopic processes underlying crystal growth. We basically proceed in two steps: (i) First we analyze possible atomic structures (adatoms, defects, clusters, steps on surfaces) and evaluate their relevance by comparing the total energies. (ii) This is succeeded by a selection of relevant atomistic processes and the calculation of energy barriers (and in the future maybe also prefactors) for the respective reaction rates.

The combination of step (i) and step (ii) defines a problem at the cutting edge of supercomputing in surface science. Up to now only very few such calculations have been performed. Usually there is a huge number of relevant atomistic processes: deposition, diffusion on a terrace, diffusion across a step edge, diffusion along a step edge, diffusion of dimers, nucleation of islands, exchange of atoms. To model these processes often unit-cell sizes of the order of $100 - 300$ atoms are required. The calculation of activation barriers requires the sampling of high dimensional reaction paths in order to find the trajectory with minimum energy saddle point. This requires a large amount of constraint molecular static and dynamics calculations using large unit cells.

For this purpose we have developed EStCoMPP [1] a parallelized *ab initio* molecular dynamics program based on the local density approximation to the DFT, norm-conserving pseudopotentials of the Kleinman-Bylander form, a plane-wave basis set for the wavefunctions and iterative diagonalization schemes for the eigenvalue problem. The convergence of the charge density to self-consistency is accelerated by quasi-Newton methods. Force calculations combined with molecular statics are used to determine the minimum energy configurations and the reaction pathways. The surface is simulated by a repeated slab model.

The central problem of solving the density-functional Kohn-Sham equations is mapped to the solution of an eigenvalue problem of dimension N in the space of the plane-wave basis set. For group III, IV, or V semiconductors, the eigenvalue problem easily reaches dimensions of $N \cong 30000 - 100000$ and is solved iteratively for M eigenstates, $M \cong 300 - 1000$.

The wavefunctions are represented in a plane-wave basis by $\psi_{k\nu} = \sum_n^N c_{k\nu}^n e^{i(k+G^n)r}$. The generic form of any iterative algorithm requires (i) the application of the Hamiltonian matrix $H_k^{n',n}(m, \{R\})$ on the wave-vector $c_{k\nu}^{n,(i)}(m, \{R\})$, $c_{k\nu}^{n',(i+1)} = \sum_n H_k^{n',n} c_{k\nu}^{n,(i)}$ and (ii) the orthogonalization: $\langle c_{k\nu}^{(i+1)} | c_{k\nu'}^{(i+1)} \rangle = \delta_{\nu,\nu'}$. These equations have to be solved for each Bloch state k, band index ν, iteration step i of the eigenvalue problem, for each self-consistency (SC) step m to reach convergence of the charge-density, and for each molecular dynamics step $\{R\}$. For the example described below this core algorithm is carried out about 45 times per Bloch state and molecular dynamics step, each time for about 500 state-vectors.

One strategy for parallelizing the iterative eigenvalue problem may proceed by distributing (i) the k-points, (ii) the eigenstates ν for each k-point, and (iii) the elements n of the wave-vectors over several processing elements (PEs), according to the 3 distinct indices of the expansion coefficients $c_{k\nu}^n$ of an eigenstate $\psi_{k\nu}$. To a good approximation each of the 3 parallelization steps can be carried out independently, and at present step (i) and

(iii) are implemented.

The distribution of the k-points over a set of PEs is equivalent to an independent execution of the iterative eigenvalue problem on each PE. The parallelization is coarse grained, the communication is at a minimum and the parallelization is easy and efficient (cf. Fig. 1). This parallelization strategy, however, fails for larger systems with typically few k-points. The memory and speed per PE is insufficient to solve a large eigenvalue problem.
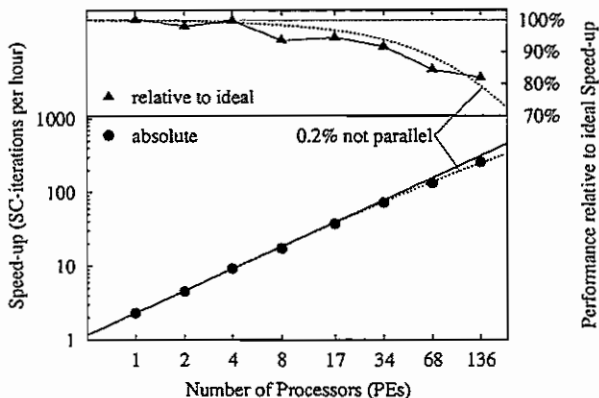

FIG. 1. Speed-up as function of the number of PEs for the k-point parallelization. Example is bulk β-Sn. The unit cell contains 2 atoms. The calculations were carried out with 272 k-points. The lower panel shows the absolute speed-up. The straight line shows the hypothetical speed-up for a program with ideal parallelization (100% parallelization, no overhead). The upper panel shows the ratio of actual speed-up to ideal speed-up. The broken lines is a fit through the data-points with the theoretical speed-up of a program for which 0.2% of the CPU-time/PE remains unparallelized.

These drawbacks are overcome by approach (iii), i.e. distributing the vector elements over many PEs. This is equivalent to distributing the eigenvalue problem over the PEs, and this is the most difficult parallelization step which requires a fine scale parallelization with frequent communication. Taking into account that the iterative eigenvalue problem requires vector-vector and matrix-vector multiplications, fast-Fourier transformations, and subspace diagonalizations, a new data-structure is compulsory for an efficient parallelization. Since the length of the vectors scales with the size of the problem, the distribution of vector-elements over the PEs is an approach that allows the use of many processors and provides scalability in the sense that the number of usable PEs scales with the problem size. Fig. 2 shows the speed-up for approach (iii) in combination with the k-point parallelization. We find an excellent speed-up for 64 PEs (32 PEs/k-point) for which the program runs 10 times faster than on a single processor of the Cray T90. A better speed-up for an even larger number of processors can be achieved by including approach (ii), which will be done in the future.

A frequently applied method for hetero-epitaxy of materials with lattice mismatch is based on the "surfactant effect". E.g. covering the surface with a monolayer of As (or Sb) changes the growth mode of Ge on Si(111) from Stranski-Krastanov (3D-islands) on pure Si(111) to layer-by-layer-growth. As a contribution to the understanding of this effect we have performed calculations for kinetic processes of Si, Ge, Sn and As adatoms on Si(111):As (1 ML).

The competition between surface diffusion and incorporation of the group IV adatoms under the surfactant layer decisively influences island nucleation on terraces and thus the growth mode for heterostructures. We have found that Si is readily incorporated [2] yielding a high island nucleation rate as found in experiment [3]. On the other hand, Ge adatoms make many diffusion jumps. They can easily reach terrace steps, which would indicate step flow. Thus, the influence of surfactants on processes at steps is important as has been suggested in the literature [4].

We are currently performing calculations for diffusion on the reconstructed clean Si(111) surface, for the stability of small adatom clusters and of steps on Si(111):As, and for Sb as a surfactant.
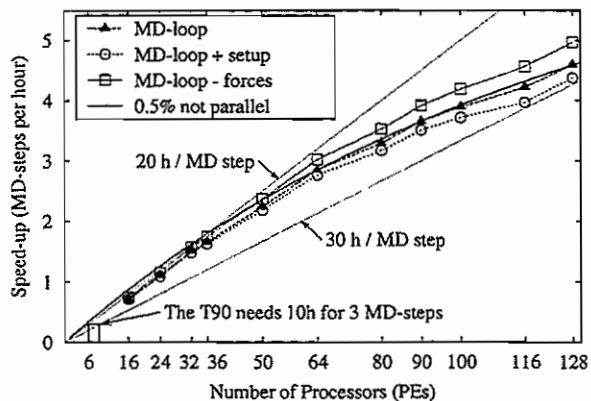

FIG. 2. Speed-up for As/Si(111) containing 110 atoms in the super-cell and two k-points. 50 % of the PEs are assigned to each k-point. The straight dotted lines show the hypothetical speed-up for a program with ideal parallelization requiring 20 or 30 hours, respectively, per MD-step on one PE. The full line is a fit through the data-points and represents a program for which 0.5% of the CPU-time/PE remains unparallelized. For comparison: A single Cray-T90-vector-processor unit needs ten CPU hours for three MD-iterations, thus six to nine T3E processors (depending on the speed-up) correspond to a single T90 processor.

[1] EStCoMPP: Electronic STructure COde for Materials Properties and Processes.
[2] K. Schroeder et al., Phys. Rev. Lett. 80, 2873 (1998)
[3] B. Voigtländer et al., Phys. Rev. B 51, 7583 (1995)
[4] D. Kandel and E. Kaxiras, Phys. Rev. Lett. 75, 175 (1996)

Multifractal structure of eigenstates in the Anderson model with long-range off-diagonal disorder

D. A. Parshin[1,2] and H. R. Schober[1]

[1] *Theorie III*

[2] *Technical State University, 195251 St. Petersburg, Russia*

The interaction of random defects (electric or elastic dipoles) in a medium can be treated by an Anderson model with long range off-diagonal disorder ($V_{ij} = (\pm)/|\mathbf{R}_i - \mathbf{R}_j|^d$) where $\mathbf{R}_i$ are Poisson distributed random points in d dimensional space. In this marginal case all states are delocalized. The most extended modes, which dominate properties such as heat conductivity, have a self-similar multifractal structure, reflected e.g. in their generalized dimensions, D_q.

Since the first paper of Anderson [1] on quantum localization of excitations in disordered systems our understanding of this difficult theoretical problem has progressed enormously. The disorder-induced localization-delocalization transition was found to manifest itself by a complex spatial behavior of the wave functions believed to have multifractal structure at the localization threshold.

Usually Hamiltonians with short range off-diagonal matrix elements are investigated. We investigate [2] the opposite case: *long-range off-diagonal disorder* where for some distance dependence of the non-diagonal matrix elements, $V(R)$, all states are delocalized. For the $3d$ case this was proven for $V(R)$ falling off $\propto 1/R^3$ or slower [1]. This dependence of transition matrix elements is characteristic for the dipole interaction between elastic defects in solids. It was shown recently that such an interaction between soft harmonic oscillators leads to the universal linear frequency dependence of the density of states above the boson peak in glasses [3]. It is remarkable that 95% vibrational states in glasses are usually neither localized nor propagating in the usual plane wave sense. Their spatial structure is still a challenge to physicists in this field as well as for the *marginal* case of the Anderson model in general.

A second motivation for this work is the increasing interest in statistical properties of large random matrixes, $N \times N$. We find drastic differences compared to the Wigner-Dyson random matrix theory for statistically independent off-diagonal matrix elements. The triangle rule for distances implied in the $1/R^d$ law introduces specific correlations between the off-diagonal matrix elements causing in turn multifractal properties of the eigenstates. The distribution of the eigenvalues is also very different. In the Wigner semi-circle the density of states at small energies is size dependent, $\propto 1/\sqrt{N}$. In our case it is size independent, i.e. it is finite in the thermodynamic limit.

We study numerically the spectrum and eigenvector statistics of large $N \times N$ real symmetric matrixes $\hat{V}$ with purely off-diagonal disorder. Without loss of generality all diagonal matrix elements are set to zero. Off-diagonal

disorder is introduced as $V_{ij} = (\pm 1)/|\mathbf{R}_i - \mathbf{R}_j|^d$. Here $\mathbf{R}_i$ are Poisson-distributed random points in d dimensional space ($d = 1, 2, 3$), and the random sign, ± 1 provides for the average value $\langle V_{ij} \rangle = 0$ corresponding to the interaction of randomly oriented electric or elastic dipoles.

We place N random points, s (oscillators) according to Poisson statistics in an d-dimensional "cube" of size $L = N^{1/d}$ ($100 \leq N \leq 10000$) thus keeping the average concentration of oscillators constant. Diagonalizing the matrix $\hat{V}$ we find a set of N orthonormal eigenvectors $e_s(j)$ with

$$\sum_{s=1}^{N} e_s^2(j) = \sum_{j=1}^{N} e_s^2(j) = 1 \qquad (1)$$

and corresponding eigenvalues, ω_j. This is repeated until the relative variance of the average values, discussed in the following, has dropped well below the percent level.
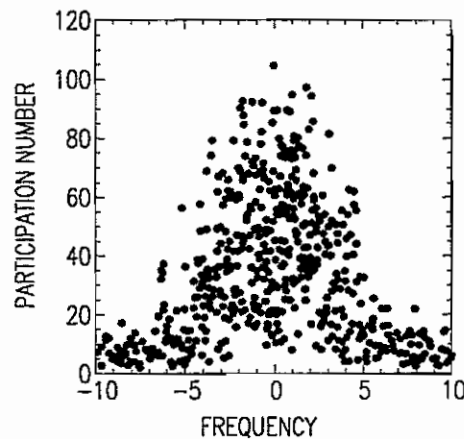

FIG. 1. Participation numbers versus frequency for a 3d system of 800 oscillators.

As the usual measure of localization of the states j we calculate the participation ratio

$$P_j = \left(N \sum_{s=1}^{N} e_s^4(j) \right)^{-1} . \qquad (2)$$

The product $NP_j \equiv N_j$, the participation number, shows how many oscillators participate in the mode j (frequency ω_j). Fig. 1 shows the participation numbers N_j versus frequencies ω_j for a $3d$-system of 800 oscillators. Striking are the strong fluctuations of N_j for small ω_j. Here we are mainly interested in the mode j_m (frequency ω_m) with the maximal participation number (ratio) which is the most extended one in the system.
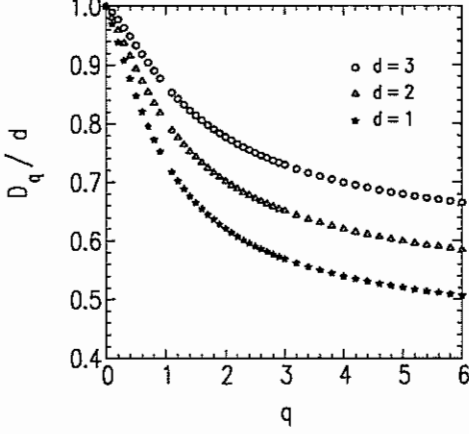

FIG. 2. Generalized dimensions for the most extended eigenstates as function of q for one, two and three dimensional systems.
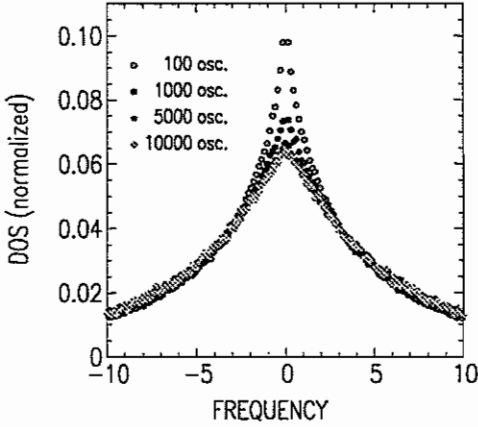
FIG. 3. Density of states for 3d system of 100, 1000, 5000 and 10000 oscillators.

To study the multifractal properties of the eigenstates we investigate the scaling with N (or equivalently system size L) of the generalized inverse participation numbers of these maximally extended modes j_m

$$M_q = \left\langle \sum_{s=1}^{N} \left[e_s^2(j_m) \right]^q \right\rangle_N \propto N^{-(q-1)D_q/d} = L^{-(q-1)D_q}.$$

(3)

Angular brackets denote averaging over the samples with given number N. If the generalized dimension D_q depends on q one speaks of a multifractal structure of the eigenstates. Fig. 2 shows the functions D_q/d for $d = 1, 2, 3$ obtained from our numerical simulation. Nonzero values of D_2 imply delocalization of the most extended states in the system. A plane-wave like state would give a constant value $D_q/d = 1$. In the multifractal analysis one usually calls D_2 the correlation dimension. We obtain values of 0.62, 1.40 and 2.33 for the $1d$, $2d$ and $3d$ cases, respectively. The corresponding values for the information dimension D_1 are 0.74, 1.61 and 2.60.

One of the important characteristics of the energy spectrum is the density of states (DOS) $g(\omega)$

$$g(\omega) = \frac{1}{N} \left\langle \sum_{j=1}^{N} \delta(\omega - \omega_j) \right\rangle_N$$

(4)

Usually this function is non critical and scale independent in the limit $L \to \infty$. Fig. 3 shows $g(\omega)$ for $3d$ system with $100, 1000$ and 5000 oscillators. For large N the DOS does no longer depend on the system size. Using this property one can introduce a length $L_\omega = (g(0)\omega)^{-1/d}$ which can be taken as the size of the system whose mean level spacing equals ω at small ω. In our case existence of such a length might be a consequence of the invariance under the transformation $(\mathbf{r}, t) \to (b\mathbf{r}, b^d t)$ due to $V(R) \propto R^{-d}$. Therefore, $1/L_\omega^d \propto \omega$ and $g(\omega) \to$ const for $\omega \to 0$. If this holds, then comparing the scaling behaviors of M_q and $C(t)$ leads to the relation $\tilde{D}_2 = D_2/d$ observed in our computer experiment. However for more definite conclusion one needs investigate the same problem for $V(R) \propto R^{-\mu}$ with $\mu \neq d$.

To conclude, we investigated numerically the spatial structure of delocalized states in the marginal case of the Anderson model with long-range off-diagonal disorder corresponding to the important dipole interaction. Because of the long-range correlations in the system these delocalized states have multifractal spatial structure causing anomalous diffusion of excitations in this system.

[1] P. W. Anderson, *Phys. Rev. B*, **109**, 1492 (1958).
[2] D. A. Parshin and H. R. Schober, Phys. Rev. B **57**, 10232 (1998).
[3] V. L. Gurevich, D. A. Parshin, J. Pelous and H. R. Schober, *Phys. Rev. B*, **48**, 16318 (1993).

Partial draining of a tethered polymer in flow

Diego Kienle[1], Roland Rzehak[1], and Walter Zimmermann[1,2]

[1] *IFF Theorie III and Forum Modellierung*

[2] *Theoretische Physik, Universität des Saarlandes, D-66041 Saarbrücken*

Deformations of a polymer fixed at one end and subjected to a uniform flow have been investi-gated by taking the hydrodynamic interaction (HI) between polymer segments into account. For the first time the so-called non-draining effect which results from the collective hydrodynamic back-flow caused by all segments, is explicitly calculated. A partial flow penetration into the polymer coil is found. Therefore neither the free-draining nor the non-draining models discussed previously de-scribe the polymer-flow interaction appropriately. Accordingly, the f-shell blob model is introduced, describing the partial draining and the transition to a free draining polymer with increasing flow velocity, similar as in simulations.

Non-Newtonian fluids exhibit astonishing flow behav-ior such as turbulent drag reduction in dilute polymer solutions and their understanding is both theoretically challenging and of high technological importance. How-ever, a generally accepted theoretical basis for the de-scription of the large scale motion of non-Newtonian flu-ids, similar to the Navier-Stokes equations for simple flu-ids, is not available yet. Only for small displacement gradients there is a broadly accepted "general linear vis-coelastic model" for incompressible viscoelastic fluids [1]. If only linear fluid deformations are required even hydro-dynamic instabilities in viscoelastic fluids may be pre-dicted. An example is the surface instability, the so-called Faraday instability, occurring in a vertically vi-brated fluid layer. Here linear viscoelasticity induces a new harmonic branch [2].

The basis of an understanding of the *nonlinear* behav-ior of non-Newtonian fluids is certainly the interplay be-tween flow and polymers. Accordingly two basic ques-tions have been addressed recently [3,4]: How does the flow field deform a polymer and how is the flow field modified by the presence of the polymer?

In classical experiments on the dynamics of polymers in solution such as light scattering, birefringence, rheome-try and small angle neutron scattering one measures only volume-averaged quantities. A huge step forward in the analysis of the crucial interplay between the flow field and the deformations of the polymers has been achieved by studying single DNA molecules. DNA can be manip-ulated with optical tweezers and when decorated with fluorescent dyes, the reaction of these polymers can be followed under an optical microscope.

In recent computer simulations of bead-spring models for tethered polymers the polymer-induced perturbation of the flow field is determined for the first time, which is no less important for the behavior of non-Newtonian fluids than the flow induced deformation of the polymer [3]. In the model the hydrodynamic interaction (HI) be-tween the polymer segments as well as the excluded vol-ume interaction (EVI) have been included, but unlike

other work averaging approximations in the treatment of the HI have been avoided. We found in simulations that the flow partially penetrates the polymer coil which questions former coarse grained models assuming non-draining polymers. Accordingly we introduce a general-ized blob model with blobs having a free-draining outer shell and a non-draining inner sphere to cover this partial draining effect [4,5]. Consequently, this model is able to describe a transition between a coiled, nearly impenetra-ble polymer and a nearly stretched free-draining polymer.
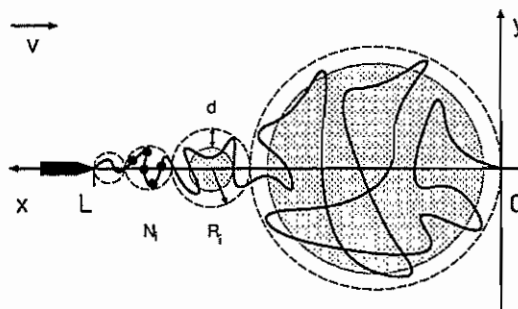

FIG. 1. Sketch of a polymer tethered at one end and ex-posed to a uniform flow field with velocity v. In the blob picture the deformed polymer with N segments (beads) is approximated by a sequence of spheres (blobs) with radius R_i and containing N_i segments. In the f-shell blob model each blob consists of a free-draining outer shell of thickness d and an impenetrable inner sphere (shaded).

The temporally averaged segment density of a tethered bead-spring chain with harmonic springs and $N = 200$ beads is shown in fig. 2 for a uniform imposed flow with velocity $v = 0.02$. The y-dependence of the x-component of the flow field $u_x(r)$, as shown in fig. 3, indicates a nonvanishing flow at the average location of the polymer coil. This apparent flow penetration is a superposition of two effects. The flow penetrates the polymer coil at any moment and due to thermal fluctuations the polymer coil does not stay at a fixed location. Nevertheless, such a mean field presentation is appropriate for comparison with temporally averaged measurements and the mean

field type blob models.

f-shell blob model. - The partial penetration of flow into the polymer coil, cf. fig. 2, may be taken into account in blob models by assuming for each blob a free-draining outer shell of thickness d and an impenetrable inner sphere, cf. fig. 1. Previously discussed non-draining and free-draining blob models are contained in this model as limiting cases. The blob radius R_k is determined by a balance between the drag force F_k acting on a blob and the thermal agitation, $R_k = k_B T / F_k$ (Pincus rule). $R_k^{non} = R_k - d$ is the radius of the non-draining inner sphere. Using the Flory scaling $R_k = b N_k^\nu$ ($b = 1.0$ is segment length) the number of segments $N_k = (R_k/b)^{1/\nu}$ within the k-th blob may be calculated as well as the number $N_k^{non} = [(R_k - d)/b]^{1/\nu}$ in the non-draining part and the number of segments $N_k^{free} = N_k - N_k^{non}$ in the outer free-draining shell. F_k is the sum of drag forces exerted by the $(k-1)$ blobs counted from the free end plus the Stokes friction acting on the k-th blob caused by both the non-draining inner sphere and by the free-draining shell, i.e. $F_k = F_{k-1} + 6\pi\eta v R_k^{non} + 6\pi\eta a v N_k^{free}$. η is the solvent viscosity and a is an effective hydrodynamic bead radius. Together this provides the recursion relation for the force F_k

$$F_k = F_{k-1} + 6\pi\eta v \left(\frac{k_B T}{F_k} - d \right)$$
$$+ \frac{6\pi\eta v a}{b^{1/\nu}} \left(\left(\frac{k_B T}{F_k} \right)^{1/\nu} - \left(\frac{k_B T}{F_k} - d \right)^{1/\nu} \right) , \quad (1)$$

with $F_0 = 0$. The sum $\sum_k R_k$ of the blob radii $R_k = k_B T / F_k$ gives the overall extension $L(v)$ of the polymer as a function of the flow velocity, cf. fig. 3. The bead radius a has been chosen such that the elongation of the polymer starts already sets in at smaller velocities in the free draining limit (dashed line in fig. 3) than in the non-draining limit (dashed-dotted line), similar as in our simulations. The intermediate curves in fig. 3 (solid lines) are for different values of the penetration depth d.

In the non-draining and the free-draining limits eq.(1) may be solved analytically with some approximations (see i.e. [4]). Then one obtains simple power laws for the polymer extension, $L(v) \sim v^2$ in the non-draining limit and $L(v) \sim v^{2/3}$ in the free-draining limit [4], when $R = bN^{\frac{3}{5}}$ is chosen. However, an exact numerical calculation of $L(v)$, cf. dashed and dashed dotted curve in fig. 3, has more structure than the simple power laws obtained by the approximate calculation, cf. straight lines in fig. 3. The power laws may be considered as upper limits for the slope $L(v)$ for very long chains. A finite penetration depth d gives a smaller slope $L(v)$ than for $d = 0$, as shown in fig. 3. According to both effects one cannot expect any scaling regime with simple power laws for $L(v)$ for molecules having less than $N \sim 1500 - 2000$ Kuhn segments which are used in experiments. Besides these investigations on the stationary polymer shape also a powerful method to determine the relaxation spectrum of polymers has been recently applied [6].
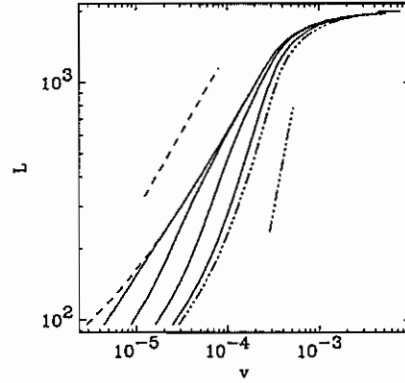
FIG. 3. Elongation $L(v)$ of the polymer calculated for the f-shell blob model with various values of the penetration depth $d = 1.0, 5.0, 15.0, 40.0$ from right to left. The dashed-dotted curve is for the non-draining limit $d = 0$ while the dashed curve corresponds to the limit $d = R_F$ it is the dashed one. The straight lines are the power laws obtained for analytical approximations. Parameters are $N = 2000$ and $b = 1.0$ with a corresponding Flory radius $R_F = bN^{3/5} = 95.6$.
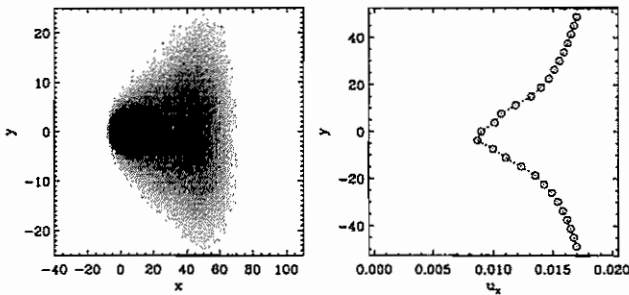

FIG. 2. Left: The time averaged density of polymer segments (beads) $\rho(x, y, z = 0)$ for a bead spring chain with $N = 200$ segments fixed at the origin with one end and subjected to a uniform flow in the x-direction with $v = 0.02$. Right: The spatially averaged x-component of the velocity field $\bar{u}(\vec{r})$ as a function of y indicates the partial penetration of the flow into the polymer.

[1] R. B. Bird, R. C. Armstrong, and O. Hassager, *Dynamics of Polymeric Liquids, Vols.* I, II, 2nd ed. (John Wiley & Sons, New York, 1987).

[2] H. W. Müller and W. Zimmermann, *Faraday instability in a linear viscoelastic fluid* Europhys. Lett. 45 169 (1999).

[3] R. Rzehak, D. Kienle, T. Kawakatsu, W. Zimmermann *Partial draining of a tethered polymer in flow* (sub. Europhys. Lett.)

[4] R. Rzehak, W. Kromen, T. Kawakatsu, W. Zimmermann, *Deformations of tethered polymers in uniform flow* (sub.)

[5] D. Kienle and W. Zimmermann, *f-shell blob model for tethered polymers in strong flow* (subm. to Macromolecules)

[6] R. Rzehak and W. Zimmermann, *Relaxation Modes and -Times for Nonlinear Polymer Dynamics and the Karhunen-Loeve Method* (unpublished).

Dynamics of Viscoelastic Flow in Ion Tracks Penetrating Glassy Materials

H. Trinkaus, H.R. Schober

Theorie III

Track formation in glassy materials under bombardment with energetic heavy ions and the associated macroscopic deformation (creep and anisotropic growth) are treated in terms of viscoelastic shear stress relaxation in regions locally heated by the ions (thermal spikes). The solutions of a system of linear viscoelastic field equations, proposed to describe these processes, reproduce all characteristic features of the observed deformation phenomena. An evaluation of appropriate experimental studies on the basis of the presented theory is, in turn, expected to provide valuable information on the glass viscosity near typical thermal spike temperatures.

During the last decade, bombardment with energetic ions has increasingly attracted interest in material science and technology, particularly in microelec- tronics where this method is used to modify the state of surface near layers systematically. However, in most employed techniques, the mechanisms underlying the observed phenomena are not yet well understood.

The interaction of energetic ions with solid materials by quasi-elastic collisions and electronic excitations results in microstructural modifications associated with specific macroscopic effects. For sufficiently high electronic stopping powers ($S_e > 10$keV/nm at ion energies >10MeV/u), continuous "tracks" with diameters of several nanometers form along the ion trajectory both in crystalline solids and amorphous materials. In crystalline solids such tracks have been identified as amorphous inclusions. In amorphous materials on the other hand, track regions are obviously in a modified glassy state whose character was, however, not known until recently. Also the macroscopic deformation effects of track formation were not understood so far: The spectacular "anisotropic growth" of (stress free) foil samples perpendicular to the ion beam direction ("Klaumünzer effect"[1]), and the large creep deformation under an externally applied stress, both occurring even at low sample temperatures, $T_o \to 0$ [2]. Thus, for glassy systems, there are two obvious questions: (1) What is the character of the material modification in an ion track, and (2) what is the relation of these mesoscopic defects to the macroscopic deformation phenomena?

In recent years, track formation and the associated macroscopic deformation phenomena were discussed, using a relatively crude approximation, in terms of viscoelastic shear stress relaxation in nano-scale "thermal spike" regions and the subsequent freezing-in of the associated shear strain increments [3,4]. In the case of anisotropic growth, the local shear stresses are defined by the thermal expansion in cylindrical thermal spike regions, and in the case of creep by the macroscopic stress field. In the frozen-in state, a so formed track is considered to represents a mesoscopic defect in the form of a cylindrical elastic inclusion. In the mean time, the postulated elastic character of ion tracks has been confirmed by etching experiments studying the effect of a macroscopic stress on track formation [5]. A semi-quantitative treatment in which the viscosity of the glassy material is assumed to drop from infinite to zero when a certain "flow temperature" is exceeded (similar to melting) yields a reasonable description of the experimentally observed steady state deformation rates for high electronic stopping powers. A weakness of this approach is the conceptional and quantitative uncertainty of the term "flow temperature", and, related to this, the fact that it is not suitable to describe the behaviour of the deformation rate at low ("threshold") stopping powers, low ("incubation") doses, and elevated temperatures.

These problems can be overcome only by dropping the unrealistic assumption of a glass viscosity which changes discontinuously with temperature, and by using a continuum approach to describe local stress relaxation. Assuming the latter to be of Maxwellian type, the following linear viscoelastic field equations for the evolution of the displacement, $u_i(r,t)$, strain, $\varepsilon_{ij}(r,t)$, and stress, $\sigma_{ij}(r,t)$, fields in the thermal spike region of an ion track have been proposed recently [6,7]

$$\varepsilon_{ij} = (\partial_i u_j + \partial_j u_i)/2 \quad , \tag{1a}$$

$$\varepsilon_{ij} = \varepsilon_{ij}^{el} + \varepsilon_{ij}^{vi} + \varepsilon_{ij}^{tr} \quad , \tag{1b}$$

$$\partial_j \sigma_{ij} = 0 \quad , \tag{1c}$$

$$\sigma_{ij} = K \varepsilon_{kk}^{el} \delta_{ij} + 2\mu \, \tilde{\varepsilon}_{ij}^{el} \quad , \tag{1d}$$

$$\tilde{\sigma}_{ij} = 2\eta \, \dot{\tilde{\varepsilon}}_{ij}^{vi} \quad . \tag{1e}$$

Here, K is the bulk modulus, μ the shear modulus and $\eta\{T(r,t)\}$ the shear viscosity of the material giving a Maxwellian relaxation time $\tau\{T(r,t)\}=\eta\{T(r,t)\}/\mu$. The displacement field defines the total strain field which consists of elastic (el), viscous (vi), and thermal expansion induced "transformation" (tr) contributions, with $\varepsilon_{kk}^{tr} = \alpha\{T(r,t) - T_o\}$ where α is the thermal volume expansion coefficient and $T-T_o$ is the local temperature increase. The

tilde restricts tensors to their deviatoric parts, for instance $\tilde{\sigma}_{ij} = \sigma_{ij} - \sigma_{kk}\delta_{ij} / 3$. Equations (1c) to (1e) express elastic equilibrium, linear elastic stress-strain relation, and viscous strain production upon Maxwellian relaxation, respectively.

Surprisingly, the inhomogeneous system of coupled first order partial differential equations (1a) to (1d) can be solved approximately or, in special cases, even rigorously for cylindrical thermal spike regions of ion tracks – independent of the specific temperature evolution. Thus, for an incompressible medium, $K \to \infty$, the viscous strain component perpendicular to the track axis is given by the rigorous solution [6,7]

$$\varepsilon^{vi}(r,t) = \frac{1}{6}\int_0^t \varepsilon_{kk}^{tr}(r,t')\exp[-I(r;t',t)]dt'/\tau(r,t')$$

, (2a)

$$I(r;t',t) = \int_{t'}^t dt'/\tau(r,t')$$

(2b)

In the general case of finite K, the solutions involve a spectrum of relaxation times centered around the Maxwellian relaxation time. The cross-section for macroscopic anisotropic growth, the "deformation rate", A , is obtained by integrating $\varepsilon^{vi}(r, t \to \infty)$ over the cylindrical cross-section at the end of the track "life-time" which, for $T_o \to 0$, may be extended to infinite, $t \to \infty$.

For more detailed solutions, $T(r,t)$, $\varepsilon_{kk}^{tr}(T)$ and $\eta(T)$ need to be specified. Thus, for Gaussian thermal spikes inducing the local thermal expansion $\varepsilon_{kk}^{tr} = \alpha T$ ($T_o = 0$) in amorphous systems characterized by an Arrhenius type temperature dependence of the relaxation time, i.e. $\tau = \tau_o \exp(E/kT)$, the appropriately normalized low temperature steady state deformation rate A can be expressed as a "universal" scaling function of the two dimensionless variables, r_o^2/r_1^2 and r_2^2/r_1^2, where $r_o^2 = \langle r^2 T(r,t=0) \rangle$, $r_1^2 = \langle r^2 T(r,t=\tau_o) \rangle = 4D_{th}\tau_o$ (D_{th}: thermal diffusivity), and $r_2^2 = kS_e /\pi E\rho C$ (ρC: specific heat per unit volume) are the radial variances of the temperature distribution, $\langle r^2 T(r,t) \rangle$, at $t = 0$, $t = \tau_o$ and for $T(t,0) = E/k$, respectively.

Introducing these functions and dimensionless variables into Eqs. (2a,b) and performing the integrations numerically, the set of curves shown in Fig.1 is obtained which describes the stopping power dependence of the deformation rate. The curves show the transition from a threshold behaviour at low S_c to an approximate linear increase at high S_c, depending on the parameter r_o^2/r_1^2. With increasing r_o^2/r_1^2, the threshold behaviour becomes increasingly more pronounced. This shape variation in the theoretical curves covers that of experimental curves [1]. Information on the material parameters involved, particularly on the high temperature viscosity parameters τ_o and E, may be obtained by analyzing experimental data in terms of such theoretical curves.

In many cases, the dose dependence of the deform- ation rate is characterized by a transient to steady state ("incubation dose"). This feature may be attributed to
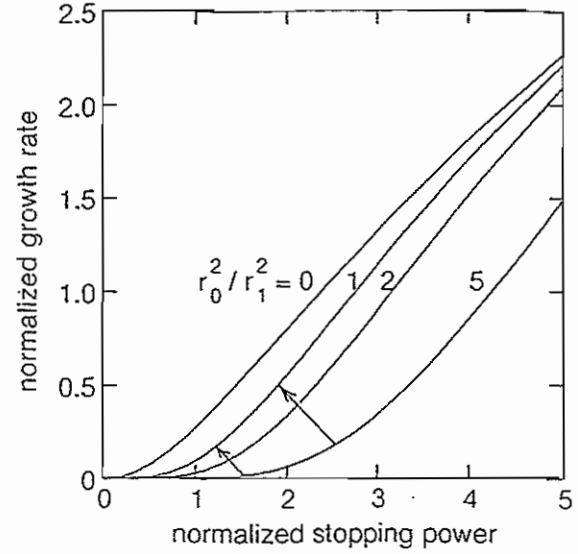

Fig.1: Normalized cross section for low temperature anisotropic growth, $3kA/2\pi\alpha D_{th}\tau_o E$, vs. normalized electronic stopping power, $r_2^2/r_1^2 = kS_e/4\pi\rho CD_{th}\tau_o E$ for various values of the parameter r_o^2/r_1^2. The arrows indicate parameter changes during the incubation period.

an ion beam induced reduction of the viscosity resulting in changes of the dimensionless variables of the scaling function as indicated in Fig. 1.

The dependence of the deformation rate on the sample temperature may be attributed to the relaxation of the stresses which are temporarily frozen-in in the track regions during cooling down of the thermal spikes. This back-relaxation can be treated in a separate second step since the corresponding relaxation time is many orders of magnitude larger than the one in the thermal spike. An evaluation of the experi- mentally observed decrease of the deformation rate at elevated sample temperatures provides information on the glass viscosity in the corresponding temperature range.

[1] S. Klaumünzer, Rad. Eff. and Def. in Solids 110 ,79 (1989).

[2] A. Audouard et al., J. Phys.: Cond. Mat. 5, 995 (1993) .

[3] H. Trinkaus, A. I. Ryazanov, Phys. Rev. Lett. 74, 5072 (1995)

[4] H. Trinkaus, Nucl. Instr. & Meth. B 107, 155 (1996).

[5] C. Trautmann, S. Klaumünzer and H. Trinkaus, submitted to Phys. Rev. Lett.

[6] H. Trinkaus and H.R. Schober, Mat. Res. Soc. Symp. Proc. 481, 359 (1998).

[7] H. Trinkaus, Nucl. Instr. & Meth. B 146, 204 (1998) .

Creep Motion of a Solidification Front in a Two-Dimensional Binary Alloy

X. Feng, E.A. Brener, D.E. Temkin and Y. Saito

Theorie III

The propagation of a solidification front in a two-dimensional binary alloy is studied by Monte Carlo (MC) simulations. A random atomic configuration is quenched and the atoms which prefer to be in the liquid phase act as quenched pinning centers to the advancing solidification front. For very small and very large bond energy ϵ, the front of a finite sized system is pinned by the quenched spacial disorder. However, for a moderate ϵ or for a large width N the pinning transition is smeared out and the front propagates steadily even in the two-phase region by thermal creep.

Interface motion in random media is observed in various disciplines of physics: random magnets, charge density waves, steps on crystal surfaces, to name just a few examples. It can be generalized to elastic manifolds as polymers, vortices in superconductors etc. In these systems quenched randomness pins the motion of the interface and at absolute zero temperature a sharp pinning-depinning transition takes place at a finite strength of an external driving force. At a finite temperature, however the pinning transition is smeared out by the creep motion of the interface.

In this work we study the motion of a one-dimensional (1D) solidification front in a two-dimensional (2D) disordered binary alloy system whose atoms in both solid and liquid phases are frozen. We know that a solidified system can have various different microstructures depending on conditions. One of the controlling parameter is the cooling rate. When it is fast enough, then we are in the glass regime in which the system is quenched so fast that the atoms do not have time to jump as the solidification front passes. Therefore all atoms in both phases can be considered as frozen. In addition, for a disordered binary alloy system there exists always spatial fluctuations of the concentration which are also quenched as atoms themselves. This quenched disorders lead to spatial and temporal correlations by the propagations of the solid-liquid interface. Our main interest lies in how this quenched disorder affects the motion of the interface when the system is very rapidly cooled.

The kinetic model we studied for such a diffusionless alloy growth was introduced by Temkin [1]. A simple square lattice is randomly occupied by A and B atoms and it is decomposed into two parts by a solid-liquid interface, liquid above solid, for example. The solidification or melting takes place only at the interface. The atomic configuration is quenched. Solidification therefore proceeds via a 'diffusionless' transformation. For simplicity we assume that the cohesive energies act between nearest neighbor atoms of the same phase but they do not depend on the type of atoms:

$$\epsilon_{AA}^{\beta} = \epsilon_{AB}^{\beta} = \epsilon_{BB}^{\beta} = \epsilon_\beta \qquad (\beta = s, l). \qquad (1)$$

Here the superscripts s and l refer to solid and liquid

state, respectively. Condition (1) leads to the mixing energy equal to zero and therefore both phases are ideal solutions. The interface thus corresponds to the place where the atomic cohesion is broken and each broken bond costs interface energy. Depending on the process (freezing or melting) and on the number $j(= 1, 2, 3)$ of nearest neighboring atoms in the same phase, there are 12 transition frequencies: six solidification frequencies denoted as $\omega_{+X}(j)$ and six melting frequencies denoted by $\omega_{-X}(j)$. Here X refers to A or B atom. These frequencies should satisfy the detailed balance condition to ensure the equilibrium phase diagram. The equilibrium phase diagram with the solidus $C_s(T)$, liquidus $C_l(T)$ and equal-free-energy $C_0(T)$ lines is shown in Fig.1. The area between the solidus and liquidus lines $(C_s(T) < c <)C_l(T)$ is the two-phase coexisting region.
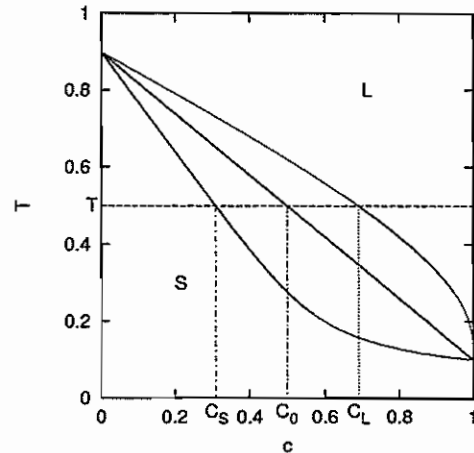

FIG. 1. The equilibrium phase diagram: temperature T versus concentration c of B-atoms. The melting temperatures of A-atoms and B-atoms are: $T_A = 0.9$ and $T_B = 0.1$.

We have systematically studied the behavior of the interface by means of Monte Carlo simulation. It has been found that the interface of a 2D alloy system has a steady-state solidification velocity in the solid phase region ($c < C_s$) and a steady-state melting velocity in the liquid phase region ($c > C_l$).

However, in the two-phase coexistence region the interface shows a rather complicated behavior depending strongly upon the width of the system N and the bond energy ϵ. The time dependence of the average displacement of the interface is found to follow a power law as $h(t) = at^\nu + b$. The simulation results of the dependence of the effective exponent ν on the bond energy ϵ and the system size N are summarized in Fig.2. We choose $c = 0.4$ and $T = 0.5$ such that the corresponding phase point is located in the two-phase coexistence region with a solid phase favored (see Fig.(1)). For simplicity, ϵ_s and ϵ_l take always the same value: $\epsilon_s = \epsilon_l = \epsilon$.
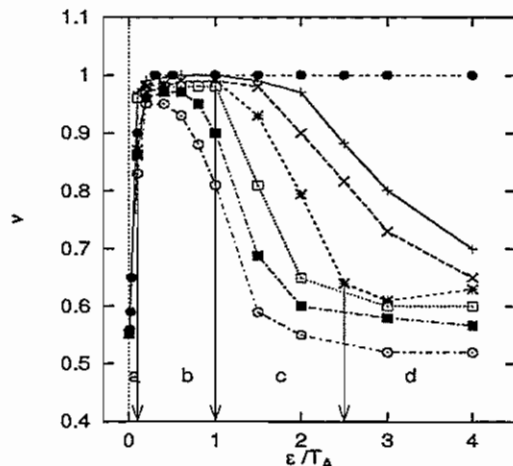
FIG. 2. Dependence of the dynamical exponent ν on the bond energy ϵ. Curves from bottom to top correspond to system sizes $N = 25, 30, 40, 50, 70, 80$ and 2000. The simulation time is up to $t = 10^6$.

Figure 2 shows an evident size- and bond energy-dependence of the interface dynamics. Taking $N = 40$ as an example, we can divide ϵ dependence of ν into four characteristic regimes

$$
\begin{aligned}
(a) & \quad \nu < 1 \quad \text{for} \quad \epsilon < 0.1T_A, \\
(b) & \quad \nu = 1 \quad \text{for} \quad 0.1T_A < \epsilon < \epsilon_c(N), \\
(c) & \quad \nu < 1 \quad \text{for} \quad \epsilon > \epsilon_c(N), \\
(d) & \quad \nu = \nu_{1D} \quad \text{for} \quad \epsilon \to \infty.
\end{aligned}
\tag{2}
$$

$\epsilon_c(N)$ is a critical bond energy which varies with the system size N.

Unlike the 1D system, the 2D system can grow steadily even in the two-phase region $(0.1T_A < \epsilon < \epsilon_c(N))$. However when $\epsilon > \epsilon_c(N)$, the interface becomes pinned such that the spatial disorder of the alloy leads to a decay of the interface velocity. In the large energy limit $(\epsilon \to \infty)$ theoretical analysis and computer simulations [3] show that the two-dimensional system behaves similarly like a 1D system. It means the interface has a constant velocity in the one-phase region and a vanishing velocity

in the two-phase coexisting region where the exponent ν has the same value as its one-dimensional counterpart ν_{1D} (=0.51 for $c = 0.4$ and $T = 0.5$ [2]).

A peculiar result occurs for small but nonzero bond energies, less than about $0.1T_A$. Here pinning occurs as would be the case for vanishing bond energy but the exponent ν is increased above the value of the one-dimensional case ($\nu \simeq 0.51$). Therefore both for very large and very small bond energy in a finite system the interface will be pinned.

For a very large system ($N \to \infty$) with a finite bond energy, the simulation reveals that the interface always moves steadily within a finite simulation time that means $\epsilon_c(N \to \infty) \to \infty$. This corresponds to the thermal creep motion. We have analyzed the dynamic behavior of the solidification front by scaling argument [3] which dates back to Imry and Ma. In the pinning region of the interface, where there are more B-atoms than the expected average value and the liquid phase is favored, three energies play a important role. They are the energy that the system has to pay in order to overcome the pinning region, the interface energy caused by the deformation of the interface and the energy gain by the driving force. It has been found that the influences of the bond energy ϵ and the driving force H, which is proportional to the concentration difference $c - C_0$, on the velocity v of the interface growth are decoupled. Numerical calculations have conformed the analytic formula in the vicinity of zero H and for sufficiently large ϵ

$$
v = 1.5e^{-\epsilon/T}e^{-0.5\Delta^2/HT}.
\tag{3}
$$

Our model can be mapped into the Random Field Ising Model and Δ in (3) is a prefactor characterizing the effective strength of the random pinning force.

In addition, we have also found that the correlation length $\xi_{//}$ along the interface increases very slowly with the time. When it reaches the system size N the whole interface becomes correlated and the interface asymptotically behaves like the one in a one-dimensional system, but as long as the system size is larger than $\xi_{//}$ the thermal creep wins over the pinning force. Thus for the system studied here the limits $N \to \infty$ and $t \to \infty$ do not commute.

[1] D. E. Temkin, Sov. Phys. Crystallogr., **19**, 291 (1974).
[2] Y. Saito, N. Tanabe and D. Temkin, Phys. Rev. E**48**, 2028 (1993).
[3] X. Feng, E. A. Brener, D. E. Temkin, Y. Saito and H. Müller-Krumbhaar, will appear in the Phys. Rev. E**59**, 1999.

Surface Instabilities in Cracks

Efim A. Brener and V.I. Marchenko
Theorie III

The surface of a propagating crack is shown to be morphologically unstable because of the non-hydrostatic stresses near the surface (Asaro-Tiller-Grinfeld instability). We find that the energy of a wavy crack becomes smaller than the energy of a straight crack if the crack length is a few times larger than the Griffith length. The local dispersion relation is derived assuming that the instability develops via mass transport by surface diffusion.

The uniform motion of a straight crack is well understood [1]. Experiments on the fracture of bulk specimens, however, show that the crack surfaces are often rough [2]. Some of these results are interpreted in the framework of models of cracks propagating in heterogeneous media. The other possibility for the roughening of the crack surfaces is the instability of the straight motion of the crack tip. Recent experiments on the fracture of thin plates [3] clearly established that many puzzling phenomena in brittle fracture dynamics are related to an oscillatory instability at velocities appreciably below the Rayleigh speed V_R.

There were several attempts in literature to investigate the stability of the propagating cracks. The linear stability analysis of the quasistatic crack has been performed by Cotterell and Rice [4] with subsequent refinement by Adda-Bedia and Ben Amar [5]. They found that the straight motion of the crack becomes unstable if the tangential loading exceeds a critical value.

In these descriptions, a crack surface is viewed as the trace left behind by the crack tip as it traverses the sample. All modes related to the further surface deformations due to a transfer of matter are assumed to be frozen. The main purpose of this report is to describe the instabilities of the crack surface related to these so far missing degrees of freedom. We will find that the surfaces of a propagating crack undergo an Asaro-Tiller-Grinfeld (ATG) instability [6,7] of purely macroscopic origin.

Asaro and Tiller [6] and later Grinfeld [7] brought out the idea that the surface of a solid which is subject to a uniaxial stress (i.e., when $\sigma_0 = \sigma_{xx} - \sigma_{yy} \neq 0$) is morphologically unstable. This instability has an elastic origin: a corrugated surface leads to a lower elastic energy than a flat one. Note that the instability implies a transfer of matter, either from a liquid phase or through surface diffusion. The interface displacement is due to redistribution of material, not due to elastic strain. Surface energy prevents short-scale deformations. The chemical potential of such a solid near the surface can be written as [8,9]

$$\mu_s = v_s[f_{s0} + \frac{1-\nu^2}{2E}(\sigma_{\tau\tau} - \sigma_{nn})^2 + \alpha K]. \tag{1}$$

Here v_s is the atomic volume of the solid phase; f_{s0} is the free energy density for a hydrostatic situation; α is the surface energy; K is the curvature of the interface (counted positive for a convex solid); σ_{ik} is the stress tensor; n and τ are subscripts referring to the normal and the tangent to the interface; ν and E are the Poisson and Young coefficients. For a small perturbation of the interface ($y(x,t) = Y_k \exp[ikx + \omega t]$), the shape dependent part of the chemical potential is [7]

$$\mu_s = v_s \left[\frac{2(1-\nu^2)\sigma_0^2}{E}|k| - \alpha k^2 \right] y(x,t). \tag{2}$$

If the surface is the interface between the solid and vacuum, the instability develops via surface diffusion; the normal velocity is proportional to the Laplacian of the chemical potential of the solid phase. This leads to the following dispersion relation

$$\omega = Dk^2 \left[\frac{2\sigma_0^2(1-\nu^2)}{\alpha E}|k| - k^2 \right] \tag{3}$$

where D is proportional to the surface diffusivity. Here elasticity plays a destabilizing role and $|k|$ reflects its nonlocal properties.

Let us discuss a two-dimensional crack subject to mode I (opening-mode) loading at infinity perpendicular to the crack: $\sigma_{yy}^\infty = P$. This crack is stable in the sense of [4,5]. However, the surface of the crack behind the moving tip becomes unstable. The crucial observation is that at the crack surface $\sigma_{nn} = 0$ but $\sigma_{\tau\tau}$ is not! Thus, we can expect the development of the ATG instability (we note that hydrostatic loading is not favorable for the ATG instability). However, the application of this theory to the surface of the crack requires some comments and modifications. We are not in a homogeneous situation due to the presence of the finite crack. The stress field is singular and should be found from the solution of the corresponding crack problem.

Due to the presence of the singular stress field there is an additional stabilizing elastic contribution to the chemical potential, Eq.(2), which leads the modified ATG spectrum [10]

$$\omega = Dk^2 \left[\frac{2P^2(1-\nu^2)}{\alpha E} \left(|k| - \frac{L^2}{(L^2 - x^2)^{3/2}} \right) - k^2 \right]. \tag{4}$$

This local dispersion relation is valid for relatively short-scale deformations, $kr \gg 1$, where $r = (L - x)$ is the distance from the tip.

The instability occurs at distances $r > r_0 \sim L_G(L/L_G)^{1/3}$ and at $k_c \sim 1/L_G$. Here we have introduced the so-called Griffith length

$$L_G = \frac{2E\alpha}{\pi(1 - \nu^2)P^2}.$$ (5)

In order to find the critical length of the straight crack at which the crack undergoes the ATG instability we must go beyond the local approximation which has been used so far. We have to calculate the change of the energy up to the second order with respect to the perturbation of the centerline $y(x)$ and to find the critical length when this energy change becomes negative for the first time.

The total energy U is a complicated functional of the perturbation $y(x)$ and depends also on the length of the crack. The optimal perturbation corresponds to the minimum of this functional and the threshold of the instability corresponds to the condition $U_{min} = 0$.

In order to estimate the critical length we use the variational procedure with a simple representation of the perturbation, $y(x) = Y_k(\cos kx - \cos kL)$ and find [10]

$$U = \frac{\pi P^2(1 - \nu^2)}{E}(kL)^2 F(kL)Y_k^2$$ (6)

where the function $F(z)$ can be expressed in terms of Bessel functions J_m

$$F(z) = (L_G/2L)[1 - \sin 2z/2z] - [J_0^2(z) + J_1^2(z)]$$

$$+2[J_1(2z) - 2J_1(z)\cos z + J_0(z)J_1(z)]/z.$$ (7)

A straight crack is stable if $U > 0$. This is always the case for small L. The bifurcation threshold corresponds to $U = 0$ and $dU/dk = 0$, see Fig.1. Thus, the straight crack becomes unstable at $L_c \approx 6L_G$ and $k_c L_G \approx 0.7$ where L_G is the Griffith length.

In the case of the fast tip motion we can expect that the described instability should be only convective in the frame of reference of the moving tip due to its slow development [10]. However, the drastic acceleration of the instability and the refining of the length scale in the nonlinear regime make still conceivable that eventually the tip motion itself could be affected by the instability. The pattern which develops on the surface of the main crack in the recent experiments on the microbranching instability [3] superficially looks similar to the pattern predicted by the nonlinear ATG instability. However, the direct relevance of our results to these experiments is problematic because of the slow surface diffusion process compared to the fast tip motion.

The described instability has a purely macroscopic origin (compared to the microscopic tip instability predicted in [11]) and it does not depend on details of the cohesive

or plastic zone. As it follows from our analysis the instability should be more efficient in the case of slow cracks.
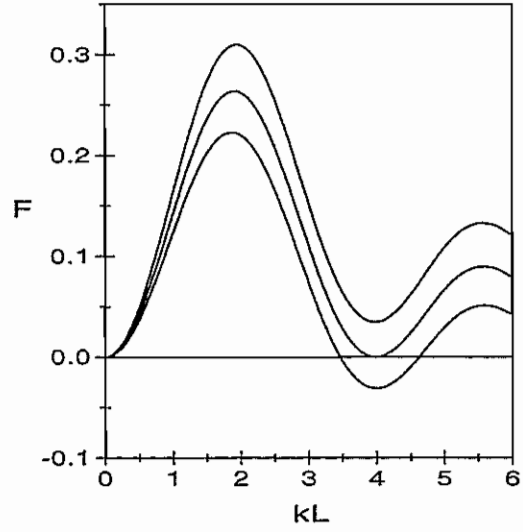

FIG. 1. The reduced energy F versus kL for three different values of the length of the crack; from the bottom to the top $L = 10L_G$, $L = 5.85L_G$, $L = 4L_G$. The crack goes unstable near $kL = 4$ where $F < 0$.

[1] L.B. Freund, *Dynamic Fracture Mechanics* (Cambridge University Press, New York, 1990).

[2] E. Bouchaud, J. Phys. Condense. Matter **9**, 4319 (1997); P. Daguier, B. Nghiem, E. Bouchaud, and F. Creuzet, Phys. Rev. Lett. **78**, 1062 (1997); S. Ramanathan, D. Ertas, and D.S. Fisher, Phys. Rev. Lett. **79**, 873 (1997); S. Ramanathan and D.S. Fisher, Phys. Rev. Lett. **79**, 877 (1997), and references therein.

[3] J. Fineberg, S.P. Gross, M. Marder, and H.L. Swinney, Phys. Rev. Lett. **67**, 457 (1991); Phys. Rev. B **45**, 5146 (1992); S.P. Gross, J. Fineberg, M. Marder, W.D. McCormick, and H. Swinney, Phys. Rev. Lett. **71**, 3162 (1993).

[4] B. Cotterell and J.R. Rice, Int. J. Fract. **16**, 155 (1980).

[5] M. Adda-Bedia and M. Ben Amar, Phys. Rev. Lett. **76**, 1497 (1996).

[6] R.J. Asaro and W.A. Tiller, Metall. Trans **3**, 1789 (1972).

[7] M.A. Grinfeld, Dokl. Akad. Nauk. SSSR **290**, 1358 (1986) [Sov. Phys. Dokl. **31**, 831 (1986)].

[8] C. Herring, J. Appl. Phys. **21**, 437 (1950).

[9] P. Noziéres, J. Phys. I **3**, 681 (1993).

[10] E.A. Brener and V.I. Marchenko, Phys. Rev. Lett. **81**, 5141 (1998).

[11] E.S.C. Ching, J.S. Langer, and H. Nakanishi, Phys. Rev. E **53**, 2864 (1996).

Institute for Scattering Methods

Modern solid state physics goes far beyond a phenomenological description and bases the understanding of solid state properties and phenomena on atomistic theories. To obtain information about the atomic structure of solids, probes with sub-nanometer spatial resolution are needed. To study the excitation spectra, an appropriate energy resolution is necessary in addition. All these requirements can be met by scattering methods. In this sense, scattering methods provide the basis of our present understanding of the structure, excitations and phase transitions of condensed matter on a microscopic level.

At the Institute for Scattering Methods (ISM), synchrotron x-ray scattering and neutron scattering are employed for the investigation of condensed matter on an atomistic microscopic level. The emphasis lies on exploiting fully the complementarity of the two probes. Besides the application of scattering methods to solid state problems, major activities are concentrated on the methodology. This includes the further development of experimental techniques by improving instrument components and data treatment algorithms, the development of new experimental methods and the corresponding instruments and the development, construction and operation of scattering instruments at large-scale facilities. At present, ISM operates five instruments at the research reactor DIDO of the Research Center Jülich and two instruments at the Hamburger Synchrotronstrahlungslabor HASYLAB. These instruments are open for the use by external groups from universities, research centers and industry. The instrument responsibles from ISM provide scientific and technical support during the experiment and the data processing. ISM is open for all research areas in condensed matter science, where scattering methods can be applied. At present, the research activities are concentrated in three fields: solid state magnetism, structural disorder in alloys, quasi-crystals and high T_c superconductors and electrocatalytic processes. For the purpose of this research, ISM is also engaged in sample preparation (e.g. by molecular beam epitaxy) and characterisation (e.g. AC and DC susceptibility and magnetisation measurements).

In the field of instrument development, the main activities in 1998 were:

1. Design and construction of a high energy side station at an undulator line of the Advanced Photon Source (APS) at Argonne National Laboratory, USA. This work is done in close collaboration with the Midwest Universities Collaborative Access Team (μCAT) at APS.
2. Development of a nuclear spin polarised ^{3}He-filter for the purpose of neutron polarisation analysis. In 1998, the activities were focussed on the design of the ^{3}He polarisation station.
3. Design and construction of a new type of small-angle scattering instrument, which employs focussing mirror optics.
4. Equipment of the diffuse neutron scattering machine DNS at the DIDO-reactor with supermirrors for neutron polarisation analysis. A progress report on this project can be found in the following pages.
5. Optimisation of the reflectometer HADAS at the DIDO-reactor for experiments on small magnetic thin-film samples and studies for the implementation of a polarisation analysis option.
6. Development of optimised target and moderators for the European Spallation Neutron Source.

Method development was done for high energy magnetic x-ray scattering in the energy range above 100 keV, for resonant exchange scattering from ferro- and antiferromagnets for inelastic x-ray scattering, anomalous small-angle x-ray scattering, characterisation of thin-film devices by means of combined neutron-, x-ray reflectivity- and diffuse scattering measurements and neutron polarisation analysis.

In the field of solid state magnetism, we addressed the following topics:

1. Determination of the frustration mechanism in disordered system with competing interaction by determining elementspecific spin pair correlations.
2. Investigation of the critical behaviour at magnetic phase transitions for frustrated and disordered systems and systems with higher order exchange interactions.
3. Investigation of the effect of fourth order exchange interaction on magnetic structure, phase transitions and low temperature magnetisation.
4. Optimisation of the growth conditions for magnetic multilayer systems by determining the interface morphologies with combined neutron and x-ray scattering experiments.

Examples for the work done at ISM this year are given by the progress reports on the following pages.

Thomas Brückel

Institute for Scattering Methods: General Overview

Modern solid state physics goes far beyond a phenomenological description and bases the understanding of solid state properties and phenomena on atomistic theories. To obtain information about the atomic structure of solids, probes with sub-nanometer spatial resolution are needed. To study the excitation spectra, an appropriate energy resolution is necessary in addition. All these requirements can be met by scattering methods. In this sense, scattering methods provide the basis of our present understanding of the structure, excitations and phase transitions of condensed matter on a microscopic level.

At the Institute for Scattering Methods (ISM), synchrotron x-ray scattering and neutron scattering are employed for the investigation of condensed matter on an atomistic microscopic level. The emphasis lies on exploiting fully the complementarity of the two probes. Besides the application of scattering methods to solid state problems, major activities are concentrated on the methodology. This includes the further development of experimental techniques by improving instrument components and data treatment algorithms, the development of new experimental methods and the corresponding instruments and the development, construction and operation of scattering instruments at large-scale facilities. At present, ISM operates five instruments at the research reactor DIDO of the Research Center Jülich and two instruments at the Hamburger Synchrotronstrahlungslabor HASYLAB. These instruments are open for the use by external groups from universities, research centers and industry. The instrument responsibles from ISM provide scientific and technical support during the experiment and the data processing. ISM is open for all research areas in condensed matter science, where scattering methods can be applied. At present, the research activities are concentrated in three fields: solid state magnetism, structural disorder in alloys, quasi-crystals and high T_c superconductors and electrocatalytic processes. For the purpose of this research, ISM is also engaged in sample preparation (e.g. by molecular beam epitaxy) and characterisation (e.g. AC and DC susceptibility and magnetisation measurements).

In the field of instrument development, the main activities in 1998 were:

1. Design and construction of a high energy side station at an undulator line of the Advanced Photon Source (APS) at Argonne National Laboratory, USA. This work is done in close collaboration with the Midwest Universities Collaborative Access Team (µCAT) at APS.
2. Development of a nuclear spin polarised ^{3}He-filter for the purpose of neutron polarisation analysis. In 1998, the activities were focussed on the design of the ^{3}He polarisation station.
3. Design and construction of a new type of small-angle scattering instrument, which employs focussing mirror optics.
4. Equipment of the diffuse neutron scattering machine DNS at the DIDO-reactor with supermirrors for neutron polarisation analysis. A progress report on this project can be found in the following pages.
5. Optimisation of the reflectometer HADAS at the DIDO-reactor for experiments on small magnetic thin-film samples and studies for the implementation of a polarisation analysis option.
6. Development of optimised target and moderators for the European Spallation Neutron Source.

Method development was done for high energy magnetic x-ray scattering in the energy range above 100 keV, for resonant exchange scattering from ferro- and antiferromagnets for inelastic x-ray scattering, anomalous small-angle x-ray scattering, characterisation of thin-film devices by means of combined neutron-, x-ray reflectivity- and diffuse scattering measurements and neutron polarisation analysis.

In the field of solid state magnetism, we addressed the following topics:

1. Determination of the frustration mechanism in disordered system with competing interaction by determining elementspecific spin pair correlations.
2. Investigation of the critical behaviour at magnetic phase transitions for frustrated and disordered systems and systems with higher order exchange interactions.
3. Investigation of the effect of fourth order exchange interaction on magnetic structure, phase transitions and low temperature magnetisation.
4. Optimisation of the growth conditions for magnetic multilayer systems by determining the interface morphologies with combined neutron and x-ray scattering experiments.

Examples for the work done at ISM this year are given by the progress reports on the following pages.

Thomas Brückel

Scientists

Dr. Berthold Alefeld	Development of neutron scattering methods; instrument responsible for lattice parameter instrument LAP; construction and development of the small angle scattering machine KWS III
Prof. Dr. Thomas Brückel	Institute director; neutron and synchrotron x-ray scattering; magnetism
Dr. Harald Conrad	European Spallation Source ESS project: target and moderators
Dr. Günther Goerigk - HASYLAB, Hamburg -	Material research with anomalous x-ray small angle scattering; instrument responsible for Juelich's user-dedicated small-angle scattering facility JUSIFA
Dr. Heinz-Günter Haubold	Anomalous small angle x-ray scattering ASAXS and x-ray absorption spectroscopy from highly dispersive systems; in-situ studies of catalysed electro-chemical processes
Dr. Ulrich Köbler	Magnetisation and neutron diffraction studies of materials with fourth-order exchange interactions
Dr. Achim Kollmar - deceased 09.03.1998 -	Development and operation of the spin echo spectrometer IN 15 at ILL
Dr. Albert Metz - HMI, Berlin, until 30.9.98 -	Heavy fermion systems
Dr. Robert Mueller	Development of the ^{3}He filter for neutron polarisation analysis
Dr. Werner Schweika	Diffuse neutron scattering for the investigation of short-range order in alloys, oxides, perovskites and quasi-crystals; instrument responsible for the diffuse neutron scattering instrument DNS

Guest Scientists

Dipl.-Phys. Carla Byloos	Shock waves in the ESS spallation target
Dr. Emmanuel Kentzinger	Neutron and synchrotron x-ray scattering from magnetic thin film materials
Dr. Thomas Zeiske - since 16.09.1998 -	Instrument responsible of the triple axis spectrometer SV 4; SV 4 upgrade and polarisation analysis option

Post-Doctorates

Dr. Wolfgang Caliebe

- HASYLAB, Hamburg -

Magnetic x-ray scattering and x-ray spectroscopy; instrument responsible of the Wiggler beamline W1

Dr. Klaus-Dieter Göcking

- until 30.09.1998 -

Development of neutron optical techniques for the small angle scattering machine KWS III

Dr. Thomas Reif

- since 01.09.1998 -

Second instrument responsible for SV 4; magnetic x-ray and neutron scattering

Dr. Ulrich Rücker

- since 01.02.1998 -

Instrument responsible for the neutron reflectometer HADAS; preparation and characterisation of magnetic thin film systems

Dr. Thomas Vad

- since 01.09.1998 -

Further development of the instrument control and data treatment programs for Juelich's user-dedicated small-angle scattering facility (JUSIFA); ASAXS measurements

Engineers and Technicians

Wolfgang Bergs

- since 15.06.1998 -

Reflectometer HADAS

Arnold Broch

Diffuse neutron scattering instrument DNS

Ludwig Dohmen

Project engineer for the small angle scattering instrument KWS III

Udo Engelbrecht

- until 30.04.1998 -

General purpose cold neutron beam EKN

Dipl.-Ing. Peter Hiller

Project engineer for the μCAT-collaboration at the Advanced Photon Source APS; x-ray small angle scattering

Christel Horriar-Esser

Ultra low-temperature magnetometry and ^{3}He filter project

Markus Hülsbeck

- 17.06.1998 - 31.12.1998 -

Small angle scattering instrument KWS III

Bernd Huy

- until 07.05.1998 -

Triple axis spectrometer SV 4

Heinrich Jungbluth

Software development for x-ray small angle scattering

Dipl.-Ing. Günther Kluck

Project engineer for the polarised thermal neutron scattering instrument

Barbara Köppchen

Secretary

Karl Kutzbach	Neutron reflectometer
Bodo Olefs	Magnetometry
Jens Rademacher	Trainee

- since 09.1998 -

| Berthold Schmitz | Triple axis spectrometer SV 4 |

- since 01.04.1998 -

| Fred Werges | Cryotechniques and molecular beam epitaxy |
| Elmar Westphal | Software development for x-ray small angle scattering |

- 01.09.1998 - 31.12.1998 -

-

PhD Thesis Student

| Dipl.-Phys. Eberhard Kümmerle | Structural investigations on proton conductors |

- until 30.09.1998 -

-

Diploma Thesis Student

| Ralf Goldstein | Spin lattice relaxation with β-NMR |

- Univ. Hannover, since 10.08.1998 -

Resonant Inelastic X-Ray Scattering of EuO, EuS, and $Eu_3Fe_5O_{12}$

Wolfgang A. Caliebe

Institut für Streumethoden

We measured resonant inelastic-scattering spectra of EuO, EuS, and $Eu_3Fe_5O_{12}$ at the Eu L_{III}-edge by monitoring the Eu $L\alpha_1$ emission. The data are compared with XMCD-data, and interpreted within a multi-electron picture. The data of EuO and EuS show a clear splitting of two transitions in the white line of $\approx 4\,eV$ and $2\,eV$, respectively. This corresponds to the splitting of the 5d-states into the t_{2g}- and e_g-orbitals due to the crystal field. The $Eu_3Fe_5O_{12}$-data show a clear separation of 2 transitions in the pre-edge region $5\,eV$ below the edge. These transitions are interpreted as transitions into 4f-orbitals. Furthermore, a splitting of $\approx 4\,eV$ of two transitions in the white line is observed, which is associated to the crystal field splitting of the 5d-orbitals in a non-cubic environment into the a_1-, a_2-, and a_3-orbitals, of which the a_1 and a_2 cannot be resolved.

For the study of magnetism in rare earth compounds, the role of the valence electrons, especially the coupling to the 4f electrons, is of great interest. In Eu compounds, the half-filled 4f-shell with a large spin and no orbital momentum gives rise to interesting features, e.g. the dependence of magnetism in the cubic compounds of chalcogenides with Eu^{+2} on the lattice constant: EuO and EuS are ferromagnetic, but EuTe with a larger lattice constant is anti-ferromagnetic. This may be related to the interactions of the 4f-electrons either due to the 4f-5d-4f coupling between two Eu^{+2}-ions, or due to the superexchange via the chalcogenide ion. Standard spectroscopic tools like near-edge absorption spectroscopy and x-ray magnetic circular dichroism (XMCD) at the L-edges lack the resolution due to the short life time of the 2p core-hole, and at the M-edges, the surface sensitivity can influence the results. These experimental difficulties are easily overcome by using 2p3d-resonant inelastic x-ray scattering (RIXS) at the L-edges. In 2p3d-RIXS, the incident energy is tuned to an L-absorption edge, and photons with an energy close to the L-fluorescence are detected. The final state corresponds to an M-absorption edge because of the hole in the 3d state. The longer life time of the 3d hole now gives a better intrinsic resolution, while the higher energies of the incident and scattered photons probe the bulk instead of the surface.

We used RIXS to investigate EuO, EuS, and $Eu_3Fe_5O_{12}$. All three samples were previously studied with XANES and XMCD at the $L_{II,III}$ (see fig.1) and $M_{IV,V}$ edges [1]. The results, however, left some open questions, concerning the origin of some spectroscopic features and the splitting of the 5d-band: (1) The splitting of the 5d-states in EuO and EuS, and wheather any quadrupolar transitions are involved. (2) The search for quadrupolar transitions in the cubic compounds EuO and EuS. (3) The nature of the pre-edge features in the L_{III} edge in $Eu_3Fe_5O_{12}$, i.e. transitions into empty 4f states, or transitions into hybridized 4f-5f states.

The experiments were performed at the inelastic x-ray scattering beamline X21 at the NSLS at Brookhaven National Laboratory in Upton, NY, USA. The energy resolution of the monochromator is 0.2 eV over an energy range from 6 to 10 keV. The monochromatic beam is focused onto the sample into a spot with a size of $500 \times 300\,\mu m^2$. The inelastically scattered x-rays are energy analyzed with a high resolution backscattering crystal spectrometer. The crystal is spherically bent in order to cover a larger solid angle. Sample, crystal and detector are on a Rowland circle. The resolution of the spectrometer depends on the Bragg angle, and improves with increasing angle. It is limited by the contribution of the source size and the intrinsic reflection width. In this experiment, the energy resolution was approximately 0.8 eV at the Eu $L\alpha$ fluorescence line with the Ge(333)-reflection at $\Theta=76.75°$. The experimental set-up is described in detail in [2].
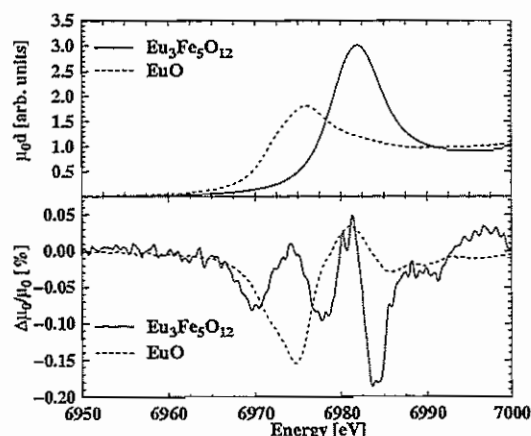

FIG. 1. Absorption edge (upper panel) and XMCD-spectra (lower panel) at the L_{III} edge of Eu in EuO and $Eu_3Fe_5O_{12}$. The difference of the energy of the edge is directly related to the oxidation state (2+ and 3+, respectively). The XMCD-spectra differ significantly in the pre-edge region: In $Eu_3Fe_5O_{12}$, two additional negative features at 6970 eV and 6980 eV appear. In EuO no structure is observed in the pre-edge region. The corresponding data of EuS are similar to the one of EuO.

In order to study the t_{2g}-e_g-splitting of the 5d-band of Eu in EuO and EuS, we tuned the incident energy through the white line and measured with high energy resolution a satellite in the Eu $L\alpha$ emission line. Due to the longer life time of the 3d-hole, we are able to resolve a structure in the white line. A small splitting of 4 eV (EuO) and 2 eV (EuS) is observed in a satellite of the emission line (see fig.2).
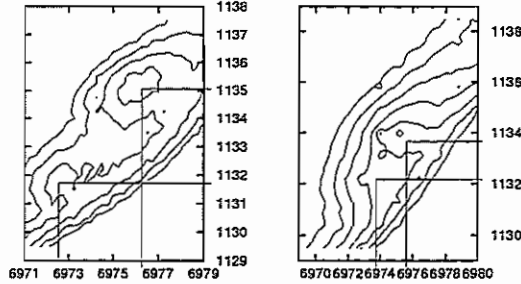

FIG. 2. Contour plots of the intensity distribution with the incident energy around the white line and the energy of the scattered photons at a satellite in the $L\alpha$ fluorescence for EuO (left) and EuS (right). The data are plotted as a function of incident energy and energy transfer. The peak for EuO splits into two with a separation of 4 eV, and the separation for EuS is 2 eV. The lines mark the positions of the transitions.

As the white lines of the Eu L_{III}-edges in EuO and EuS split into two lines with approximately equal strength and a separation of 4 and 2 eV, respectively, we conclude that the structure in the XMCD-spectra is due to dipole transitions into the 5d-band, and that transitions into the half filled 4f-orbitals do not occur. The energy separation decreases with the chalkogenide from O to Te, which was already studied with XPS by Eastman et al. [3]. If there were an excitation into an empty 4f-orbital, we would expect a larger separation of the peaks in the energy transfer direction, and a ratio of at least 1:100 between the quadrupolar and dipolar transition, which should be visible. We also looked at lower incident energies for further transitions as we would expect any existing quadrupolar transition into an empty 4f orbital at about 6 eV lower energy due to the coupling with the core hole [3], but we did not observe any significant structure although any transition with a strength of 1:250 of the dipolar transition would have resulted into a significant feature.

In order to study the transitions in the pre-edge region of the Eu L_{III}-edge in $Eu_3Fe_5O_{12}$, just a few emission scans at selected energies were measured because the intensity of the emission was lower. This is a direct result of the higher absorption of the sample due to the iron, and the lower absorption of Eu in the pre-edge region. The result of a few selected scans is shown in fig.3: When the incident energy is tuned to the pre-edge region at E_i=6970 eV and 6975 eV, two small additional peaks are observed at energy transfers 1124.6 eV and 1126.6 eV, respectively. By scanning the energy of the incident and scattered photons together with a constant energy trans-

fer at the corresponding energy transfers, just two resonances at E_i=6970 eV and 6975 eV were observed. For the higher incident energy, a small contribution of the first transition is still detected as a small shoulder on the low-energy transfer side of the peak. By increasing the energy of the incident photon, these structures disappear, and the line-shape of the emission line narrows.
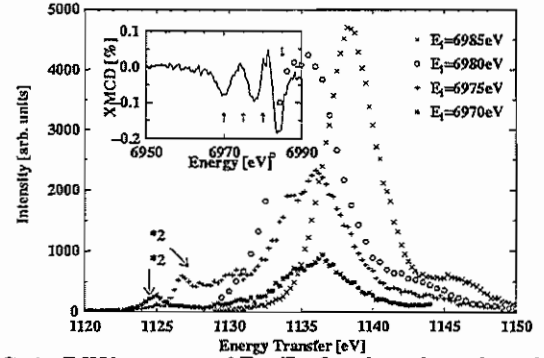

FIG. 3. RIXS spectra of $Eu_3Fe_5O_{12}$ for a few selected incident energies. For comparison, the energies are marked with arrows in the XMCD-data in the inset. The RIXS-spectra for the two lowest incident energies (E_i=6970 eV and 6975 eV) were multiplied with 2 to have similar scales. Two additional peaks are observed at ΔE=1124.6 eV and 1126.6 eV, respectively. With increasing energy, the line shape of the main emission line at ΔE=1136 eV changes, and shifts linearly with the incident energy for energies above the absorption edge as expected.

The two additional peaks at 10 eV below the main emission line are associated with transitions into empty 4f orbitals. Their strength compared with the dipol transition into the white line is about 1:30, which is quite strong for a quadrupolar transition. The local environment of Eu in $Eu_3Fe_5O_{12}$, however, is not cubic, so that the 4f orbitals hybridize with 5d orbitals. Therefore, the transition into the 4f orbitals is not of purely quadrupolar nature, which explains the high intensity.

The change in line shape of the main emission line is explained with a splitting of the 5d orbitals into three bands (a_1, a_2, and a_3), of which the transitions into the a_1 and a_2 bands, which cannot be separated, have about equal intensity as the a_3 band which is separated by ≈ 2 eV.

This combination of different spectroscopic measurements – XMCD and RIXS – yields more information than one of the measurements alone. A detailed data analysis is in progress.

[1] K. Attenkofer, thesis, Universität Würzburg (1999)

[2] W.A. Caliebe, thesis, Christian-Albrechts-Universität, Kiel (1997)

[3] D.E. Eastman, F. Holtzberg, S. Methfessel, Phys. Rev. Lett. **23**, 226 (1969)

Nanostructrual Characterization of Hydrogen Diluted a-SiGe:H Alloys by Anomalous Small-Angle X-ray Scattering Studies

G. Goerigk

Institut für Streumethoden

The nanostructure of hydrogenated amorphous silicon germanium alloys, a-$Si_{1-x}Ge_x$:H, prepared by different plasma enhanced chemical vapor deposition techniques was analyzed by anomalous small-angle X-ray scattering (ASAXS) experiments. The Ge component was found to be inhomogeneous distributed with correlation lengths between 1.0 and 1.24 nm. From the analysis of extended ASAXS measurements from samples prepared under high hydrogen dilution the volume fractions and the densities of the Ge-rich phases are estimated.

F&E-Nr: 23.89.1

Hydrogenated amorphous silicon germanium alloys, a-$Si_{1-x}Ge_x$:H, play an important role in amorphous silicon-based solar cell technology. The Ge is added to produce lower bandgap material to absorb the longer wavelength photons of the solar spectrum and to achieve higher efficiencies. However, Ge alloying invariably results in degraded opto-electronic properties compared with the base a-Si:H material [1,2]. The extent to which this behavior is intrinsic (atomic scale potential fluctuations, intrinsic defects, preferential H bonding) or extrinsic (non-optimized deposition conditions, poor nanostructure) to the alloy is not established. The nanostructure of thin films prepared by different plasma enhanced chemical vapor deposition (PECVD) techniques can be well characterized by small-angle X-ray scattering [3-6]. Especially when using synchrotron radiation and applying the well-established technique of anomalous small-angle X-ray scattering (ASAXS), the Ge-related nanostructure of the alloy can be determined. The ASAXS-technique is used in order to separate the scattering due specifically to Ge composition fluctuations other than those associated with voids or surface roughness. The Ge-related nanostructure of the films can be correlated with the opto-electronic properties of the materials [7].

Different alloys obtained from different deposition techniques at United Solar Systems Corporation (USSC) and at the Indian Association for the Cultivation of Sciences (IACS) have been examined. The ASAXS measurements were carried out at the JUSIFA beamline at HASYLAB, DESY Hamburg.

Figure 1(a) shows scattering curves of two samples prepared by two different deposition techniques (MW = microwave and RF = radio frequency deposition) obtained at energy E_1. The curves of Figure 1(b) correspond to the separated scattering obtained from the difference of the normalized scattering curves measured at E_1 =11.1 and E_2 =10.725 keV. Thus, these films clearly reveal a significant contribution from non-uniformly distributed Ge in the amorphous matrix. The solid lines passing through the separated scattering curves are fitted model functions according to the q-dependence described by Eq.1 and an additional q^{-4}-term describing some type of large inhomogenities.

$$\Delta\frac{d\sigma}{d\Omega}(q,E_{1,2}) = b\cdot\frac{a^3}{(1+a^2q^2)^2} + \frac{c}{q^4} \qquad (1)$$

The first term of the fitted model function represents an early correlation model proposed by Debye et al. [8] to allow interpretation of SAXS caused by inhomogeneities of random shape and size. From the fits correlation lengths of a=1.0 nm and 1.24 nm were obtained for the MW-sample and the RF-sample, respectively.
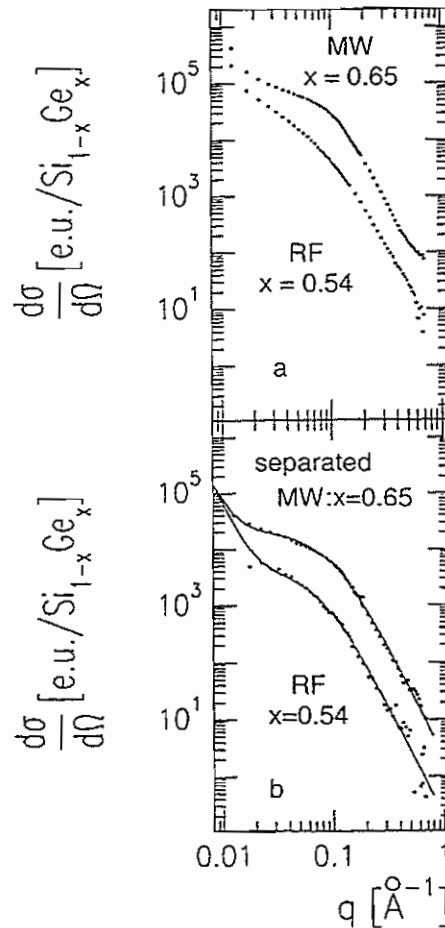

Figure 1a: Scattering curves of MW- (x=0.65) and RF-sample (x=0.54) at energy E_1. From the SAXS measurements at two different energies E_1 and E_2 the separated scattering of Ge was obtained (Fig.1b).

Especially RF-samples prepared under high hydrogen dilution have attracted attention. From a study of films prepared at the IACS, a reduced Ge nanostructural heterogeneity was found for this deposition technique, which correlated with improved opto-electronic behavior /7/. From earlier comparisons with films prepared under high hydrogen dilution at USSC, strong differences were found, because the USSC films seemed to reveal stronger nanostructural heterogeneities. Additional tests were made to search for possible microcrystallinity in the high dilution samples, but no evidence for microcrystallinity was found /4/. For explanation of the differences in the properties of the materials resulting from the different preparation techniques, additional information is required concerning the properties of the Ge-rich phase such as the volume fraction, the density and the concentration of Ge. Information is obtained for instance from flotation density measurements and the results were attributed to a combination of different influences like voids, H-alloying or density reduction due to the amorphous state /4/.

Additionally information can be obtained from extended ASAXS measurements using more than two energies. As can be seen from Eq.2, the factor b from Debye's correlation model is related to the volume fraction Φ of the Ge-rich phase and the contrast $\Delta\rho$ of the two

$$\Delta\frac{d\sigma}{d\Omega}(q,E_{1,2}) =$$

$$8\pi\frac{\Phi(1-\Phi)}{n}\left(\frac{\Delta\rho^2(E_1)}{|\bar{f}(E_1)|^2} - \frac{\Delta\rho^2(E_2)}{|\bar{f}(E_2)|^2}\right)\frac{a^3}{(1+a^2q^2)^2} \qquad (2)$$

phases α and β, which contain the average atomic densities n_α, n_β, the chemical concentrations x_α, x_β and $f_\alpha(E)$ and $f_\beta(E)$, the appropriate scattering factors for the two phases composed of the atomic scattering factors of Ge and Si (Eq.3):

$$\Delta\rho^2(E) = \left|n_\alpha f_\alpha(E) - n_\beta f_\beta(E)\right|^2$$

$$f_\alpha(E) = (1-x_\alpha)f_{Si}(E) + x_\alpha f_{Ge}(E) \qquad (3)$$

$$f_\beta(E) = (1-x_\beta)f_{Si}(E) + x_\beta f_{Ge}(E)$$

A linear approximation /9/ can be applied to Eqs.2,3, which relates a modified difference of the anomalous dispersion corrections $\Delta F'(E_1,E_2)$ to the difference of the separated scattering $\Delta d\sigma/d\Omega(q=0)$ at E_1 and E_2 extrapolated to q=0. In order to obtain the information from the linear approximation, the ASAXS measurements must be extended to more than two energies. Extended ASAXS measurements with four different energies (10.719, 11.051, 11.083 and 11.095 keV) from two alloys (x=0.47, 0.57), deposited under RF conditions with additionally applied hydrogen dilution were performed. From the four energies six different separated scattering curves with the scattering extrapolated to q=0 according to Eq.1 were obtained. Figure 2 summarizes the result of the linear approximation. The slopes and the intersections with the y-axis of the straight lines are related to

the volume fractions Φ, the average atomic densities n_α and the Ge-concentrations x_α of the Ge-rich phase. For instance assuming a high Ge-concentration of nearly 100% in the Ge-rich phase yields volume fractions of about 31% and 43% for x=0.47 and x=0.57, respectively. Slightly smaller values of about 90% for the average atomic densities are calculated for the Ge-rich phase with respect to the average densities of the samples.
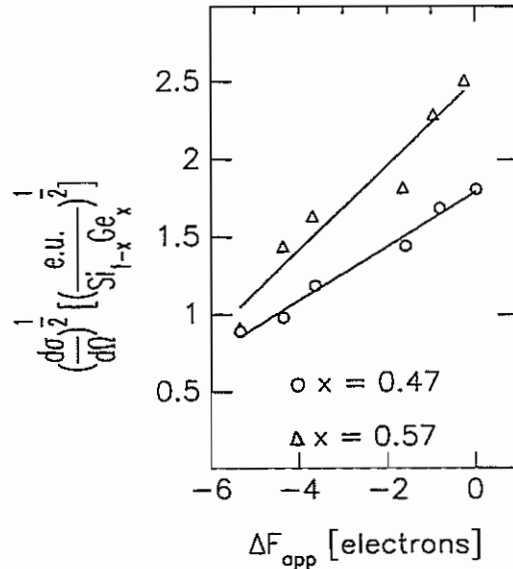

Figure 2: The slopes and the intersections with the y-axis of the linear approximations are related to the volume fractions, the average atomic densities and the concentrations of the Ge-rich phase.

/1/ W. Paul, J.H. Chen, E.Z.Liu, A.E. Wetzel, and P. Wickboldt, J. Non-Cryst. Solids 164-166, 1 (1993)
/2/ W. Paul, R.A. Street, and S. Wagner, J. Electronic Mats. 22, 39 (1993)
/3/ S.J. Jones, Y. Chen, D.L. Williamson, R. Zedlitz, and G. Bauer, Appl. Phys. Lett. 62, 3267 (1993)
/4/ D.L.Williamson, Mat. Res. Soc. Symp. Proc. 377, 251 (1995)
/5/ A.R. Middya, S. Ray, S.J. Jones, and D.L. Williamson, J. Appl. Phys. 78, 4966 (1995)
/6/ P. Wickboldt, D. Pang, W. Paul, J.H. Chen, F. Zhong, C-C. Chen, J.D. Cohen, and D.L. Williamson, J. Appl. Phys. 81, 6252 (1997)
/7/ G.Goerigk, and D.L.Williamson, Sol.Stat.Com.,Vol. 108, No. 7, pp.419-424 (1998)
/8/ P. Debye, H.R. Anderson, and H. Brumberger, Jou. Appl. Phys. 28, 679 (1957)
/9/ G.Goerigk, H.-G.Haubold, C.Klingshirn, and A.Uhrig, J. Appl. Cryst. (1994). 27, 907-911

Competing magnetic interactions in Gadolinium-Europium-Sulfide mixed crystals

D. Hupfeld, W.A. Caliebe and Th. Brückel

Institut für Streumethoden

We report on a study of the effects of competing magnetic interactions in the mixed-crystal series $Gd_xEu_{1-x}S$ using neutron- and resonance exchange scattering of synchrotron radiation. For the first time we were able to reveal a different temperature dependence for two magnetic ions Gd^{3+} and Eu^{2+} occupying the same site stochastically. We propose a quantitative model of the frustration mechanism leading to a spin glass phase. With resonance exchange scattering we were able to observe the short range correlations in the spin glass state.

F&E-Nr: 23.89.1

Introduction In contrast to the more traditional tools of magnetic neutron- or nonresonant magnetic x-ray diffraction, x-ray resonance exchange scattering (XRES) offers the unique possibility to distinguish the magnetic order of different elements in a magnetic alloy by tuning the x-ray energy to the absorption edges of the magnetic elements. This is of particular interest for highly disordered and frustrated systems. An excellent example is given by mixed crystals of the series $Gd_xEu_{1-x}S$. While GdS is an antiferromagnetic metal, EuS is a ferromagnetic insulator. At intermediate concentrations of both elements in the mixed crystal $Gd_xEu_{1-x}S$, a metal-insulator-transition and a low temperature spin glass phase exits.

We have investigated five samples of the $Gd_xEu_{1-x}S$ mixed crystals in a concentration range from x = 1.0 to x = 0.6. In this report we present the results of measurements of a $Gd_{0.8}Eu_{0.2}S$- and a $Gd_{0.67}Eu_{0.33}S$-sample. The first one orders antiferromagnetically, the second one shows a spin glass behaviour at low temperatures.

Sample Preparation The examined samples were prepared by direct reaction of stoichiometric amounts of the constituent elements at 600° C for two weeks. The resulting powder was pressed and heated in a tungsten-crucible to about 50° C below the corresponding melting temperatures for three weeks [1].

Investigation of $Gd_{0.8}Eu_{0.2}S$: an antiferromagnetically ordered system First element specific measurements with XRES at the $Gd_{0.8}Eu_{0.2}S$-sample showed that the Gadolinium- and Europium-ions both participate in the antiferromagnetic order of type II below a Néel-temperature of 53.316(8) K. The sample was characterised at room temperature by diffraction measurements with x-rays and with a x-ray microscope. No inhomogeneities or decompositions were observed.
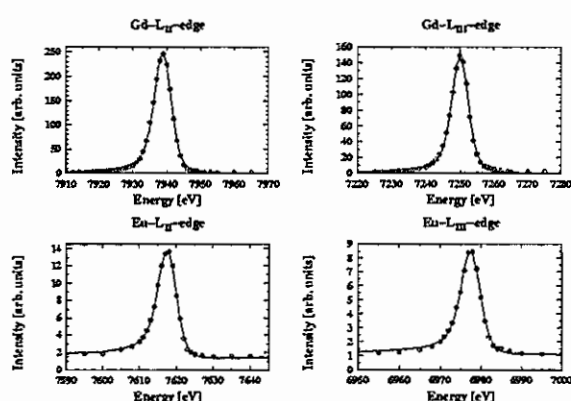
Figure 1: Absorption corrected energy dependence of the intensity of the $\left(\frac{1}{2}\frac{1}{2}\frac{9}{2}\right)$ magnetic Bragg-peak at the Gadolinium- and Europium-L_{II}- and -L_{III}-edges. The data were taken from the $Gd_{0.8}Eu_{0.2}S$-sample at 4 K.

In figure 1 the energy dependence of the absorption corrected XRES intensities at the four Gadolinium- and Europium-L_{II}- and -L_{III}-edges is shown. The absorption coefficient was determined from the energy dependence of the fluorescence yield. A polarisation analysis of the scattered intensity from pure GdS demonstrated that in these compounds XRES is dominated by electric dipole transitions into the conduction band. We were able to observe electric quadrupole transitions, which were weaker by a factor of 300, and therefore are negligible. The asymmetry of the energy dependence is caused by contributions of nonresonant magnetic scattering [2]. A simplification of the energy dependence of the scattering amplitude given by [3] is:

$$A(E) = iA_{mag} + \frac{1}{E} \cdot \frac{ia_{res}}{\Delta E - i\frac{\Gamma}{2}}$$

Where A_{mag} is the contribution of nonresonant magnetic scattering, a_{res} is proportional to the contribution of XRES, ΔE is the difference

between the x-ray energy E and the energy of the excited state and Γ is the lifetime of the excited state. The solid line in figure 1 represents a fit of the square of the absolute value of the scattering amplitude (equation 1) convoluted with the instrumental energy resolution. The lifetime Γ averages to 0.2 fs.

The investigation of the temperature dependence of the XRES of $Gd_{0.8}Eu_{0.2}S$ revealed a complete different behaviour of the Gadolinium- and Europium-ions. In contrast to neutron scattering, XRES as a second order perturbation process is not necessarily proportional to the sublattice magnetisation. Therefore additional measurements with hot neutrons were performed at the instrument D9 of the ILL. With neutron scattering the average magnetisation of the two atomic species is observed. In figure 2 the reduced sublattice magnetisation measured with XRES and neutron scattering is compared. The weighted sum of the sublattice magnetisation of Gadolinium and Europium coincides with the neutron data.
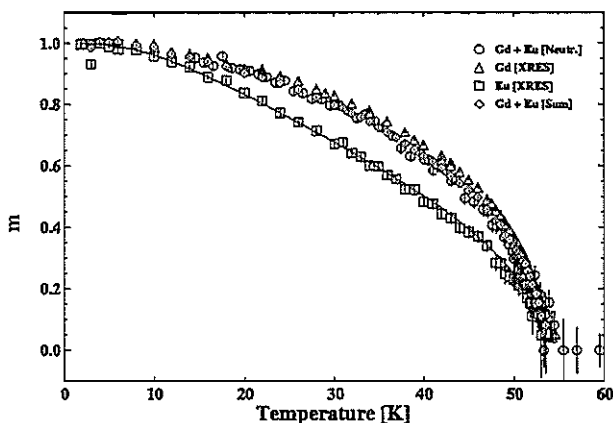
Figure 2: Temperature dependence for the $Gd_{0.8}Eu_{0.2}S$ crystal. XRES has been used to determine separately the behaviour of the Gadolinium- and Europium-ions. With magnetic neutron scattering only the average magnetisation is accessible. For comparison with the neutron data the weighted sum of the two XRES measurements is shown.

The sublattice magnetisation of the Gadolinium ions can be described by a Brillouin-function with spin 7/2. The behaviour of the sublattice magnetisation of the Europium ions is due to frustration effects. The antiferromagnetic exchange between the Gadolinium ions and the ferromagnetic exchange between the Europium ions can not be satisfied simultaneously. A simple model, which takes the frustration effects of Europium pairs surrounded by Gadolinium ions into account, was used to describe the temperature dependence of the sublattice magnetisation of the Europium ions

[2]. The solid line in figure 2 represents the fit with the so called "frustrated"-Brillouin-function. Close to the Néel-temperature the critical exponent of the sublattice magnetisation was determined to be β = 0.451 (2). This value is close to the exponent of the meanfield model β $\approx$ 0.5. This differs significantly from the critical exponent β = 0.384 (5) observed for pure GdS, which is consistent with the Heisenberg-model β = 0.3645 (25) [4].

We also investigated a $Gd_{0.73}Eu_{0.27}S$-sample which showed a behaviour comparable to the $Gd_{0.8}Eu_{0.2}S$-sample. The determined Néel-temperature and critical exponent were 36.4 (1) K and β = 0.47 (2), respectively.

Investigation of $Gd_{0.67}Eu_{0.33}S$: a spin glass system The $Gd_{0.67}Eu_{0.33}S$-sample was expected to show a spin glass-behaviour at low temperatures. An initial search did not reveal magnetic Bragg scattering at the expected positions in reciprocal space. Therefore we used a polarisation analysis setup with a pyrolytic graphite crystal to suppress background due to charge scattering in $\sigma \rightarrow \pi$ geometry. Measurements have been performed at all four Europium- and Gadolinium-L_{II}- and L_{III}-edges. Only at the Gadolinium-L_{II}-edge magnetic scattering has been observed. Figure 3 shows diffuse magnetic scattering centred

around the $\left(\frac{1}{2}\frac{1}{2}\frac{9}{2}\right)$ position. The data were

taken at 2 K in resonance at the Gadolinium-L_{II}-edge with a Q-scan in [111]-direction. The width of the peak corresponds to a correlation length of 105 (12) Å. The peak intensity is 0.6 c/s on a background of 1.5 c/s. These measurements were carried out at beamline W1 of HASYLAB at DESY. To improve the statistics of the data and to search for antiferromagnetic correlations between the Europium-ions we have repeated these measurements at the ESRF. The intensity was about six times larger and the peak-to-background ratio was improved by a factor of two. We did not find antiferromagnetic correlations for the Europium-ions.

Q-scans in the [001]-, [110]- and [111]-directions at the ESRF lead to correlation lengths of 46(4)Å, 73(6)Å and 168(11)Å, respectively. The reason for this anisotropy is not yet understood. It is not due to an anisotropy of the susceptibility [2].

We also measured the energy dependence of the XRES at the Gadolinium-L_{II}-edge which is shown in figure 4. The curve form is comparable to those observed for the GdS-, $Gd_{0.8}Eu_{0.2}S$- and $Gd_{0.73}Eu_{0.27}S$-samples.
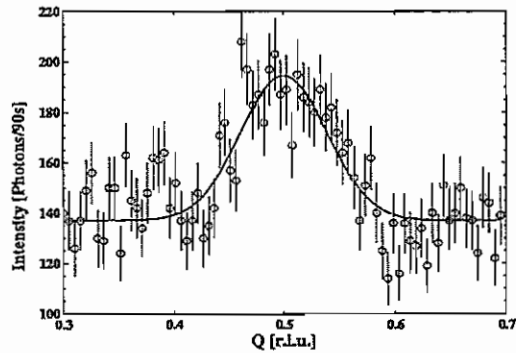
Figure 3: Q-scan (4.3 0.3 0.3) → (4.7 0.7 0.7) around the $\left(\frac{1}{2}\frac{1}{2}\frac{9}{2}\right)$-position of the $Gd_{0.67}Eu_{0.33}S$-sample. The sample time was 90 seconds for each datum point. The energy was tuned to the Gadolinium-L_{II}-edge; the temperature was 2 K. A polarisation analyser with $\sigma \to \pi$ geometry was used. The solid line represents the fit of a Gaussian curve to determine the integrated intensity.
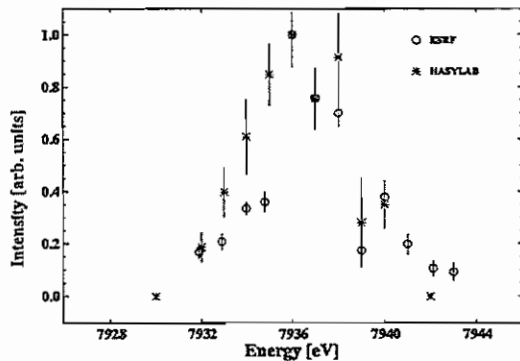
Figure 4: Energy dependence of the magnetic scattering around the $\left(\frac{1}{2}\frac{1}{2}\frac{9}{2}\right)$-position at the Gadolinium-L_{II}-edge of the $Gd_{0.67}Eu_{0.33}S$-sample.
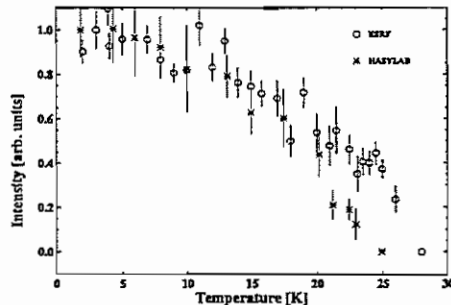
Figure 5: Temperature dependence of the magnetic scattering around the $\left(\frac{1}{2}\frac{1}{2}\frac{9}{2}\right)$-position at the Gadolinium-L_{II}-edge of the $Gd_{0.67}Eu_{0.33}S$-sample.

In figure 5 the temperature dependence of the integrated intensity of the diffuse scattering measured with XRES is displayed. Above a temperature in the range of 23 K to 26 K the intensity vanishes. Additional measurements of the AC-susceptibility are planned to determine the freezing temperature of the system.

As a second sample in the spin glass-regime a $Gd_{0.67}Eu_{0.33}S$-crystal was investigated. The measurements were performed in the same way as with the \gdc-sample. We were not able to observe magnetic diffuse scattering with XRES. We suggest that the correlation length of the antiferromagnetically ordered clusters are too short.

Conclusions We have investigated the magnetic behaviour of the $Gd_xEu_{1-x}S$ mixed crystals. XRES has been proven to be a versatile tool to determine element specific the properties of highly frustrated systems. We were able to observe the development of the spin glass state on a microscopic scale. In the Gadolinium rich samples the Europium-ions exhibit an antiferromagnetic order. Frustration effects lead to a deviation of the reduced sublattice magnetisation of the Europium-ions from the Brillouin-function with spin 7/2. This is due to a ferromagnetic coupling in Europium-clusters with two or more ions. This was demonstrated with a model calculation. With further increasing Europium concentration the Europium-clusters become larger and the ferromagnetic coupling dominates. This leads to a breakdown of the long range antiferromagnetic order.

For the first time it was possible to observe the short range antiferromagnetic order in a spin glass state with XRES. The correlation length has been determined to be in the range of some 10 Å up to 100 Å.

This work was done in collaboration with N. Bernhoeft (ESRF), K. Mattenberger (ETH Zuerich), G. McIntyre (ILL), J. Strempfer (DESY), A. Stunnault (ESRF) and F. Yakhou (ESRF).

[1] K. Mattenberger, L. Scherrer, and O. Vogt, J. Cryst. Growth 67, 467 (1984).
[2] D. Hupfeld, Dissertation. Universitaet Hamburg, 1998.
[3] M. Blume, *Magnetic effects in anomalous dispersion in Resonant anomalous x-ray scattering*, edited by C. S. G. Materlik and K. Fischer (Elservier Science B. V., Amsterdam, 1994), pp. 231 - 256.
[4] J. le Guillou and J. Zinn-Justin, Phys. Rev. B 21, 3976 (1980).

Interface and magnetic characterization of Fe/δ-Mn/Fe sandwich structures using scattering methods

E. Kentzinger, U. Rücker, W. Caliebe, G. Goerigk, F. Werges, B. Alefeld and *C.Fermon**

Institut für Streumethoden

**DRECAM/SPEC*, CEA Saclay, 91191 Gif sur Yvette cedex, France*

Using reflectivity and small angle diffuse scattering of synchrotron radiation and neutrons, we characterize the interface morphology and the magnetic structure of Fe/δ-Mn/Fe trilayers. We find high correlated roughness of the interfaces. MOKE measurements as a function of Mn thickness revealed 90° or non-collinear coupling between the Fe layers for thickness of Mn around 0.8 nm, in agreement with polarized neutron reflectivity measurements.

In contrast to all other 3d transition metals, Mn does not have a simple fcc or bcc structure at room temperature: the α-Mn phase has a structure with 58 atoms in the cubic unit cell. The δ-phase (body centered cubic) in bulk Mn is stable at high temperature (from 1410 K up to the melting point at 1517 K) and cannot be obtained at room temperature by quenching. However, we were able to stabilize δ-Mn in the form of thin epitaxial films by molecular beam epitaxy.

We are interested in determining the magnetic structure of δ-Mn as a function of temperature and, when it is sandwiched between two ferromagnetic layers, correlate it with the magnetic coupling between these layers and with the interface roughness or interdiffusion.

We present here first results on the characterization of Fe/δ-Mn/Fe sandwich structures using synchrotron radiation and neutron scattering methods.

For this study, we grow Fe/Mn bilayers on Fe(001), Ag buffer and GaAs(100) substrate. *In-situ* LEED experiments show that Mn grows epitaxially on Fe and stays mono-crystalline up to 4 nm. Synchrotron radiation diffraction experiments are currently undertaken to determine the in-plane lattice parameter and the possible tetragonal distortion of the Mn layers.

To reveal the interface morphologies, we perform reflectivity and small angle diffuse scattering of synchrotron radiation using the CEMO and JUSIFA beamlines of HASYLAB at DESY in Hamburg. On the CEMO beamline, a well collimated and monochromatic beam impinges on the surface under an incident angle α_I, is scattered and detected under an exit angle α_F by a single detector. On this experiment, intensities are recorded over a high dynamical and a large angular range. On the JUSIFA beamline, the scattered x-rays are collected by a 2-dimensional position sensitive detector, giving access to a large solid angle for detection.

When α_I and α_F are kept equal, a specular reflectivity scan is performed: the scattering vector lies perpendicular to the sample surface and only density modulations averaged over planes parallel to this surface are accessible. When α_I is different from α_F, a non-specular (diffuse) scan is performed: the scattering vector has a component parallel to the sample surface and density modulations along planes parallel to it can be determined.
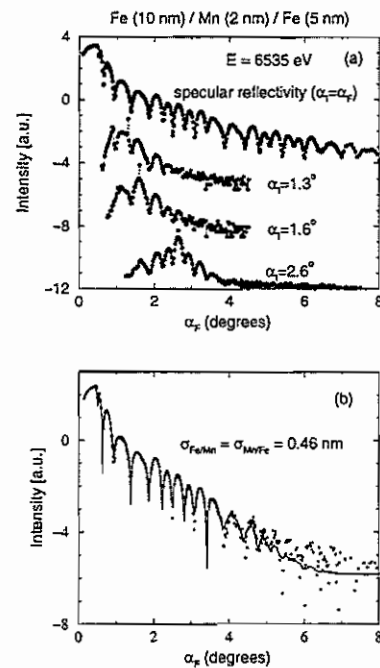

FIG. 1. (a): Specular reflectivity and diffuse scattering measured on the CEMO beamline on a Fe/Mn/Fe trilayer. Intensities are on a logarithmic scale in arbitrary units. For clarity the different scans are shifted one with respect to the other on the intensity scale. Fe and Mn are neighbors in the periodic table of the elements. Therefore the energy E of the x-rays was chosen close to the absorption edge of Mn (6539 eV) in order to increase the contrast between the form factors of Fe and Mn.

(b): True specular reflectivity obtained by substracting the diffuse background from the specular reflectivity. This diffuse background is measured by scaning α_I and α_F with $\alpha_F = \alpha_I + \epsilon$ where ϵ is small and chosen in an appropriate manner. The solid line is a fit. The fitted parameters defining the interface roughness or interdiffusion between the first Fe layer and the Mn layer ($\sigma_{Fe/Mn}$) and between the Mn layer and the second Fe layer ($\sigma_{Mn/Fe}$) are equal and given in the figure. See [1] for an exact definition of the roughness parameter σ.
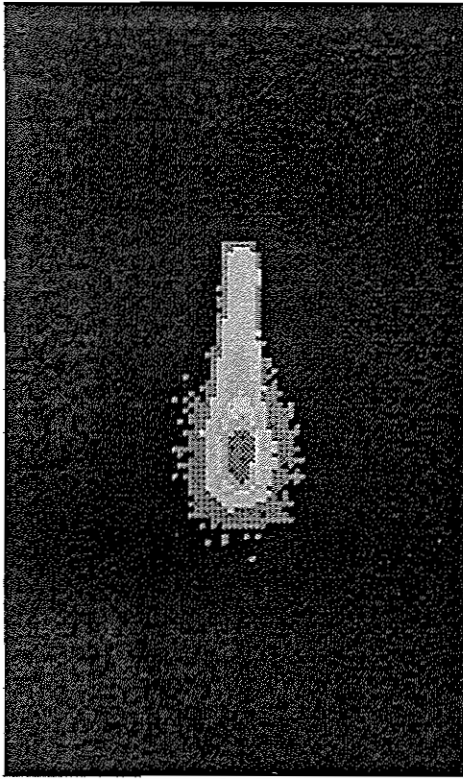
FIG. 2. Measurement at the JUSIFA beamline of the diffuse scattering of a polished GaAs substrate. The peak at the critical angle of total external reflection is the Yoneda peak [3]. Intensities are displayed on a log-scale. The maximum of intensity is 94 in arbitrary units.
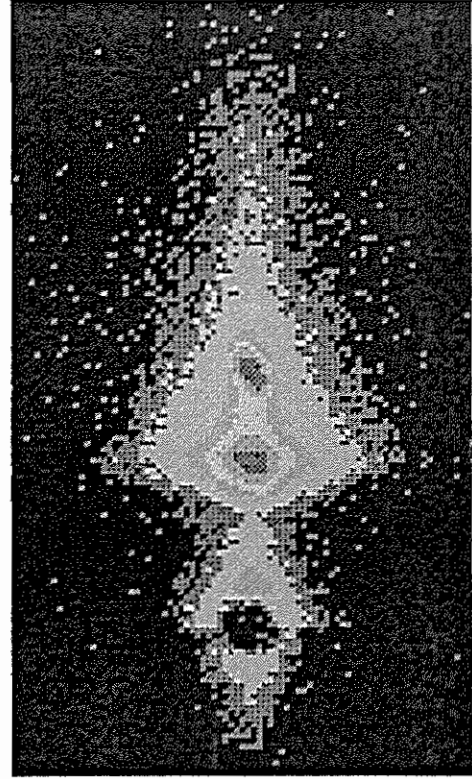

FIG. 3. Measurement at the JUSIFA beamline of the diffuse scattering of an annealed GaAs substrate. The incident angle α_I of the x-rays is the same as in figure 2. Again we see the Yoneda peak. The second peak is the specular reflex. The maximum of intensity is 4.2 in the same units as in figure 2.
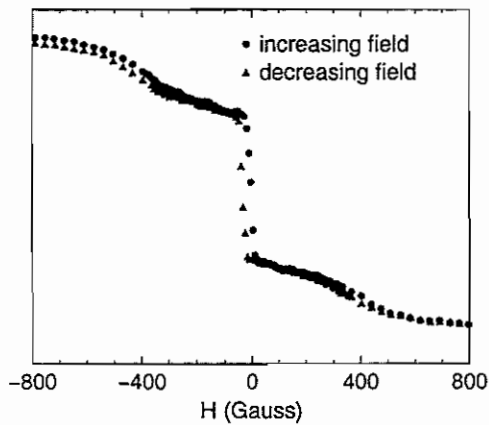

FIG. 4. Longitudinal MOKE hysteresis measurement on Fe/Mn(0.8nm)/Fe. The external field H is applied along the [100] easy axis of magnetization.
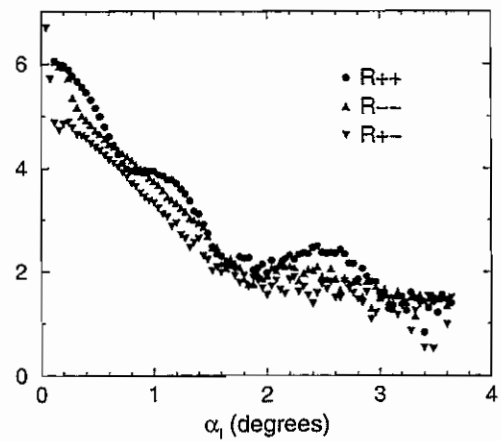

FIG. 5. Polarized neutron reflectivity on the same sample as in figure 4 under an external field of 40 G applied along the [100] axis. + or - in the legend correspond to the neutron spin orientation with respect to the external field (parallel or anti-parallel, respectively) before (first position) and after (second position) reflection by the sample. Intensities are on a log-scale in arbitrary units.

An example of such scans performed on CEMO is given in figure 1.a. The sharp peaks at $\alpha_F = \alpha_I$ in the diffuse scans show that the specular reflectivity is the superposition of a "true specular" component and a "diffuse background". At $\alpha_I = 2.62°$ the true specular component is already very small. Above 4°, it is almost equal to zero so that the modulated intensity we observe in the specular reflectivity scan is pure diffuse scattering.

As an example of our measurements on JUSIFA, the diffuse scattering from a polished GaAs substrate and the one from a GaAs substrate after annealing at 630°C are displayed in figure 2 and 3, respectively. (We use this stage of annealing for oxygen desorption before deposition of our layers). Comparing the two pictures we see that, in the case of the annealed GaAs, the intensities are lower and the diffuse scattering extends over a larger area than with the non-annealed sample, showing that the annealing stage introduces surface roughness.

We are currently analyzing the CEMO and JUSIFA measurements in the framework of the dynamical theory, where interdiffusion, uncorrelated roughness and both in-plane and layer-to-layer correlated roughness profiles are considered [2]. From the analysis of the true specular reflectivity, we can already state that our Fe/Mn/Fe trilayers show either high interdiffusion or roughness (figure 1.b). However, the strong oscillations in all the diffuse scans we measured (see figure 1.a) can only be explained in terms of correlated roughness [2].

First MOKE measurements performed on our Fe/Mn/Fe trilayers show almost no magnetic coupling between the Fe layers or pure ferromagnetism inside the whole trilayer, except for Mn thickness around 0.8 nm where evidence of 90° or non-collinear coupling is present (figure 4). This result is independent on temperature between 20 and 300 K.

To determine in a model-independent way the nature of the coupling and the magnetism of the Mn layers, we perform polarized neutron reflectivity (PNR) measurements. PNR is the method of choice for this study, as it gives a completely vectored picture of the projection of the magnetic moments on the sample surface [4]. Test measurements on PADA at the LLB-Saclay on some of our samples showed a non-zero R+- signal, signature of a non-zero component of the magnetization perpendicular to the applied field (figure 5). In a near future, PNR works will be possible in the guide hall of the neutron research reactor of Jülich as we plan to equip the HADAS reflectometer with polarizers and spin-flippers.

To conclude, we have launched a program to study the magnetism of Mn in Fe/Mn/Fe trilayers in correlation with the interface morphology and the magnetic coupling. Specular and non-specular reflectivity of synchrotron radiation give us access to the interfaces morphologies. Once a good recipe will be found to build layered structures of Fe and Mn with sharp interfaces, the magnetic structure of δ-Mn will be determined using neutron scattering (PNR and high angle diffraction).

F&E-Nr.: 23.89.1

[1] X.L. Zhou and S.H. Chen, *Physics Reports*, **257**, 223 (1995)
[2] V. Hóly and T.Baumbach, *Phys. Rev. B*, **49**, 10668 (1994)
[3] Y. Yoneda, *Phys. Rev.*, **131**, 2010 (1963)
[4] S.J. Blundell and J.A.C. Bland, *Phys. Rev. B*, **46**, 3391 (1992)

Wide-angle neutron scattering with polarization analysis - structural investigations of Polyalkylmethacrylat polymer glasses

W. Schweika

Institut für Streumethoden

The diffuse neutron scattering instrument DNS in the cold neutron guide hall of the Juelich research reactor has been equiped with sets of supermirrors to produce polarized neutrons and to analyze scattered neutrons over a wide angular range. To demonstrate the new capabilities we discuss first measurements of the wide-angle of four different partially deuterated samples of Polyalkylmethacrylat polymer glasses, where the intensities have been separated into coherent and spin-incoherent parts of the elastic scattering.

Polarisation Analysis Due to its magnetic moment the neutron is a sensitive probe to explore structural and dynamic properties of magnetic materials. However, the neutron spin also causes the spin-dependent nature of the nuclear scattering. In order to separate all of these different scattering contributions, the technique of polarisation analysis provides a unique and important tool. For instance in case of nuclear scattering only, the spin-flip scattering consists of 2/3 of the incoherent scattering, while the non-spin-flip scattering contains the total coherent scattering and 1/3 of incoherent scattering. At low temperatures the elastic incoherent part is independent of the scattering vector (reflecting the randomness of nuclear spin states), which can be used as an excellent intrinsic calibration of the coherent scattering part into absolute intensities.

Similar to the prototype instrument D7 at the ILL we also used polarizing multilayers in our analyzers. The multilayers of $TiN/Fe_{50}Co_{48}V_2$ have been produced by sputtering technique on a thin float-glass substrate (P.Boeni, PSI) and their performance was found to be very good. An essential difference to the D7-instrument is the focussing and defocussing layout of the polarizers, a slightly bended stack of such multilayers, in the primary and secondary part of the spectrometer. Hence, especially studies on small samples will benefit from a gain in intensity (by a factor of approximately four). The final version is designed for 22 analyzing units. Meanwhile 11 units are ready for routine operations.

Polyalkylmethacrylat Polymer Glasses There is only very little work concerned with the structure factor of amorphous polymers involving the technique of neutron spin-polarization analysis [1,2]. The work by Gabrys *et al* on polymethylmethacrylat aimed primarily to explain the crystallisation properties in stereoregular polymers in terms of short range ordering, whereas the work by Lamers *et al* combined scattering experiments with computer simulations of amorphous cell models to elucidate the relationship of macroscopic properties and microscopic structure in polycarbonates. The present work is initiated from previous light scattering results of unusual dynamic properties of Polyhexylmethacrylat with regard to the longitudinal acoustic branch [3]. It was found that within the series of polyalkylmethacrylats the Brillouin dispersion becomes more and more decoupled from the main-chain rubber relaxation (indicative of softening of the structure) the longer the alkyl side chain is [4]. This is an anomalous finding and is yet not fully understood. Therefore a series of incoherent quasi-elastic neutron scattering experiments have been undertaken in order to find correlations between structure and dynamics. Since obviously the length of the side chain is important we have investigated two different side-chain lengths $-C_2H_5$ (*-ethyl*) and $-C_6H_{13}$ (*-hexyl*). On the other hand it is essential to distinguish effects coming from the main chain from those stemming from the side chain. Therefore the materials were selectively deuterated.

Measurements and Results Most of the measurements have been performed at low temperatures (8K) collecting all of the scattering of the frozen-in structure within the elastic resolution of the instrument. Nonetheless, the time-of-flight method was used to improve the signal-to-background ratio. In principle, it is not necessary to apply the polarization analysis of the scattering to obtain the coherent scattering cross-section. However, polarization analysis has proved to give an essential qualitative improvement, since there is a clear separate determination of coherent and incoherent scattering, avoiding further systematic errors by using the incoherent scattering as an intrinsic calibration to absolute intensities.

The experimental results for Polyethylmethacrylat and Polyhexylmethacrylat, see Fig. 1, can be distinguished into two groups. The side-chain protonated polymers, exhibiting a single peak structure (open symbols in Fig. 1), and the main-chain protonated polymers, exhibiting a double peak structure (filled symbols in Fig. 1). Following the Polyethylmethacrylat data interpretation with regard to S(Q), we may tentatively relate the low-Q peak in case of (a) and (c) to the inter-chain correlation, since in the longer side-chain material (c) the peak shifts towards lower Q and may hence reflect the inter-chain separation. The cases (b) and (d) are different as they clearly show two maxima. Again the low-Q peak is attributed to the inter-chain distance while in both cases the second peak at Q = 1.4 $Å^{-1}$ reflects the typical repetition unit along one chain. On the other hand, for the deuterated side chains (cases (a) and (c)) the contrast for the coherent scattering amplitudes of these atoms is rather weak. A more elaborate analysis of the

structure is planed with comparative computer simulations [5]. This work has been done in collaboration with G. Meier, MPI.

[1] B. Gabrys, J. Higgins, O. Schaerpf, J. Chem. Soc. Faraday Trans. 82, 1929 (1986)

[2] C. Lamers, D. Richter, W. Schweika, J. Batoulis, K. Sommer, and O. Schärpf, Short-Range Order in Amorphous Polycarbonates, Physica B, 180 - 181, 515 (1992).

[3] G. Meier, F. Kremer, G. Fytas, A. Rizos, J. Poly. Sci. Phys. Ed. 34, 1391 (1996).

[4] R.Y. Li, O.Z. Jiang, G. Fytas, C.H. Wang, Macromolecules 19, 778 (1986).

[5] K. Kremer, private communication.
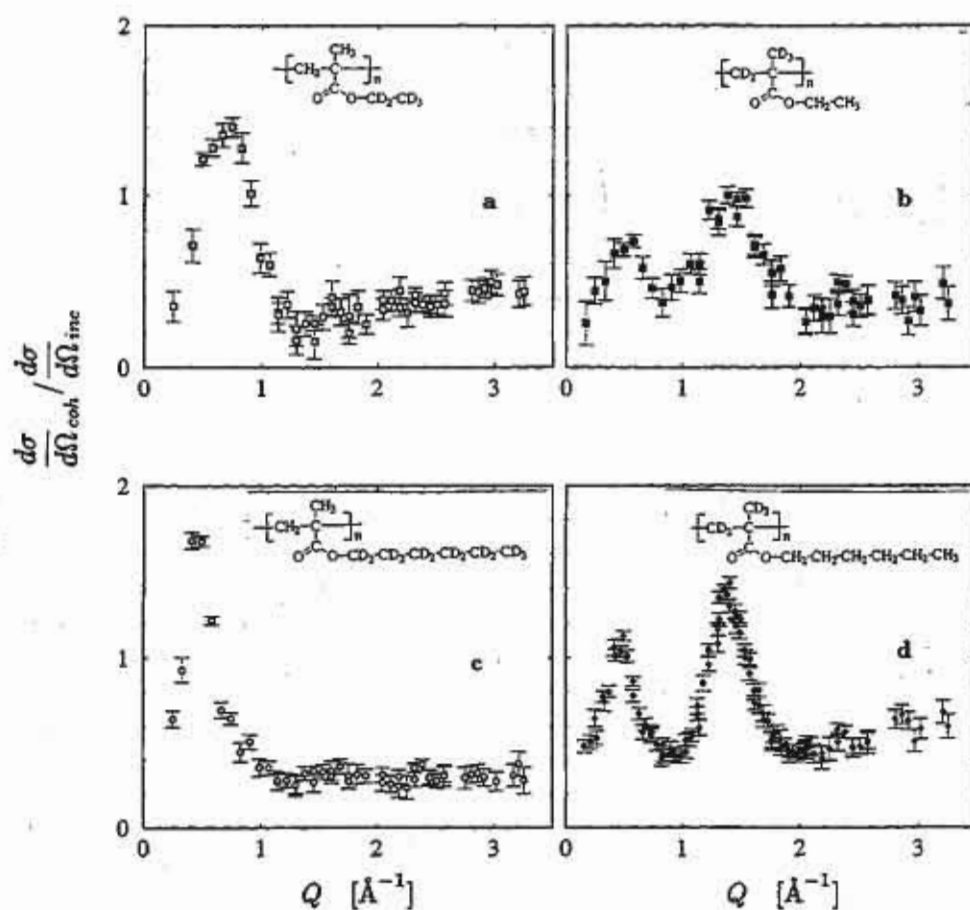
Figure 1: Coherent scattering of partially deuterated/protonated Polyalkylmethacrylat at T = 8 K (normalized by its incoherent scattering); Polyethylmethacrylat (a) main-chain protonated, (b) side-chain protonated, Polyhexylmethacrylat (c) main-chain protonated, (d) side-chain protonated.

Institute for neutron scattering: General overview

In 1998 the research reactor FRJ-2 was delivering neutrons for 151 days. Altogether 191 experiments were performed at the different neutron scattering instruments. 143 or 75% of them with external participation. These numbers include experiments performed within the Institute for Scattering Techniques, the Institute for Neutron Scattering (INS) and the different external Collaborating Research Groups. The external users came from 53 different institutions. Fig.1 displays the distribution of the external users with respect to their origin. As may be seen, the FRJ-2 attracted large interest not only in the national but also in the international community. At this point I like to thank in particular the reactors operation department for the very good cooperation between users and operators.
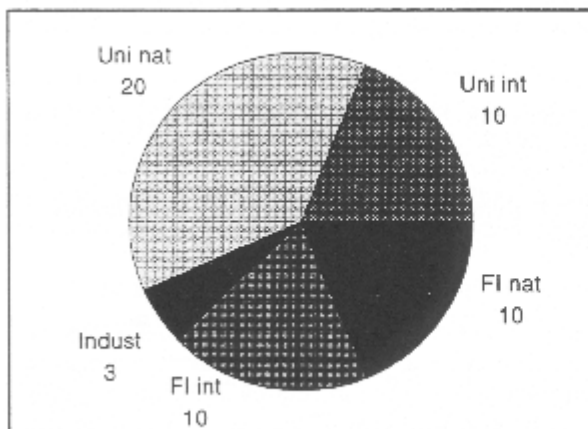

Fig. 1: Origin of the user groups performing neutron scattering experiments at the FRJ-2 in 1998: FI: research organisations outside the university; Uni: universities; Indust: industry.

In 1998 a neutron laboratory course was hold for the second time. This course comprised 20 hours of lectures and one week of practical experiments at seven different neutron instruments. Among the more than 100 applicants from different Universities in Germany and beyond 35 participants were accepted. The neutron laboratory course was very well received by the students. In 1999 a third course is foreseen.

Neutron instrumentation FE 23.89.1

In 1998 the construction of the new thermal time of flight instrument was completed. First test experiments revealed a high thermal flux 2×10^8 integral at sample position from this number a pulsed intensity of about 2×10^5 n/cm^{2}s may be estimated. Unfortunately, due to manufacturing problems of the very delicate high speed background chopper, some delays in the commissioning of the instrument occurred.

With respect to this chopper, we like to acknowledge the cooperation with the IGV within the Forschungszentrum - provision of the magnetic bearings - and the jet engine manufacturer MTU - manufacturing of the chopper.

The double crystal diffractometer was furnished with new channel cut perfect silicon crystals which improved the resolution characteristics of this instrument significantly. In particular the broad wings of the resolution function are now strongly reduced. Finally, in 1998 we commenced with design studies for a new back scattering instrument at the Munich reactor

FRM-II, which is supported by the federal government. In particular the properties of the phase space transformation by a fast turning wheel was studied in detail (report Kirstein).

In 1999 the main activities will be concentrated on the construction of the back scattering instrument mentioned above. We will participate in the development of neutron time of flight spin echo, where we develop broad band flippers and are actively engaged in the test experiments at the instrument IN15 in Grenoble. Furthermore, it is planned to consider also the zero field NSE technique as a complementary way to perform NSE experiments.

Polymers, membranes and complex fluids (FE 23.30.0)

The research activities within the INS are focussed in the field of polymer physics and complex fluids. In order to be successful here, a close cooperation between polymer synthesis which by itself is an object of research, and physics investigation is necessary. In the following I discuss the different main topics.

Polymers synthesis

In 1998 the synthesis of branched polymers and blockcopolymers were the backbone of the activity. Star polymers of different functionalities and very high molecular weight were prepared as well as H-shaped polymers which are important in the frame of a European Brite-Euram project for polymer processing. In order to investigate aspects of the reptation model, high molecular weight PVCH polymers were synthesized $M_W > 10^6$. In order to deepen our understanding of mixed polymer and surfactant systems, for the first time an organic synthesis of fully deuterated nonionic surfactants was accomplished in our laboratory. In addition quite a large number of homopolymers or simple diblockcopolymer were synthesized. Finally I would like to emphasize the collaboration between the Institute for Biotechnology and the polymer laboratory on the development of organic cathalysts which are fixed at a polymer backbone.

For 1999 it is foreseen to synthesize in particular H-shaped and comb like polymers for the BRITE-EURAM project. In addition further amphiphilic polymers and star polymers are on the agenda.

Finally experiments on the living polymerization with SANS are going to be extended to in situ experiments of the polymerization kinetics and the associated aggregation states.

Polymer dynamics

The core activity of the institutes relates to dynamical properties of soft condensed matter systems. Thereby we cover dynamical features from the large scale motions of long chains in the melt to the local relaxation processes and the soft vibrational properties. Starting from the high frequency side, X-ray and neutron Brillouin scattering experiments were performed on polybutadiene melts. From a direct comparison of the results it is clear that above 1.5 meV energy transfer the X-rays are superior. Below this energy the better resolution of neutron experiments favors neutron scattering.

In this low energy transfer regime new dynamical features were observed, which are proportional to the density of states and visible down to a momentum transfer of 0.1Å^{-1}.

In the regime of the α-relaxation Q-dependent incoherent neutron scattering experiments addressed the question whether this process is heterogeneous. The neutron results favor a homogeneous nature of the α-relaxation at least in the temperature range, where neutrons can resolve the relaxations. On the results from neutron scattering experiments on the glass transition under confined geometry we report separately (report Zorn). In order to increase our experimental portefeuille, a laboratory for dielectric spectroscopy was implemented, which will allow complementary experiments with a large dynamic range.

On polyisobutylene the dynamic response was studied over two orders of magnitude in momentum transfer covering all processes from translational diffusion, the Rouse modes, the intrachain viscosity, the α-relaxation, to local relaxation processes. Thereby the single chain response was successfully related to the collective dynamics (report Arbe).

Exploiting the possibilities of IN15, the large scale motions of long chain polymer melts was systematically investigated varying the chain molecular weight. Furthermore, studies were undertaken, where labeled sections were placed at different positions along the chain. Over all a very good agreement with the reptation model is found - actually no other formulated theory is able to explain the data. Furthermore, apparently contour length fluctuation processes are directly visible in the dynamic response. Large scale motion was also investigated on diblockcopolymers around the order disorder transition to the lamellar phase. Thereby the different aspects of the dynamic response were fully studied in using different chain contrasts.

The experimental results were compared with the most advanced dynamical random phase approximation theory. Severe deviations were found with respect to the predicted collective response. The experiments reveal strong indications for the importance of surface excitations in the dynamic response of the microphase separated domains.

In 1999 most of these activities are going to be continued. New emphasis will be placed on the study of dynamic form factors in the high frequency regime, where the new time of flight instrument SV29 will be very helpful. This instrument will also allow to address again the question of the dynamical heterogeneity. Furthermore, the dynamics of polymer containing microemulsions will be addressed.

Association, Aggregation and structure formation in polymer solutions

Aside of the dynamic experiments this field is another stronghold of the activities within the institute. The most important discovery of 1998 was the realization that small additions of amphiphilic polymers to microemulsions increase the emulsification properties significantly. This feature was documented in terms of phase diagrams. Neutron small angle scattering experiments on the structure of polymer containing microemulsions and the confirmations of the polymers within these systems were just started (report Willner).

The micellarization properties of blockcopolymers were investigated on the amphiphilic systems as well as on polymers with architecture. I would like to mention particularly new experiments on the exchange kinetics of unimers between polymer micelles, which can be uniquely accessed by contrast variation in small angle neutron scattering.

In this frame also the aggregation behavior of carbo hydride copolymers, which are used as fuel additives should be mentioned. Polymers of only two blocks of polyethylene and polyethylenepropylene aggregate into platelet shaped micelles, which act as nucleation centers for wax crystals in diesel fuel and suppress the cold filter plugging point. In 1998 we studied random copolymers of these two components, which aggregate to form loose networks with a large number of crystalline connecting points. Unexpectedly we found a characteristic mesoscopic length scale in these structures which indicates some order in the chaos.

In 1999 the study of the amphiphilic blockcopolymers both with respect to the micellarization behavior as well as concerning their action in microemulsions will be continued.

Furthermore, the structure formation in mixed star polymer and colloidal systems is on the agenda. In addition the conformation of systematically structurally modified branched nylon molecules will be studied.

Phase transitions in polymer melts

In this field in particular ternary systems of two homopolymers and a compatibility providing diblockcopolymer were undertaken. The phase transitions and the phase diagrams in such systems were explored; of particular interest is a composition range were complete compatibility in a homogeneous phase is observed (report Schwahn).

Branched polymers and polymer networks

After having identified the effect of topological constraints on rubber elasticity, the focus of the ongoing research is the effect of filler particles in rubbers. Here experiments on SiO_2 fillers are undertaken and a systematic characterization of the systems is performed.

This concerns both, the surface properties of the SiO_2 filler as well as the exploration of different cross linkers. Aside of the work on rubbers SANS experiments on the deformation of branched polymers under external stress are performed.

These experiments are connected to rheological studies and aim on an exploration of how the non linear viscosity can be influenced by specific branching, in order to improve polymer processing conditions.

Further research activities.

Aside of the polymer research, three other topics are investigated by neutron scattering.

1. Dynamics of microemulsion: With the investigation of mixed polymer microemulsion systems this field is now conncected to the polymer research.
2. Tunneling phenomena and molecular crystals (see report M. Prager)
3. Dynamics of small molecules in porous media. In 1998 the dynamics of ethane propane and benzene in MCM 41, a micro crystalline material with tubes of 5 nm size, were studied. Both translational diffusion as well as reorientational motion were

identified. The main conclusion of these experiments is that the molecules adsorbed at the channel walls have a mobility similar to the liquid phase. These experiments are accompanied by computer simulations which are performed by the collaborating chemical institutes

Dieter Richter

The Institute for Neutron Scattering - Coworkers and area of activity

Scientific Staff

Dr. J. Allgaier	Polymer synthesis	23.300
Prof. U. Buchenau	Dynamics of glassforming materials	23.300
Dr. H. Grimm	Molecular crystals, oriented macromolecules. Responsable: Backscattering spectrometer BSS1	23.300
Dr. M. Monkenbusch	Dynamics of polymers and complex liquids Responsable: Spinecho Spectrometer NSE	23.300
Dr. M. Prager	Rotational tunneling Responsable: Thermal time of flight spectrometer SV29	23.150
Dr. W. Pyckhout-Hintzen	Polymer networks; branched polymers	23.300
Prof. Dr. D. Richter	Structure and dynamics of polymers, glass transition, complex liquids	23.300
Dr. D. Schwahn	Phase transitions in polymer systems Responsable: Small angle neutron scattering KWS1 and double crystal diffractometer DKD	23.300
Dr. R. Stockmeyer	Dynamics of adsorbed molecules, diffusion in porous media Responsable: Cold time of flight spectrometer SV5	23.150
Dr. L. Willner	Polymer synthesis, polymer micelles	23.300

Technical Staff

U. Bünten	Technician at SV29	23.891
Ms. M. Hintzen	Technician in the polymer laboratory	23.300
Dipl.-Ing. M. Heiderich	Engineer responsible for the KWS1 and DKD instruments	23.891
M. Jungen	Technician at SV5	23.891
Dipl.-Ing. T. Kozielewski	Engineer backscattering spectrometer FRM-II	23.891
P. Pickartz	Instrument electronics	23.891
Ms. U. Sausen-Malka	Electronics laboratory	23.891
Dipl.-Ing. R. Schätzler	Engineer responsible for the NSE and BSS1 spectrometer	23.891
K. Schönknecht	Technician at BSS1 and NSE	23.891
Dipl.-Ing. G. Vehres	Electronics engineer, head of electronics laboratory	23.891
Ms. M.-L. Schüsseler	Secretary	
Ms. S. Oubenkhir	Secretary	

Other Scientific Coworkers

Dr. M. Heinrich	Polymer processing, influence of branched polymers	23.300
Dr. St. Kahle	Dielectric spectroscopy, relaxations in complex polymer systems	23.300
Dr. N. Karibiants	Lightscattering, microemulsions, polymer micelles	23.300
Dr. O. Kirstein	Project scientist for backscattering instrument at FRM II	23.891
Dr. W. Leube	Micellarisation and gelation of partially crystallizable polymers	23.300
Dr. J. Sänger	Synthesis of branched polymers	23.300
Dr. W. Schmidt	Instrument responsable IN12 at the ILL	23.891
Dr. J. Stellbrink	Star polymers and living polymerization	23.300
Dr. A. Wischnewski	Instrument development pulsed spin echo, topological constraints in polymer melts	23.891
Dr. habil. R. Zorn	Rubbery electrolytes, glasstransition	23.300

Thesis Students

Dipl.-Chem.B. Abbas	(Univ. Münster) Critical concentration fluctuation; in block-copolymer melts	23.300
Dipl.-Phys. A. Botti	(Univ. Münster) Microscopic deformation in polymer networks	23.300
M.Sc.H. Endo	(Univ. Münster) The role of amphiphilic polymers in the emulsification properties of microemulsions	23.300
Dipl.-Chem. H. Frielinghaus	(TH Aachen) Investigations of critical fluctuations in polymer blends under pressure	23.300
M.Sc. M. Goad	(Univ. Münster) Dynamic modulus and entanglement formation in polymer melts of polymer blends	23.300
Dipl.-Phys. S. Hoffmann	(Univ. Münster) Dynamics of polymer blends	23.300
Dipl.-Ing. H. Kaya	(Univ. Münster) Micellarisation of amphiphilic polymers	23.300
Dipl.-Chem. M. Kreitschmann	(Univ. Münster) Influence of polymer architecture on the aggregation properties of PI-PS blockcopolymers	23.300
Dipl.-Ing. M. Mihailescu	(Univ. Münster) Dynamic of microemulsions - influence of amphiphilic polymers	23.300
Dipl.-Chem. A. Poppe	(Univ. Münster):Micellarisation and exchange kintetics of PEO-PEP diblockcopolymers in selective solvents	23.300
Dipl.-Phys. A. Westermann	(Univ. Münster) Influence of topological interactions and fillers on the chain deformation in polymer networks	23.300

Guests

Dr. A. Arbe	(Univ. of the Baskenland San Sebastian, Spain) Primary and secondary relaxations in polymer glasses	23.300
Prof. J. Colmenero	(Univ. of the Baskenland San Sebastian, Spain) $\alpha - \beta$ relaxations in polymers	23.300
Dr. L.-J. Fetters	(Exxon Annandale) Living polymerisation with small angle neutron scattering	23.300
Dr. H. Montes	(ESPCI Paris) Dynamics of concentration fluctuations and single chains in diblockcopolymers	23.300
Dr. A. Rupprecht	(Univ. Stockholm) Setup and commissioning of a spin apparatus for DNA	23.300
Dr. A. Sokolov	(Univ. Mainz) Dynamics around the glass transition and of biopolymers	23.300
Prof. E. Straube	(Univ. of Halle) Influence of topological constraints on the microscopic deformation in polymer networks	23.300
Dr. S. Borbely	(Research Institute for Solid State Physics and Optics, Budapest) Experiments on the spinodal decomposition of polymer blends by the neutron double crystal diffractometer	23.300
M.Sc. K. Marton	(Univ. of Miskolc, Ungarn) Aggregation behaviour of partially crystalline polymer	23.300
Dr. S. Koizumi	(JAERI Tokai) Heterogeneity in polymer glasses	23.300

Trainees

J. Thelen
S. Thoma
R. Stollenwerk

Crossover from Rouse Dynamics to Local Bond Relaxation

In this work we tried to address the question how the chain dynamics of a polymer crosses over from the universal Rouse dynamics to local bond dynamics observed close to the first maximum of the static structure factor $S(Q)$. This study required to cover a large Q-range ($0.03 \leq Q \leq 3\text{Å}^{-1}$) and to push from the two limits: (i) The investigation of the coherent dynamic structure factor of the single chain $S_{chain}(Q,t)$ (deuterated melt containing a fraction of protonated chains) in the low Q-range allows to characterize the chain relaxation. (ii) The dynamic structure factor $S_{coll}(Q,t)$, revealing the collective dynamics, can be followed on fully deuterated melts in the neighborhood of the first and second maxima of $S(Q)$, i.e. $0.6 < Q < 3\text{Å}^{-1}$. The difficulty of this study lies in the extension towards high Q for $S_{chain}(Q,t)$ and towards low Q of $S_{coll}(Q,t)$, due to the low scattering, cross sections in both cases in the intermediate Q-range ($0.4 - 0.8\text{Å}^{-1}$).

The sample chosen was Polyisobutylene (M_W = 3800). Measurements of $S_{chain}(Q,t)$ were performed by means of the IN11 neutron spin echo (NSE) spectrometer at the Institut Laue-Langevin (ILL, Grenoble, France). The chain dynamics can be well investigated at Q-values lower than 0.5 Å^{-1}; above this value, the scattering of the chain becomes too weak. In the case of the deuterated sample, we used the Jülich NSE spectrometer for thoroughly exploring the Q-range, where the static structure factor of PIB has its first maximum. In addition, previous IN11 measurements at higher Q-values were also available /1/.

A phenomenological description of the dynamic structure factors in terms of stretched exponentials

$$S_{KWW}(Q,t) = \exp\left[-\left(t/\tau_{KWW}\right)^{\beta}\right]$$

leads to the results shown in Figure 1(a) for the average relaxation time $\langle\tau\rangle$ defined as

$$\langle\tau\rangle = \int_0^{\infty} S_{KWW}(Q,t)\,dt =$$

and in Figure 1(b) for the shape parameter β^0. A Q-dependence close to a single power law starting from the lowest Q up to 3.0Å^{-1} is observed for $\langle\tau\rangle$ which is interrupted in the region of the structure factor maximum by an oscillation. This continuity in the time was unexpected. It is worthy to note that the modulation of the time scale of the collective dynamics with $S(Q)$ becomes clear only with the better Q-resolution of the Jülich NSE spectrometer. Concerning the shape of the functions, the collective dynamics shows a more stretched decay than the chain structure factor when approaching to the overlapping Q-regime, as can be deduced from Figure 1(b).

In this phenomenological description, the chain scattering function can be parametrized by KWW laws [Eq.(1)] with a time scale given by a power law in Q $\langle\tau\rangle \approx Q^{-3.1}$, see Fig. 1(a)]. This behavior might be extrapolated to the higher Q-region ($Q > 0.5 \text{ Å}^{-1}$), where a β parameter close to 1 would be expected for this dynamic structure factor. Based on this description for $S_{chain}(Q,t)$ we tried to connect both dynamics by renormalizing this function in the spirit of the Sköld approach /2/. Assuming the chain itself to be the dynamical unit in the sample, the collective structure factor would be given by $S_{coll}(Q,t) = S_{chain}\left(Q/\sqrt{S(Q)},t\right)$. The result of this approach gives an astonishing good agreement between the calculated and the measured average timescales for the collective dynamics (see Figure 2), indicating that the collective response of the chain ensemble can be well connected to the single chain dynamics. However, as expected from the results of the phenomenological KWW description, the shape of the collective response function cannot be predicted in this way.

These results strongly support a common underlying mechanism driving both dynamics. The timescale of the collective dynamics seems to be determined by the single chain dynamics, implying an essential role of the intramolecular interactions in the collective dynamics. The discrepancies found in the functional form would be related to the influence of the inter- interactions on the collective dynamics.
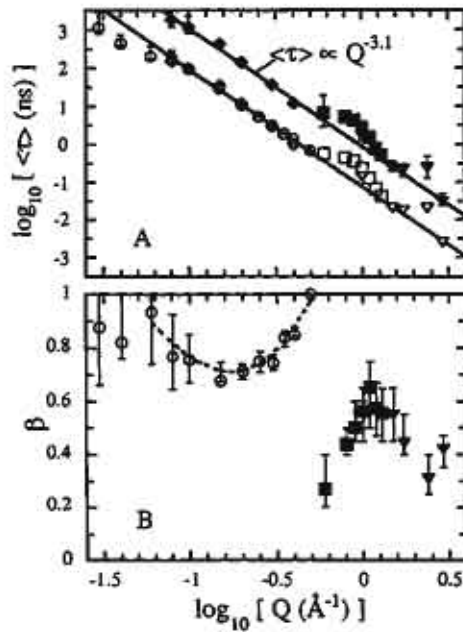

Figure 2: Q-dependence of the product $<\tau>Q^{3.1}$ in comparison to the results from the modified Sköld Ansatz for the coherent scattering function starting from the single chain structure factor (solid line).

/1/ D. Richter, A. Arbe, M. Monkenbusch, J. Colmenero, B. Farago and R. Faust, Macromolecules 31, 1133 (1998)
/2/ K. Sköld, Phys. Rev. Lett. 19, 1023 (1967)
/3/ L. Harnau, R. G. Winkler, and P. Reineker, J. Chem. Phys. 102, 7750 (1995); J. Chem. Phys. 106, 2469 (1997)
/4/ See, e.g., G. Allegra and F. Ganazzoli, Advances in Physical Chemistry Vol. 75, 265 (1989)

A. Arbe, M. Monkenbusch, J. Colmenero, D. Richter FE 23.30.0

Figure 1: (a) Average times $<\tau>$ obtained from the KWW description of the single chain structure factor at 390 K (◆) and 470 K (O), and the collective structure factor: IN11 /1/ (▼) and new Jülich data (■) at 390 K. The empty symbols correspond to the shifted timescales to 470K. (b): Q-dependence of the shape parameter β.

Microscopic Dynamics of a confined glass-forming liquid

The dynamics of glass-forming liquids in confinements is currently a topic of high interest for theory as well as experiment. The theoretical interest is mainly based on the question of the existence of a length-scale of the glass-transition, e.g. the „cooperativity length" [1]. Experimental studies have been enabled recently by the commercial availability of nanoporous glasses as Gelsil and Vycor.

Most of these studies have used dielectric spectroscopy as a tool to probe the dynamics of the liquids. The most recent results [2] indicate that the dynamics near the glass-transition is **accelerated** in the confinement–in accordance with cooperativity length arguments. Nevertheless, some uncertainty is involved in these experiments because it is not obvious how to separate the dielectric susceptibility of the enclosed liquid out of the total response measured.

The aim of this experiment was to study the influence of spatial confinement on the dynamics of a glass-forming liquid on a microscopic length scale by using neutron scattering. Because of the weak interaction of neutrons with matter the correction for the matrix contribution reduces to a simple subtraction of an „empty" sample.

The experiments were done on a sample of Salol (phenylsalicylate) in Gelsil A025, porous amorphous silica with an average pore diameter of 25 Å. In order to avoid adsorption of the Salol molecules to the silica surface, the Gelsil glass was treated with hexamethyldisilazane covering the internal surface with trimethylsilyl groups. Deuterated silazane was used to reduce inelastic scattering from its methyl group dynamics. A reference sample of bulk Salol was measured under identical conditions. The experiments were done on IN6, a time-of-flight spectrometer, and on IN16, a backscattering spectrometer, at the Institut Laue Langevin in Grenoble.

Fig. 1 shows a representative IN6 spectrum at low temperature. Detectors at different angles were interpolated to constant Q, the absolute units of $S(Q,\omega)$ have been established by normalising to the elastic intensity at 2 K. Because the resolution function of the IN6 has a strong „tail" the elastic line was subtracted.

The most striking result of this experiment can be seen in the **vibrational** dynamics: While the inelastic intensity (and consequently the vibrational density of states) is identical for confined and bulk Salol for energies ≥ 1.5 meV it is strongly reduced for smaller energies.

Interestingly, this reduction can be qualitatively explained in a simple picture where the inelastic scattering is due to sound waves: The confinement introduces an upper boundary for the wavelength which corresponds to a limit in frequency below which sound waves are forbidden. The inset of fig. 1 shows the ratio between the inelastic scatter-
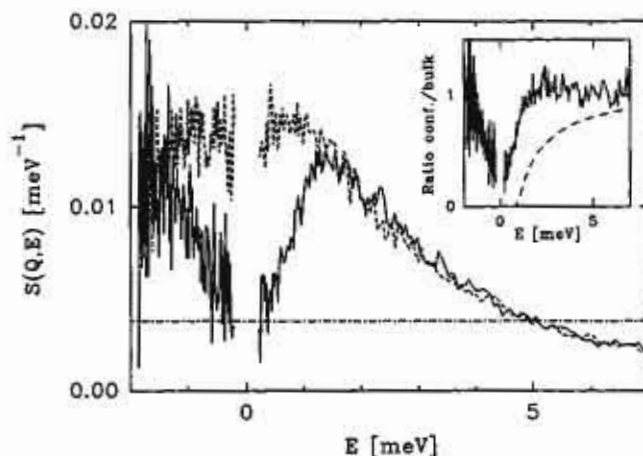
Fig. 1: Scattering function $S(Q,\omega)$ of confined (continuous line) and bulk (dashed line) Salol at 100 K obtained from IN6 at constant $Q = 1.64$ Å^{-1}. The inset and the dot-dashed line (sound wave level) are explained in the text.

ing of confined and bulk sample compared to a crude model assuming spherical confinements: The eigenmodes of vibrating spheres with the elastic constants of bulk Salol in a completely rigid confinements were calculated. The distribution of eigenfrequencies was averaged using a distribution of diameters, 25 ± 8 Å. The location of the cut-off at about 1 meV is well described. This gives support to ideas of the „sound wave nature" of low frequency vibrations in glasses [3]. But the detailed shape is not correctly represented by the model probably because the pores in Gelsil are not spherical but rather form a network of cylinders. A model-free test experiment with samples having *different pore diameter* will be done soon: From the ideas presented here we predict that the cut-off scales inverse-proportionally with the diameter.

It has to be noted that despite this intriguing possibility of explaining the *ratio* of the vibrational densities of state their *absolute values*–as usual in glasses–show a strong enhancement (boson peak) over the level expected from the Debye theory of sound waves, $S(Q,\omega) \propto g(\omega)/\omega^2 \equiv const$, indicated by the dot-dashed line in fig. 1.

In order to explore the **relaxational** dynamics at temperatures near and above the glass transition ($T_g = 218$ K) inelastic neutron scattering data from IN6 and IN16 were combined in the time domain. After subtracting the empty Gelsil matrix the data were Fourier transformed and divided by the respective resolution functions to obtain the dynamic structure factor $S(Q,t)$. The results are shown in fig. 2. Due to the strong crystallisation tendency of bulk Salol no reference data could be obtained between 250 and 310 K.
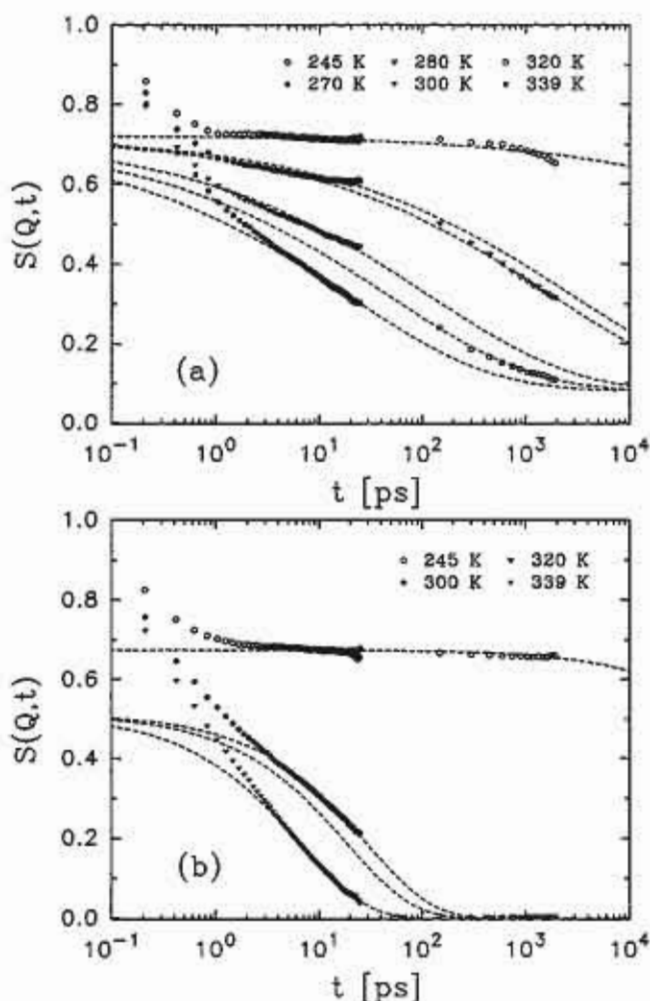
Fig. 2: Dynamic incoherent structure factor $S(Q,t)$ of confined (a) and bulk (b) Salol obtained from IN6 and IN16 by Fourier transform, $Q = 1.42$ Å^{-1}. The dashed lines represent the Kohlrausch fits explained in the text.

As a first approach to obtain relaxation times from these data, the Kohlrausch function $f \cdot \exp(-(t/\tau_K)^\beta)$ was fitted. The fits were unsatisfactory for confined Salol. This problem could only be resolved by assuming an elastic contribution, i.e. a fraction of about 13% of Salol molecules being completely immobilised. Nevertheless, the fit is still not perfect and the possibility of a continuous distribution of partially immobilised molecules has to be taken into account.

Fig. 3 shows the average logarithmic relaxation times $\langle \log_{10} \tau \rangle$ for both samples. It has to be noted that the Kohlrausch exponents β were significantly smaller for confined Salol: $\beta = 0.31$, to be compared with the bulk value $\beta = 0.67$. This broadening of the relaxation corresponds to what was earlier detected by dielectric measurements [2].

For comparison the same quantity, $\langle \log_{10} \tau \rangle$, obtained from those dielectric measurements on identical samples has
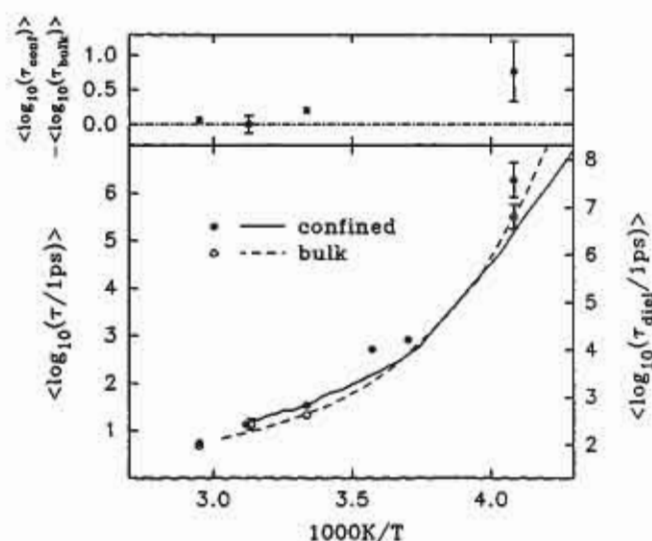

Fig. 3: Circles, left axis: average logarithmic relaxation times obtained from the fits shown in fig. 2 (filled: confined, open: bulk). Lines, right axis: dielectric average logarithmic relaxation times [2] (continuous: confined, dashed: bulk). The upper part of the graph shows the differences between the neutron scattering $\langle \log_{10} \tau \rangle$ of confined and bulk Salol.

been added as lines to fig. 3. (Because of the Q dependence of neutron scattering data no *identity* of the values can be expected but only *proportionality*. Therefore, the axis of the dielectric data has been shifted to match in the high temperature region.) It can be seen that for bulk Salol the dielectric and neutron scattering relaxation times are proportional over the whole temperature range. In contrast, the data from confined Salol behaves opposedly for the two experimental methods: The relaxation observed by neutron scattering seems to be **slower** in the confinement at low temperatures, while the dielectric data suggest **faster** dynamics.

In order to clarify this crucial question future experiments have to be done in which the crystallisation of the reference sample is suppressed, different confinement sizes are studied, and higher resolution in the backscattering part is deployed.

[1] E. Donth, „Relaxations and Thermodynamics in Polymers" (Akademie Verlag, Berlin, 1992)
[2] M. Arndt, R. Stannarius, H. Groothues, E. Hempel, F. Kremer, *Phys. Rev. Lett.* 79 2077 (1997)
[3] U. Buchenau, A. Wischnewski, D. Richter, B. Frick, *Phys. Rev. Lett.* 77 4035 (1996)

Reiner Zorn, Lutz Hartmann*, Dieter Richter, Friedrich Kremer*, Bernhard Frick*

FE 23.15.0
*Universität Leipzig
+Institut Laue Langevin, Grenoble/Frankreich

Isotropic Lifshitz Critical Behavior in a Mixture of a Homopolymer Blend and Diblock Copolymer

A three component mixture of a critical binary homopolymer blend and the corresponding symmetrical diblock copolymer leads to a rather complex phase diagram. The main interesting issue of those systems might be the occurrence of the isotropic Lifshitz critical point. For this universality class one expects significant renormalization due to thermal composition fluctuations as its upper critical dimension - above which fluctuations are not relevant- is two times larger ($d_U=8$) than that of binary blends ($d_U=4$). This makes it difficult to calculate the critical exponents. They are not known neither from theory nor from earlier experiments.

In Figure 1 the phase diagram of a ternary mixture of a partially deuterated poly(ethyl ethylene), PEE, and poly(dimethyl siloxane), PDMS, has been depicted versus the copolymer content. It was determined from measurements of thermal composition

PEE/PDMS/PEE-PDMS
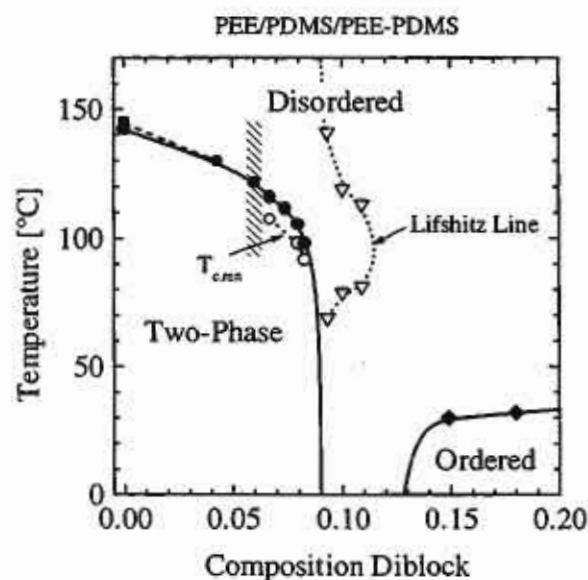
Figure 1: Phasediagram

fluctuations with small angle neutron scattering. The disordered regime at high temperatures is separated by the Lifshitz line; at diblock compositions below and above the

Lifshitz line, the maximum intensity occurs at $Q=0$ and at a finite Q-value, respectively. This also means that below this line ordering occurs on a macroscopic scale by phase separation while above this line ordering occurs on a mesoscopic scale. The Lifshitz line of this system is estimated at the constant diblock composition of 6%. The observed one, however, depends on composition; at around 100°C it is modified between 9% and 11%. In Figure 2 the structure factor S(Q) of
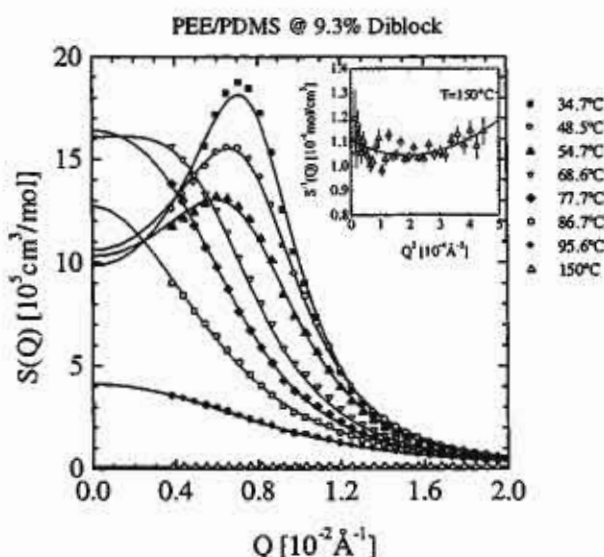
PEE/PDMS @ 9.3% Diblock

Figure 2: Structure factor

the 9.3% sample is shown as an example: For temperatures above 141°C (see inset) and below 69°C the maximum intensity occurs at a finite Q while for temperatures in between at Q=0. Mesoscopic ordering could only be observed for diblock contents of $\Phi=15\%$ and larger.

The Lifshitz critical point is a multiple critical point at the connection of the macroscopic and mesoscopic ordering transition lines. It can, however, only be realized if fluctuations are not relevant; thermal fluctuations destroy the Lifshitz point as according to the Ginzburg criterion they stabilize the disordered phases in blends and diblock copolymers differently strongly. In

Figure 3 the inverse susceptibility $S^{-1}(0)$ versus $1/T$ is shown. The critical temperatures obtained at $S^{-1}(0) = 0$ decrease with diblock
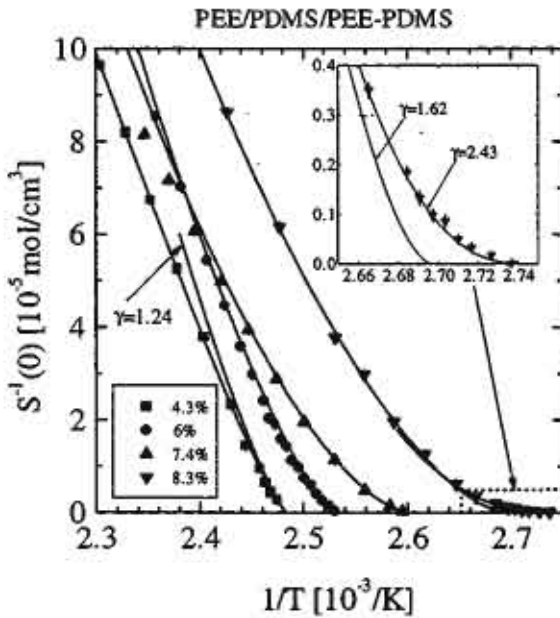

Figure: 3 Inverse susceptibility

content as depicted in the phase diagram. The $\Phi = 4.3\%$ mixture behaves similarly to blends, namely, from high to low temperatures a transition from *mean field* to *3d-Ising critical behavior* is observed. This is demonstrated by the fit (solid line) of a crossover function which has been extensively used for polymer blends. A second line through some of the 4.3% data represents the asymptotic 3d-Ising scaling law with the critical exponent $\gamma = 1.24$. The inverse susceptibilities of the samples with the diblock content of $\Phi = 6, 7.4$ and 8.3% are characterized by curvatures far beyond that of the $\Phi = 4.3\%$ one. Such larger curvature corresponds to an increase of the γ-exponent, indicating a crossover to the universality class of the *isotropic Lifshitz case*. These susceptibilities could be analyzed by the scaling law according to $S^{-1}(0) = C_+ t^\gamma$ with the reduced temperature, $t = (T - T_c)/T$, and the critical exponent, γ (solid lines). A similar analysis has been performed for the correlation length according to $\xi = \xi_{0+} t^{-\nu}$ with the critical exponent ν. The obtained

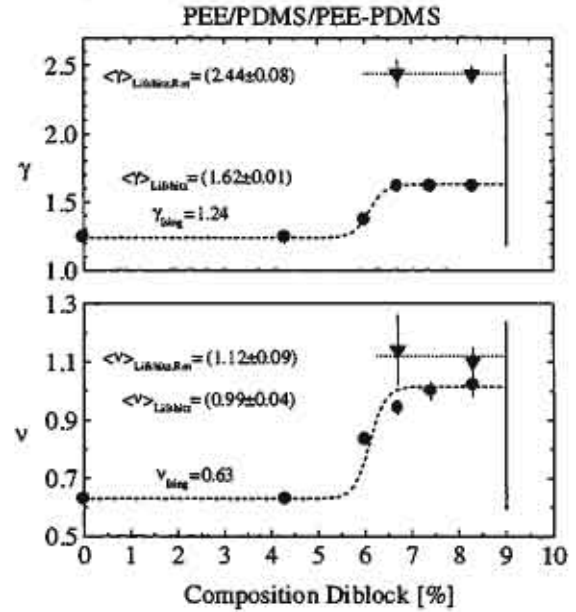critical exponents are plotted versus the diblock content in Figure 4. In two samples

Figure 4: Critical exponents

with composition 6.7% and 8.3% an additional crossover was observed very near the critical temperature as demonstrated for the 8.3% sample in the inset of Figure 3. The values of the corresponding exponents are also plotted in Fig.4. Such an additional crossover was only observed if the experiments were performed sufficiently slowly near T_C. We abbreviate this additional crossover as the *renormalized Lifshitz critical behavior*. An interpretation of this crossover might be related to rearrangements of the diblock copolymers caused by the strong thermal fluctuations which further stabilize the sample against phase decomposition. The corresponding critical temperatures have been plotted as open dots in the phase diagram of Figure 1.

Dietmar Schwahn, Kell Mortensen*, Henrich Frielinghaus*, Kristoffer Almdal*

Constrained dynamics of ordered star polymer solutions: determination of the microscopic confinement size using NSE

Star polymers, i.e. f monodisperse linear chains tethered to a central microscopic core, can actually be viewed as hybrids between polymer-like entities and colloidal particles establishing an important link between these different domains of physics. With increasing concentration star polymers show ordering phenomena as known from hard sphere fluids, but opposite to those star polymers start to interpenetrate each at the overlapp concentration $c^* = \frac{3}{4\pi R_g^3} \cdot \frac{N_A}{M_w}$. The structural properties of dense star polymer solutions can be described on a microscopic basis by a logarithmic interaction potential[1]. However, the dynamics of star polymers are far less understood, especially in dense solutions. Recently, a dynamic light scattering study[2] gave evidence for the existence of a structural glass transition above c*. Unfortunately, due to the experimental accessible Q range, light scattering is restricted to a mesoscopic spatial resolution of several hundred nanometers. Therefore, the interaction effects in dense star polymer solutions, which are most pronounced at the peak of the static structure factor $Q_m \approx 0.05\text{Å}^{-1}$, cannot be investigated using light scattering techniques. These problems can be overcome using neutron spin echo spectroscopy (NSE), a high resolution neutron scattering technique with an spatial resolution of several tenths of angstroms and an experimental time window in the pico- and nanosecond range.

Here we report an experimental study on the microscopic dynamics of an 18-arm polyisoprene star polymer, M_w=7500g/mol per arm, in a good solvent methylcyclohexan well above the overlapp concentration c^*. Using the H/D labeling technique it was possible to synthesize star polymers where only the inner quarter, the *core*, of each star polymer was protonated, i.e. visible for the NSE experiment. Not only, this was the first NSE study on dense star polymer solutions, moreover, during this study we were able to extend the NSE time range for the first time up to 350ns. This could be realized using the new spin echo spectrometer IN15 at the ILL (IN15 is a joined project of IFF(FZ Jülich), HMI(Berlin) and the ILL(Grenoble), specially designed for the use of long neutron wavelength). This extreme high resolution was necessary to investigate the microscopic dynamics of dense star polymer solutions above c*. In this concentration regime star polymers show a pronounced *deGennes* narrowing at Q_m. This very slow structural relaxation can not be resolved in the conventional time window of NSE instruments. I.e., until the development of IN15 it was not possible to decide wether the intermediate scattering function decays to a final plateau or not.

Fig. 1 shows the normalized intermediate scattering functions $S(Q,t)/S(Q,0)$ at Q_m=0.075Å at three different concentrations, 20%, 25, and 30% volume fraction($c^* \approx 10\%$). It can clearly be seen that at each concentration a final plateau is reached at $\tau \approx 180$ns. Due to the increasing amount of structural arrest with increasing concentration, the height of the plateau depends on concentration. The restricted motion of the star polymers can be approximated by the following dynamic structure factor (solid lines in fig. 1):

$$S(Q,t) = \exp(-1/3\, Q^2 <r^2>) + \left[1 - (\exp(-1/3\, Q^2 <r^2>))\right] H(Q,t)$$

with $H(Q,t)$ the Zimm dynamic structure factor[3] and $<r^2>$ the mean square displacement or the average size of the star confinement. The obtained values of

$\langle r^2 \rangle \approx 15$ Å are considerably smaller than the size of the star, $R_g=75$Å. The insert of fig. 1 shows the the concentration dependence of $\langle r^2 \rangle$ compared to those of the blob size ξ obtained from dynamic light scattering experiments. Obviously the star confinement relates to the blob size of the entangled star polymer solution. For all concentrations we obtain a characteristic ratio $\langle r^2 \rangle/\xi \approx 1.42$. The obtained slope is somewhat smaller than the predicted value 3/4 from scaling theory.

Thus, the available thermal energy kT enables each star core to perform a restricted motion over a spatial extent equal to the blob size ξ of the surrounding entangled star polymer solution. This relationship between kT and ξ is also known from solutions of linear polymers, and emphasizes the hybrid character of star polymers. These first results are a promising approach to elucidate the complex dynamics of entangled star polymer solutions by combining NSE and DLS.
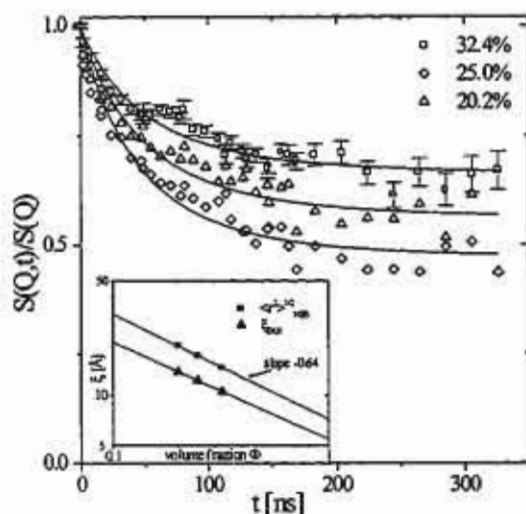
Literature

1. C. N. Likos, H. Löwen, M. Watzlawek, B.Abbas, O. Jucknischke, J. Allgaier, and D. Richter; *Phys. Rev. Letters*, **80**, 4450, (1998).
2. J. Stellbrink, J. Allgaier, and D. Richter; *Phys. Rev. E* **56**, 3772 (1997).
3. E. Dubois-Violette, P. G. deGennes; *Physics*, 3,181 (1968)

J. Stellbrink, J.Allgaier, M. Monkenbusch and D. Richter IFF, FZ Jülich

G. Ehlers and P. Schleger, ILL, Grenoble
FE 23.30.0

Amphiphilic block copolymers:
Micellarization and Emulsification Properties

Recently, we reported the synthesis of new poly(ethylene-propylene)-polyethylene oxide (PEP-PEO) block copolymers /1/. PEP-PEO is a combination of the highly apolar aliphatic polyhydrocarbon PEP, soluble in non-polar solvents, and PEO, which is polar and watersoluble. The material also can be regarded as the polymeric equivalent to the low molecular weight C_mE_n surfactants due to the same chemical structure. In this report we will focus on micellarization in aqueous solution and on emulsification properties in water/oil microemulsions of PEP-PEO block copolymers.

1. Micellarization

The aim of this work was to study the structural changes of the micelle by varying systematically the block copolymer composition. This study was ideally carried out by small angle neutron scattering (SANS) involving contrast variation experiments. The system PEP-PEO/water is particularly suitable for this investigation for two main reasons:

i) The block copolymer can be prepared free of homopolymer with small polydispersities ($M_w/M_n < 1.04$) by anionic polymerization for any desired molecular weight and composition. ii) Due to the strong hydrophobicity of PEP the cmc is very low, the micelles have high aggregation numbers, and self-assembling still occurs in a very asymmetric block copolymer composition with high PEO content.

Six block copolymers were investigated by SANS which differ in the PEO content over a large range up to a factor of 24, while the PEP size was kept constant in all polymers. Data analysis was performed by a spherical core/shell model with either constant or radially decreasing density profile in the corona and constant density in the core for both cases.

It was found that micelles with low PEO content could be analyzed by the model with homogeneous density distribution. The fit results reveal that these micelles have large aggregation numbers, P, large cores and thin coronas with high polymer concentration. On the other hand micelles formed by the polymers with high PEO content could be
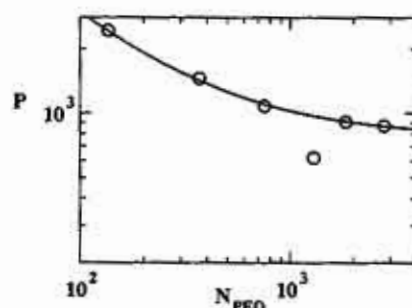

Figure 1: Aggregation number versus degree of PEO polymerization

analyzed only by the core/shell version with radial decreasing polymer density in the shell. In these cases the aggregation numbers as well as the core radii of the micelles are smaller, while the overall micellar radii are large. The polymer concentration in the corona is low and falls off with $r^{-4/3}$ as predicted for star polymers in a good solvent. Obviously, due to the increase in PEO content the micelles undergo a transition from a micelle with homgeneous density distribution to a micelle with starlike or hairy structure. This can also be seen from Figure 1 where the aggregation number is plotted as a function of the degree of PEO polymerization, N_{PEO}. A strong decrease of P is visible for micelles with increasing PEO content for small N_{PEO} while at higher N_{PEO} the aggregation number is within experimental error constant.

This behavior can be interpreted in terms of two thermodynamical models. The first one was developed by Nagarajan and Ganesh /2/ on the basis of Flory-type mean field calculations. This model quantitatively predicts that $P \sim N_{PEO}^{-0.51}$ for block copolymers in water with PEO as the soluble block. The solid line in Figure 1 well represents this behavior and confirms the validity of this model for PEP-PEO micelles with homogeneous density distribution and high polymer concentration in the corona. The second model was presented by Halperin /3/. He has performed a scaling analysis on

micelles with starlike structure in which the r^- $4/3$ density profile is considered. The model predicts that P is independent of N_{PEO} for block copolymer micelles in which the soluble part is much larger than the core forming block. Figure 1 demonstrates the validity of this prediction for the micelles with high PEO content and starlike structure.

2. Emulsification properties

Non-ionic C_mE_n form microemulsions together with water and oil. In this project, we investigate the emulsification properties of PEP-PEO which is the polymeric equivalent to C_mE_n. It is important to note that the non-polar PEP-block is soluble in oils, i.e. aliphatic hydrocarbons. For most other amphiphilic block copolymers the hydrophobic part is insoluble in oils and therefore such materials cannot be used for our investigation. Due to the high amphiphilicity of PEP-PEO, it is not expected that the pure polymer also form microemulsions together with water and oil. For that reason we focused on using PEP-PEO as additive to C_mE_n.

The investigations were carried out using the surfactant $C_{10}H_{21}$-(O-CH$_2$-CH$_2$)$_4$-OH ($C_{10}E_4$) together with equal amounts of water and decane as the oil. Several block copolymers of different compositions and molecular weights were examined. The molecular weights ranged between 1,000g/mol and 22,000g/mol for the PEP block and between 1,000g/mol and 50,000g/mol for the PEO block.

Adding small amounts of polymer to $C_{10}E_4$, we found that the surfactant efficiency increased dramatically. This means that much less of the surfactant mixture is needed to transform a certain amount of water and oil into a microemulsion than it is the case for pure $C_{10}E_4$. For example the addition of 10% of polymer to $C_{10}E_4$ caused an increase in surfactant efficiency by a factor of 3 to 5. This behavior is documented in Figure 2. Without the addition of polymer (left side) the amount of surfactant used in the experiment only allows the solubilization of small amounts of oil and water in the microemulsion phase. If enough polymer is added, oil and water is solubilized (right side).
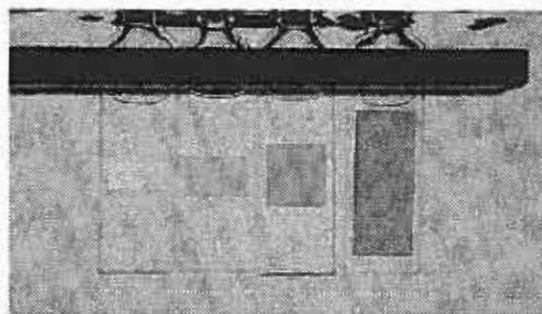

Figure 2: Expansion of the microemulsion phase in the system water/decane/$C_{10}E_4$ with increasing amount of polymer: uppper phase: oil excess phase; middle phase: microemulsion; lower phase: water excess phase.

The increase in surfactant efficiency was found for all PEP-PEO block copolymers. In additional experiments it was found that the polymer also increases the efficiency of other nonionic and ionic surfactants. For this reason our finding is expected to be very valuable for commercial application /4/. From this standpoint another feature of the polymeric additive is important. Without the polymer microemulsions, having higher contents of surfactants, form lamellar phases, which are disadvantageous for washing processes. If the system contains polymer lamellar phases were not found.

In order to explain the effect, further experiments are now on the way. It is planed to investigate the structure of the microemulsions and of the block copolymers by small angle neutron scattering experiments.

References /1/J. Allgaier, A. Poppe, L. Willner and D. Richter, Macromolecules 30, 1582, (1997).
/2/R. Nagarajan, K. Ganesh, J. Chem. Phys., 90, 5843, (1989).
/3/A. Halperin, Macromolecules 20, 2943, (1987).
/4/ J. Allgaier, L. Willner, D. Richter, B. Jakobs, T. Sottmann und R. Strey, not yet published patent application DE 19839054.8-41.

L. Willner, A. Poppe, J. Allgaier, D. Richter, FE 23.30.0
B. Jakobs, T. Sottmann, R. Strey, Universität Köln

Probing a Second Order Phase Transition in a Perovskite by Rotational Tunnelling Spectroscopy

Because of its simple tunnelling spectrum and the large tunnel splitting of $\hbar\omega_{A\to T} = 58\mu eV$ $(NH_4)_2PdCl_6$ was a candidate to show the large isotope effect in rotational tunnelling. Unexpectedly, the deuterated compound $(ND_4)_2PdCl_6$ transforms from the common $Fm3m$ high temperature (HT) phase into a monoclinic low temperature (LT) phase $P2_1/n$ at T_c=30.2K [1]. The predominant change at this phase transition is a large angle rotation of the ammonium tetrahedra. Similar phase transitions occur in many perovskites A_2BC_6 [2]. They are usually of second order, the low temperature phase is mostly tetragonal and the characteristic soft mode is a libration of the BC_6 octahedra.

X-ray and neutron crystallography of the mixed protonated/deuterated ammonium palladium chloride showed that T_c approaches zero at a deuteration $c_D \sim 0.3$. It was the aim of the experiment to study this well-known phase transition via rotational tunnelling of the ammonium ions. Due to proton exchange NH_4 and NH_3D can be used as probes. Spectra at low degree of deuteration, $c_D = 0.1$, were taken at the backscattering spectrometer in Jülich in an energy range up to $33\mu eV$, samples with c_D=0.3 and 0.5 were investigated using IN10B of the ILL, Grenoble. Here the energy regime could be extended up to $60\mu eV$.

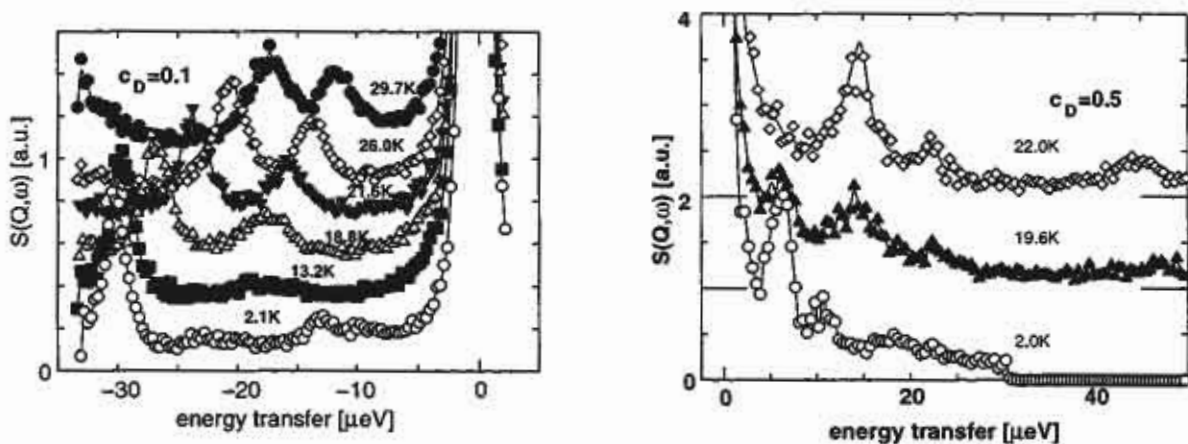Figure 1: Tunnelling spectra of $(NH_4)_{2(1-c_D)}(ND_4)_{2c_D}PdCl_6$

At the highest temperatures, e.g. $T = 29.7K$ at $c_D = 0.1$, the sample is in the HT cubic phase and spectra can be straightforwardly explained: the lines at 17.3/34.6(partly visible)μeV represents the known T→E/A→T splitting of the threedimensinal NH_4 rotor in a tetrahedral environment. The new single line at 11.9μeV is due to NH_3D. Its intensity is quantitatively described by the statistical occurrence probability of NH_3D at full H-D exchange and the inelastic structure factor of a one-dimensional threefold rotor. The transition energy is close to that estimated by a rule of thumb from a potential strength obtained by scaling up the NH_4-potential by the ratio of the related rotational constants [3].

For $c_D = 0.5$ fully protonated ammonium ions are a minority. The main intensity is contained in the NH_3D tunnelling line. The spectrum measured at T=22K has the same explanation as above. At $T = 2K$ the sample is in the monoclinic LT phase. The tunnel splittings (cor-

rected for temperature effects) have decreased by a factor ~ 2 which can be related to a $\sim 30\%$ increase of the height of the rotational barrier of both species.

The most interesting regime is that of the critical fluctuations above T_c before the transformation to the LT phase. Unexpectedly the two ammonium isotopomers - occupying crystallographically identical sites - develop differently with lowering temperature. While NH_4 lines just shift according to the usual T-effect, the NH_3D line broadens and represents finally a wide distribution of tunnel splittings. The reason of this behaviour is searched in different properties of NH_4 and NH_3D and disorder of mixed crystals.

Similar broad tunnelling spectra are measured in mixed ammonium-alkali halides. It is well known that $(KI)_{1-x}(NH_4I)_x$ forms a dipolar glass phase at low temperature. In this system the discrepancy between molecular and site symmetry leads to an off-centre position and a tilted orientation of the ammonium ion. Due to polarization of the environment a strong induced dipole moment is observed. The corresponding long range interaction in combination with occupational disorder leads to an orientational glass phase around $x \geq 0.17$ [4].

In ammonium hexahalo compounds distances between the ammonium ions are larger than in ammonium halides. Consequently the quickly, $\sim r^{-7}$, decaying octopole-octopole interaction between them is has only a weak influence on the ammonium rotational potential [5]. The situation becomes different for NH_3D. Due to its lower symmetry the molecule represents a dipole with a long-range, $\sim r^{-3}$, dipole-dipole interaction with other NH_3D's. Because of missing experimental information a possible size of the electrical dipole moment is es-

timated the following way: We assume that the crystallographic ammonium site coincides with its centre-of-mass. In an undistorted lattice this is also the centre of charges of the environment. The centre-of-charges of the ammonium ion, however, is still at its centre-of-geometry: the nitrogen position. This separation of positive and negative charges leads to a calculated dipole moment of the NH_3D ion of about 0.1D. At the intermolecular distance of nearest ammonium ions the dipole-dipole energy amounts to ~ 20k, k being the Boltzmann constant. In the temperature regime around T_c where the lattice approaches an instability the weak additional dipole-dipole interaction of the NH_3D molecules can determine locally the shape of the rotational potential, eventually towards that of the final LT phase. The random occupation of ammonium sites with NH_3D leads to orientational disorder in a likely orientational glass phase.

Further experiments are necessary and planned to verify the model.

[1] I.P. Swainson, B.M. Powell, R.D. Weir, J. Sol. State Chem. **B131**,221 (1997)

[2] J. Winter and K. Roessler, Phys. Rev. **B21**,2920(1980)

[3] Y. Ozaki, K. Maki, K. Okada, J.A. Morrison, J. Phys. Soc. Jpn. **54**, 2595(1985)

[4] J.-F. Berret, C. Bostoen, B. Hennion, Phys. Rev. **B46**,13747(1992)

[5] M. Prager, W. Press, K. Roessler, J. Mol. Struct. **60**,173(1980)

M. Prager, H. Grimm, P. Schiebel
FE023.15.0

Design studies of the phase space transforming backscattering spectrometer for the FRM II

Based on the design and performance of existing backscattering spectrometers (e.g. [1], [2]) a next generation high flux instrument shall be installed at the cold neutron source of the FRM-II reactor in Munich in 2003.
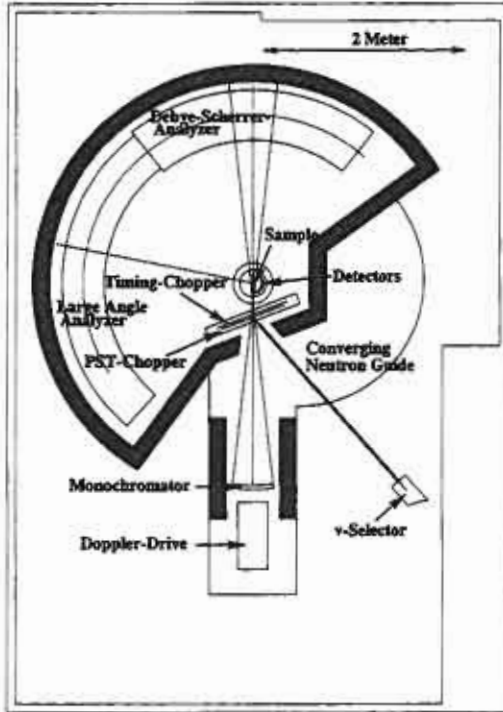

Figure 1: Schematic sketch of the backscattering spectrometer.

In addition to well established experiments like the IN16 at Grenoble we will use a new device not only to enhance the neutron flux at the backscattering energy ($E_0 = 2.08$ meV using the lattice vector $\vec{G}_{Si111}$), but also to optimize the ratio of signal to noise and the width and shape of the elastic peak. This device is called a Phase-Space-Transformation chopper [4]. The PST chopper consists of a disk of diameter 1.2 m. The disk is divided into six sectors as a result of the analyzer geometry and alternate sectors will be covered with pyrolitic graphite crystals (lattice vector $\vec{G}_{PG002}$). The basic principle is as follows (Fig. 2): The incoming beam of neutrons has an angular divergence due to the critical angle of reflection inside the neutron guide ($\alpha \approx 1^\circ$ around direction $\vec{n}_{NG}$) and a

large longitudinal spread of wave vectors Δk is 'extracted' due to the offered broad distribution η of $\vec{G}_{PG002}$ lattice vectors. After diffraction, the outgoing neutron beam will have a smaller spread Δk but a broader divergence ($\approx 9^\circ$). Ideally, the arc of diffracted neutrons is aligned orthogonally to the outgoing wave vectors by the chosen speed $\vec{v}_{PST}$ of the chopper.

In order to accommodate the enlarged divergence, both the PST chopper and the Si monochromator are composed of many individual crystals. Qualitatively, this 'phase space transformation' enhances the usable flux (increased divergence) without impairing the energy resolution of the instrument. The optimiza-

Figure 2: MC simulation of the Bragg diffraction from PG crystals with $\eta = 4$ and $\alpha = 1^\circ$. Chopper speed: 300 m/sec.

tion of the instrument thus implies the two questions:

(i) which values are to be chosen for the vectors $\vec{v}_{PST}$ and $\vec{n}_{NG}$ and

(ii) which orientational correlation is to be maintained within the individual pairs of $\vec{G}_{PG002}$ and $\vec{G}_{Si111}$ vectors?

In order to inspect those questions, the mapping of two distributions (incoming wave vectors $p_i(\vec{k}_i)$ and lattice vectors $p_G(\vec{G})$ onto the distribution of outgoing wave vectors $p_f(\vec{k}_f)$ via momentum and energy conservation [3] has been extended to possibly misaligned central vectors and moving crystal. Since for neutrons, energy is quadratic in $\vec{k}$, the map is equivalent to the Radon transform [5] of the product $p_i * p_G$ along the direction $< \vec{k}_i > +\vec{v}$. It is interesting to note that this map is also the basis for image reconstruction in medical applications of x-ray transmission (CT).
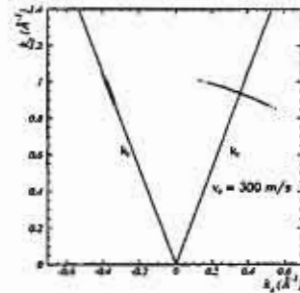
The results are:

(i) The condition of 'orthogonality' depends on the gain factor η/α, only (Fig. 3). A value of 4 entails a speed of $v_{PST} \approx 300$ m/sec and a composition of e.g. 10 or 5 tilted PG crystals with an individual mosaic of $0.4°$ or $0.8°$, respectively. Vertical focusing favours the smaller, costs the larger individual mosaic.
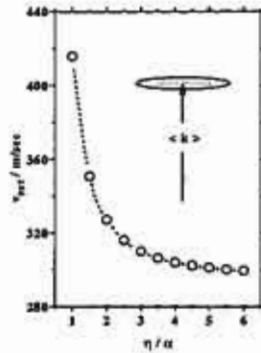

Figure 3: Relation between the gain factor (beam divergence/PG mosaic) and the speed of the PST chopper.

(ii) The Doppler effect experienced by the tilted crystals is non negligible. A partial beam (divergence $\Delta\alpha = 0.1° - 0.2°$) emerging at $NGdev \geq 0$ off from the direction $\vec{n}_{NG}$ needs tilt angles of the PG crystals $PGdev$ according to

$$PGdev = {}^{+4.8}_{-3.6} \sqrt{NGdev} \qquad (1)$$

whereas $NGdev < 0$ cannot be used.

(iii) Those two solutions supply the left and right halves of the Si monochromator. The inclination is $Sidev = {}^{2.2}_{2.5} PGdev$. The deviation of those mirror conditions from the usual value of 2 results from the moving PG crystals. Δk in μeV and relative intensity of the partial beams ($\delta\alpha = 0.1°$) after passing the PG and Si crystals are displayed in Fig. 4. As can be seen, the intensity is negligbly small for regimes with unacceptable resolution.

(iv) The chosen origin or reference beam for the angular fluctuations in the scattering plane ($NGdev, PGdev, Sidev$) refers to the geometrical direction of the neutron guide and untilted crystals. It follows from Fig. 4 that this orientation of the spectrometer relative to the neutron guide has to be shifted by about the limiting angle of total reflection for maximum intensity.
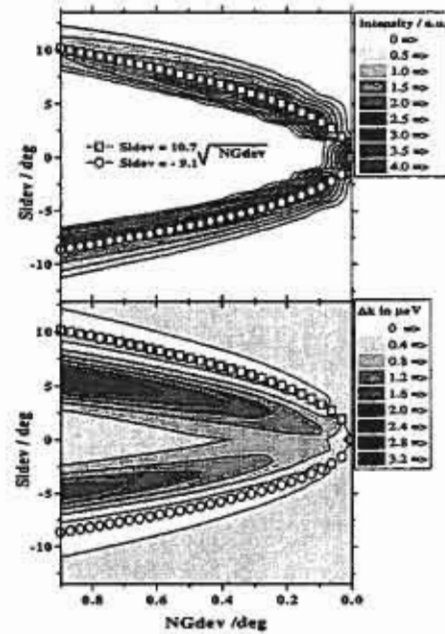

Figure 4: Energy resolution and relative intensity of a partial beam after passing the PG and Si crystals. Angular offset: $\Delta\alpha = 0.1°$ around $\vec{n}_{NG}$.

In order to optimize the spectrometer we look for alternatives to the PST chopper. Today, it seems to be possible to increase the neutron flux using a focussing supermirror guide ($m \approx 3.5$) and a PG crystal with a large mosaic ($\eta_{FWHM} \approx 5°$). This would be advantageous due to mechanical reasons (lower weight and size of the chopper disk) and it would also result in a much simpler construction. To make a decision between the alternatives, both will be checked using an analytical and Monte Carlo method.

[1] B. Alefeld, T. Springer, A. Heidemann,
    Nucl. Sci. & Eng. 110 (1992) 84

[2] P. M. Gehring, C. W. Brocker,
    D. A. Neumann,
    Mat. Res. Soc. Symp. Proc. 376 (1995) 113

[3] H. Grimm,
    Nucl. Instr. & Meth., 219 (1984) 553

[4] J. Schelten, B. Alefeld,
    in Proc. Workshop on Neutron Scattering
    Instrumentation for SNQ, ed. by R. Scherm,
    H. H. Stiller, report Jül-1954 (1984)

[5] J. Radon,
    Ber. Verh. Sächs. Akad. 69 (1917) 262

O. Kirstein, H. Grimm, M. Prager

FE-023.89.0

Institute Materials Development: General Overview

The Institute of Materials Development participates in three Research and Development programs of the research centre:

- GaAs- GaAs defect physics and crystal growth research ("fundamental research for the information technology" program)
- Crystal growth research and sample preparation of intermetallic systems, quasi-crystals and other multicomponent systems ("materials science" program)
- Research on perovskites with high hydrogen solubility and mobility ("high temperature proton conducting materials for fuel cells" program)

High quality research samples are prepared in four service groups:

- Crystal growth, sample preparation and characterisation laboratory (6 staff members). Intermetallic compound crystals (Ni3Al), rare earth chalcogenide crystals (EuO), and large Bi-crystals are three examples of current activities.

- Thin film laboratory (1 staff member, UHV-thin film preparation by sputtering and evaporation methods). Equipment and know-how will be transfered to the new institute of electro-ceramics.

- Thermoanalysis laboratory (1 staff member)

Two important research projects are funded by external research grants:

- GaAs-crystal growth, defect-physics and process chemistry research and development of Tammann/Bridgman-type crystal growth methods for growing large high-quality GaAs-crystals. Industrial technology transfer is based on a contract with the german GaAs production company (see report by Sonnenberg).
- Growth of quasi-crystals for the german quasi-crystal research community. The successful growth methods by the Czochralski and Tammann/Bridgman-technique have been extended to new flux growth methods with large development potential which will improve crystal output rate and crystal quality.

In collaboration with the *Institut für Kristallzüchtung* in Berlin-Adlershof materials and methods for growthing SiC crystals by gas phase transport have been tested. This expertise has also been used for hydrogen cleaning of SiC wafers for thin film deposition in the Institute of Thin-film and Ion Technology of the Juelich Research Center (Fattah).

Testing of the GaAs Hot-Wall Czochralski industrial prototype unit (Leybold-IGV-project) has been frequently interrupted by repeated equipment failure due to unreliable components. In principle, this technology would still be interesting for GaAs crystal growth research although its industrial use is hampered by complexity, unreliability and high costs. On the contrary, our Tammann/Bridgman GaAs technology is now well advanced and has demonstrated its superiority for the industrial production of large and high-quality crystals since it is simple, reliable and economical.

Thermodynamic modelling has been used as an important part of the crystal growth research activities. Model and data collections have been developed in cooperation with the *Institut für Theoretische Hüttenkunde, RWTH Aachen*, and the company *Gesellschaft für Thermophysik und Thermochemie* in Herzogenrath for the systems Ga-As-B-Si-C-O-H, Si-C-H-O and electro-ceramic materials including charged sublattice defect species together with electronic charge carriers. The results are available in the form of graphical phase diagrams which provide information for those not interested in the thermodynamic details. Thermodynamic properties of selected systems have been measured in collaboration with the *Institut für Gesteinshüttenkunde*, *RWTH Aachen*, *the Institut für Kristallzüchtung* in Berlin and the *Bergakademie Freiberg*.

The following reports by the leading scientists of the institute provide more detailed insight into selected research results of the year 1998.

H. Wenzl

Staff members of the institute of materials development 1998

Prof. Dr. H. Wenzl

Scientists:

Dr. J. Hauck	Chemistry, crystallography, crystal structure systematics, especially in view of oxides and hydrides (Materials-oriented solid state research)	23.55.0
Prof. Dr. T. Schober	Proton-conducting perovskites	23.90.0
Dr. K. Sonnenberg	GaAs-crystal growth research, advanced, industrially-oriented crystal growth systems (Fundamental research for the information technology)	23.42.0
Dr. M. Noack	GaAs crystal growth project (Fundamental research for the information technology)	23.42.0

Research engineers and technicians:

Dipl.-Ing. M. Beyß	Quasi-crystals, intermetallic compounds, alloys (Materials-oriented solid state research)	23.55.0
Dipl.-Ing. A. Fattah	Crystal growth, GaAs Hot-Wall Czochralski project, intermetallic compounds, SiC (Materials-oriented solid state research)	23.55.0
Dipl.-Ing. K. Fischer	Crystal growth, bismuth, rare earth chacogenides, oxides (Materials-oriented solid state research)	23.55.0
Dipl.-Ing. K. Bickmann	Cristallography, thermo-analysis (Materials-oriented solid state research)	23.55.0
Dipl.-Ing. J. Friedrich	Metallography, electron microscopy, oxides	23.90.0
Dipl.-Ing. D. Triefenbach	Sample preparation of electro-ceramic materials	23.90.0
Dipl.-Ing. E. Küssel	GaAs-crystal growth projects (Fundamental research for the information technology)	23.42.0
H. Gier	GaAs crystal growth projects, cold crucible development (Fundamental research for the information technology)	23.42.0
Frau K. Sellinghoff	Semiconductor chemistry laboratory, sample preparation (Fundamental research for the information technology)	23.42.0
Frau R. Fischer	X-ray crystallography and crystal orientation (Materials-oriented solid state research)23.55.0	
Frau E. Würtz	Metallography, electron microscopy (Materials-oriented solid state research)	23.90.0

GaAs crystal growth and defect studies

K. Sonnenberg

We continued to develop the technology of GaAs crystals growth employing the vertical Tammann/Bridgman/Stockbarger methods and to study defects in GaAs especially by using the different contrast techniques of infrared light microscopy.

1. Technical development

(i) The BMBF-project "Semi-insulating 100mm diameter GaAs single crystals with low dislocation density has been continued (Dr. M. Noack). The main objective was the optimization of the temperature field in the growth furnace to achieve lower dislocation densities and a more homogeneous distribution of dislocations. The obtained dislocation density of 3000-400 cm^{-2} is more than an order of magnitude lower than in standard LEC-crystals. Substantial improvements in the homogenisation of the dislocation distribution have been achieved.

(ii) A copy of one of our crystal growth furnaces has been tested extensively by the company FCM (Freiberger Compound Materials) which plans to use the FZJ-Technology for its new GaAs production line. After initial difficulties have been solved by us (E. Küssel) excellent growth results have been achieved. Our growth technology appears to provide a yield value close to 100%. It is capable to provide material with higher quality as compared to the standard technique at much lower investment costs.

(iii) Because of this success FCM has signed a contract with FZJ for the design of an upgrade of our furnace system for crystals with 150 and 200 mm diameter to become the world leader regarding in GaAs crystal size and to gain important advantages on the market. The 150 mm substrate wafer which are produced from the new material exhibit very low dislocation densities, are superior in the overall homogeneity and contain low inherent elastic distortions. Low elastic stresses are particular import for growing high quality epitaxial layers and reduce wafer losses by fracture during their handling.

2. Outsourcing of a company

After the retirement of Prof. Wenzl and Dr. Sonnenberg and after completion of the BMBF-project the development of the crystal growth technology for large semiconductor crystals will be terminated in the third quarter of 1999. On the basis of the existing technology Dr. Noack has founded a small crystal growth company "VB-tec" (Vertical Bridgman technology) which will start operating after the end of his contract with the crystal growth projects.

VB-tec will try to produce various crystals for the research and industrial market (InP crystals for optoelectronics, Si-doped GaAs crystals for high-power lasers, Ge crystals as substrates for GaAs solar cells, for example). Preliminary contacts with possible industrial partners in this connection have already been beneficial for the IFF-research groups:

the company Union miniere has grown a dislocation free Ge-crystal for us which is required for manufacturing a high-quality neutron diffractometer (Dr. Schwahn). Initially, VB-tec will have to rely heavily on laboratory space and special equipment to be rented from the department to cut down the initial surge in fund requirements. It will start experimental development work with its own crystal growth furnace based on the FZJ-technology.

3. Defect studies in GaAs

These studies concentrated in the passed year on the reactions of native point defects with dislocations in GaAs. Clumb processes of dislocations caused by these reactions have been studied through the method of birefringence contrast. We were able to slow experimentally as well as theoretically, that edge dislocations, when observed in the direction of the Busgers-vector, appear as a sharp transition of a bright to dark contrast at the dislocation line. This, however, is only the case if the crystal is also subjective to a material homogeneous elastic background thesis. The half lattice plane associated with the dislocations appears either bright or dark depending on the sign of the background stress. We were also able to show that the background stress can be easily simulated by optical means, i.e. through an optically anisotropic plate which is inserted into the beams line of the microscope. With this technique the sign of the dislocation can be easily determined and as a result also the sign of the climb process, if the initial position of the dislocation is known. This position can be found – as indicated in Fig. 1b – through the decoration of the dislocation by As-precipitates. The climb process shown in Fig. 1a (half-plane appear dark) – which is typical for GaAs in the as grown state – obviously is due to a shrinkage of the half plane i.e. it must be caused by a vacancy absorption process.
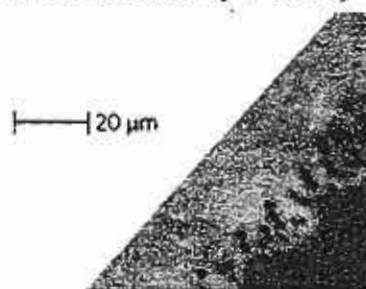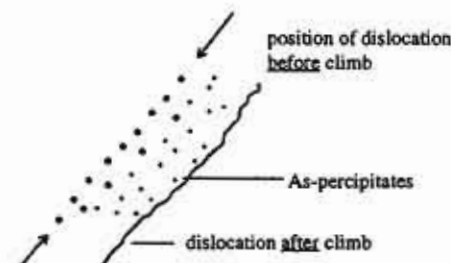

Figure 1a

Figure 1b

Since GaAs grown from a stoichiometric melts is always slightly As-rich, one must assume the that climb process is governed by absorption of Ga-vacancies, V_{Ga}. This, however is in conetration to general assumption in the literature, that the excess of As in GaAs is As-interstitials. Absorption a As-interstitial at dislocation would result in a growth of the half plane which is in contact to our experimental observation. From Fig. 1a and in particular from Fig. 2a we must also conclude that the climb process does not take place before the formation of As-precipitate (i.e. not at higher temperatures), but very likely together with it. This is plansiblee because both processes are likely to be goverened by the same kinetics, i.e. the diffusion of Ga-vacancies to the dislocation.
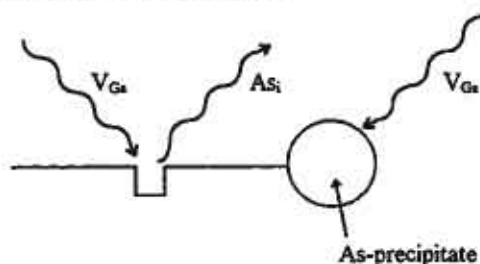

Figure 1c

As-precipitates are formed through the agglomeration of Ga-vacancies with a subsequent absorption of As-interstitials, which in turn are generated or absorbed during the climb of dislocation (see Fig. 1c) through a so called Petroff-Kimerling process.
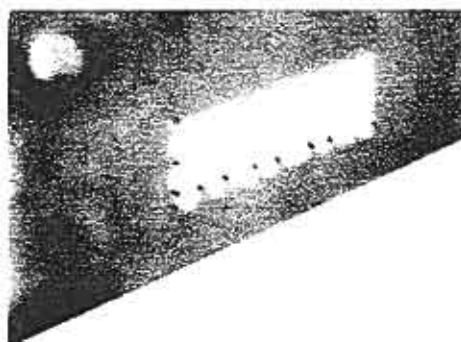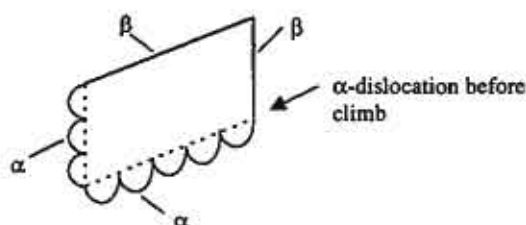

Figure 2a

Figure 2b

Since the formation of As-precipitates takes place in the temperature region between 900 and 1000°C, we shall assume the climbing process to occur within the same temperature region. The fact that both processes occur simultaneously also makes it understandable that the area across which the dislocation moved during its climb process appears, decorated with As-precipitates. This is obvious from Fig. 3a and 4a.
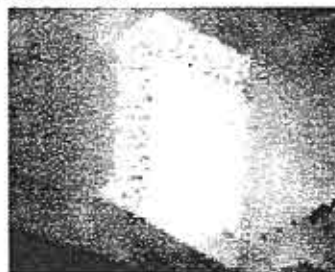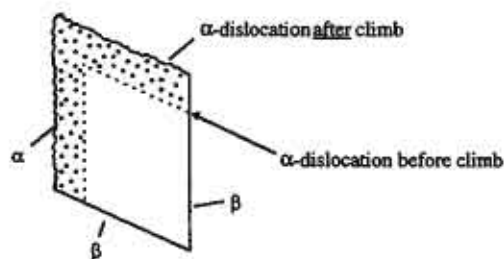

Figure 3a

Figure 3b

One can also recognize (particularly from Fig. 4a) that those As-precipitates which are uncleated earlier have grown for a longer size. Dislocations with a (KI)-glide plane appear in a so called α- and β-dislocations (see Fig. 2 and 3) along [112]-directions. Our results show, that climb processes are only observer for α-dislocation. They are also preferentially decorated by As-precipitates. This result is rather plausible since Ge-vacancies are acceptors on the one hand and α-dislocations very likely exhibit a donor character. Since there is a general agreement that dislocation only appear in the so called "glide"-configuration the half plane associated with α-dislocation must be terminated by a row of As-atoms (β-dislocation by Ga-atoms in contrast). As a result α-dislocation behave like donors.

Figure 4a

α-dislocation _after_ climb

β

β

intermediate positions of
α-dislocation

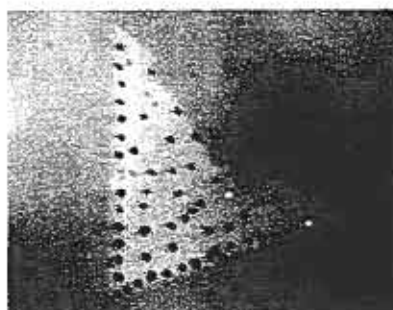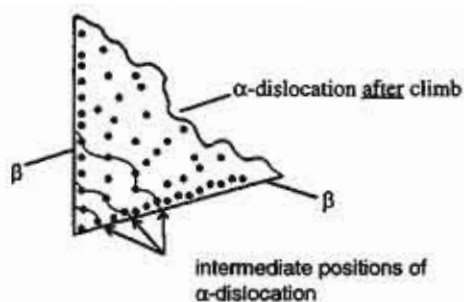*Figure 4b*

The dislocation loops shown in Fig.2 and 3 are very likely
formed by reactions between dislocations during glide
processes. Subsequently climb processes led to the
appearance of the loops shown in Fig.2 and 3. In Fig. 4a an
example of a loop is shown which is very likely caused only
by climb processes as indicated in Fig. 4b. This
interpretation is also confined by the fact, that the area
within the loop is decorated by As-precipitates as well as by
the observation that those precipitates close to the left edge
of the loop are larger (since they are uncleated first).

Injection of protons into inert gases using a high-temperature proton conductor

T. Schober, J. Friedrich, D. Triefenbach

F&E-Nr.: 23.90.0

High-temperature proton conductors are ceramics which absorb water vapor at elevated temperatures. The protons introduced in this way into the lattice are rather mobile and may be transferred to electrodes on the outside using electric fields provided that the electronic conduction is sufficiently low. In the present work we used the substance $Sr(Zr_{0.8}Ce_{0.2})_{0.8}In_{0.2}O_{3-\delta}$ [1] which has oxygen vacancies in the dry state and absorbs water vapor according to the classic equation

$$(H_2O)_{gas} + V_o^{\cdot\cdot} + O_o^x \Leftrightarrow 2OH_o^{\cdot} \qquad (1)$$

The protons become embedded into the electron cloud of oxygen ions. In the present experiment (Fig. 1) the proton conducting ceramic had the shape of a tube sealed at one end which could be heated internally using a heating rod. Incidentally, this arrangement is the same as used in internally heated λ-sensors for automobiles where the ceramic is Y-stabilized zirconia and the mobile species are oxygen ions.
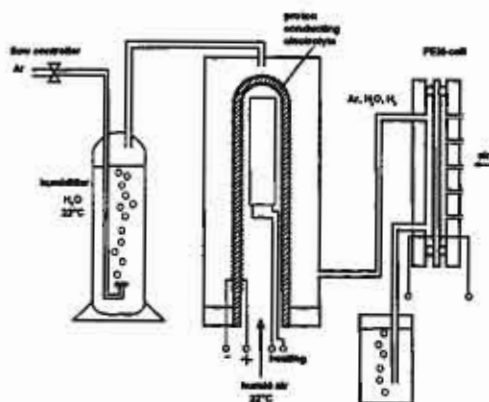

Fig. 1. Schematic of the testing arrangement. The 8YSZ sensor is not shown but is inserted in the same position as the PEM cell

The key question to be solved in this experiment was whether it is possible to transport protons from the wet air side across the proton conducting ceramic tube to the argon side and to inject them as hydrogen molecules into the inert gas stream.

The proton conducting tube had an O.D. of 6mm, an I.D. of 4 mm and a length of 40 mm. Pt electrodes were applied to the out- and inside of the tube. Hermetic sealing of the tube in a annular ceramic spacer and a chamber was achieved using a special glass solder. Wet Ar gas was first admitted to the chamber and then transferred to either a small commercial PEM fuel cell or to a standard 8YSZ-type oxygen sensor. The PEM fuel cell contained Nafion as the electrolyte for protons and served to demonstrate the presence of hydrogen molecules in the gas stream. In case our device produced a partial pressure of hydrogen, the PEM cell would display a EMF of about 1 V typical of a difference in a partial pressure of oxygen across the membrane of about 24 orders of magnitude as given by the well-known formula:

$$EMF = RT/4F \ln(p_{O_2}^1 / p_{O_2}^2) \qquad (2)$$

where F Faraday's constant. In the other case, where no hydrogen evolution occurs at the inner electrode, the EMF would be 50-100 mV reflecting the p_{O_2}-difference between air and argon gas.

Results: Using a humidified stream of 5 ml Ar/min and *no* enforced proton transport the EMF measured by the 8YSZ oxygen sensor was about 95 mV which is typical of high-purity Ar gas.

However, using a current of 10 mA across the interface with the correct polarity the EMF registered by the PEM fuel cell as well as the 8YSZ oxygen sensor approached 900 mV. This high value demonstrates that protons must have been injected into the gas stream resulting in a wet Ar-H_2 mixture. It is thus evidence for proton conduction in the electrolyte. Assuming a transport number of about 10% for the present substance we can calculate the number of moles, n_{H_2}, transferred to the Ar gas by the current i:

$$n_{H_2} = i/2F \qquad (3)$$

References:

[1] T. Schober, J. Friedrich, Solid State Ionics (in press)

Ordered bcc alloys

J. Hauck, K. Bickmann, R. Fischer and K. Mika

The ordered body-centred alloys M_xN_y can be characterized by the self-coordination numbers (s-CN) $T_1 T_2 T_3$ of the M atoms with M atoms and the composition $r=y/x$. The T_i values of M atoms and the maximum T_i^{max} values 8 6 and 12 for i=1-3 are correlated to the short-range order parameters α_i by $\alpha_i T_i^{max} = T_i^M - (T_i^{max} - T_i^M) x/y$. The T_i or α_i values (i=1-3) of all possible structures with $x+y \leq 8$ were determined numerically and plotted in a structure map. For MN composition the s-CN values 8 6 12 of W are reduced to 0 6 12 (CsCl), 4 0 12 (NaTl), 4 4 4 (TiCu), 2 4 6, 4 2 4 or 6 4 6, which are at corners of a decahedron [1] (Fig.1/Tab.1).
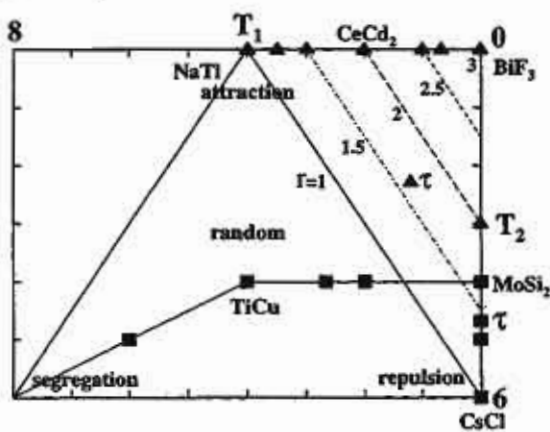

Figure 1: Structural map of ordered bcc M_xN_y alloys $T_1 T_2 T_3$; y/x at different r=y/x with the numbers T_1 and T_2 of M atoms in the first and second coordination sphere of M atoms as parameters for layered [0 0 1] (■) and [1 1 1] (▲) compounds and aperiodic sequences (τ).

The interactions between M atoms can be analyzed from the location at the structure map as repulsive in CsCl, attractive in NaTl and clustering in TiCu. Segregation or disorder of M and N atoms occurs at 8 6 12 or 4 3 6 respectively. The 0 4 4; 2 ($Mo Si_2$), 2 0 6; 2 ($CeCd_2$), 0 3 9; 2 ($Si Fe_2$), 4 4 4; 2, 4 2 2; 2, 0 0 12; 3 ($Bi F_3$, $Al Fe_3$), 0 2 4; 3 (($Mo,U) U_3$), 2 0 0; 3, 4 2 2; 3 and 2 2 0; 3, structures are at corners of the structure maps at MN_2 or MN_3 composition. Most ordered M_xN_y alloys can be classified in two families, which are named by the pioneers, who investigated the structures of the first examples: Au_2Nb_3, Ti_2Cu_3 and Ti_3Cu_4 of the Schubert series [2], Pb_2Li_7 and Pb_3Li_8 of the Zalkin & Ramsey series [3]. The structures of the Schubert series can be described by the sequences of metal atoms in [0 0 1] direction as e. g. MoSiSi (=b) for $MoSi_2$, Ti_2Cu_2 (=d) for TiCu and $TiCu_2 Ti_2Cu_2$ (=bd) for Ti_3Cu_4. The structures of the Zalkin, Ramsey series can be described by sequences of metal atoms in [1 1 1] direction as e. g. Ce Cd Cd (=k) for $CeCd_2$, AlFeFeFe (=l) for $AlFe_3$ and $PbLi_3PbLi_2PbLi_3$ (=lkl) for Pb_3Li_8. In some other structures part of the M atoms of CsCl (MN) are substituted by N atoms in [0 0 1] layers with composition MN, N_2 (($Mo, U) U_3$), M_2N_2, N_4 (Au (Zn, Au)$_3$) or [1 1 1] layers M_6N, N_7 (Pu_3Pd_4) and $M_3 N_4$, R_7

($Zn_3 Ga_4 Pd_7$). The structures with a partial filling of the M sublattice occur mainly at repulsive interactions of M atoms, while attractive interactions or clustering are increasing in the [1 1 1] and [0 0 1] layered compounds. Structures with long sequences of structural units like $Pb_3 Li_8$ (lkl) or clustering like TiCu ($Ti_2 Cu_2$) can segregate to 2 $PbLi_3$ (l) + $PbLi_2$ (k) or Ti+Cu. The ordering of metal atoms in superconducting oxides corresponds to the [0 0 1] series as e. g. Mo Si_2 ($CuLa_2O_4$) or Os_2Al_3 ($Cu_2La_3O_7$) [1].

One-dimensional quasicrystalline phases can be obtained e.g. for (0 0 6 ; 5) ($Ni_2\square Al_3$) structure [4], if the composition is varied to $Ni_{1.85}\square_{1.15}Al_3$ and the sequence of vacancies $\square$(NiAlNiAl$\square$Al) alters to the Fibonacci sequence at 0 0 6; 4.22. Other aperiodic one-dimensional sequences of M and N atoms can occur at $MN_2/MN=1.62$, if the valence electron concentration of e. g. Ti_3Pd_5 ($TiPd_2TiPd_2TiPd$) or Os_2Al_3 ($OsAl_2OsAl$) is varied similar as in many other systems [2].

Table 1: Sequences of layers and s-CN values of ordered bcc alloys

$M_x N_y R_z T_{z'}$	layer sequence	$T_i (M)$
layered [0 0 1] structures (Schubert [2])		
Cs Cl	a (M N)	0 6 12 ; 1
Mo Si$_2$	b (M N$_2$)	0 4 4 ; 2
M N$_3$	c (M N$_3$)	0 4 4 ; 3
γ-TiCu	d (M$_2$ N$_2$)	4 4 4 ; 1
Au$_2$ Nb$_3$	e (M$_2$ N$_3$)	4 4 4 ; 1.5
M N$_2$	f (M$_2$ N$_4$)	4 4 4 ; 2
M N	g (M$_4$ N$_4$)	6 5 8 ; 1
Os$_2$ Al$_3$	a b	0 5 8 ; 1.5
Ti$_3$ Pd$_5$	b a b	0 4.7 6.7 ; 1.7
Fibonacci	b/a = τ	0 4.8 7.1; τ
Ti$_3$ Cu$_4$	b d	2.7 4 4 ; 1.3
Ti$_2$ Cu$_3$	b d b	2 4 4 ; 1.5
Re Al (Re, Al)$_2$	M R N R	0 4 4 ; 3 (M, N)
layered [1 1 1] structures (Zalkin & Ramsey [3])		
Cs Cl	h (M N)	0 6 12 ; 1
Ce Cd$_2$	k (M N$_2$)	2 0 6 ; 2
Bi F$_3$, Al Fe$_3$	l (M N$_3$)	0 0 12 ; 3
M N$_4$	m (M N$_4$)	0 0 6 ; 4
M N$_5$	n (M N$_5$)	0 0 6 ; 5
Na Tl	o (M$_2$ N$_2$)	4 0 12 ; 1
Al$_2$ Li$_3$	p (M$_2$ N$_3$)	3 0 9 ; 1.5
M N	q (M$_3$ N$_3$)	4 2 8 ; 1
Fibonacci	k/h = τ	1.2 2.3 8.3; τ
Si Fe$_2$	hl	0 3 9 ; 2
Si$_2$ Li$_5$	kl	1 0 9 ; 2.5
Pb$_3$ Li$_8$	lkl	0.7 0 10 ; 2.7
Pb$_2$ Li$_7$	lm	0 0 9 ; 3.5
Ga$_4$ Li$_5$	op	3.5 0 10.5 ; 1.25
Ge$_2$ Cu$_2$ Li$_5$	MNR$_2$ NMR$_3$	1 0 6 ; 3.5 (N)
(Nb, Al) (Nb, Ti) Ti$_2$ Al$_2$	M R T N T R	0 0 6; 5 (M, N)
Sn Li Mg Pd	M N R T	0 0 12 ; 3 (all)
Al Mn Cu$_2$	M R N R	0 6 12 ; 1 (Cu)
Ag Sb Li$_2$	M N R R	4 0 12 ; 1 (Li)
Ni$_2$ □ Al$_3$	M R M R N R	0 0 6 ; 5 (□)

References

[1] J. Hauck and K. Mika, in Studies of High Temperature Superconductors 25, 1 edited by A.V. Narlikar, Commack NY; Nova Science (1997)

[2] K. Schubert, Kristallstrukturen zweikomponentiger Phasen (Crystal Structures of Binary Phases), Berlin, Springer (1964)

[3] A. Zalkin and W.J. Ramsey, J. Phys. Chem. 60 (1956) 234 and 1275

[4] K. Chattopadhyay, S. Lele, N. Thangaraj and S. Ranganathan, Acta metall. 35 (1987) 727

Institute of Electroceramic Materials

The research areas of the institute comprise (1) technologies for the integration of electroceramic materials into microelectronics and microsystems, (2) dielectric and ferroelectric properties of oxide ceramics, and (3) the defect structure in the vicinity of internal and external interfaces in oxides. These areas are complementary to the research areas of the Institute for Materials in Electronics 2 (IWE 2) at the Aachen Technical University (RWTH). Project groups often comprise staff members and students from both institutes.

Research within the area of integration technologies is focussed on the fundamental understanding of *dry processes*. The deposition of oxide thin films is performed by means of MOCVD (MOCVD = Metal Organic Chemical Vapor Deposition) systems. In cooperation with AIXTRON AG, a multiwafer planetary reactor is used for the development and optimization of modified $(Ba,Sr)TiO_3$ films as part of an ESPRIT project. In addition, a horizontal MOCVD reactor has been built for the deposition of new material systems and for the development of alternative vaporizer systems. For the patterning of the ceramic films and electrode / ceramic film stacks, Reactive Ion Beam Etching (RIBE) and Reactive Ion Etching (RIE) techniques will be employed. In contrast to the situation in the standard Si and compound semiconductor technologies, dry etching processes of oxide ceramics have hardly been investigated as yet and, hence, represent a research area in which basic studies and industrially funded applied research can be linked in a beneficial manner. The integration processes are complemented by metallization methods based on electron beam and sputter techniques. Within this area, our studies aim at a better understanding of the processes and material parameters which govern the adhesion, the mechanical stress, and the microstructure. The complementary methods at RWTH Aachen are solution-based deposition (CSD = Chemical Solution Deposition) and etch techniques with topics more strongly concentrated on the design and fabrication of integrated devices.

The second research area focuses on the *dielectric and ferroelectric properties* of oxide thin films and bulk materials, which are being investigated in Jülich as well as in Aachen. The material systems are based on compositions used for practical devices and model systems, e.g. $SrTiO_3$, $BaTiO_3$, $SrBi_2Ta_2O_9$, $Pb(Zr,Ti)O_3$ and $(Ba_{1-x}Pb_x)TiO_3$. One of the research topics is the microscopic understanding of ferroelectric hysteresis including new approaches for the separation of *reversible* and *irreversible* contributions to polarisation based on the analysis of frequency-dependent small and large signals. These studies are linked to the *aging* (imprint) phenomenon, i.e. the polarisation-dependent shift of the hysteresis curve with time and to the ferroelectric *fatigue* process, i. e. the reduction of the remanent polarisation by cycling. Both aging and fatigue processes play an important role in the operation of the novel non-volatile memories (Ferroelectric Random Access Memories, FeRAM). Up to now, they are only partially understood. In cooperation with external research groups, single domain processes in ferroelectric thin films are studied by means of scanning probe techniques. In addition, scaling effects (grain size effects in ceramics, thickness effects in films) on the transition from the ferroelectric to the superparaelectric state are investigated.

Impedance spectroscopy in the lower GHz regime is employed to determine the relaxation of the ferroelectric *domain wall* motion and to separate this contribution from the contribution of the crystal lattice. By varying the microstructure of the ceramics and by comparison between bulk ceramics and thin films, the model of Arlt will be extended with respect to the impact on 2D constraints imposed by mechanical stress due to the presence of substrates. For *dielectric*

ceramics, impedance spectroscopy is used to elucidate the interrelation of *extrinsic* losses and lattice defects. This activity includes the development and characterization of new microwave ceramics and is embedded into a cooperation with the Institute for Microstructural Research (Urban) and Norbert Klein's group within the framework of a BMBF-Leitprojekt (leading project for the Federal Ministry of Education, Science, Research and Technology (BMBF).

In the case of ferroelectric materials, existing theories will be further developed and extended towards a more quantitative description of the dielectric, piezoelectric, and elastic properties. Numerical *finite-element-methods* are used to describe the mutually coupled mechanical, thermal, and electrical properties of ceramic components such as multilayer capacitors and actuators. In a new activity, these methods will be extended to piezoelectric microactuators which will be designed and fabricated in cooperation with Prof. Mokwa's group at Aachen.

The third research area comprises the lattice disorder in the vicinity of internal interfaces (grain boundaries) and external interfaces (surfaces and electrode interfaces) and their impact on electronic and ionic charge transport. In the case of acceptor and donor doped titanate ceramics, the studies are focused on the formation of space charge depletion layers at grain boundaries as well as the related potential barriers and the transport of charge carriers along and across the grain boundary barrier. A hot-pressing technology has been developed to decorate the grain boundary area with additional dopants and to study the influence of these artifical grain boundary states. In some material systems, such as titanate-zirconate solid solutions, it is necessary to determine the equilibrium constants of the defect reactions and the diffusion constants of the system in order to create the basis for the research on interfaces. In this respect, the comparison of bulk ceramics and thin films of the same composition is of vital interest. In thin film systems, the significant influence of the electrode metals, the unexpectedly high stability under conditions of dc-voltage-induced resistance degradation, as well as the tolerance of the lattice concerning the incorporation of non-stoichiometries represent current research topics.

Continuing the cooperation with the Research Center's fuel cell project of the Research Center, proton-conducting ceramics are studied with respect to their suitability for solid oxide fuel cells (SOFCs). In addition, a new activity on thin film oxide conductors has been started as a part of a national priority program by the German Research Association (DFG).

Research on electronically conducting perovskites can be divided into studies on *semiconducting* and on *metallically conducting* oxides. In semiconducting, donor-doped $SrTiO_3$, the emphasis is placed on the interrelationship between point defects and extended defects involved in oxidation and reduction processes using single crystals and ceramics. The metallically conducting manganates and cobaltates are investigated with respect to their magnetoresistive and ferromagnetic properties. By comparing epitaxial and polycrystalline thin films, the influence of the grain boundaries on charge transport and magnetic properties is studied.

Rainer Waser

Institute for Electroceramic Materials

Head: Prof. Dr.-Ing. Rainer Waser

Secretariat: Maria Garcia

Tel. (02461) 61 5811; Fax: (02461) 61 8209

e-mail: r. waser@fz-juelich.de/m.garcia@fz-juelich.de

SCIENTISTS:

Arons, R.R.:	Structure of magnetoresistive and ferroelectric oxides; charge transport in proton conductors
Bohn; H.G.:	Mechanical and dielectric relaxation in solids. Impedance spectroscopy. Defect chemistry. Electrochemical characterization of ceramic conductors.
Ehrhart, P.:	MOCVD methods for electroceramical thin films; X-ray diffraction and optical spectroscopy.
Hoffmann, S.:	High-permittivity electroceramic thin films: MOCVD, dielectric properties, charge transport, defect chemistry
Kohlstedt, H.H.:	Reactive ion beam etching of ceramic and metallic materials, superconducting and magnetic multilayers
Krasser, W.:	Optical excitation-processes in electroceramic materials;light-annealing processes
Meuffels, P.:	Processing of electroceramic materials; defect chemistry of electroceramic materials
Otterstedt, R.:	Development of microwave ceramics; dielectric characterization; extrinsic losses in microwave ceramics
Schroeder, H.:	Technology and properties of (metal) electrodes of electroceramic thin films; mechanical properties and electromigration in thin films and interconnects.
Waser, R.:	Electronic ceramics and integration of ceramic thin films

TECHNICAL ENGINEERS:

Bierfeld, H.:	Ceramic technology and sputtering techniques
Dedek, U.:	Electrical characterization of electronic ceramics; design of measuring setups.
Haselier, H.:	Metallization and thin film technology as well as clean-room technology
Hermanns, B.:	MOCVD, RIBE, sputtering of magnetic materials
John, H.:	Clean-room technology, microlithography and optical laboratory; LRP
Speen, R.:	Relaxation spectroscopy and electrochemical characterization

Ph.D. STUDENTS

Baldus, O. (TH Aachen):	Laser annealing of CSD, MOCVD electroceramic thin films
Barton, M. (Uni Bonn):	Synthesis and characterization of single crystals of the high temperature protonic conductor $Ba_3(Ca_{1+x}Nb_{2-x})O_{9-\delta}$
Fitsilis, F. (TH Aachen):	Thin film capacitors for future DRAM applications using the MOCVD technique
Huck, H. (TH Aachen):	Characterization of oxide perovskites with optical methods
Rickes, J. (TH Aachen):	Reconfigurable multimedia processors based on ferroeletric RAM (FeRAM)
Schmitz, S. (TH Aachen):	Influence of the contact metal on leakage current and dielectric permittivity of electroceramic thin film capacitors.
Schmitz, R.:	Magnetic tunnel junctions, fabrication and experiments
Schneider, St. (TH Aachen):	Reactive ion etching (RIE) and reactive ion beam etching (RIBE) of ceramic thin films.
Schäfer, P. (TH Aachen):	Evaluation of novel MOCVD systems for the deposition of ferroelectric thin films.

GRADUANTS:

Hövelmann, J. (TH Aachen):	Computer control system for a laser annealing device
Ohly, Ch. (TH Aachen):	Investigations of the high-temperature conductivity of doped titanate thin films

GUEST SCIENTISTS:

Dr. St. Hwang (Univ. of California, USA):	Polarization switching models in polycrystalline ceramics
Dr. W. Ma (Southeast Univ., Nanjing, China):	Growth, microstructure and electrical property of ferro-electric thin films of perovskite-type oxides by MOCVD
Prof. J. Scott (Univ. of New South Wales, Australia):	Theory of charge distribution and leakage currents in BST type thin films
Dr. K. Szot (Univ. Katowice, Poland):	Study of surface layer of perovskite materials of ABO_3 structure

Colossal Magnetoresistance (CMR) in acceptor doped Lanthanum Manganites

R.R. Arons [1], U. Hasenkox [3], C. Osthöver [2] and Ch. Sauer [2]

[1] Institut für Elektrokeramische Materialien

[2] Institut für Elektronische Eigenschaften

[3] Institut für Werkstoffe der Elektrotechnik II, RWTH Aachen

F23.42.0

The recently for the first time observed Colossal Magnetoresistance effect (CMR) in acceptor doped lanthanum manganites has revived the scientific interest of the early fifties in this system /1/. This CMR is related to the transition from the semiconducting, paramagnetic into the ferromagnetic, metallic state below T_c. Therefore these systems are believed to be potential candidates for applications like magnetic sensors. In order to optimize the CMR-effect a fundamental understanding of the driving mechanism for the ferromagnetic (FM) ordering is required.

The undoped perovskite-type compound $LaMnO_3$ is an antiferromagnetic (AF) semiconductor. Upon doping of D^{2+}-ions on the La^{3+}-sites, $La_{(1-x)}D_xMnO_3$, D = Ca, Sr, Ba, becomes a FM metal with a maximum T_c for $x \approx 0.3$. This transition is generally ascribed to the $Mn^{3+} \rightarrow Mn^{4+}$ valence fluctuation accompanied by the D^{2+}-hole doping on the La-sites (the so-called Zener's Double Exchange (DE) Model /2/). Recently we have investigated epitaxial $La_{0.67}Ca_{0.33}MnO_{3-\delta}$ films on $LaAlO_3$, prepared by sputtering in oxygen /3/. From this it was shown that the maximum T_c only is reached for a stoichiometric oxygen composition ($\delta = 0$) and that T_c is reduced by the oxygen vacancy concentration in the films /3/. Accordingly, the Mn^{4+} / Mn^{3+} ratio grows as a function of the D^{2+} doping on the La^{3+}-sites, while it decreases with the oxygen vacancy concentration.

In order to obtain further understanding of the DE-mechanism, we have also doped the Mn-sites in $\{La_{0.67}Ba_{0.33}\}\{Mn_{1-y}A_y\}O_3$ with A = Fe^{3+}, Cr^{3+} /4/. While T_c was found to decrease only slightly from 350 K for y = 0 to 310 K upon y = 0.1 Cr doping, a strong decrease down to 190 K was obtained for y = 0.1 Fe. From this, the coupling between Cr and Mn was believed to be FM, whereas the Fe-Mn coupling was proposed to be AF. This agrees with the electronic configurations of $3d^3$ for Cr^{3+} and $3d^5$ (half-filled 3d-shell) for Fe^{3+}. Also the temperature dependence of the resistance was found to be completely different for the two compounds. While for Cr the maximum resistance coincides with T_c, as expected from the DE-model, the maximum for 0.1 Fe was observed at 140 K, thus far below T_c. From subsequent ^{57}Fe Mössbauer experiments (ME) it was concluded that the Fe-moments are subjected to fluctuating hyperfine (hf) fields down to temperatures far below T_c /5/. These fluctuations
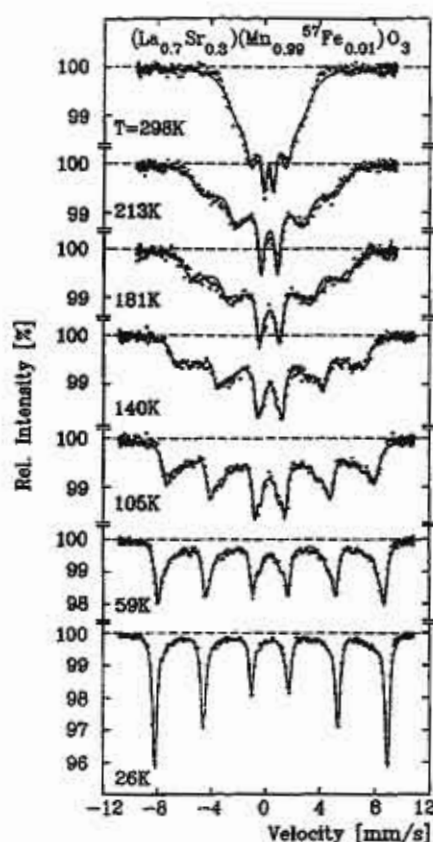

Fig. 1. Mössbauer effect spectra of $\{La_{0.7}Sr_{0.3}\}\{Mn_{0.99}Fe_{0.01}\}O_3$ at various temperatures. The spectra measured in the temperature range from 181 – 298 K were fitted using a simple Ising type relaxation model, whereas the spectra at T ≤ 140 K were fitted using a superposition of 6 magnetically split 6-line subspectra.

of the Fe-moments down to low temperatures were ascribed to the competing Fe-Mn and Fe-Fe interactions, which are both AF. This assumption, that the Fe-Fe and Fe-Mn coupling are comparably strong in case of 10 per cent Fe doping on the Mn-sites, is supported by the very high Néel temperature of the pure $LaFeO_3$, indicating that the Fe-Fe coupling is very strong. Accordingly, the corresponding fluctuations of the Fe-moments down to low temperatures might be responsible for the fact that the semiconducting-metal transition in

$\{La_{0.67} Ba_{0.33}\}\{Mn_{0.9}Fe_{0.1}\}O_3$ is shifted from $T_c = 190$ K to 140 K.

In this work we present ^{57}Fe Mössbauer experiments on $\{La_{0.7} Sr_{0.3}\}\{Mn_{1-y}Fe_y\}O_3$ for y = 0.01 and 0.10, in order to compare the temperature dependence of the hf-fields at high Fe concentrations with the diluted Fe case, in which the Fe-Fe coupling is believed to be strongly reduced compared with the Fe-Mn coupling. For this a sample was prepared using ^{57}Fe instead of natural Fe. We have chosen Sr rather than Ba, in view of its higher T_c value of 372 K instead of 350 K for the pure manganite (y = 0).

Fig. 1 shows the ^{57}Fe Mössbauer spectra of $\{La_{0.7} Sr_{0.3}\}\{Mn_{0.99}Fe_{0.01}\}O_3$ in the temperature range from 26 K to 298 K, i. e. in the FM ordered state ($T_c = 360$ K). At 26 K, near to magnetic saturation, a hyperfine (hf) split six-line spectrum is observed. From the splitting the hyperfine (hf) field is calculated to be 53 T, a value typical of Fe^{3+} ions in ionic compounds like Fe oxide. This is rather surprising, since the compound shows metallic behaviour below T_c. From the sharp lines observed, it follows that the distribution of the hf-fields at the different Fe-sites must be rather small. In contrast to this, the 10% Fe doped sample showed at 4 K broad lines representative of a broad distribution of hf-fields at the Fe-sites. This distribution in the 10% Fe sample was ascribed to the competing
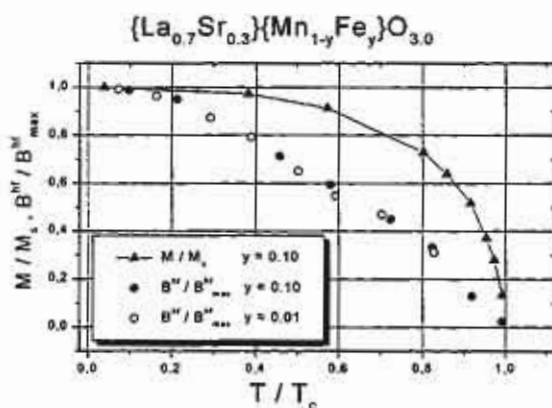

$$\{La_{0.7}Sr_{0.3}\}\{Mn_{1-y}Fe_y\}O_{3.0}$$

Fig. 2. Temperature dependence of the magnetic hyperfine fields and spontaneous magnetization for $\{La_{0.7} Sr_{0.3}\}\{Mn_{1-y}Fe_y\}O_3$ for y = 0.01 and 0.10.

antiferromagnetic Mn-Fe and Fe-Fe interactions. These competitive interactions, which lead to frustration of the Fe-moments at low temperatures, do not appear in the diluted 1% Fe sample.

In the range from 60 K to 298 K the spectra display typical spin relaxation features, which become more pronounced at increasing temperatures. This indicates that the Fe-moments are subjected to fluctuating fields, which vary with a frequency in the range of the Larmor frequency of about 10^8 s^{-1}. Above T_c, these relaxation phenomena are expected to vanish in view of the high frequencies of these fluctuations. However, our Mössbauer apparatus does not allow measurements up to the T_c value of 360 K of the 1% Fe-sample. In a rough approximation one can fit the six-line spectra with strongly broadened line widths in the temperature range from 60 K to 300 K in order to obtain an average hf-field as function of temperature. In Fig. 2 the open circles represent the reduced hf-fields of the 1% Fe sample as a function of T / T_c. For comparison we have also plotted the average hf-field (solid circles) and the spontaneous magnetization obtained from SQUID-magnetization measurements (solid triangles) for the 10% Fe sample. Whereas the temperature dependence of the hf-field is nearly identical for the two Fe compositions, it is seen that the magnetization of the Mn-moments reaches its saturation value already at much higher temperatures. Apparently the Fe-moments are subjected to fluctuating hf-fields down to temperatures, at which the Mn-moments have reached nearly their saturation value. For the 10% Fe-sample this feature was explained from the competing Fe-Mn and the Fe-Fe interactions. However, since in Fig. 2 the same behaviour is obtained for the 1% Fe sample, in which the Fe-Fe coupling is expected to be very weak, a different mechanism seems to be responsible for this effect. Further experiments must reveal, whether these hf-field fluctuations at the Fe-sites might be caused by local $Mn^{3+} \rightarrow Mn^{4+}$ valence fluctuations.

References
1) for a recent review, see A.P. Ramirez, J. Phys. Condens. Matter 9 (1997) 8171
2) C. Zener, Phys. Rev. 82 (1951) 403
3) C. Osthöver, K. Schmidt and R.R. Arons, Materials Science & Engineering B56 (1998) 164
4) C. Osthöver, P. Grünberg and R.R. Arons, J. Mag. Magn. Materials 177-181 (1998) 854
5) C. Osthöver, C. Sauer and R.R. Arons, Australian J. Phys. 51 (1998) 379

The nature of perovskites of ABO₃-type at elevated temperatures

K.Szot[1], W. Speier[2], J. Herion[3], A. Mück[3]
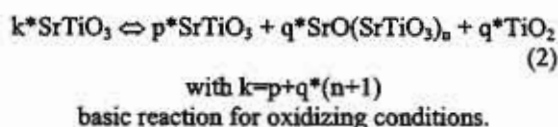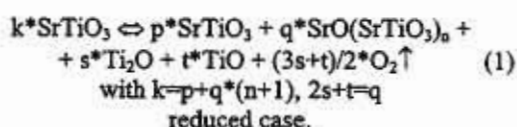
[1]Institute for Electroceramic Materials
[2]Institute of Chemistry and Dynamics of the Geosphere
[3]Institute of Thin Film and Ion Technology

F23.42.0

The special role of the surface layer of crystalline perovskites of ABO₃-type has been recognised and investigated since in the fifties. In the literature one finds terms such as „Känzig"-layers or „skin" [1]. The surface contributes to anomalous behaviour of ferroelectrica. Examples are the existence of a tetragonal distortion in this surface layer up to as much as 400°C above T_c in the case of BaTiO₃, the differences in mobility of domain walls compared to the bulk or the pyroelectrical properties of the surface layer in the cubic phase. A different kind of interpretation of the properties of the surface of the perovskite crystals has been developed by means of surface sensitive analytical methods. Very similar to standard materials such as Si or Ge, one speaks also in the case of perovskites of phenomena such as rumpling, reconstruction or relaxations within the uppermost monolayers [2]. The estimated thickness of the surface layer on the basis of surface spectroscopy (XPS, Auger or Photoelectron spectroscopy with synchrotron radiation) and „classical" methods (electrical conductivity, optical absorption or small angle x-ray diffraction) varies between 0.2nm and 10⁵nm. In most of the descriptions of the surface layer one assumes that this layer is chemically homogeneous and that the only type of relevant defects are point defects (predominantly oxygen vacancies) with a statistical distribution.

On the basis of empirical evidence we have developed a new model of the near-surface region bringing into focus segregation phenomena and changes in the chemical composition at elevated temperatures. For example, careful x-ray diffraction analysis of a wide range of single-crystals of ABO₃-perovskites, e.g. BaTiO₃, SrTiO₃, PbTiO₃, KTaO₃, KNbO₃,[3,5-7] shows that new chemical phases develop already at temperatures as low as 500°C. The fraction of additional phases increases with temperatures and heating time. The restructuring of the near-surface region, which is in fact a solid state reaction, can be observed for both reducing as well as oxidizing conditions. X-ray diffraction experiments *in situ* have demonstrated that only small range of partial pressure of oxygen exists at elevated temperatures where the composition of the near-surface region actually corresponds to the bulk of the crystalline material. According to analysis of the x-ray diffraction the reactions at reducing or oxidising conditions can be summarised as follows:

$$k*SrTiO_3 \Leftrightarrow p*SrTiO_3 + q*SrO(SrTiO_3)_n +$$
$$+ s*Ti_2O + t*TiO + (3s+t)/2*O_2\uparrow \quad (1)$$
with k=p+q*(n+1), 2s+t=q
reduced case.

$$k*SrTiO_3 \Leftrightarrow p*SrTiO_3 + q*SrO(SrTiO_3)_n + q*TiO_2$$
$$(2)$$
with k=p+q*(n+1)
basic reaction for oxidizing conditions.

The observed massive chemical reorganisation of the near-surface region is a consequence of the redistribution of A-cations or AO-complexes. Depth profiles by secondary ion mass spectrometry (see fig. 1) for single-crystals ABO₃ with (100)-orientation heated in oxidising conditions show that AO-complexes are segregated from deeper parts of the near-surface region to the surface [6,7].

This leads to a sandwich-like structure as illustrated in figure 2 with Ruddlesden-Popper-type phases on and close to the surface and BO₂-rich phases below. Under reducing conditions the redistribution of AO-complexes or A is in the opposite direction so that the order of chemical phases is reversed with respect to the oxidising situation.

For such reactions, which already occur at relatively low temperatures, the presence of extended defects play an important role [4,6]. By means of diffusion experiments using ¹⁸O [6] as tracer secondary ion mass spectrometry allowed to demonstrate that the diffusion coefficient along such extended defects is higher by an order of magnitude compared to the „classical diffusion coefficient" on the basis of random walk diffusion. Furthermore, the restructuring of the near-surface region manifest itself as a change in the topography of the surface. The Ruddlesden-Popper-type phase A₂BO₄, which grows on the surface under oxidising conditions, gives rise to the occurrence of characteristic step-like terraces with a step-height of app. 12Å (see fig. 3b). Also for crystals treated under reducing conditions the surface (see fig.3c) shows dramatic changes compared to the original flat monoatomic surface as can be taken from figure 3a.

This short description of the restructuring of the near-surface region of perovskites of ABO₃-type gives an indication of the variety of chemical and physical processes involved at elevated
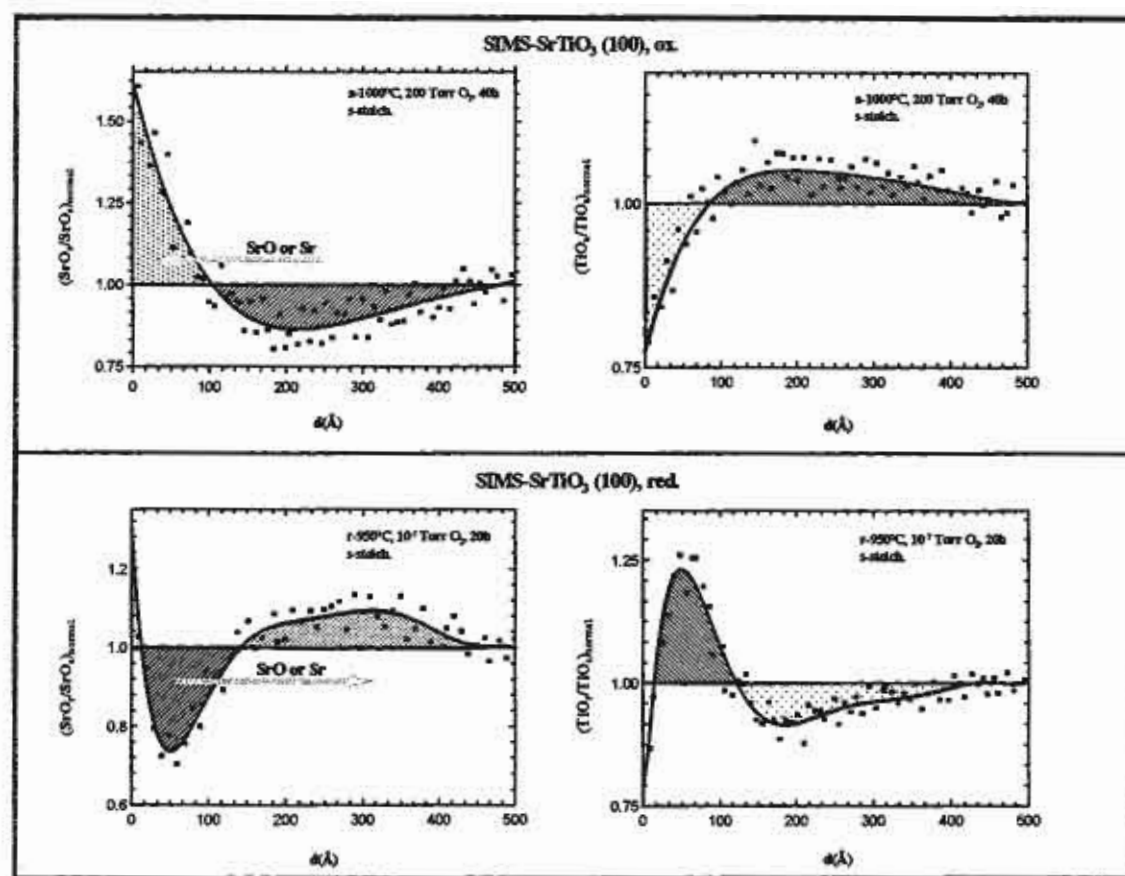
Fig.1: Depth profiles with SIMS of oxidized and reduced ABO$_3$-crystals (SrTiO$_3$).

Fig 2: Schematic illustration of the chemical heterogeneity in the surface region of ABO$_3$ - crystal induced by oxidation or reduction at elevated temperatures.

	Oxidation	Reduction
S1	AO×(ABO$_3$)$_x$	B$_2$O, BO, BO$_2$
S2	BO$_2$	AO×(ABO$_3$)$_x$
B	ABO$_3$	

SrTiO₃ (100), RT
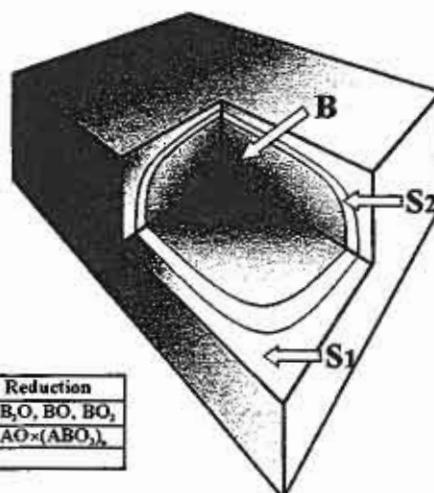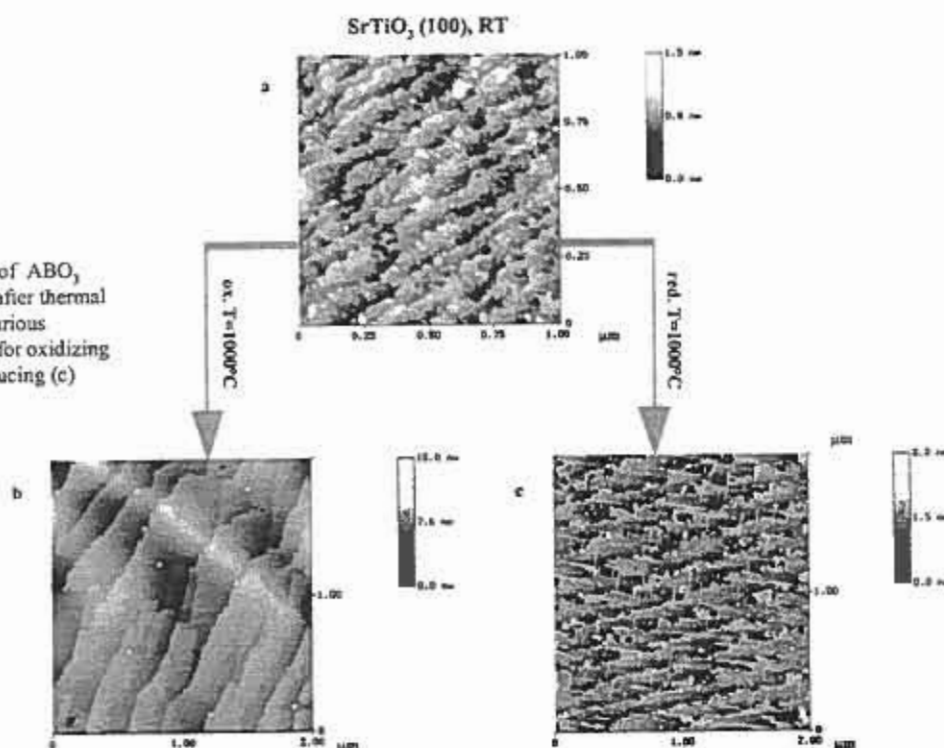
Fig.3:
AFM images of ABO₃ (100) surface after thermal treatment at various temperatures for oxidizing (b) and reducing (c) conditions.

temperatures. This also makes evident that a new interpretation of the electronic structure of the surface is necessary. This new concept of the restructuring of the near-surface region is important for an analysis of the catalytic reactions on perovskite surfaces and provides new insights to the anomalous behaviour of the ferroelectric perovskites. With detailed knowledge of the restructuring one can even hope to grow specific layered sequences of phases with A-enrichment and adepletion in a controlled manner on perovskite crystals.

1) F.Jona, G.Shirane: *Ferroelectric Crystals* (Pergamon, Oxford 1962)

2) C.Nougera: *Physics and chemistry of oxide surfaces* (Cambridge 1996)

3) K. Szot, C.Freiburg, and M.Pawełczyk, **Appl. Phys. A 53**, 563, (1991).

4) K.Szot, W. Speier, and W.Eberhardt ,**Appl. Phys Lett. 60**,1190, (1992).

5) K.Szot, M.Pawełczyk, J.Herion, Ch.Freiburg, J.Albers, R.Waser, J.Hulliger, J.Kwapuliński, J.Dec, **Appl. Phys. A 62**, 335,(1996).

6) K.Szot, W.Speier, S.Cramm, J.Herion, Ch.Freiburg, R.Waser, M.Pawełczyk, and W.Eberchardt, **J. Phys. Chem Solids 57**, 1765, (1996).

7) K.Szot, W.Speier, J.Herion, Ch.Freiburg, **Appl. Phys.A 64**, 55, (1997).

Ba-zirconate: an old high temperature proton conductor revisited

H.G. Bohn, T. Schober, J. Friedrich, D. Triefenbach

*Institute for Electroceramic Materials*

F23.90.0

Perovskite-type cerates and zirconates of the form ABO_3 (A=Ba, Sr; B=Ce, Zr) are known to dissolve significant amounts of water when doped with trivalent elements like Y or Yb. The protons are mobile and these systems become good proton conductors at elevated temperatures (high temperature proton conductors, HTPCs). It has been reported that cerates are better HTPCs than zirconates, and the best proton conducting system known up to now was $BaCeO_3$:5%Y. The disadvantage of this system (and in general all cerates) is that it becomes chemically instable in CO_2 containing atmosphere as it readily forms carbonates. This prohibits applications such as electrolytes in SOFCs or hydrogen sensors. Thus research activities (in particular in this institute) have concentrated in recent years on a new family of HTPCs, namely complex perovskites of the form $A_3B'_{1+x}B''_{2-x}O_{9-\delta}$ and here in particular on $Ba_3Ca_{1.18}Nb_{1.82}O_{9-\delta}$ (BCN18). This material is now well understood in many details and turned out to be a HTPC with electrical conductivity (in the grain interior) rather close to that of Ba-cerate [1]. However, the drawbacks of this system are unfavorable grain boundary properties such as high impedance, blocking of proton transport, and formation of cavities at the grain boundaries in reducing environment. These might be overcome by suitable material preparation procedures which require a totally new research project.

K.D. Kreuer (MPI Stuttgart) recently reported [2] that he could not reproduce the literature data on Ba-zirconate [3]. Therefore we have decided also to take a new look at this system which is (like most zirconates) chemically stable under most conditions. Ceramic samples of $BaZr_{0.9}Y_{0.1}O_3$ were prepared along the standard mixed-oxide route. Surprisingly water uptake up to 8% (the theoretical limit being 10%) was observed by *in situ* thermogravimetry. This already is considerably higher than reported previously. The electrical conductivity was then investigated by means of impedance spectroscopy. This technique allows to separate between contributions from the grain interior and the grain boundaries. Following the procedure successfully applied to BCN18 one sample of $BaZr_{0.9}Y_{0.1}O_3$ was first vacuum dried at 700°C and then charged with water to proton concentrations of 3.1, 4.6 and 6.2%. After each step the electrical conductivity σ was measured as a function of temperature T. The results are shown in figure 1 where we have plotted σT vs. $1/T$ on a
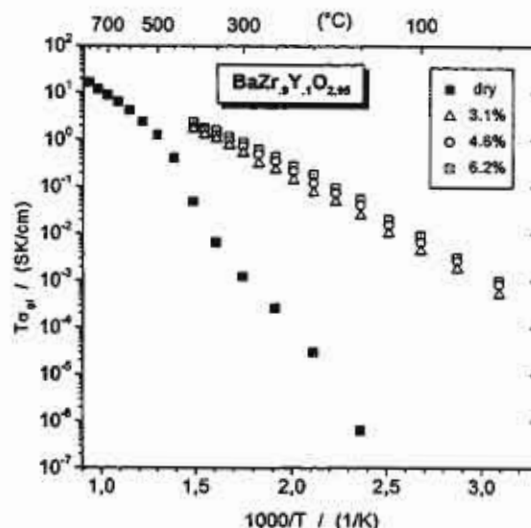
Figure 1: Grain interior conductivity of $BaZr_{0.9}Y_{0.1}O_{2.95}$ in the dry state and after charging to three different proton concentrations.
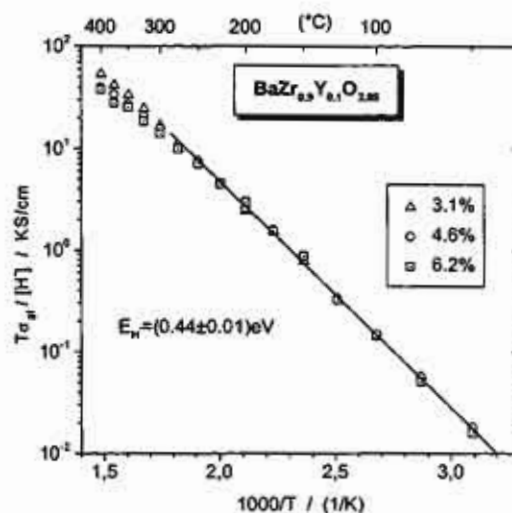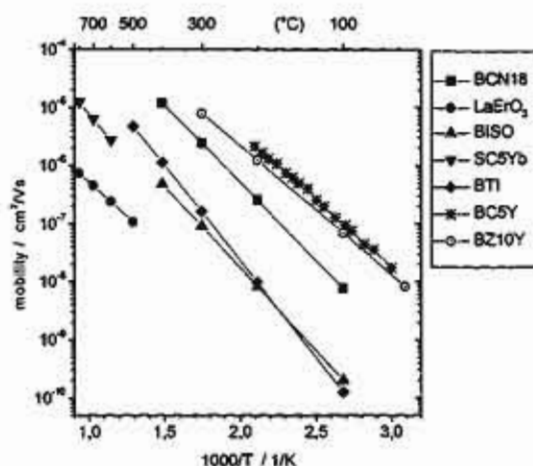

Figure 2: Temperature dependence of the normalized grain interior conductivity. The solid line represents a least squares fit to the data.

semi-logarithmic scale. Details of the curves have to be further analyzed but it is clearly seen that below 400°C the conductivity is considerably increased upon incorporation of water (e.g. by more than 3 orders of magnitude at 200°). It further

increases linearly with increasing proton content. The proton conductivity is given by $\sigma = const\,[H^\bullet]\mu_{H^\bullet}$ where $[H^\bullet]$ denotes the proton concentration and $\mu_{H^\bullet}$ the proton mobility. Below 300°C the curves show almost perfect Arrhenius behavior which indicates that the proton concentration does not change with temperature, i.e. the proton content is frozen in. This then allows a very precise determination of the proton mobility which is given by $\mu_{H^\bullet} = \dfrac{\mu^0_{H^\bullet}}{T}\exp(-\dfrac{E_{H^\bullet}}{kT})$.

Figure 2 shows a plot of $\sigma T/[H^\bullet]$ vs. $1/T$ for all the data presented in Fig. 1. In fact below 300°C all data fall on the same line. From the slope an activation energy of 0.44 eV for the proton diffusion is obtained and the pre-exponential factor results to $\mu^0_{H^\bullet} = (66\pm1)\,Kcm^2/(Vs)$. The absolute values of the conductivity and the mobility are significantly higher then reported previously for this material. In figure 3 we show mobility data gathered from the literature together with the newly obtained results for Ba-zirconate. It is seen that Ba-cerate is still the favorite material with the highest proton mobility ever observed, but our revisited Ba-zirconate comes very close !

chemical stability and no grain boundary problems so far.
The reason for the severe discrepancies to previously published data is unclear.

[1]   For a recent overview see: IFF Bulletin 53/1998.
[2]   K.D. Kreuer, communication at the 9th International Conference on Solid State Protonic Conductors (Bled, Slovenia, 17.-21.8.1998).
[3]   H. Iwahara, T. Yajima, T. Hibino, K. Ozaki, and H. Suzuki, Solid State Ionics **61** (1993) 65.

Figure 3: Temperature dependence of the proton mobility for selected HTPCs (BCN18: H.G. Bohn; LaErO$_3$:Y. Larring; BISO=BaIn$_{0.5}$Sn$_{0.5}$O$_{2.75}$:T. Schober; SC5Y=SrCe$_{0.95}$Yb$_{0.05}$O$_{2.975}$: H. Uchida; BTI=BaTb$_{0.6}$In$_{0.4}$O$_{2.8}$: R.R. Arons; BC5Y=BaCe$_{0.95}$Y$_{0.05}$O$_{2.975}$: K.D. Kreuer; BZ10Y: this report).

The grain boundary conductivity has not yet been analyzed in detail, but at first sight it is not limiting the proton conduction of the material.
These first results strongly suggest Ba-zirconate to be the favorite proton conducting material as it shows high proton mobility, high proton solubility (thus high proton conduction), mechanical and

Melting experiments on the proton conducting oxide BCN18 using microwave heating

M. Barton, P. Meuffels, R.R. Arons

Institute for Electroceramic Materials

Since the proton conducting properties of the perovskite type oxide, $Ba_3(Ca_{1.18}Nb_{1.82})O_9$, (BCN18) are strongly affected by the presence of grain boundaries, measurements on single crystals of this material are important.

In view of the high melting temperature of about 2000 °C and the high oxygen partial pressure of 200 mbar needed for the chemical stabilization of the melt, usual crucible techniques for crystal growth were discarded. Therefore we used a modified skull melting in a cold crucible.

In the case of skull melting a water-cooled copper crucible is filled with the powder of the material to be melted. A high-frequency electromagnetic field (MHz) is transmitted by a coil surrounding the crucible and powder. In view of the very low electrical conductivity of many ceramic compounds at low temperatures, a starter, e. g., carbon is added. Due to its absorption of the HF energy, the starter material is heated up, causing the surrounding oxide powder to melt. The conductivity of the molten oxide itself is sufficiently high to absorb energy from the HF field from which additional melt can be built. On the other hand, melting of the oxide close to the copper crucible surface is prevented by the cooling of the crucible. Accordingly, the melt is embedded in a crucible formed by a crust of its own material.

Subsequently, for growing of crystals the HF power must be reduced in a controlled way. Along the temperature gradient the melt crystallizes starting from the crust. By suitable crystal seed selection it should be possible to collect rather large single crystals in the center of the upper part of the crucible.

However, the success of this procedure depends on the skin depth and thus on the **electrical conductivity** of the material at higher temperatures. At the frequencies applied ($f \approx 10$ MHz) this skin depth should be of the order of a few centimeters. In case of larger skin depths, larger crucibles have to be used, leading to an increase of the HF power needed. For BCN18 we expected skin depths of 8 – 10 cm at $f \approx 10$ MHz, so that crucibles with diameters of about 15 – 20 cm and amounts of materials larger than 30 kg were necessary. By raising the frequency, the skin depth δ is reduced according to the relation $\delta \propto f^{-1/2}$, so that smaller crucibles and less amount of material can be used. In fact, an established and rather inexpensive technique exists at a frequency of 2.45 GHz, i. e., in the microwave range. From the discussion above it follows that at this frequency the skin depth in BCN18 at high temperatures amounts to about 1 cm. Additional coupling to the microwave field might arise from the appearance of dielectric losses in the GHz range. Since this coupling also appears at low temperatures, the use of a starter material might be avoided.

For the crystal growth experiments a 12 kW microwave generator with an optimized single
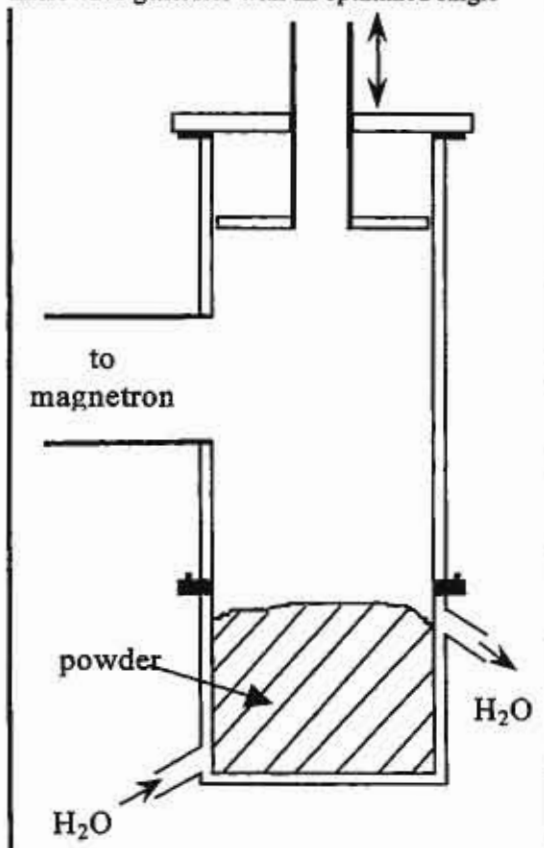
Fig.1: Single mode cavity resonator for melting up ceramic powder.

mode cavity resonator was used. The lower end was constructed as a cooled crucible of 10 cm diameter (see Fig. 1). Indeed, the powder could be heated up and locally melted without using a starter material. The cavities caused by the volume difference of the melted and powdered material were refilled with fresh powder and the material was melted again. This procedure was repeated several times until the cavities were negligibly

Fig.2: SEM-picture of fused ceramic from BCN18 showing the grain size of about 400 μm

small. As a final result we obtained a partly molten and coarse grained ceramic (fused ceramic) with maximum grain sizes of 300 – 600 μm (Fig. 2). In spite of the variation of many experimental parameters like heating and cooling rates as well as the maximum microwave energy used, we were not able to produce larger grains.

Obviously, with this method we did not succeed in producing larger amounts of melt which are needed to create better conditions for crystallization. We believe that the conductivity of the BCN18 melt is much higher than expected. This might be caused by the production of additional free electrons arising from the valence fluctuation of niobium. Due to its high conductivity the main part of the microwave energy is absorbed by the melt. Correspondingly, the skin effect in the melt is strongly enhanced, screening off the solid material

below. The volume of the melt does not grow by increasing the MW radiation energy either, since - in contrast to metals - the thermal conductivity of the ceramic is not sufficiently high to melt the surrounding powdered material. Only overheating of the melt is obtained leading to the evaporation of metal atoms. The MW energy is now completely absorbed by the plasma arising from the evaporated metal atoms. This results in a solidification of the melt and an interruption of the experiment.

That the conductivity of the molten material plays an essential role seems to be confirmed by experiments on materials with lower conductivity values of the liquid, e. g. Al_2O_3. In this case much larger amounts of material could be molten and crystallites with sizes of the order of 1 – 2 mm could be obtained.

Institute for Microstructure Research

General

The Institut für Mikrostrukturforschung (Institute for Microstructure Research) is working in a number of scientific fields. These were selected with an emphasis on modern-materials aspects, on the importance of an atomistic and microstructural understanding for their performance and, if possible, on the possibility of an evolution of research work into technical devices. The goal is an interdisciplinary research group working on a spectrum of scientific problems sufficiently wide to allow a flexible and rapid reaction to new scientific developments. In some of these fields the competence should span the whole range from materials preparation via basic physics investigations to technical devices. In others access to interesting materials and device problems is provided by qualified collaborations inside and outside the Jülich research center. Besides this general-physics and technology part of the institute there is a second part of special competence, the structural research by means of the most modern equipment in transmission electron microscopy and scanning tunneling microscopy. This work is carried out within the Center for High-Resolution Electron Microscopy which is operated by the institute and which at the same time serves a wider community of users.

Research Fields

The research fields can be characterized as follows:

(1) Ceramic Superconductors: Here the emphasis is (a) on thin-film and heterostructure production, Josephson effects, tunneling devices and their application in magnetometer systems and spectroscopic techniques. In addition (b) our investigations on high-frequency properties of ceramic superconductors has evolved into the technology of dielectric resonators and filters for communication applications.

(2) Semiconductors: Here the emphasis is on III-V compounds. In collaborations with various research groups we are studying, mainly by transmission electron microscopy, the growth of thin films and heterostructures. In recent years the problems related to the production and application of low-temperature GaAs have been of special interest. Another topic is the application of scanning tunneling microscopy to the study of the electronic states in compound semiconductors. Here a technique is employed which was pioneered in our group and which permits, via the detection of the far-reaching Debye screening effects of charged doping or impurity atoms at the surface, an investigation of defect related phenomena in the bulk of the samples.

(3) Metallic Alloys: Here the emphasis is on quasicrystalline alloys and their closely related normalcrystalline approximants. Our crystal-growth group is growing large single-quasicrystals for our own research but also for users world-wide, in particular for the participants in the DFG priority program on quasicrystals. Our own work on quasicrystals and approximants concentrates on plasticity and surface physics.

(4) Electroceramics: In the field of electrocermic materials we take advantage of our long-standing experience with respect to perovscitic materials both in preparation and in microstructure research by means of transmission electron microscopy. In collaboration with the Institute of Electroceramic Materials (Prof. Waser) we dedicate a large research capacity

to the investigation of the structural aspects of the production and properties of thin electroceramic films.

(5) High-Resolution Electron Microscopy: Although in the beginning primarily considered as a tool for high-quality materials investigations in atomic dimensions the theoretical, methodical and technical aspects of atomic-resolution transmission electron microscopy have become in recent years one of the central fields of interest of our group. We have developed special competence in the theory of high-resolution electron microscopy. Advanced application packages for the exit wave-function reconstruction are installed and serviced by us world-wide in electron-microscopic user facilities. Since 1991 and 1997 we have in collaboration with EMBL Heidelberg and Technical University of Darmstadt developed the word's first aberration-corrected transmission electron microscope with record resolution, 1.3 Å at 200 kV. These developments are continued (see below).

Equipment

With respect to the equipment the state can be described as follows:

The institute has at its disposal sputtering deposition machines, some of them with three-target facilities which were developed and built in the institute for the high-precision deposition of ceramic superconductor thin film and heterostructures, in particular dc-SQUID devices. In addition for this device production local clean room facilities, structuring and packaging facilities are available.

For high-frequency superconductivity measurement equipment for up to 20 GHz and spectroscopic equipment in the frequency range of 100 GHz up to 2 THz is available. The design of dielectric resonators and filters is optimized by means of finite-element calculations.

The institute operates together with the Institut für Streumethoden (Prof. Brückel) the laboratory for crystal-growth which was part of the former Institut für Materialentwicklung (Prof. Wenzl). This permits to maintain part of the outstanding expertise of this institute in the field of crystal growth. Beyond doubt the whole Department will take advantage of such a materials preparation facility.

The Institute für Mikrostrukturforschung operates the Jülich Center for High-Resolution Electron Microscopy. This contains two 400 kV JEOL machines of the type 4000 EX/FX, a JEOL 2000 EX, a PHILIPS CM 20 FEG and a JEOL 840 A scanning microscope. The most recent instrument is the spherical-aberration corrected PHILIPS CM 200 FEG, the world's first aberration-corrected transmission electron microscope developed by the institute in a collaboration financed by the Volkswagen-Stiftung. This instrument is now in a good working condition and it is operated as a user facility with national and international guests.

The priority in scanning tunneling microscopy is on high-temperature investigations a field only rarely served by other competing groups. Our scanning-tunneling microscopy group has at its disposal two microscopes with in-situ cleavage facilities and ex-situ heating up to 750 °C. These machines were designed and built inside the institute. An in-situ heating STM has been ordered from Omicron to be delivered in May 1999.

Although the institute has an extended in-house program for materials plasticity since about five years it never operated its own deformation machine. We received funds from various sources which permitted us to install (together with the group of Prof. Ullmaier) end of 1998

our own ZWICK mechanical testing system. The excellent collaboration in the plasticity field with the MPI für Mikrostrukturphysik, Halle, (Prof. Messerschmidt) will be continued.

Special results and developments

The cooperation with BOSCH in the framework of the BMBF-Consortium "High-Temperature Superconductor Systems for Satellite Communication" is very productive. In particular the multipole filters designed in the PhD-thesis work of St. Schornstein have received considerable attention. We consider it as an outstanding success that our institute, as partner of BOSCH, has won the competition for one of the five priority programs (Leitprojekte) of the German Federal Minister of Science and Technology (BMBF). The Title: "High-Temperature Superconductivity for the Communication Technology of the Future". The institute also succeeded in a competition for funding of a project with the same title by the "Strategiefonds of the Hermholtz-Gemeinschaft Deutscher Forschungszentren (HGF)".

Our dc-SQUIDs on the basis of ramp-type junction geometry continue their success both in performance and in their acceptance in application and on the market. As a supplier of TRISTAN Company (USA, formerly Conductus) we deliver a larger number of SQUIDs and magnetometers per month. New developments concern flux transformers and gradiometers where the market demands (and commercial orders) directly meet our scientific interests. Our dc-SQUIDs are also employed in a number of projects carried out together with the Institut for Thin-Film and Ion-Technology (Prof. Braginski) and the ZEL (Prof. Halling).

Our developments of Hilberttransform spectroscopy on the basis of Josephson-Junctions are bearing ample fruit. Hilberttransform spectroscopy provides an excellent and novel tool for spectroscopy in the frequency range of 10^{10} to 10^{13} Hertz, more than three orders of magnitude faster than Fourierspectroscopy. Here we have an excellent collaboration with the Institute for Radioelectronics in Moscow. We succeeded in acquiring a BMBF-project for the development of a fast gas-spectromer and a project with DESY, Hamburg. The latter is a consequence of our successful test of Hilberttransform spectroscopy for the determination of the shape of electron bunches in the beam in the TESLA accelerator test facility in Hamburg. This technology has the chance to become the basic technology for beam diagnostics in the final installation. Other projects concerning this novel technique have been submitted to international funding agencies.

The successful project of the spherical-aberration corrected transmission electron microscope described above has triggered a priority program of the DFG. In the framework of this new program granted in 1998 our institute will develop in collaboration with CEOS Company, Heidelberg, and Zeiss-LEO, Oberkochen, the world's first Subangström-Instrument. Besides ultra-high resolution the 200 kV machine will contain a monochromator and an in-column energy filter of the Krahl-type. Another two instruments further optimized for high-resolution analytic functions will be installed at the University of Münster and at the MPI für Metallforschung in Stuttgart. Delivery is planned for 2003. This will maintain the institutes position as a pioneer in advanced instrument development.

The institute is partner of PHILIPS ELECTRON OPTICS with respect to the theory and application of exit-wave function reconstruction techniques in high-resolution transmission electron microscopy. In this field our institute is respected as a key institute. Advanced application packages for the exit wave-function reconstruction are installed and serviced by us

world-wide, under PHILIPS contract in electron-microscopic user facilities. The key role in this field is further illustrated by a large number of visits by international experts.

The quasicrystal group has currently three DFG funded projects which, after running now for two years, will enter the second phase in May 1999. In these as well as in other parts of our research program the shortage in manpower has not been without influence. Delays resulting from problems to find good PhD students and post-docs were and are unavoidable. It is the clear institute policy to maintain high-quality standards and, in the extreme, to return funds rather than yield to the personnel-related difficulties. Great efforts went into a new PhD program with the Russian Academy of Sciences and other GUS state universities and universities in China. In the framework of this special program designed by the institute and the partners abroad the PhD students are working two years in Jülich on a grant supervised by the Jülich Doktorandenausschuß, but they will pass their examina in their home university. Two PhD students are working now in the institute on this basis. Others financed by other sources (e.g. by the Humboldt Foundation) come from China.

Knut Urban

Institute for Microstructure Research

Staff

(Total 14 - 7 Scientists)

DI W. Evers	Physical Experimental Technique, Low Temperature Technique, Thin Film Production	(23.55.0, 23.42.0)
DI K.-H. Graf	Electronics, Electronic Data Processing, Scanning, Tunnelling Microcopy	(23.55.0, 23.42.0)
Dr. B. Grushko	Crystal growth, phase diagrams of alloys	(23.55.0)
J. Hanssen	Technical Maintenance of High Resolution Electron Microscopy	(23.55.0, 32.42.0)
Dr. C.L. Jia	Characterization of microstructures, interfaces, grain boundaries and defects in superconductor, diamond and electronic ceramic films by high resolution electron microscopy	(23.42.0)
Dr. B. Kabius	Cs-corrected Transmission Electron Microscopy for Imaging of interfaces in Semiconductors, Electron microscopy of superconducting materials	(23.42.0)
Dr. N. Klein	Microwave applications of HTc-superconductors	(23.42.0)
D. Meertens	Metallography, Semiconductor Preparation, Scanning- and Transmission Electron Microscopy	(23.55.0, 23.42.0)
Dr. U. Poppe	Superconductivity, Tunneling Spectroscopy High-Tc Superconductor Thin Films and Multilayers, Scanning Tunnelling Microscopy	(23.42.0)
I. Radloff	Secretary	
Dr. A. Thust	Reconstruction techniques in high-resolution electron microscopy	(23.55.0)
Prof. Dr. K. Urban	Head of Institute; Microstructure of crystal lattice defects and interfaces in metals and semiconductors, phase transformations in alloys, electron microscopy	
G. Waßenhoven	Photolaboratory, Photography Technique	(23.55.0, 23.42.0)
R. Peters	Photolaboratory, Photography Technique	(23.55.0, 23.42.0)

Post-docs (Total 6)

Dr. Ph. Ebert	Scanning tunnelling microscopy of semiconductor interfaces	(23.42.0; 23.55.0)
Dr. M. Feuerbacher	Plasticity of Quasicrystals	(23.55.0)
Dr. H. Klein	Plasticity of Quasicrystals	(23.55.0)
Dr. M. Lentzen	Microscopy of seminconductor heterostructures, Reconstruction techniques in high-resolution electron microscopy	(23.42.0)

| Dr. M. Luysberg | Transmission Electron Microscopy of semiconductor heterostructures, Low temperature GaAs und microcrystalline Si | (23.42.0) |
| Dr. H. Yi | Cryogenic dielectric Filters | (23.42.0) |

Doctor students (Total IO)

V. Chirotov	Broadband Hilbert-Transform Spectroscopy with high-Tc Josephson junctions	(23.42.0)
B.Jahnen	Interdiffusion in Antimonid-based heterostructures	(23.42.0)
Ch. Lei	Investigation of Lattice Defects in Electro-ceramic Thin Films by High Resolution Electron Microscopy	(23.42.0)
R. Rosenfeld	Phase reconstruction techniques in high-resolution electron microscopy, Electron Microscopy of electrocerainic Materials	(23.42.0)
P. Schall	Plasticity of Quasicrystals and related intermetallic phases	(23.55.0)
D. Schemion	Investigations of ferrite materials at cryogenic temperatures and microwave applications in conjunction with high temperature superconductors (23.42.0)	
St. Schornstein	Microwave Filters based on high temperature superconductors, Construction of HTc-based Band Pass Filters	(23.42.0)
F. Kluge	Scanning tunnelling microscopy of quasicrystals	(23.42.0)
M. Winter	Microwave Frequency Standards	(23.42.0)
M. Yurechko	Formation of intermetallic phases in ternary alloys of aluminium with transition metals	(23.55.0)

Diploma students (Total 4)

R. Ott	Production of structured dielectric layer systems and investigation of their dielectric properties in dependence of morphologyand granularity.	(23.42.0)
P. Quadbeck	Scanning Tunnelling Microscopy of Si and Te-doped GaAs	(23.42.0)
M. Heggen	Investigation of Plastic Behaviour of icosahedral Zn-Mg-Re Quasicrystals	(23.55.0)
D. Joussen (FH)	New Circuits for Hybride Oszillators	(23.42.0)

Guests (Total 3)

Dr. J. Chen	Cs-corrected Transmission Electron Microscopy	(23.42.0)
Dr. Y. Divin	Hilbert-Spectroscopy (Russia)	(23.42.0)
Dr. M. Faley	High-Tc-Superconductor SQUIDs (Russia)	(23.42.0)

Cryogenic dielectric resonators for future microwave communication

I.S.Ghosh [3], D.Schemion [1], S.Schornstein [2], M.Winter [1] and N.Klein [1]

[1] *Institut für Mikrostrukturforschung ,* [2] *presently employed at Softlab, Köln,* [3] *presently employed at Philips Research Center, Aachen*

Abstract - Cryogenic dielectric resonators machined from various single crystalline materials exhibit a strong increase of quality factor. Therefor they are excellent suited for various microwave applications. We have developed a dielectric C-band quasielliptic four-pole filter for use in output multiplexers of future cryogenic satellite transponders and a demonstrator for a low phase noise oscillator at 23 GHz, based on a sapphire whispering gallery resonator with piezoelectric frequency tuning. A sapphire/rutile compensated whispering gallery resonator is realized for secondary frequency standard application.

I. DIELECTRICS FOR MICROWAVE APPLICATIONS

Dielectric resonators based on microwave ceramics are of great importance for current microwave technology. In most cases, they are used either as frequency stabilising elements for microwave local oscillators, or as resonators each forming one or two poles of a microwave filter. For applications at room temperature polycrystalline ceramics are in use and tremendous progress has been made recently in achieving high permittivity, high Q, low temperature coefficient of the resonant frequency, and low fabrication costs [1].

Single crystals of various dielectric materials exhibit a strong decrease of the loss tangent $tan\delta$ at microwave frequencies upon cooling to cryogenic temperatures. As an example, high-purity sapphire at X-band frequencies exhibits $tan\delta$ (300K) $\approx 1 \cdot 10^{-5}$, $tan\delta$ (77K) $\approx 1 \cdot 10^{-7}$, and values for T$\rightarrow$ 0 of 10^{-9} to 10^{-8}, depending strongly on the level of impurities in the crystal [2]. However, at room temperature some microwave ceramics exhibit very low losses close to single crystals. As an example, a polycrystalline Ba-Mg-Ta-O compound manufactured by MURATA with a permittivity of about 22 exhibits a $Q \cdot f = f / tan\delta$ of 350 THz [3], the corresponding value for single crystalline LaAlO$_3$ is 500 THz [4]. The advantage of ceramics is a temperature coefficient of the resonant frequency of a dielectric resonator of less than 1 ppm/K, the corresponding value of LaAlO$_3$ is 55 ppm/K [4]. The optimisation of microwave ceramics with lower losses down to cryogenic temperatures would be very challenging for the applications described in the next section.

II. CRYOGENIC DIELECTRIC FILTERS FOR SATELLITE OUTPUT MULTIPLEXERS

Our filter approach described in detail in [5] is based on the fundamental mode of a dielectric hemisphere. For this mode – similar to the TE$_{018}$-mode of a dielectric cylinder – the electric field is oriented nearly parallel to the contour of
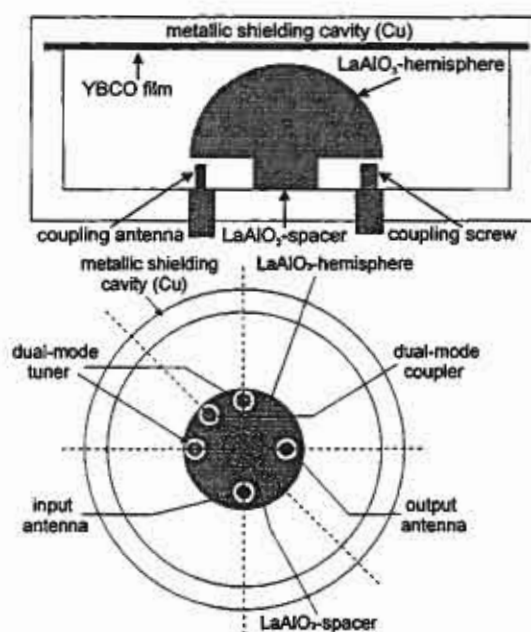

Fig. 1. Schematic view of a dual-mode filter based on two degenerated modes in a dielectric hemispheres. The top view (bottom) indicates the position of the coupling and tuning elements.

the hemisphere. If the hemisphere is mounted on a metallic plane, this mode is equivalent to the 3-times degenerated TE$_{018}$-like mode of a dielectric sphere, with the metallic plane acting as an electromagnetic image plane. Consequently, this mode is 2-times degenerated allowing for dual-mode operation. In order to minimise the loss contribution of the metallic shielding cavity the hemisphere is arranged on a dielectric cylinder, usually machined from the same material as the hemisphere.

This configuration results in a very high electric field in the airgap underneath the hemisphere to achieve sufficiently strong external coupling by coaxial probes and dual-mode splitting by dielectric tuning rods (Fig. 1). Plots of the electromagnetic field distribution can be found in [5]. A quasielliptic four-pole filter was constructed by arranging two hemispheres in one metallic shielding cavity, one being separated from the other by a metallic aperture. Fig. 2
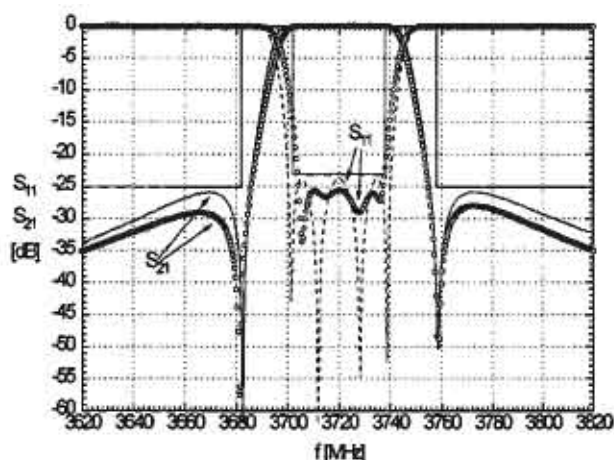
Fig. 2. Measured frequency response of a C-band quasielliptic four-pole filter based on lanthanum aluminate hemispheres (s_{11}: reflected signal (circles), s_{21}: transmitted signal (squares)) in comparison to an equivalent circuit simulation (lines), (PUFF, [6])).

Fig. 3. Magnification of s_{21} indicating the low value of the in-band insertion loss.

shows the measured filter characteristic of a C-band filter with a centre frequency of 3.72 GHz and a bandwidth of 32 MHz (s_{11}: reflected power, s_{21} : transmitted power). The Q_0 of the filter was i) measured from the 3 dB bandwidth under weak coupling conditions ii) determined indirectly from the measured in-band insertion loss using an equivalent circuit model of our filter [6]. The filter was measured both with and without HTS-thin film endplate. At room temperature, the insertion loss was found to be – 0.08dB with a silver plated shielding cavity. The corresponding Q_0 is 46,000, which is extremely low in comparison to cavity filters or conventional dielectric filters employing polycrystalline dielectrics. At $T = 77$ K the insertion loss was measured to be –0.04 dB (Fig. 3), indistinguishable with or without HTS endplate. However, the accuracy of this measurement performed with a calibration at 77K is only 0.03 dB. For the filter without HTS endplate, this value remains constant up to $T = 120$K. In liquid nitrogen ($T = 77$ K) the power handling capability of the filter was found to be 180 W (based on a 0.1 dB change of insertion loss) for both configurations. For the version with the HTS endplate this power level corresponds to a maximum rf magnetic field of only 4 Oe at the surface of the HTS film. At present, we are still optimising the coupling in order to avoid a power handling limitation by multipacting apparent during operation in vacuum, which currently limits the capability of our filter to about 35 W.
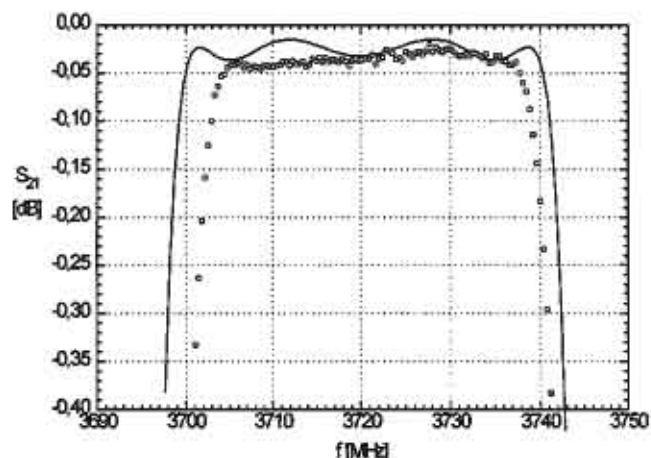
III. CRYOGENIC DIELECTRIC WHISPERING GALLERY RESONATORS IN LOW PHASE NOISE OSCILLATORS

Dielectric resonators with Q-values $> 10^6$ at T = 77 K have been employed to build an oscillator at 23 GHz for Satellite communication in cooperation with Bosch Telecom GmbH. In order to achieve ultimate Q-values we have used sapphire Whispering Gallery Mode resonators. The key advantage of this resonator structure is that $\approx$90% of the electric field energy is confined within a central cylinder made of air; only $\approx$10% are stored in a sapphire structure acting as reflector for the resonant radiation.

In order to set the oscillator frequency accurately we have investigated the performance of a mechanical and electrical tuning mechanism. The mechanical tuning is done by reducing the distance between the top endplate and the central dieletric. The tuning range for this kind of
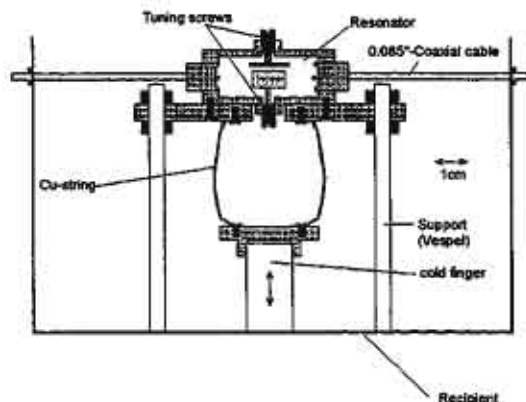

Fig.5. Mechanically de-coupled resonator on cold finger of commercial Stirling cooler.

mechanism without reducing the resonator Q by more than 10% is about 40 MHz. The electrical tuning is done by a piezoeletrical tuning element. We achieved a frequency shift of 40 kHz and 100 kHz.

We have incorporated this oscillator on a commercial Stirling–type miniature cooler. (AEG SL200; max. cooling power at 77 K = 3 W.) To mechanically de-couple the resonator from the cold finger of the Stirling cooler we connected the resonator with the cold finger via stranded copper wires which absorb most of the vibrational energy.

An integrated two staged HEMT Amplifier has been build for the active element in the oscillator, which has an integrated varactor phase shifter to fullfill the oscillator condition of 2π.

According to Leesons Model [7] and the noise contribution of each Amplifier, investigated in the work done by [8], we expected phase noise values of about -130 dBc/Hz at 1 kHz offset.

IV. CRYOGENIC DIELECTRIC WHISPERING GALLERY RESONATORS IN SECONDARY FREQUENCY STANDARDS

Single crystal dielectric materials such as sapphire demonstrate remarkably low values for the dielectric loss tangent even at rather modest cryogenic temperatures (40-80 K) which are readily achieved using Gifford-McMahon closed cycle coolers. We have taken a resonator design shown in Fig. 6, previously reported in [9] for a composite dielectric resonator incorporating both sapphire and rutile single crystal elements and further improved the Q value while raising the frequency versus temperature compensation point to greater than 60 K. At the same time the geometrical size of the dielectric pucks has been increased while still using the same closed cycle cooler so that a compact loop-oscillator system is realised at a frequency of close to the Cs atomic clock hyperfine frequency and an operating temperature of 63.5 K. Unloaded Q values as high as 10^7 have been achieved under these conditions for this composite resonator.

Allan variance measurements on the resonator temperature indicate that a few tens of microkelvin stability at averaging times out to at least $\tau=10^3$ s are already achievable. A Pound stabilisation technique is being used to reduce the effects of drifting in room temperature circuit components. Sidebands at ±100 kHz are imposed using an electronic phase shifter. The reflected signal from the resonator input has a component at 100 kHz if the oscillator is not tuned exactly to the resonator centre frequency. This error signal is detected by the lock-in and applied to the phase-shifter to correct the resonant frequency.

In addition we have used the oscillator as a low phase noise source and have measured its phase noise performance, achieving a level of less than -120 dBc/Hz for offset frequencies greater than 1 kHz.
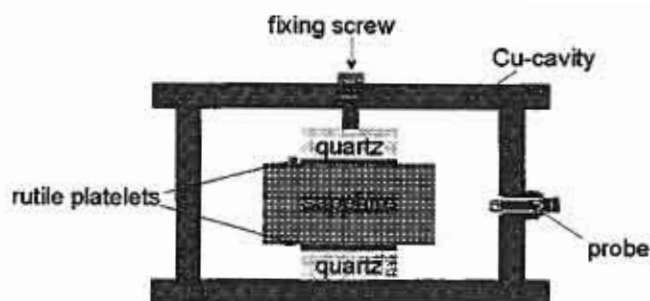

Fig. 6. Resonator design for composite sapphire/rutile whispering gallery resonator

REFERENCES

[1] K. Wakino, "Recent development of dielectric resonator materials and filters in Japan", *Ferroelectrics*, vol. 91, pp. 69-86, 1989 and commercial information by MURATA Industries, Japan.

[2] V.B.Braginsky, V.S. Ilchenko, and Kh. S. Bagdassarov, "Experimental observation of fundamental microwave absorption in high quality dielectric crystals", *Phys.Lett. A*, vol. 120, pp. 300 - 305, 1987.

[3] T.Kässer et al., "A satellite repeater comprising superconducting filters", *IEEE MTT-S Int. Microwave Symp. Digest*, pp. 375-378, 1998.

[4] C.Zuccaro et al., "Microwave absorption in single crystalline lanthanum aluminate", *J. Appl. Phys.*, vol. 82, pp. 5695-5704, 1997.

[5] S.Schornstein, I.S. Ghosh, and N.Klein, "High temperature superconductor-shielded high power dielectric dual-mode filter for applications in satellite communications", *IEEE MTT-S Int. Microwave Symp. Digest*, pp. 1319-1322, 1998.

[6] S.W. Wedge, R.Compton, D.Rutledge, "PUFF", *Computer Aided Design Software for Microwave Integrated Circuits*, Version 2.0.

[7] Leeson D B 1966 *Proc. IEEE* 54 329-330

[8] Schemion D, Diplomathesis 1997, IFF, FZ-Jülich GmbH

[9] L.Hao, N.Klein, W.J.Radcliffe, J.C.Gallop and I.S.Ghosh "Temperature compensated cryogenic whispering gallery mode resonator for microwave frequency standard applications" Proc. 12thEFTF (1998, Warschau) pp112-114

Operation of HTS dc-SQUID Sensors in High Magnetic Fields

M.I.Faley[1], U.Poppe[1], K.Urban[1], E.Zimmermann[2], W.Glaas[2], H.Halling[2], H.-J.Krause[3], M.Bick[3], D.N.Paulson[4], T.Starr[4], and R.L.Fagaly[4]

[1] Institut für Festkörperforschung, FZ-Jülich GmbH, D-52425 Jülich, Germany
[2] Zentrallabor für Elektronik, FZ-Jülich GmbH, D-52425 Jülich, Germany
[3] Institut für Schicht- und Ionentechnik, FZ-Jülich GmbH, D-52425 Jülich, Germany
[4] Tristan Technologies inc., San Diego, CA 92121 USA

For HTS dc-SQUID sensors operating in high magnetic fields we have used quasiplanar HTS Josephson junctions, HTS films prepared at optimized conditions with a high oxygen pressure dc-sputtering technique, a capsulation with a heater, and a proper dc-SQUID layout. DC-SQUIDs tested in magnetic fields up to about 100 mT demonstrate no reduction of the critical current. With the use of a digital feedback a dynamic range of about 160 dB was achieved. For the magnetometers with flip-chip flux antennas a resolution of about 40 fT/√Hz was obtained in unshielded environment [1].
F&E-Nr: 23550

Many applications require high-T_c dc-SQUID magnetometers operating at liquid nitrogen temperature in a magnetically unshielded environment and even in the presence of high static magnetic fields. A magnetic field dependence of the involved junctions should be avoided.

Josephson junctions demonstrate a Fraunhofer like oscillating dependence of the critical currents on external magnetic fields, normal to the current flow. For planar Josephson junctions the affecting magnetic field is parallel to the substrate surface. The magnetic field $H_\parallel$ leads to an appearance of shielding currents in the film. The first minimum of the critical current I_c corresponds to the shielding current density reaching the critical current density of the junctions. The magnetic field $H_{c\parallel}$ at which the film becomes normal is depending on the film thickness:

$$H_{c\parallel} = 2\sqrt{6}\frac{H_c\lambda_c}{d}$$

where H_c is the thermodynamic critical field and $d \approx 0.2$ μm is the film thickness. The penetration depth λ_c is about 0.7 μm at low temperatures. Taking into account a temperature dependence $\lambda_c(T) = \lambda_c(0)/(1-(T/T_c)^2)^{1/2}$ typical for YBa$_2$Cu$_3$O$_7$ (Y*) films we find λ_c(77K) ≈ 1.3 μm, leading to

$$H_{c\parallel} \approx 32 H_c \qquad (1).$$

A similar effect probably appears for quasiplanar Josephson junctions [2]. The only direction in which the quasiplanar junctions are opened for the external field is the direction parallel to the substrate plane and perpendicular to the current flow (from side). In this direction the effective area, where the interference of supercurrent in the junction appears is about 0.2 μm². This would correspond to a first minimum in I_c(H) dependence at magnetic field of about 10 mT. But due to reduction of shielding currents in the superconducting electrodes according to (1) the first minimum is shifted up to about 300 mT. This could explain the absence of a reduction of the critical current in the quasiplanar Josephson junctions for the investigated range of magnetic fields up to about 100 mT [2].

This opens up a new possibility to measure large magnetic fields with high accuracy. Thus the dynamic range of the constructed system exceeded 160 dB. This value one should compare with the one for Hall sensors of about 100 dB, which are typically used for this range of magnetic fields. Hall sensors can operate in high fields, but have a poor sensitivity of about 10 nT/√Hz. The periodic dependence of the dc-SQUID voltage on the external flux allows a counting procedure for signals much larger than a flux quantum. This in principle can lead to a dynamic range up to about 32 bit. Within one period a conventional analog compensation of the magnetic flux is used.

Important for many application is the operation of sensitive magnetometers including a multilayer flux transformer in unshielded environment. We have demonstrated the stable operation of the flip-chip magnetometers with a sensitivity of 1.6 nT/Φ_0. To reduce the effect of the external noise some of the measurements were performed in rural environment with less electromagnetic noise. There was neither a suppression of the bias current of the magnetometers nor any increase of the white noise (of about 40 fT/√Hz) of the measuring system.

To strengthen the flux pinning in multilayer structures we have used the inclusions of secondary phases (like Y$_2$BaCuO$_5$, BaCuO$_2$, and CuO) inside Y* films. It is remarkable that the inclusions can be epitaxially covered by following layers or by the same film, sputtered at different conditions. A Pt heater placed near the SQUID inside the capsulation allows to remove trapped magnetic flux from Y* films and thus helps to improve the noise properties of the magnetometer in high magnetic fields.

[1] M.I.Faley, U.Poppe, K.Urban, E.Zimmermann, W.Glaas, H.Halling, H.-J.Krause, M.Bick, D.N.Paulson, T.Starr, and R.L.Fagaly, *Applied Superconductivity Conf.*, Sept. 13-18, 1998, Palm Desert, USA. Report EHA-02.

[2] M.I.Faley, U.Poppe, K.Urban, H.Hilgenkamp, H.Hemmes, W.Aarnink, J.Flokstra, and H.Rogalla, *Appl.Phys.Lett..*, vol.67, No.14, 2087-2089, 1995.

Formation of As precipitates in Be doped non-stoichiometric GaAs and their influence on the electrical properties

M. Luysberg and K. Thul

Institut für Mikrostrukturforschung

Isothermal and isochronal annealing studies of highly Be doped non-stoichiometric GaAs were performed to study the influence of Be doping on structural and electrical properties. In both, undoped and Be doped material, As precipitates are formed upon annealing. However, a considerably higher activation energy of As precipitate formation following the Ostwald ripening mechanism is found for the Be doped case when compared to its undoped counterpart. Therefore, Be retards the As diffusion in low temperature grown GaAs. The electrical conduction behavior of the as-grown material is characterized by hopping conduction. Short annealing times turn the material resistive, despite the high Be doping levels. Only longer annealing times or higher temperatures result in p-type conduction. These changes of the electrical properties cannot be described by the buried Schottky barrier model, which assumes the precipitates to govern the conduction behavior. Instead, the electrical properties are dominated by the residual point defect concentrations.

The excess As incorporated during the low temperature growth of GaAs (LT-GaAs) by molecular beam epitaxy is made responsible for the unique properties of this material, such as the high electrical resistivity and the ultrashort carrier trapping time. The As rich LT-GaAs films contain a high concentration of point defects. In particular, the As antisite defect (As_{Ga}) has a considerable impact on electrical and optical properties owing to its deep double donor nature [1]. Upon annealing the excess As conglomerates to As precipitates (e.g. [2,3]). Recently, Be doped material was shown to have superior optical properties in view of the carrier trapping times being even shorter than in the undoped counterpart [4]. Furthermore, the material is more thermally stable, i.e. annealing at moderate temperatures does not induce significant structural changes [4,5]. The mechanisms leading to this thermal stabilization by Be doping for the case of high Be doping levels are investigated. In addition, the change of the electrical properties upon annealing is studied, in particular with respect to the structural changes.

Non-stoichiometric Be doped GaAs films (10^{20} cm^{-3}) as well as an undoped reference sample were grown by MBE at a substrate temperature of 190°C and BEP ratios of 10 and 20. Isochronal and isothermal annealing series were studied in a temperature range from 600°C to 850°C. Structural properties were determined by transmission electron microscopy (TEM). The temperature dependence of the electrical conductivity was measured using a standard van der Pauw configuration.

Upon annealing both, the undoped reference sample and the highly Be doped material undergo qualitatively the same structural changes: using annealing temperatures below 750°C results in a homogeneous distribution of crystalline precipitates [5]. The precipitates show the typical Moiré fringe contrast (Fig 1a and c), which was utilized for identification of the phase of the precipitates as hexagonal As. At high annealing temperatures, i.e. 800°C and 850°C, the precipitates are amorphous causing a homogeneous dark contrast in Fig.1 b and d. By energy dispersive X-ray
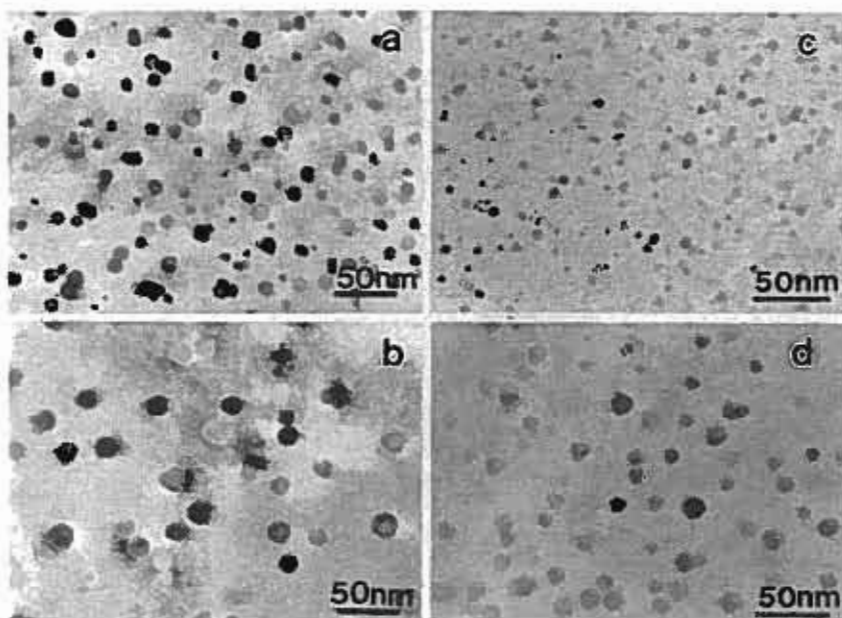
Fig. 1: TEM bright field images showing precipitates in undoped (a, b) and Be doped (c, d) LT-GaAs. Samples were annealed at 700°C (a, c) and 800°C (b, d) for 30 min. A considerably smaller precipitate size is observed in the case of Be doping.

analyses these precipitates were shown to consists of As. A considerably smaller precipitate size is observed in Be doped material compared to it's undoped counterpart (Fig. 1). The quantitative evaluation of the precipitate densities reveals a smaller value in LT-GaAs:Be [5].

With increasing annealing time and/or temperature the precipitates grow larger according to an Ostwald ripening mechanism. This behavior is also seen for undoped and Be doped material, respectively, in Figure 1, where the precipitates are significantly larger at the higher temperature (800°C Figs. 1 b and d).The quantitative evaluation of the activation energy of precipitate coarsening results in a much higher value of about 2.5 eV for the Be doped samples compared to 1.4 eV obtained for the undoped reference sample. Therefore, it can be concluded that Be doping retards the As diffusion.

The low activation energy of the undoped LT-GaAs was previously attributed to the migration energy of the As_{Ga} in a V_{Ga} assisted diffusion process [3]. The formation energy of V_{Ga}, which usually has to be considered as well, can be neglected in the case of As diffusion in LT-GaAs, because a supersaturation of V_{Ga} is incorporated during the low temperature growth [2]. The reduced diffusion in the Be doped samples may therefore be explained by a reduced V_{Ga} concentration governing the vacancy assisted diffusion of As_{Ga}. However, other mechanisms may have to be considered as well to explain the suppressed As diffusion, like the formation of Be_{Ga}-As_{Ga} complexes. This would require to overcome the binding energy of the complex to allow for the diffusion of the As_{Ga}.

The electrical properties obtained after different annealing conditions are shown in Figure 2. The as-grown sample shows a high conductivity. Temperature dependent measurements revealed the typical hopping conduction behavior [5]. Annealing at 600°C for short times (< 6h) leads to a decrease of the conductivity, whereas longer times and/or higher temperatures result in p-conductive samples. Following the buried Schottky barrier model [6], where zones around the metallic As precipitates are assumed to be depleted of carriers, As precipitates could be responsible for this conduction behavior [9]. The overlap of
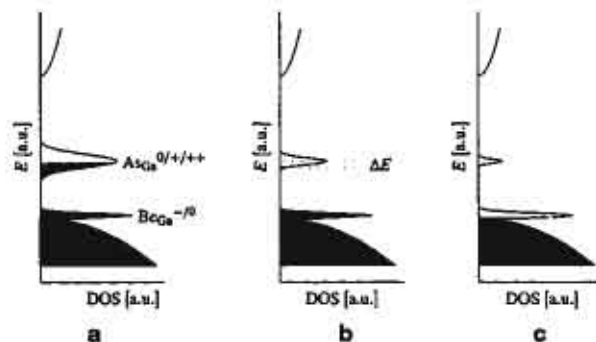
Fig.3: Density of states diagram for electrons for as-grown material (a), after short annealing times (600°C,<6h) (b), and after long annealing times and/or higher temperatures (c). The 0/+ and the +/++ band of the As_{Ga} donors are merged for simplicity, the V_{Ga} acceptor band is omitted

these depleted regions may explain the resistive material obtained after short annealing times, where the precipitate density is highest [5]. However, by quantitatively measuring the sizes and densities of precipitates in our samples, we obtain the volume of the depleted zones to be at most 2.6% [5]. We conclude that the buried Schottky barrier model is not suitable to describe the conduction behavior in highly Be doped LT-GaAs.

Instead, residual defects have to be taken into account, as shown schematically in Figure 3. According to this model, the as-grown sample is characterized by a high As_{Ga} concentration with a large fraction of As_{Ga}^{+} (corresponding to the Be acceptors) pinning the Fermi level midgap (Fig. 3a). Annealing the samples only shortly results in a decrease of the As_{Ga} concentration (Fig. 3b). However, there are still enough midgap defects present to pin the Fermi level in the lower half of the band gap. According to the reduced defect concentration, hopping conductivity within the As_{Ga} band becomes less dominant and the resistivity rises. Only large annealing times and/or higher annealing temperatures make the material p-type, since finally the As_{Ga} concentration becomes smaller than the Be acceptor concentration (Fig. 3c).

[1] X. Liu, A. Prasad, W. M. Chen, A. Kurpiewski, Z. Liliental-Weber, and E. R. Weber, *Appl. Phys. Lett.* 65, 3002 (1994)

[2] M. Luysberg, H. Sohn, A. Prasad, P. Specht, Z. Liliental-Weber, E. R. Weber, J. Gebauer, and R. Krause-Rehberg, *J. Appl. Phys.* 83, 561 (1998)

[3] Z. Liliental-Weber, X. W. Lin, J. Washburn, and W. Schaff, *Appl. Phys. Lett.* 66, 2086 (1995)

[4] P. Specht, S. Jeong, H. Sohn, M. Luysberg, A. Prasad, J. Gebauer, R. Krause-Rehberg, and E. R. Weber, *Mater. Sci. Forum* 258-263, 951 (1997)

[5] M. Luysberg, P. Specht, K. Thul, E. R. Weber, and Z. Liliental-Weber, *Proc. of the SIMC-14*, Berkeley (1998), accepted for publication.

[6] A. C. Warren, J. M. Woodall, J. L. Freeouf, D. Grischowsky, D. T. McInturff, M. R. Melloch, and N. Otsuka, *Appl. Phys. Lett.* 57, 1331 (1990)
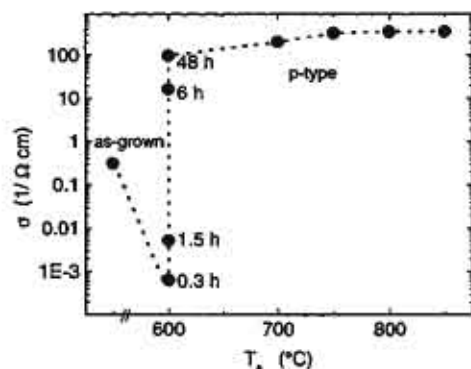
Fig.2: Change of room temperature conductivity of Be doped LT-GaAs upon annealing. The as-grown conductivity is high due to hopping conduction. Short annealing times turn the sample resistive before it finally becomes p-type at longer times and/or higher temperatures.

A novel type of dislocation in an Al-Pd-Mn quasicrystal approximant

H. Klein, M. Feuerbacher and P. Schall

Institut für Mikrostrukturforschung

A single crystal of the ξ'-AlPdMn phase was plastically deformed in a three-point bending geometry. The deformed crystal shows a periodic lattice of phason lines. In an HREM study a novel dislocation type, termed meta-dislocation, with a Burgers vector of magnitude 165 Å was observed. At the core of the meta-dislocation a dislocation of the ξ'-structure is found. Its structure and Burgers vector were determined by HREM. It is equivalent to the most common Burgers vector in the icosahedral quasicrystal. The structural relationship between the dislocation and the meta-dislocation is discussed.

As in crystalline solids, the predominant plastic deformation mechanism in quasicrystals (QCs) is the motion of dislocations. This has been shown for QCs of icosahedral [1] and decagonal [2] structure. In contrast to periodic crystals, however, icosahedral QCs show no work hardening. They even become softer the more they are plastically deformed [3], i.e. the flow stress decreases with increasing strain.

In the compositional vicinity of quasicrystalline phases one often finds periodic phases with large unit cells. These 'approximants' represent an intermediate state between crystals and QCs. They are periodic in structure and therefore crystals and they are close in local order, chemical composition and physical properties to QCs [4]. One should therefore expect to find a similar behavior of approximants regarding the plastic deformation mechanism. On the other hand, due to the large cell parameters in approximants, a complete dislocation would necessitate a Burgers vector of more than 10 Å in magnitude, which would involve very high defect energies compared to what is observed in simple crystals, making its existence improbable.

As yet, no experimental investigations of the plastic deformation behavior of approximants have been published and no dislocations in approximants have been observed. Klein et al. [5] proposed a geometrical model for the plastic deformation of an approximant (ξ'-phase) of the icosahedral Al-Pd-Mn phase which does not involve dislocations. The model employs a new kind of linear defect which can move under an applied stress and carry plastic flow.

In this paper we present an HREM (high resolution electron microscopy) study of plastically deformed ξ'-AlPdMn approximants. For the first time dislocations are observed and characterized in an approximant phase. The Burgers vector is equivalent to the most commonly observed Burgers vectors in icosahedral Al-Pd-Mn. We report on the interaction of the dislocation with the phason lines which results in dislocations on another length scale.

The orthorhombic ξ'-AlPdMn approximant has a chemical composition of approximately $Al_{73.5}Pd_{22.4}Mn_{4.1}$ [6], which is close to that of the icosahedral phase $Al_{70.5}Pd_{21}Mn_{8.5}$. HREM at an incident electron beam parallel to the b axis of this structure shows flattened hexagons in rows of two different orientations as the salient structural feature (Fig. 1(a)) The contrasts on the hexagon vertices have been shown to correspond to columns of clusters of icosahedral symmetry containing 54 atoms, so-called Pseudo-Mackay icosahedra.

In the model of plastic deformation of the ξ'-phase proposed by Klein et al. [6], defects can be introduced into the perfect lattice of flattened hexagons where they can be characterized by a banana-shaped polygon attached to a regular pentagon (labeled 'A' in Fig. 1(b)). They can be introduced at the crystal surface and they can move parallel to the c direction through successive jumps of hexagon vertices. Note that these defects are linear defect lines, i.e. they are extended parallel to the b axis that is perpendicular to the image plane. The defect labeled 'B' in Fig. 1(b) is identical to 'A' except for a kink in its defect line. This leads to elongated defect contrasts in HREM images.

The defects have been termed phason defects in reference to phason defects in QCs, because the atomic jumps involved in the motion of a defect result in a local rearrangement of the structural building blocs while leaving the structure unchanged at large distances [7]. In the following we will refer to the defects as phason *lines* in order to emphasize their linear character. Note that the orientation of the flattened hexagons is changed in two rows below the phason line in Fig. 1(b) which corresponds to the trace of the moving phason line. This leads to a local structure change.

A single crystal of the ξ' phase obtained by Bridgman growth was plastically deformed at 750 °C under creep conditions, i.e. at constant load, in 3-point bending geometry. Its b axis was parallel to the bending axis and the c axis parallel to the applied force.
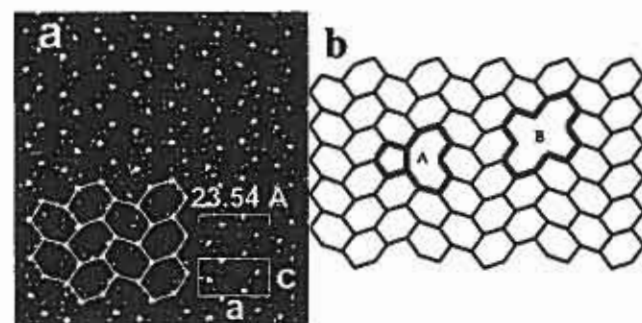

Fig. 1: a) HREM image of the ξ'-AlPdMn phase seen along its b axis. b) Phason lines in the tiling of flattened hexagons. Defects 'A' and 'B' are identical except for a kink in the defect line of 'B'.

HREM observations on the deformed sample revealed the presence of a periodic arrangement of phason lines, changing the periodicity in the c direction from 12.34 Å in the original structure to 81.66 Å in the deformed crystal (Fig. 2(a)). Thus, a structural transition has taken place during plastic deformation by the creation and motion of phason lines. The periodicities of the a and b directions remain unchanged. Dislocations were also observed in the deformed sample. The line directions of all dislocations are parallel to the b axis yielding end-on contrasts when the electron beam is parallel to the b axis. From Bragg contrast extinction conditions in different two-beam cases the Burgers vectors were determined to be parallel to the c axis.

The periodic lattice of phason lines contains structural defects. Fig. 2(b) shows a dislocation where six half-planes of phason lines are inserted on the left-hand side. In the core of this 'meta-dislocation' the perfect tiling of flattened hexagons of the ξ' phase is observed. Drawing a Burgers circuit around the core of the meta-dislocation a Burgers vector parallel to the c axis can be defined whose magnitude is approximately 165 Å.

A new polygon is observed near the six inserted half-planes (Fig. 3(a)). A Burgers circuit drawn around it doesn't close, it reveals a Burgers vector parallel to the c direction with a magnitude equal to $(2\tau-3)d=1.83$ Å, where $d=7.76$ Å is the edge length of the tiles. This corresponds precisely to the most frequently observed Burgers vector in the plastically deformed icosahedral Al-Pd-Mn phase [8, 9].

The polygon characterizing the dislocation core can be embedded in a tiling of flattened hexagons if one allows rows of parallel hexagons (Fig. 3(b)).Introducing six half-planes of phason lines one can modify the tiling around the dislocation core in such a way as to regain a perfect tiling of rows of hexagons in alternate orientations (Fig. 3(c)). Entire planes of phason lines can therefore be built again.

The observed dislocation is a partial dislocation with a Burgers vector whose magnitude is an irrational fraction of the cell parameter $c=12.34$ Å. This is achieved in the material by a rearrangement of the basic structural units, i.e. Pseudo-Mackay icosahedra. In this way a dislocation with a Burgers vector much smaller than the cell parameter can be incorporated in the crystal without changing the local order. In contrast, partial dislocations in simpler structures, e.g. simple ordered intermetallics, massively change the local order, which results in the formation of stacking faults.
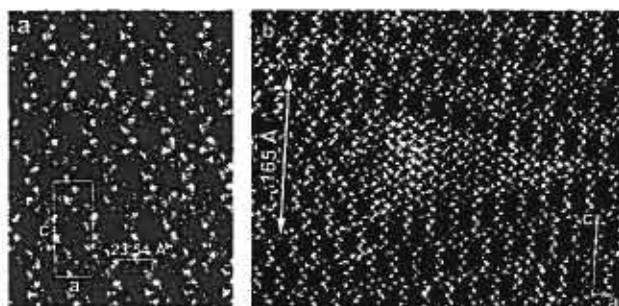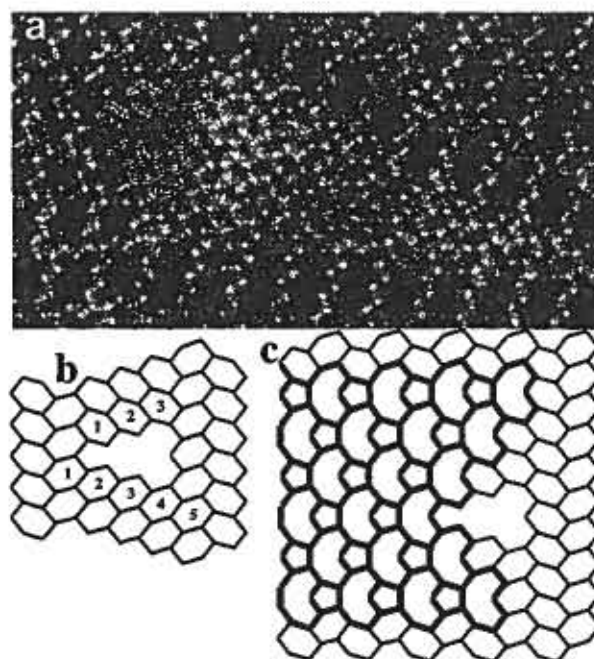

Fig. 3: a) HREM taken along b of the core region of the meta-dislocation. b) The polygon can be embedded in a tiling of flattened hexagons if one allows for rows of parallel hexagons. c) The alternate orientations of flattened hexagons can be recovered above and below the defect by introducing 6 half-planes of phason lines.

In conclusion, we identified the Burgers vector direction and magnitude of a dislocation in the ξ' approximant of the Al-Pd-Mn icosahedral phase. It is equivalent to the most frequently found Burgers vector in the icosahedral phase.

In the periodic lattice of phason lines observed in the plastically deformed ξ' phase this dislocation is a nucleation site of a structural defect in the phason line lattice. This meta-dislocation was observed to have six inserted half-planes of phason lines leading to a Burgers vector of 165 Å.

[1] M. Wollgarten, M. Beyss, K. Urban, H. Liebertz and U. Köster, *Phys. Rev. Lett.*, **71**, 549 (1993)
[2] M. Feuerbacher, M. Bartsch, B. Grushko, U. Messerschmidt and K. Urban, *Phil. Mag. Lett.*, **76**, 369 (1997)
[3] S. S. Kang, J. M. Dubois., *Phil. Mag. A*, **66**, 151 (1997)
[4] C. Janot, "Quasicrystals, A Primer", *Clarendon Press*, Oxford (1992)
[5] H. Klein, M. Audier, M. Boudard, M. de Boissieu, L. Beraha and M. Duneau, *Phil. Mag. A*, **73**, 309 (1996)
[6] M. Boudard, H. Klein, M. de Boissieu, M. Audier and H. Vincent, *Phil. Mag. A*, **74**, 939 (1996)
[7] L. Beraha, M. Duneau, H. Klein and M. Audier, *Phil. Mag. A*, **76**, 587 (1997)
[8] M. Feuerbacher, C. Metzmacher, M. Wollgarten, B. Baufeld, M. Bartsch, U. Messerschmidt and K. Urban, *Mat. Sci. Eng. A*, **233**, 103 (1997).
[9] R. Rosenfeld, M. Feuerbacher, B. Baufeld, M. Bartsch, U. Messerschmidt, M. Wollgarten, G. Hanke, M. Beyss, and K. Urban, *Phil. Mag. Lett.*, **72**, 375 (1995)

Fig. 2: a) HREM image of the plastically deformed ξ' phase seen along b. Dark areas represent phason lines. b) A meta-dislocation in the lattice of phason lines.

Observation of the atomic structure of a $\Sigma=3$ {111} twin boundary junction in a BaTiO$_3$ thin film by phase-retrieval electron microscopy

C.L. Jia, R. Rosenfeld, A. Thust and K.Urban

Institut für Festkörperforschung, Forschungszentrum Jülich GmbH, D-52425 Jülich, Germany

The technique of focal-series reconstruction in high-resolution electron microscopy is applied for the investigation of the atomic structure of a multiple-twin-lamella junction in a BaTiO$_3$ film. In the observed junction area, four types of twin variants including two groups of nanotwins meet each other, resulting in a complicated global boundary with a mixture of $\Sigma=27$ and $\Sigma=3$ segments. For the global boundary, a boundary structure-unit is identified in which some of the [110] BaO columns are found to be partially occupied.

Our previous research [1,2] showed that a high density of nanotwins exists in individual grains of BaTiO$_3$ thin films. The high density of these twin boundaries was related to the existence of a hexagonal structure modification in the BaTiO$_3$ compound at high temperature since the atoms near the twin boundaries exhibit the same arrangement as a sub-unit of the hexagonal unit cell [3]. The twinning involves a {111} BaO$_3$ plane as the boundary plane and the nearby oxygen octahedra share the face instead of the corner, as is the case for the perfect cubic and tetragonal structure. Since the twinning occurs along the four {111} planes which are crystallographically equivalent for the room-temperature structure of BaTiO$_3$, intersections between twin boundaries can be frequently observed within a grain. The core area of such twin intersections exhibits a morphology different from that of undisturbed single twin boundaries and is often considerably more complicated in structure. Therefore, the local atomic arrangement at the core area is of interest.

In this work, we characterize the atomic structure of a multiple twin junction in a BaTiO$_3$ polycrystalline film [4] by means of the numerical reconstruction of the electron wavefunction at the exit plane of the object using a focal series of high-resolution images as input [5]. Whereas single high-resolution images often suffer from nonlinear contrast artifacts, transfer gaps and severe optical distortions introduced by the objective lens of the electron microscope, the quantum mechanical electron wavefunction at the exit plane of the object is free of such imaging artifacts and depends only on the object structure and the properties of the incident electron beam.

For the wavefunction reconstruction, a focal series of 20 images was acquired at equally spaced defocus values using a Philips CM20ST FEG electron microscope operated at 200 kV. The numerical reconstruction of the EPW was carried out using the Philips/Brite-Euram focal-series reconstruction package [6].

Figures 1 (a) and (b) show two high-resolution images of a BaTiO$_3$ grain taken along the [110] zone axis as representatives of the complete focal series. In both images the twin structure can be recognized only coarsely. The images show a vertical $\Sigma=3$ twin boundary intersecting two groups of nanotwin lamellae. The exact atomic arrangement in the junction area of the twin variants cannot be recognized due to the strong optical blurring which is typical of present-day electron microscopes equipped with field-emission electron guns.
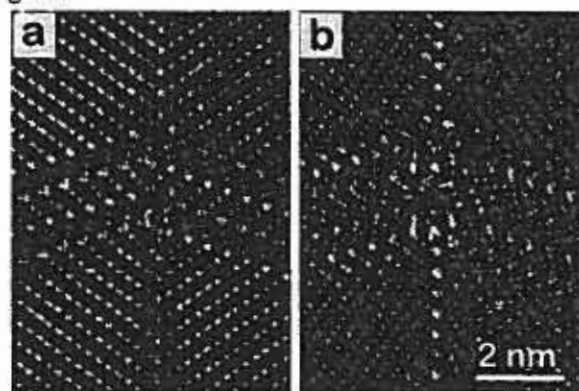

FIG. 1. Two high-resolution images of a focal series recorded from an area of a BaTiO$_3$ thin film including multiple twin variants viewed along the [110] direction. Image (a) was recorded at a defocus value of -137 nm and image (b) at a defocus value of -225 nm.

Figure 2 displays the phase of the exit plane wavefunction (EPW) reconstructed from the focal series. In strong contrast to the two representative experimental images shown in Fig. 1, an intuitive impression of sharpness is already evoked by inspecting the phase image. This indicates that the severe imaging artifacts caused by the microscope could be successfully eliminated. In Fig. 2 one can clearly observe two types of phase maximum (bright dots), one being very prominent, the other being relatively weak compared to the background phase. According to the simulation of the EPW, as shown by the inset 'S' in Fig. 2, the prominent phase maxima coincide with Ti columns viewed in the [110] direction and the faint streaks connecting these maxima arise from the O columns located between the Ti columns. The weak phase maxima coincide with BaO columns.
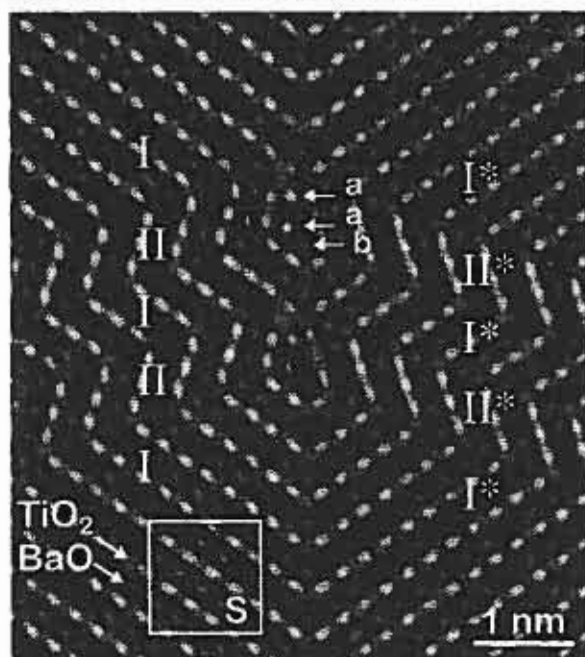

FIG. 2. Phase of the EPW reconstructed from the focal series shown partly in Fig. 1. For comparison, the inset 'S' displays the phase of the simulated EPW for a sample thickness of 9 nm. Note the excellent fit between simulation and reconstruction.

In the phase image of Fig. 2 one observes four different twin variants which are designated variants I, II, I* and II*. From the EPW simulation it is concluded that all $\Sigma=3$ {111} twin boundary planes between the twin variants I and I*, I and II, and I* and II* are in coincidence with one of the {111} BaO_3 planes. The $\Sigma=3$ twinning relation is no longer maintained between variants II and II*. The misorientation between the two variants leads

to a $\Sigma=27$ boundary. Therefore, the intersection of these twin variants leads to a mixture of $\Sigma=27$ boundary segments and $\Sigma=3$ twin boundary segments. A repetition of the global boundary structure is observed along the vertical direction.

The characteristic structure unit of the global boundary is a polygon bordered by the TiO_2 planes of the surrounding twin variants. Within each of the two polygon units one finds three phase maxima which differ from each other significantly in height, as denoted by arrows in Fig. 2. Two phase maxima (arrows 'a') in the $\Sigma=27$ segment of the polygons exhibit a similar phase value which is higher than that of the third maximum (arrow 'b'). Taking into account the surrounding atom environment and following the atomic stacking sequence from the surrounding twin variants, the three maxima within each of the two polygon units should coincide with BaO columns. Based on a simulation of the EPW for a structure model of the boundary junction [7] the weak phase maximum denoted by arrow 'b' reflects a 100% occupancy of the underlying BaO column while the two strong phase maxima marked with arrows 'a' reflect a column occupancy of only 50%.

In conclusion, the focal-series technique for the reconstruction of the exit-plane wavefunction in high-resolution electron microscopy was applied successfully for the investigation of a complex twin junction in $BaTiO_3$. Compared to the traditional interpretation of single images, the extraction of object information is enormously simplified, since one obtains an almost direct insight into the structure.

[1] C.L. Jia, K.Urban, M. Martin, S. Hoffmann and R. Waser, Phil. Mag. A 77, 923 (1998).
[2] C.L. Jia, K.Urban, S. Hoffmann and R. Waser, J. Mater. Res. 13, 2206 (1998).
[3] R. D. Burbank and H.T. Evans, Jr., Acta Cryst. 1, 330 (1948).
[4] M. Mertin, PhD thesis, RWTH Aachen (1996).
[5] W.M.J. Coene, A. Thust, M. Op de Beek and D. Van Dyck, Ultramicroscopy 64, 109 (1996).
[6] A. Thust, M.H.F. Overwijk, W.M.J. Coene, and M. Lentzen, Ultramicroscopy 64, 249 (1996).
[7] Jia, R. Rosenfeld, A.Thust and K.Urban, Phil. Mag. Lett. (1999) in press.

The IFF-Institute "Electronic Properties"

The electronic structure constitutes the microscopic basis for all materials properties. The electronic interactions determine whether a solid is metallic, insulating, or semiconducting, whether it is transparent or exhibits a distinctive color, whether it is a magnet or a superconductor. Even the elastic properties and the thermal conductivity and heat capacity are determined by the electronic structure. Accordingly, the research program of the IFF institute 'Electronic Properties' is devoted towards the investigation of the electronic structure of atoms, molecules and solids. The ultimate goal is the development of an understanding and consecutively the control of the properties of new materials.

The electronic structure of elementary solids consisting of a regular lattice formed by one or two atomic constituents, like pure metals or semiconductors such as GaAs, is quite well understood. Thin film systems introduce a modification of these intrinsic materials properties due to quantization as well as the electronic interactions at the surface and the interfaces. These effects which were originally introduced by quantum mechanics have led to the concept of 'atomic engineering of materials', whereby the materials properties are controlled by a variation of the atomic constituents at the microscopic atomic level. These concepts establish the central and interconnecting aspect of our research program, where we use both experimental as well as theoretical tools for our investigations. In our research we are not only investigating the ground state properties but also the dynamic short time response to an external stimulus, as for example a short light pulse.

We are especially interested in classes of materials where the microscopic control and the variation of the atomic constituents have a dominating influence on the technological application. Accordingly, the present research efforts of the institute are oriented in the following areas:

(1) Magnetic thin films and multilayers; from basic research to sensors and MRAM's
(2) Clusters and Cluster-Materials.

Additionally in our institute there is an effort to develop new **(3) Methods and instrumentation** for our research, whereby the application of synchrotron radiation plays a central role. This includes the design and construction of beamlines and instruments for research with synchrotron radiation. As a part of a center of the newly founded 'Helmholtz Gemeinschaft' we can use the well developed infrastructure to a special advantage in the area of designing large scale instrumentation.

Wolfgang Eberhardt

The IFF Institute 'Electronic Properties'

General Description of the Research Program

The research program of the IFF institute 'Electronic Properties' is devoted towards the investigation of the electronic structure of atoms, molecules, clusters, and solids. The ultimate goal is the development of an understanding and thus a base for the control of the properties of (new) materials. The electronic structure constitutes the microscopic origin for all materials properties. The electronic interactions determine whether a solid is metallic, insulating, or semiconducting, whether it is transparent or exhibits a distinctive color, whether it is a magnet or a superconductor. Even the elastic properties and the thermal conductivity and heat capacity are determined by the electronic structure.

The electronic structure of simple solids consisting of a regular lattice formed by one or two atomic constituents, like pure metals or semiconductors such as GaAs, is quite well understood. Thin film systems introduce a modification of the intrinsic materials properties due to the interaction at the surface and the interfaces. In structures where at least one of the dimensions is in the nanometer range, the interface or surface properties in conjunction with quantum size effects result in large modifications of the original materials properties. This has led to the concept of 'atomic engineering of materials', whereby the materials properties are controlled by a variation of the atomic constituents at the microscopic atomic level. These concepts establish the central and interconnecting aspect of our research program, where we use both experimental as well as theoretical tools for our explorations. In our research we are not only interested in the ground state properties but also in the dynamic short time response to an external stimulus, as for example a short light pulse.

A large part of our research program is devoted towards the development of a microscopic understanding of classes of materials with a direct connection to a technological applications. Such materials where the microscopic control and the variation of the atomic constituents have a dominating influence for the technological application include semiconductor layer systems and heterostructures as well as thin film magnetic systems for sensors and storage media.

Oriented towards these technological applications the research efforts of the institute are organized in the following areas:

1. **Magnetism of solids and thin films**; From basic research to Magnetoelectronics
2. **Clusters as new Materials.**
3. Additionally in our institute there is an effort to develop new **Methods and Instrumentation** for our research. Hereby plays the application of synchrotron radiation a central role. This includes the design and construction of beamlines and instruments for research with synchrotron radiation.

Institute "Electronic Properties"

May 1999

Prof. Dr. W. Eberhardt   Secretary:J. Gollnick

Director:

Tel.: 4428, Fax: 2620

Groups	**Research Areas**
Dr. C. Carbone	Thin film magnetism
Dr. K. Maiti	Spin-polarized photoemission and CMXD
A. Dallmeyer (PhD-student)	with synchrotron radiation
M. Malagoli (PhD-student)	
Dr. L. Baumgarten	F-sec laser photoemission and high resolution
S. Link (PhD-student)	photoemission from solids
C. Zilkens (PhD-student)	
Dr. S. Cramm	Beamlines at DELTA and BESSY II
Dr. S. Eisebitt	Soft x-ray emission spectroscopy
A. Karl (PhD-student)	STM microscopy and spectroscopy
R. Scherer (PhD-student)	
G. Kann (PhD-student)	
I. Wirth (Diploma-student)	
M. Freiwald (Diploma-student)	
Dr. S. Blügel	Electronic structure theory of solids and
Dr. G. Bihlmayer	multilayers
Dr. S. Clarke	STM-theory
Dr. X. Nie	
P. Kurz (PhD-student)	
D. Wortmann (Diploma-student)	
Dr. P.S. Bechthold	Electronic structure, geometry and materials
Dr. M. Neeb	properties of clusters
R. Klingeler (PhD-student)	F-sec dynamics of clusters
G. Lüttgens (PhD-student)	
N. Pontius (PhD-student)	
Dr. B. Kessler	Electronic properties of cluster materials
J. Morenzin (PhD-student)	and polymer systems
D. Schondelmaier (Diploma-student)	

J. Lauer	Electronic-Laboratory
H. Pfeifer	
K. Bickmann	Vacuum-Laboratory
B. Küpper	

Research Group "Magnetic Multilayers"

Prof. Dr. P. Grünberg	Magnetic multilayers for sensors and
Dr. D. Bürgler	memory applications
Dr. C. Sauer	
Dr. S.-S. Yan	
D. Olligs (PhD-student)	
P. Rottländer (PhD-student)	
J. Wingbermühle (PhD-student)	
M. Buchmeier (Diploma-student)	
F.-J. Köhne	
R. Schreiber	

Electronic structure and magnetism of 1-D nanostructures

The electronic structure and the magnetic behaviour of a material can be significantly modified by reducing its dimensions along one or more directions in space. Quantum-size effects give rise to electronic and magnetic properties for low-dimensional systems, which have no counterpart in the bulk. The physical realization of these systems opens the possibility of designing new kinds of materials ("atomic engineering of materials"). Nearly two-dimensional (2-D) systems, such as ultrathin films and superlattices, have recently been the aim of intensive investigations. However, very little is known so far about the electronic and magnetic structure of systems with still lower dimensionality. The manipulation of single atoms and their displacement on surfaces is already possible with the STM. But this technique does not allow to prepare nanostructured large-area samples, which are required by standard methods for band structure determination, such as angle-resolved photoemission.

In molecular beam epitaxy the growth of monatomic nanowires can be obtained exploiting self-organization mechanisms of adatoms on suitable substrates.

An array of monatomic chains forms by deposition of submonolayer amounts of Au on Ni(110), as shown in Fig.1. The Au atoms initially alloy into the Ni(110) surface. At coverages larger than 0.4 ML the development of a quasi 1-D Au dimer-trimer chain structure with a chain-chain distance of approximately 8 surface lattice constants can be observed ("dealloying phase separation").
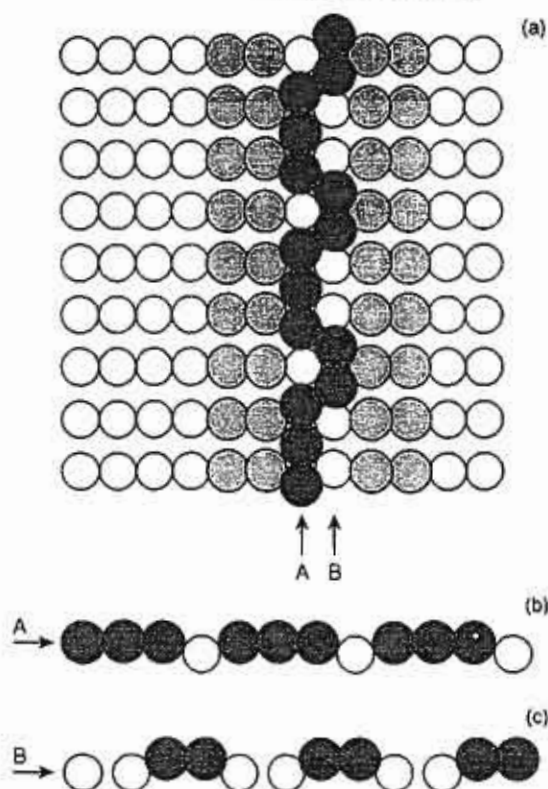

FIG. 1. a) [001]-directed dimer-trimer chain structure of the Au/Ni(110) alloy with four adjacent columns of substituted Au-atoms (white, grey=Ni, Au) taken from [1]. In b) and c) the atomic arrangements along the [001]-column containing the Au trimers and dimers are shown.
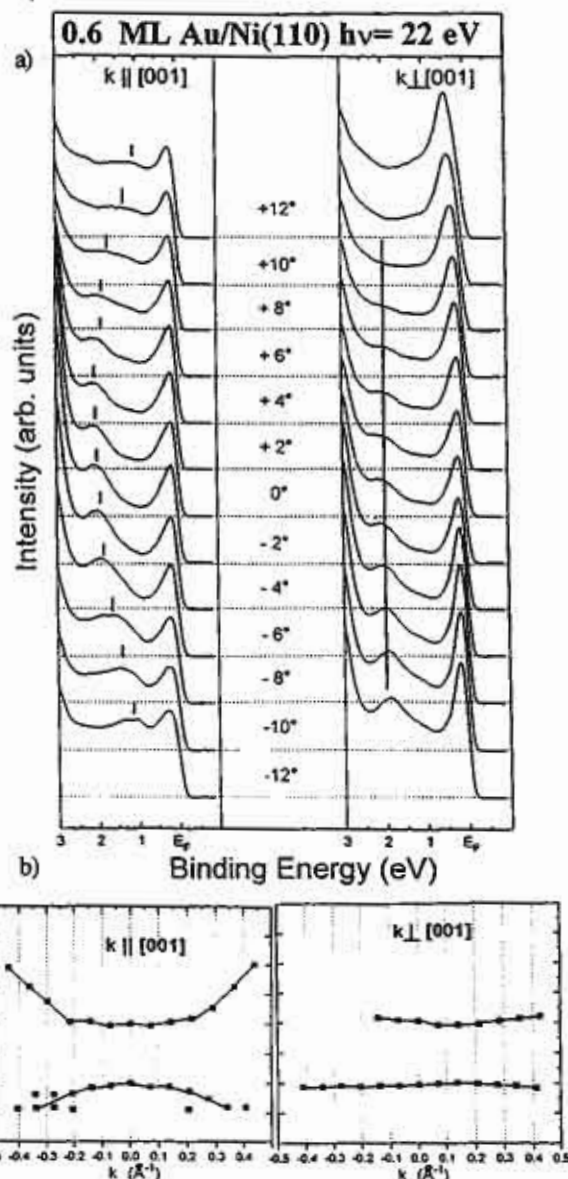

FIG. 2. a) Angle-resolved photoemission spectra taken at hν=22 eV and b) the corresponding experimental band structure. Dispersion of the chain-induced Au s,p-states can only be observed, when the electron wave vector is changed parallel to the [001]-directed chains. Perpendicular to the chains these states remain at constant binding energy.

The electronic states of the Ni(110) substrate and their changes with increasing Au coverage were determined with angle-resolved photoemission. In correspondence with the chain formation the appearance of Au 5d- and 6s,p-states with binding energies of 3.0 eV and 1.8 eV, respectively, can be observed for 0.4 ML. Varying the electron wave vector parallel or perpendicular to the [001]-directed chains, different dispersion behaviour of the chain-induced states is found as depicted in Fig. 2. Along the chains the 6s,p- and the 5d-band (not shown in Fig. 2. a) exhibit a dispersion of 1 eV and 0.5 eV, respectively, while perpendicular to the chains these states remain nearly at constant binding energy. This observation shows that there is electron confinement perpendicular to the chains and no confinement parallel to the chains reflecting their 1-D character. As the electrons are only free to move in one direction, the Au-chains actually represent monatomic nanowires.

1-D nanostructures can also be obtained by molecular beam epitaxy on stepped single-crystal surfaces. Pt(997) consists of a regular distribution of (111)-terraces separated by monatomic steps (shown in Fig. 3), that can be used as a template for growing nanowires exploiting step decoration.
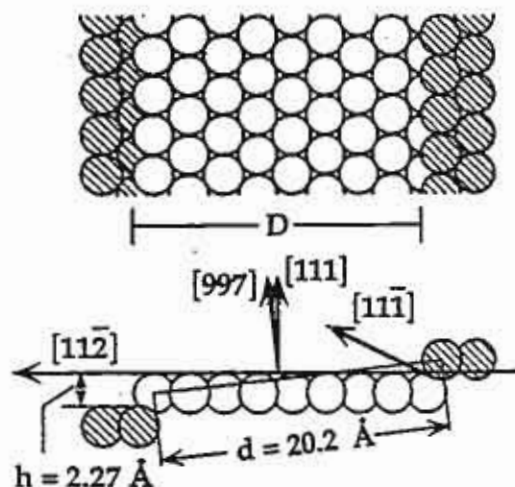

FIG. 3. A schematic view of the Pt(997) surface. The (111) terraces are 20±2 Å (8±1 atomic rows) wide and separated by monatomic steps, which serve as a template for growing nanowires exploiting step decoration.

STM and thermal He-scattering show that monatomic chains of various elements (Xe, Kr, Ag, Co, Cu) can be grown on the Pt(997) surface. Under appropriate growth conditions these chains are arranged into a regular array with a high degree of longitudial coherence and with an even lateral spacing [2].

For studying the electronic structure of Co- and Cu-wires, whose formation is complete at coverages of approximately 0.12 ML, the sensitivity of the photoemission experiment to these small amounts of deposited material can be enhanced taking advantage of the Pt 5d-Cooper minimum, where the photoionization cross section of the substrate is strongly reduced. Photoemission spectra of Co and Cu on Pt(997) taken at $h\nu=122$ eV show that 3d-induced structures can already be found for smallest coverages (<0.05 ML). In Fig. 4 the contribution of the Co-chains (0.12 ML) to the photoemission features, which was determined by subtracting the spectrum of the clean Pt(997)-surface, is shown in comparison to a 1 ML Co-spectrum.
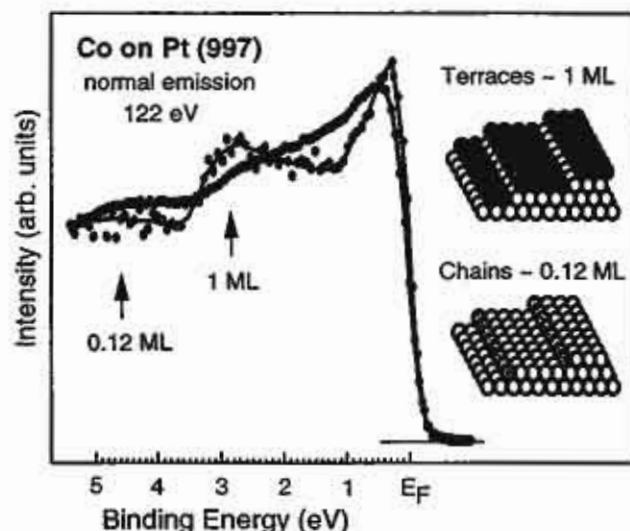
FIG. 4. Difference spectrum showing the Co-induced states for 0.12 ML (chains) in comparison to a 1 ML Co-spectrum. A two-peak structure is found for the Co-chains in contrast to a single Cu-peak, which is observed for Cu-wires on Pt(997).

A double-peak feature is associated to the 3d-emission from the Co-monatomic wire. Only a single photoemission structure was instead observed for the Cu-wires, suggesting for the Co-wires the presence of an exchange split-band and of sizable local magnetic moments. By increasing the coverage an evolution of the electronic states follows as the deposited material develops a 2-D and a 3-D character.

[1] L. Pleth Nielsen et al., PRL, 74, 1159 (1995)
[2] V. Marsico et al., PRL, 78, 94 (1997); P. Gambardella et al., to be published

A. Dallmeyer, R. Kläsges, C. Carbone, W. Eberhardt
Institut für Festkörperforschung, Forschungszentrum Jülich, D-52425 Jülich
C. Pampuch, O. Rader, W. Gudat
BESSY GmbH, Lentzeallee 100, D-14195 Berlin
P. Gambardella, K. Kern
Institut de Physique Expérimentale, EPF-Lausanne, CH-1015 Lausanne

The influence of NiO and CoO outerlayers on the GMR effect

Spin valves systems (SV) are very promising for the application as magnetoresistive sensors. The presence of a NiO exchange bias layer on top of the spin valve system enhances the GMR effect [1,2]. This enhancement is still not completely understood, although it has been suggested that it originates from specular reflection of the electrons at the interface with NiO [3]. A similar effect could, in principle, be expected from a CoO exchange bias layer. The lower Néel temperature of CoO (292 K bulk, compared to 570 K for NiO bulk) enables a study of the influence of the antiferromagnetism by changing the temperature, in a temperature range where the samples are not subject to interdiffusion.

The samples Si(111)/NiFe/Co/Cu/Co are prepared by thermal evaporation under UHV conditions (base pressure $< 10^{-10}$ mbar). The layers are evaporated using a shadow mask, enabling the simultaneous production of sixteen resistivity elements on one single 6×16 mm^2 substrate. The Cu layer is evaporated using the "wedge-technique", which produces a different Cu thickness for each element. In this way one can study the dependence of the resistivity and coupling on the Cu layer thickness on elements grown under the same conditions. The bottom NiFe layer is evaporated in the presence of an field of 3.2 kA/m (40 Oe) applied parallel to the longitudinal axis of the elements. The top NiFe layer is evaporated with a field of 4.8 kA/m (60 Oe) perpendicular to the longitudinal axis. On top of the upper NiFe layer an exchange bias layer is deposited. Different exchange bias layers are used, all deposited with a magnetic field applied: CoO and NiO (10nm) are prepared by reactive evaporation of Co or Ni in an oxygen atmosphere (10^{-6} mbar), and FeMn (10 nm) is coevaporated from two sources.
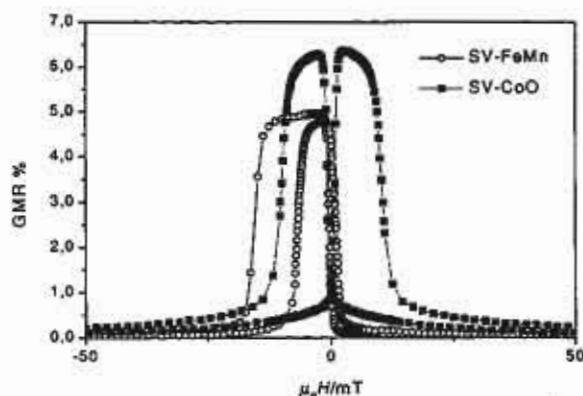
The FeMn and reactively evaporated CoO and NiO spin valves are capped with a NiFe (5 nm) layer to prevent corrosion. The magnetoresistance of the samples is measured using a four probe method.

In Fig. 1 the GMR curves at room temperature of spin valves with CoO and FeMn exchange bias layer are plotted. The FeMn spin valve behaves like a typical exchange biased sensor. The CoO is above its Néeltemperature and no exchange bias is present, but the coercive field of the Co layer is still increased. The magnetisations of both ferromagnetic layers are therefore seperated and an antiparallel alignement is achieved. In comparison to the FeMn spin valve the GMR effect in the CoO spin valve is enhanced.

In Fig. 2 the GMR effect at room temperature for spin valves with CoO and FeMn exchange bias layers is shown. In the FeMn spin valve the GMR is reduced due to shunting in the metallic FeMn layer. For comparison we plotted also the corrected GMR effect of the FeMn spin valve without shunting. Both spin valves show an increase of the GMR effect with increasing Co layer thickness. The GMR effect in the CoO spin valve is clearly larger than in the FeMn spin valve, also if shunting is taken into account. For a Co thickness of 1.6 nm the GMR effect of the CoO spin valve is no more enhanced in comparison to the FeMn spin valve. A similar effect was found by Swagten et al [4], the origin of this reduction is not yet understood.
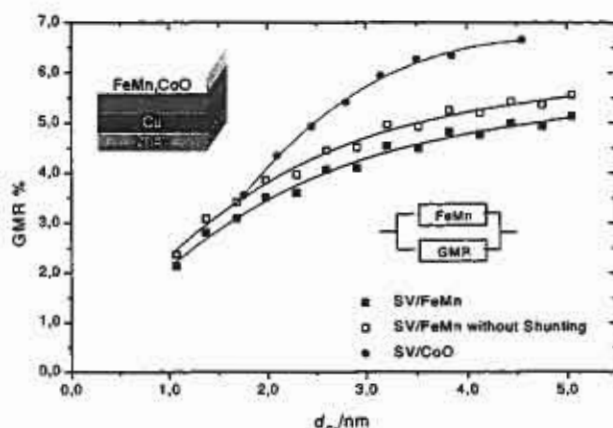
FIG. 2. GMR ratio at room temperature of spin valves NiFe$_{10nm}$/Co$_{0.5nm}$/Cu$_{4nm}$/Co$_{0-5nm}$ with an exchange bias layer of CoO and FeMn

The temperature dependences of the GMR ratios for the FeMn, CoO and NiO spin valves are shown in Fig. 3. With decreasing temperature the GMR effect of the spin valves increase. The NiO and CoO spin valves have the same quantitative behaviour up to room temperature. The GMR effect for the CoO spin valve does not depend on the crossing of the Néel temperature. Above

FIG. 1. Magnetoresistance at room temperature of spin valves NiFe$_{10nm}$/Co$_{0.5nm}$/Cu$_{4nm}$/Co$_{4.5nm}$ with an exchange bias layer of CoO and FeMn

the Néel temperature of CoO (292 K bulk) the exchange biasing vanishes, but still the coercive field of the upper cobalt layer is enlarged. In the CoO layer, the spins located close to the interface still couple to the Co layer even above the Néel temperature. The temperature dependence might differ from the behaviour of the rest of the CoO layer.

layers have been prepared. The GMR effect of the CoO and NiO spin valves is enhanced in comparison to the FeMn spin valve. The GMR effect of the CoO spin valve shows the same enhancement as a NiO spin valve. No influence of the antiferromagnetism of CoO on the GMR has been observed.
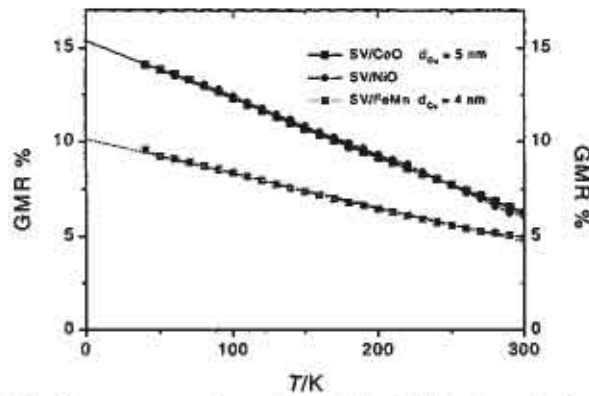
FIG. 3. Temperature dependence of the GMR effect of spin valves NiFe$_{10nm}$/Co$_{0.5nm}$/Cu$_{5nm}$/Co$_{0-5nm}$ with an exchange bias of CoO, NiO and FeMn

Spin valves with CoO, NiO and FeMn exchange bias

[1] T.C. Anthony, J.A. Brug, and S.Zhang, IEEE Trans. Magn. 30, 3819 (1994)
[2] W.F. Egelhoff, Jr.T. Ha, R.D.K. Misra, Y. Kadmon et al, J. Appl. Phys. 78 (1), 273 (1995)
[3] H.J.M. Swagten, G.J. Strijkers, P.J.H. Bloemen, M.M.H Willekens, and W.J.M. de Jonge, Phys. Rev. B 53 (14), 9108 (1996)
[4] H.J.M. Swagten, G.J. Strijkers, R.H.J.N. Bitter, W.J.M. de Jonge, and J.C.S. Kools, IEEE Trans. Magn. 34, 948 (1998)

F. Voges, P. Grünberg and R. Schreiber

Tunnelling Magnetoresistance Structures with Barriers Produced by UV Oxidation

Ferromagnetic tunnel junctions attract special interest due to their possible applications in magnetic sensors and information storage devices. Our activities in this field are in close collaboration with H. Kohlstedt, E. Girgis, R. Schmitz and J. Schelten of the Institute for Ion- and Thin Film Technology (ISI) of the Research Centre. Other partners are Université Paris Sud, the TU Eindhoven and IMEC, Leuven (B) in the academic part, and Thomson, Orsay (F) and Philips in Eindhoven as industrial partners.

One of the key problems for the preparation of tunnel junctions is the preparation of the tunnel barrier. It is usually made of metallic aluminium which is oxidized after deposition. The most successful ways of oxidation up to now – plasma oxidation and oxidation in air – result in high area resistances $(R \cdot A)$ of the tunnel elements. This is in contrast to what is required for highly integrated systems as magnetic RAMs. Following an idea by Fritzsch et al. [1], we present as an alternative way of oxidation the in situ oxidation with ultraviolet light illumination.

Using this method, we obtain low area resistances of $0.2 \ldots 15 \, \mathrm{k}\Omega \, \mu\mathrm{m}^2$ with magnetoresistance ratios $\Delta R/R$ of well above 10%. Through the choice of the oxidation method, it is possible to adjust the resistance of tunnelling magnetoresistance (TMR) devices for different applications as sensors and memory cells: With a given size of the TMR element an appropriate resistivity can be chosen with only little influence on the magnetoresistance.
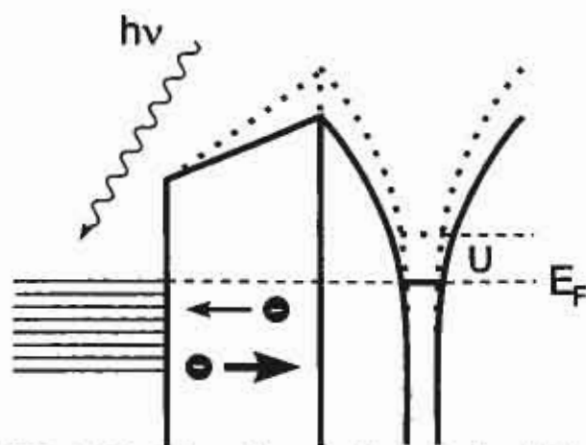
For oxidation, the preparation chamber has been fitted with a 4 W low pressure mercury lamp. It emits main ultraviolet wavelengths of 254 nm and the ozone generating 185 nm. Apparently the generation of ozone plays a minor role compared to the following process proposed by Cabrera and Mott [2]: During natural oxidation of aluminium without UV light, electrons tunnel through the already formed oxide layer and build up a surface charge. This results in a field which pulls aluminium ions through the oxide. The oxide stops to grow if the field is too low to help the ions over the potential barrier between two interstitial positions. UV light illumination excites electrons in the metal, so that some of them pass through the oxide barrier and are trapped at the surface. This increases the surface charge, and thus the field and the limiting thickness.

The oxidation time is usually one hour. Longer oxidation does not give a noticeable effect and we believe that it is possible to drastically reduce the oxidation time.

After deposition, contacts are patterned (Fig. 2) by optical lithography and subsequent Ar ion beam etching (IBE). The progress of the etching is controlled by a secondary ion mass spectrometer (SIMS). To define the junctions, a self-aligned process is applied, where the same photoresist mask is used for etching through the top electrode and deposition of the insulator. The mask is designed to allow for a four probe measurement with two separate gold contacts on the top electrode. This allows to check for tunnelling between the top electrode and the wiring.

FIG. 1. The Cabrera-Mott model of natural oxidation of Al (solid) and the changes due to UV light (dashed)
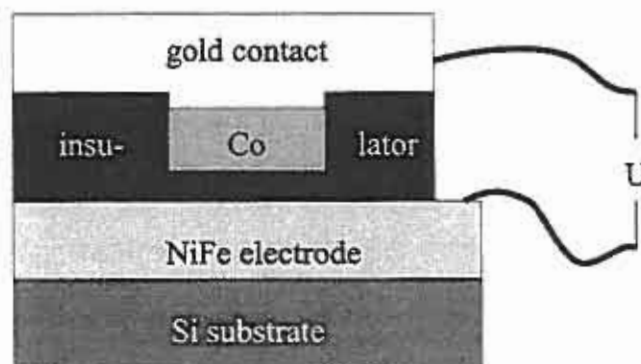
FIG. 2. Schematic cross section of a tunnel junction. The bottom magnetic layer acts as a lead

Our samples are grown by sputtering on thermally oxidized Si substrates, which have a rms roughness of about 0.4 nm. The ferromagnetic electrodes, usually 19 nm Permalloy ($Ni_{80}Fe_{20}$) and 15 nm Co, are rf sputtered, the Al barrier is dc sputtered and later oxidized. The base pressure in the recipient is 10^{-6} mbar.

Prior to patterning, all samples are characterized by MOKE measurements which gives information about the magnetic behaviour of the structures. A typical example is shown in Fig. 3 (solid line) with two distinct steps for the magnetization reversal of Co and NiFe. In contrast, in trilayers without oxidation of the Al layer, both magnetic layers are strongly coupled so that they reverse their magnetization at the same time.
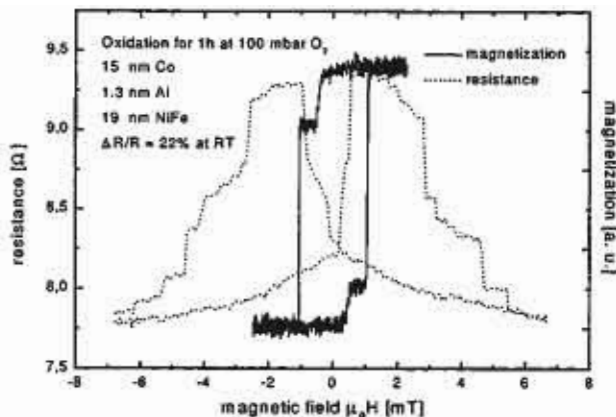
FIG. 3. Magnetization and magnetoresistance curve at room temperature

FIG. 5. Magnetoresistance curves at different temperatures

All patterned junctions whose magnetoresistance curves are shown here have a surface area of $25 \, \mu m^2$. In Fig. 3, it is possible to compare magnetization and magnetoresistance curves of the same trilayer with 1.3 nm Al thickness before oxidation. The junction shows a TMR effect of 22% at room temperature. The Co layer became magnetically harder due to the small size of the junction. The NiFe layer, which acts as bottom lead and therefore still has large areas, is nearly magnetically unchanged.

For lower temperatures the resistance and magnetoresistance ratio increase. This is shown in Fig. 4 for a (different) sample with 1.3 nm Al and in Fig. 5 for a sample with 1.0 nm Al. From the latter figure one sees also an increase of the coercitivity of the Co layer which is probably due to a coupling of the Co to the antiferromagnetic CoO at the unprotected surface of the top electrode.

In conclusion, it has been shown that the Al barrier of tunnel junctions can be oxidized with help of ultraviolet light. This results in higher resistivities than for oxidation in pure O_2, but much lower resistivities than with oxidation in air or with plasma oxidation. The resulting barriers are of high quality in the sense that it is possible to regularly achieve magnetoresistance ratios of more than 10% with a maximum of 22% at room temperature. With our usual pressure of 100 mbar, it is difficult to decide if ozone plays a major role in oxidation. Experiments on this topic are in progress.

FIG. 4. Temperature dependence of conductance and TMR effect

[1] L. Fritzsch et al. *Physica C*, 296(3-4):319, 1998.
[2] N. Cabrera and N. F. Mott. *Rep. Progr. Phys.*, 12:163, 1949.

P. Rottländer, H. de Gronckel and P. Grünberg (FE 23.42.0)

Photoelectron Spectroscopy of La$_2$O$_n$: Experiment and Theory

Continuing the recent investigations on LaO$_n$ clusters [1] we present the latest results on La$_2$O$_n$ (n=0-6). In order to gain more insight into the electronic and geometric structure of these clusters we have combined experimental and theoretical methods: photoelectron spectroscopy of size-selected cluster anions on the one hand as well as both density functional theory (DFT) and configuration interaction (CI) on the other hand.

The work function of several metals can effectively be lowered by covering the surface with a thin layer of mono- or divalent metaloxides. This phenomenon is technologically used to enhance the electron yield of thermal cathodes. The oxides of barium and cesium are effective materials to lower the work function. Lanthanum is placed right next to barium and cesium in the periodic table. The work function of solid lanthanum oxide (La$_2$O$_3$) is 2.8 eV. Small lanthanum oxide clusters have a considerably lower electron affinity than the bulk material as revealed in the present manuscript. Furthermore the electron affinity, which corresponds to the work function of a solid, becomes reduced with an increase of the number of O atoms. This is in contrast to several other metal oxide clusters for which the electron affinity increases with the number of chemisorbed oxygen atoms as has recently been shown for small iron- and aluminum oxide clusters [2,3].

The lanthanum oxide anions shown in Fig. 1. have been generated in a pulsed laser vaporization plasma source. After an adiabatic expansion the cluster anions are accelerated and focused by a Wiley-McLaren ion optic. The anions are mass selected by their time of flight prior to the detachment process. Electrons are detached by a Q-switched Nd:YAG laser pulse (3.495 eV). The kinetic energy of the emitted electrons is analyzed in a magnetic-bottle time-of-flight analyzer.

Fig. 1 shows the photoelectron spectra of La$_2$O$_n$ (n=1-6). Common to all spectra (except for La$_2$O$_4^-$) is an intense peak at lowest binding energies which represents the transition into the neutral clusters ground state. This indicates the electron affinity of the corresponding neutral cluster. The dominating peak is followed by an intensity gap at higher binding energies and a continuous emission signal. The latter indicates a most complex electronic density of states, caused by the d and s electrons.

In this context the question arises weather there are charge transfer processes and how they are related to the electronic structure and electron affinity. It turns out that the electron affinity of La$_2$O$_n$ drops continuously with the number of chemisorbed oxygen atoms (Fig. 2.). This decline stands in contrast to the behaviour of several other metal dimer oxide clusters
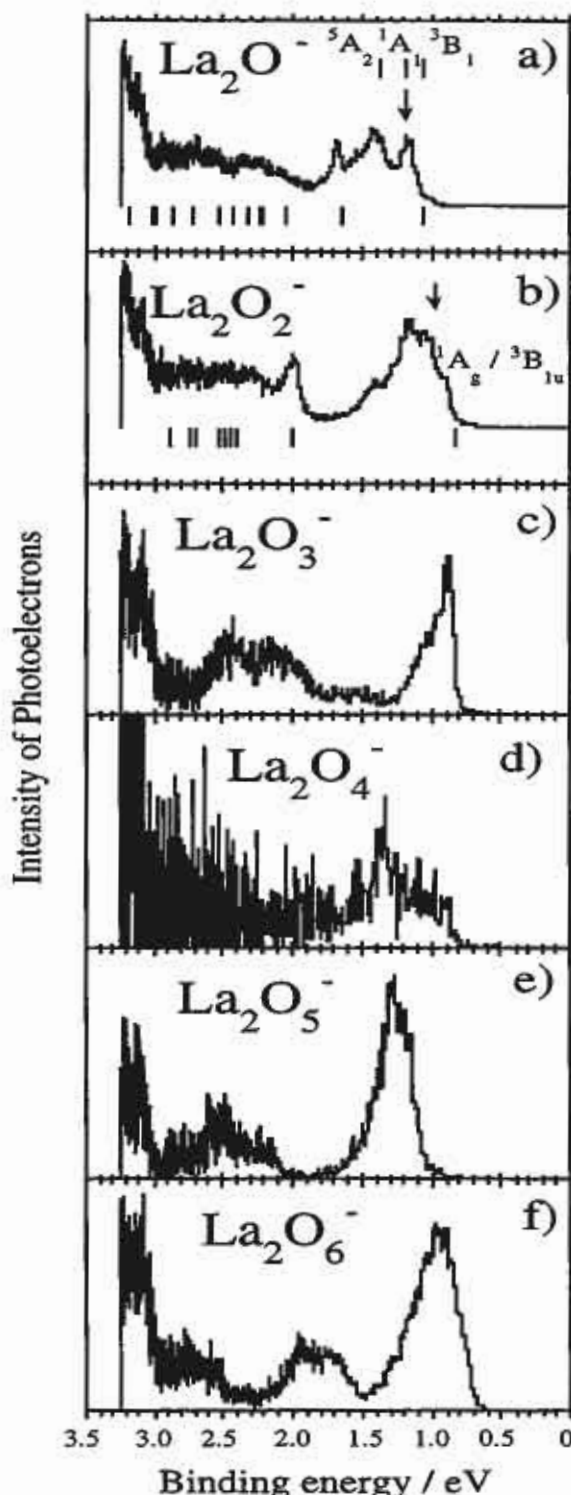

Fig. 1. Photoelectron spectra of La$_2$O$_n^-$ (n=1-6) at 3.49 eV photon energy. The line spectra below the photoelectron curve in a) and b) represent the results of CI calculations, the upper line spectra represent the energies of states with different multiplicities, each relative to the respective measured electron affinity. The arrows indicate the calculated electron affinity.

[2,3] which shows that an increasing electron affinity upon increasing oxidation is not common to transition metal dimer clusters. For example, the electron affinites of Al_2O_n and Fe_2O_n increase as a function of n. Concerning the Fe_2 dimer, this can be viewed as a sequential oxidation of the dimer where each oxygen atom is individually bound to the two iron atoms with a similar amount of charge transfer from Fe to O [2].
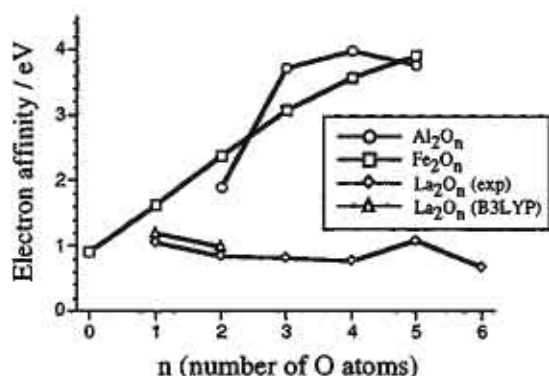

Fig. 2. Electron affinities of metal dimer oxide clusters as a function of the number of oxygen atoms. While the oxides of iron and aluminum [2,3] show increasing electron affinities, these of the lanthanum dimer oxide clusters decrease.

In the case of lanthanum dimer oxide clusters an electrostatic model seems to be insufficient to explain the bonding between lanthanum and oxygen. It is rather appropriate to consider the exact electronic structure and covalent character of the bonds. Similar results have been obtained for the lanthanum monomer oxides [1].

Density functional (DF) calculations using Becke's three parameter Hybrid method along with the Lee/Young/Parr correlation functional (B3LYP) and configuration interaction calculations (CI) have been performed on La_2, La_2O and La_2O_2. The most stable geometries revealed from the DFT are those in which the oxygen atoms are individually bound to the dimer, accompanied by a 0.74 lel charge transfer. This is supported by CI calculations on these geometries, resembling the experimental data very well.

The valence region of the lanthanum dimer is labelled by a complexity which arises from the high density of d-derived states. The chemisorption of oxygen leaves the valence region widely lanthanum dominated, although low-lying O2p-like orbitals exhibit a significant covalent character due to about 25% La5d

admixture. As the highest occupied orbitals of the lanthanum dimer have a bonding character a charge transfer from lanthanum to oxygen results in a prolongation of the distance between the two lanthanum atoms. This is consistent with the calculated geometries (Fig. 3.).
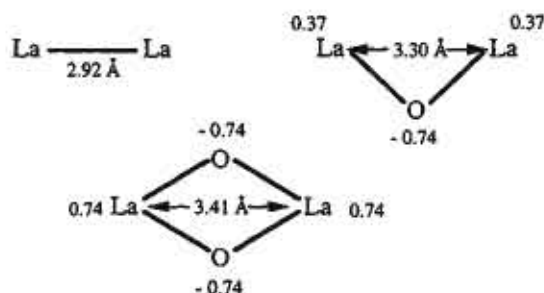
Fig. 3. Schematic drawings of the calculated most stable geometries for La_2, La_2O and La_2O_2. Note the increase of the distance between the two lanthanum atoms as the amount of oxygen increases.

The pure lanthanum dimer [4] as well as La_2O and La_2O_2 exhibit several low lying states with different multiplicities near the ground state. This leads to a ambiguity in determining the exact ground state configuration and indicates the crucial role of exchange and correlation effects in these systems. Single particle considerations are insufficient in describing the correlation between electronic structure and electron affinity.

It might be interesting to perform high resolution spectroscopy experiments on these clusters in order to uncover vibrationally excited states and identify them as normal modes of the geometries as revealed from DFT. Additional DF calculations have to be performed on La_2O_n (n=3-6). Further experiments on lanthanum trimer and tetramer oxide clusters should additionally shed light on the electronic structure of these systems and on the particular role of the lanthanum d electrons.

[1] R. Klingeler, G. Lüttgens, N. Pontius, R. Rochow, P. S. Bechthold, M. Neeb, and W. Eberhardt, Eur. Phys. J. D, in press
[2] H. Wu, S. R. Desai, and L.-S. Wang, J. Am. Chem. Soc. 1996, 118, 5296
[3] H. Wu, C. M. Rohlfing, L.-S. Wang, J. Chem. Phys. 106, 1309 (1997)
[4] M. Dolg, H. Stoll, and H. Preuss, J. Mol. Struct. (Theochem) 277, 239 (1992)

R. Klingeler, M. Neeb, P. S. Bechthold

Improved charge generation efficiency of an organic photoreceptor material by C60

Organic photoconductors like metal-free H_2-Phthalocyanine (H_2-Pc) are already in use in charge-generation layers for laser printers and xerografic devices /1/. The charge generation efficiency is limited by the competing process of recombination of the photo excited excitonic state. An admixture of the electron acceptor C_{60} is expected to increase this efficiency due to a lowered recombination rate of the charge separated state (the electron is transferred onto the C_{60}, the hole stays on the H_2-Pc-molecule) in comparison to the excitonic state. Our investigation by photoelectron spectroscopy and X-ray absorption near edge spectroscopy has demonstrated that the electron transfer is energetically possible, because the charge separated state is lower in energy than the excitonic state (see fig.1) and therefore an improvement of the photoreceptor is expected upon an admixture of C_{60} /2/.
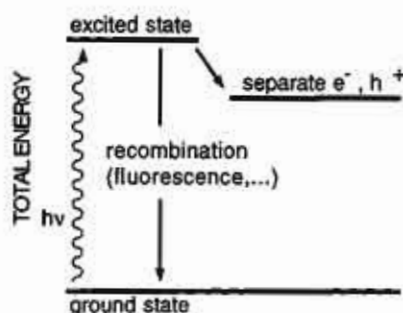
Fig.1: *Schematic total energy scheme of photoexcited and charge separated state for H_2-Pc with C_{60}.*

We now verify the effect of C_{60} onto the charge generation efficiency of H_2-Pc by looking at the fluorescence yield and the photoconductivity of the composite material for different amounts of C_{60}.

The samples for the conductivity measurements were prepared by a co-evaporation of H_2-Pc and C_{60} onto either ITO or Au-coated glass substrates, and a second Au electrode was deposited on top. A typical thickness for the organic composite material was 200nm. To reduce the influence of oxygen on the electric properties, the sublimed samples were annealed under vacuum for 4h at 150 deg C. The top Au electrode was deposited immediately after the annealing process. For fluorescence or absorption studies H_2-Pc with C_{60} was deposited on quartz substrates.

The fluorescence yield was measured with a monochromator after irradiating the sample with an argon ion-laser at a wavelength of 514 nm.

The I/U-curves were measured using a Knick constant-voltage supply and a Keithley electrometer. For the photoconductivity measurements the samples were irradiated through the glass/Au side. With an Au electrode of 30nm thickness about 50% of the light reaches the gold/Pc interface. We used monochromatic light at a wavelength of 650nm. Metal-free phthalocyanine has a large absorption coefficient ($\alpha = 2.5 * 10^4 cm^{-1}$), thus not the whole volume of the organic layer was illuminated homogeneously. Therefore the total dark- and photoresistance of the sample was measured and the photoconductivity was calculated from the following equation:

$$R_{ph} = \frac{1}{A} \int_0^L \frac{1}{\sigma(x)} dx \quad ; \quad \sigma(x) = \sigma_d + \sigma_{ph} e^{-\alpha x}$$

Here we assume an exponential decline of the light intensity into the Pc/C_{60}-layer, where R_{ph} is the total resistance under

light, σ_d is the dark conductivity, σ_{ph} the photo conductivity and A the illuminated area of the sample. L is the thickness of the Pc/C_{60} layer.
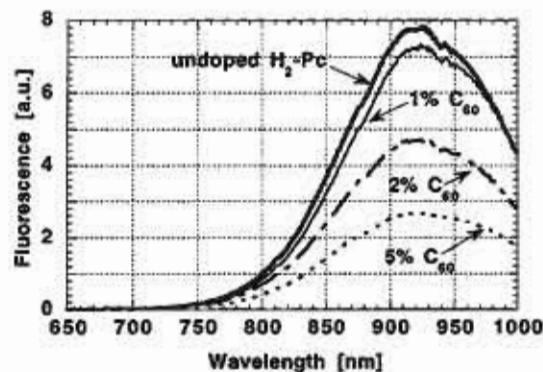
Fig.2: Fluorescence of C_{60}-doped H_2-Pc layers.

Figure 2 displays the quenching of the fluorescence yield with increasing amounts of C_{60} in the wavelength region between 650nm and 1000nm. The observed broad peak corresponds to the recombination of the singlet excitonic state. The quenching proves that C_{60} is able to reduce the recombination rate and therefore the doped material is expected to yield a higher efficiency for the charge-generation probability per incoming photon.
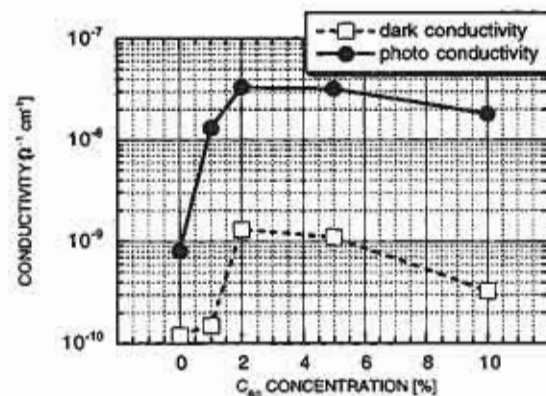
Fig.3: Conductivity for H_2-Pc+C_{60} as a function of the C_{60} concentration.

The results of the opto-electrical data for sublimed samples measured a few hours after the preparation are displayed in fig.3. A large improvement of the photoconduc-

tivity and the contrast (defined as , the ratio between photo- and dark-conductivity) can be seen due to the influence of C_{60}. The dark conductivity increases by admixing C_{60}, but decreases again for higher concentrations. We suppose that such a large quantity of C_{60} reduces the hole mobility through the organic photoconductor layer by disturbing the crystal structure.

On the other hand oxygen has a large influence on the photoelectric properties in a way that both dark- and photoconductivity are increased but the contrast is decreased if the samples are stored for a few days under normal atmospheric conditions (not shown). Therefore for possible applications oxygen diffusion has to be avoided in order to maintain the high contrast values of the C_{60}-doped phthalocyanine.

Our measurements of a fluorescence quenching of in H_2-Pc with an increasing quantity of C_{60} indicate a photo-induced charge-transfer from Pc to C_{60}. This is established by opto-electrical measurements, which show that the photoconductivity of C_{60}-doped samples is increased by more than one order of magnitude compared to the undoped ones. The contrast is also greatly enhanced by C_{60}, which makes H_2-Pc/C_{60} composites interesting for electrophotographic purposes as long as any influence by oxygen is kept low.

/1/   K.-Y.Law, Chemical Reviews 93, 449 (1993).
/2/   B.Kessler, Appl.Phys.A 67, 125 (1998).

J.Morenzin, C.Schlebusch, B.Kessler

Electronic Structure of Single Wall Carbon Nanotubes in Buckypaper

Carbon nanotubes have in recent years attracted increasing interest as a new modification of carbon, related to the fullerenes and graphite. For single-wall carbon nanotubes (SWNTs) in particular, interesting electronic properties were predicted quite early on [1–3]. For these nanotubes, the electronic structure strongly depends on the chirality vector defining the type of nanotube: (n, n) tubes ("armchair" type) are predicted to be metallic, while (n, m) tubes with $n \neq m$ are wide-gap or near-gap semiconductors, depending on the particular m and n. If $2n + m$ or $n + 2m$ is an integer multiple of 3, the SWNT is predicted to be a near-gap semiconductor with good room-temperature conductivity.

This behavior can be understood in a straightforward quantum confinement approach starting from the band structure for a single graphene sheet. We will briefly review the relation of the electronic states in nanotubes to the ones in graphite or a graphene layer, as this will enable us to discuss our experimental data on SWNTs in connection to data on graphite.
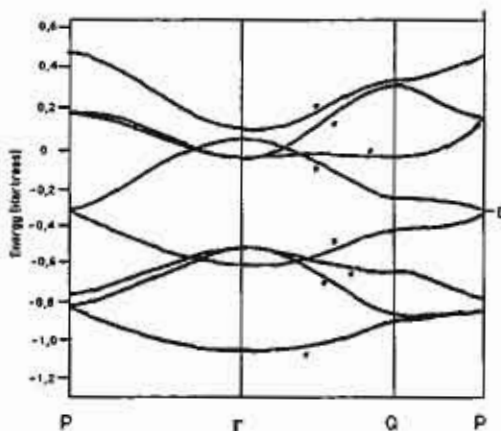

FIG. 1. Band structure of a single graphene sheet. Adapted from Ref. [4] Please note that E_F is located at about -9 eV (-0.33 Hartrees) on the energy scale.

In a nanotube, the electronic states with $\mathbf{k}_\perp$ vectors in the plane of the "rolled-up" graphene sheet but perpendicular to the tube axis have to satisfy periodic boundary conditions, hence only a set of discrete $\mathbf{k}_\perp$ are allowed [1,5]. The allowed $E(\mathbf{k})$ states in a nanotube are therefore, to a very good approximation, a subset of all the states allowed in a graphene sheet [6]. More precisely, only states on discrete lines through the two-dimensional Brillouin zone (BZ) of a graphene sheet are allowed. The slices are parallel and cut the BZ into equally wide parts. The states along each slice trough the BZ form a one-dimensional band of electronic states for the nanotube, the continuous wavevector $\mathbf{k}_\parallel$ is directed along the tube axis. In nanotube band-structure calculations, this di-

rection is typically labeled $\overline{\Gamma X}$, but it is important to note that for different tubes $\overline{\Gamma X}$ represents different sets of slices through the two-dimensional graphene BZ.
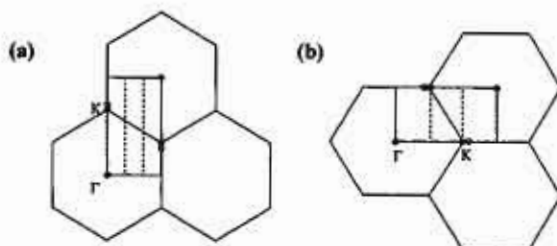
FIG. 2. Illustration of the slices through the 2-dimensional BZ of Graphene in order to find the SWNT states fulfilling the periodic boundary condition. Γ and K point are indicated by full circles, the degenerate point close to K is marked by an open circle. The rectangular Brillouin zones of the SWNTs and the slices (dashed lines) are shown. (a) SWNT of (n, n) "armchair" type. A slice will always cut through the degenerate point. (b) SWNT of $(n, 0)$ "zigzag" type. A slice can only cut through the K point (and hence in the immediate vicinity of the degenerate point) if the BZ is cut into an integer multiple of 3 equal parts. Adapted from Refs. [1,3].

Just as in graphite or a graphene sheet, where the metallicity stems from degenerate states at the K point in the BZ (Fig. 1), the nanotube will only be metallic if the K point [7] is contained in the set of allowed states. For simple geometric reasons, this is always the case for (n, n) nanotubes, as shown in Fig. 2. Further BZ geometry reveals that for all other nanotubes, a slice cuts through K only if $2n + m$ or $n + 2m$ is an integer multiple of 3. In nanotubes, however, the degenerate point is slightly shifted away from the K point [1]. As a result, the degenerate point can be reached exactly in only (n, n) SWNTs; for $(m, n \neq m)$ nanotubes the calculations show a gap of at least a few meV (near-gap SWNTs) [3].

Recently, a purification process for large batches of previously generated raw material containing SWNTs has been shown to produce samples with a high degree of SWNTs, distributed over a narrow diameter range. [8] The final product is a paper-like felt, nicknamed "buckypaper".

We have investigated the SWNTs in buckypaper, prepared by pulsed laser vaporization (PLV) and purified as described in Ref. [8] (4'' oven material). The buckypaper was investigated by two different techniques: a study of the electronic structure using *resonant inelastic soft x-ray scattering* (RIXS) was carried out at the Advanced Light Source, Berkeley (BL 7.0.1) [9], in addition, the topology and the electronic structure were studied by *scanning tunneling microscopy (STM) and scanning*

tunneling spectroscopy (STS). [10]

Both RIXS and STM/STS were performed on the *intact* buckypaper sample, *i.e.* on free-standing buckypaper. In both cases, the buckpaper was neither disentangled nor dissolved and hence the distribution of SWNTs is unchanged from the freshly purified sample. For STM/STS, the sample was cooled to 23 K.
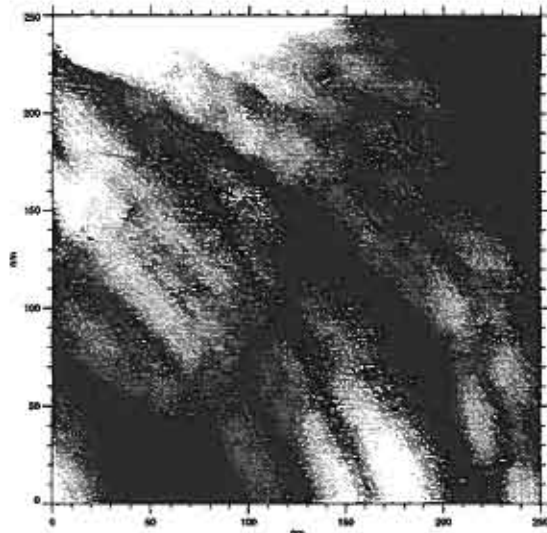
FIG. 3. Parallel SWNTs (fine diagonal lines) form microbundles about 30 nm in diameter, which in turn aggregate to form ropes in the buckypaper.
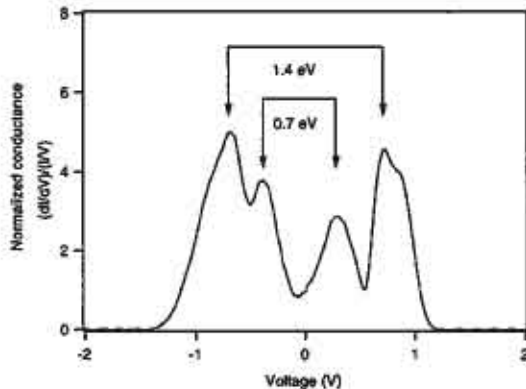
FIG. 4. Normalized differential conductivity $\frac{dI/dV}{I/V}$ on a wide gap SWNT. The positions of the singularities allow a precise determination of the bandgap.

A zoomed-in STM image on a free standing sheet of buckypaper is shown in Fig. 3. Clearly visible are two ropes with diameters between 70 and 120 nm. These ropes are not individual SWNTs, but metastructures with SWNTs as the individual building blocks. Such ropes have been observed for nanotubes produced by different techniques. Depending on the growth conditions, the organisation of the individual nanotubes into larger

structures can be different. [11–14]

The organisation of SWNTs into larger structures within our buckypaper sample can be seen. Individual SWNTs are 1.0-1.5 nm in diameter, they show up as thin stripes in the image. They form microbundles of about 30 nm in diameter. In the microbundles, the SWNTs are organized in a parallel fashion. The microbundles aggregate to ropes of about 70-120 nm diameter. Overview images show that the ropes are woven which each other, forming a dense network which constitues the buckypaper.
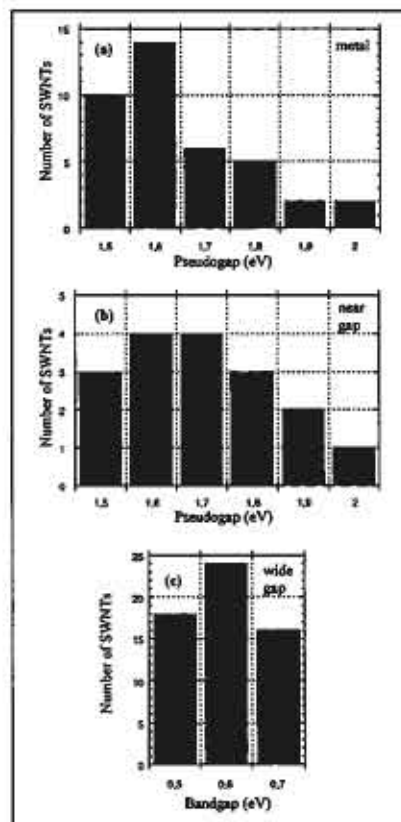
FIG. 5. Distribution of SWNTs with a given pseudogap (a,b) or bandgap (c) in the buckypaper as determined by STS on 114 randomly choosen SWNTs in the sample. The energy spacing between the innermost singularities for (a) metallic, (b) near gap, and (c) wide gap SWNTs is shown.

The distribution of SWNTs with regard to their electronic structure has been studied by STS. I(V) curves were recorded at 114 randomly choosen positions on different SWNT ropes. In order to study the electronic structure of the SWNTs we investigate the shape of the normalized differential conductivity, $\frac{dI}{dV}/\frac{I}{V}$, which represents in good approximation the shape of density of states (DOS) of the sample. [15] In agreement with the theoretical expectations [3], we observe pronounced peaks in the DOS corresponding to the typical singularities in the DOS for low dimensional systems. One example is shown

in Fig. 4. The energy spacing of these peaks in connection with the presence/absence of features around zero bias can be used to classify the SWNTs into the categories metallic, near gap and wide gap. Furthermore, the energy spacing between the innermost singularities measures the band gap (for wide gap SWNTs) or the pseudogap (for metallic and near gap SWNTs). (See Ref. [10] for details)

In the histograms in Fig. 5 we present the detailed distributions of bandgaps or pseudogaps of the metallic, near gap and wide gap SWNTs in the buckypaper. We determine the (metallic : near gap : wide gap) ratios at the surface of our buckypaper sample to be $(34 \pm 6\%$: $15 \pm 4\%$: $51 \pm 7\%)$. This result indicates that metallic SWNTs (n_1, n_2) are preferentially produced. If this was not the case, one would expect a distribution of $(4 \pm 1\%$: $35 \pm 3\%$: $61 \pm 3\%)$ on the basis of the diameter distribution determined by TEM in Ref. [8] We would like to emphasize that the gap distributions obtained characterize the intact buckypaper, in contrast to studies after dissolution of the sample, which can be affected by enrichment/depletion of certain SWNT species.

From the gap distributions shown in Fig. 5, we have determined the SWNT diameter distribution in the buckypaper [10] (not shown), assuming that the theoretically derived relations between SWNT diameter and gap are valid. [16] If the deviations of the SWNTs from "ideal" nanotubes in the buckypaper is taken into consideration, we find good agreement between our results and Ref. [8].

In order to specifically study the electronic states responsible for the RT conductivity in the metallic and near gap SWNTs, we have performed RIXS experiments.

In RIXS, a core electron is promoted into a previously unoccupied state by the absorption of a soft x-ray photon. This excited state can decay radiatively when a valence electron fills the core vacancy. Energy and intensity of the emitted photons are monitored in RIXS as a function of the excitation energy. The technique measures the density of electronic states (DOS) of a certain part of the Brillouin zone (BZ). [17] More accurately, only states with the propper symmetry (s,p,d...) compatible with the dipole transition (*partial* DOS) at the type of atom where the core vacancy has been created (*local* DOS) is probed. The excitation energy determines which parts of the BZ are probed.

Using selective excitation, we can now preferentially study the metallic and near gap SWNTs within the bulk of the buckypaper sample. For excitation energies just above the C 1s absorption threshold, we select those wavevectors within the BZ, which correspond to the unoccupied states of lowest energy. A metallic sample will have occupied states at the same wavevectors.

In Fig. 6, we present the C 1s RIXS spectra of our buckypaper sample in comparison to graphite. For different excitation energies, the x-ray emission intensity as a function of the emission energy is shown for bucky-

paper and graphite. Non-k-selective contributions have been subtracted. (For details see Ref. [9].)
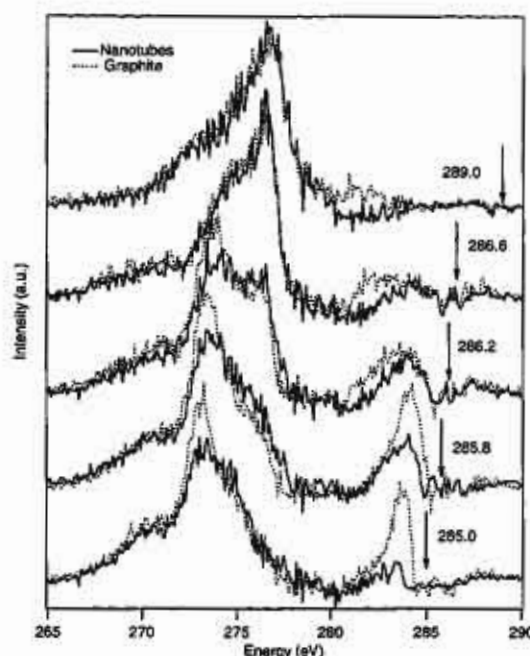
FIG. 6. Resonant inelastic soft x-ray scattering spectra of single wall carbon nanotubes (solid line) and non-oriented graphite (dotted line). The non-k-selective contributions to the raw data have been subtracted, as well as a Voigt curve to account for the diffuse reflection/recombination (arrows). The excitation energies, from bottom to top, are: 285.0 eV, 285.8 eV, 286.2 eV, 286.6 eV and 289.0 eV. Features A and B arise due to states at the K point in the BZ. For details see Ref. [9]

In the graphite RIXS spectrum excited at 285.0 eV, the broad emission feature at 270 eV emission energy labeled B is due to emission from the lowest two occupied bands at the K point, corresponding to states around 13 eV below E_F in the bandstructure reproduced in Fig. 1. These states can be unambigously assigned, as they are the only states in this binding energy range within the whole BZ. Preferential emission from the K point is expected for this choice of excitation energy just at the absorption threshold, as the core electron is promoted into the first available unoccupied states, which are at the K point (see Fig. 1).

For the SWNT sample excited at 285.0 eV, we observe an emission feature of the same shape and at the same emission energy as in graphite. For the same reasons as in graphite, we assign this feature to emission from low energy states at the K point. This is consistent with threshold excitation into the lowest unoccupied states, as those are always derived from states in the immediate vicinity of the K point, as outlined above. We would like to point out, that RIXS with threshold excitation probes selectively those SWNTs within the buckypaper which

have their lowest unoccupied states as low in energy as possible, *i.e.* at E_F. Due to the finite width of the radiation used for excitation (0.4 eV) and the C 1s core level involved in the absorption transition (width 0.09 meV), we can not distinguish metallic and near-gap SWNTs, but wide gap SWNTs are easily discriminated against.

We now turn our attention to the highest energy RIXS feature labeled A in Fig. 6. This feature is located around 284.1 eV emission energy. For graphite, this feature has been assigned to emission from the highest occupied states, located at the K point. For the SWNTs, we observe intensity in the RIXS spectrum at the same energy. For the same k-conservation reasons as in graphite, this feature can unambiguously be assigned to emission from states at the K point. We can therefore directly observe those occupied states at E_F which are degenerate (or quasi-degenerate) with the unoccupied states at K and which are responsible for the high room temperature conductivity of SWNTs with suitable (n, m).

Emission from these states can be seen more clearly in the RIXS spectra when the excitation energy is increased to 285.8 eV. Comparing the spectra from the SWNTs and the graphite, we see that the emission feature is clearly visible in the SWNTs spectrum, but it is less intense than in graphite. This difference in intensity is due to the fact that at this energy wide gap nanotubes can be excited as well. These nanotubes do not contribute to the high energy emission feature, as they have no occupied states close to E_F.

When the excitation energy is further increased, more states within the BZ are probed according to the dispersion of the unoccupied bands. As a result, the spectra are not specific for the K point anymore. This behavior is traced by the continuous decrease of feature B in the spectra.

In conclusion, we have studied the electronic structure of single wall nanotubes in intact buckypaper by STM/STS and RIXS. From STS, we find metallic, near gap and wide gap SWNTs with a ratio of $(34 \pm 6\% : 15 \pm 4\% : 51 \pm 7\%)$, respectively, indicating that metallic SWNTs are indeed preferentially produced, as had been suggested earlier. The bandgap/pseudogap distribution of the SWNTs within these groups could be quantified. RIXS allows us to directly display those occupied states which are responsible for the room temperature conductivity in metallic and near gap SWNTs.

RIXS Work: Annette Karl, Stefan Eisebitt

STM Work: Ingo Wirth, Gunther Kann, Stefan Eisebitt

[1] N. Hamada, S. Sawada, A. Oshiyama: Phys. Rev. Lett. **68**, 1579 (1992)

[2] R. Saito, M. Fujita, M.S. Dresselhaus, M.S. Dresselhaus: Appl. Phys. Lett. **60**, 2204 (1992)

[3] M.S. Dresselhaus, G. Dresselhaus, P. Eklund: *Science of Fullerenes and Carbon Nanotubes* (Academic Press, San Diego 1996)

[4] G.S. Painter and D.E. Ellis, Phys. Rev. B **1**, 4747 (1970).

[5] Similar approaches have been used to study a variety of quantum confined systems, see e.g. S. Eisebitt, S.N. Patitsas, J. Lüning, J.-E. Rubensson, T. Tiedje, T. van Buuren, W. Eberhardt: Europhys. Lett. **37**, 133 (1997)

[6] Derivations from this simple picture arise for nanotubes with small radii, as σ and π states, which are perpendicular in graphene, start to hybridize. See e.g. X. Blase, L.X. Benedict, E.L. Shirley, S.G. Louie: Phys. Rev. Lett. **72**, 1878 (1994)

[7] The K point in the graphite BZ corresponds to the P point in the BZ for a single graphene sheet. Similarly, the M point in the 3D system corresponds to the Q point in the 2D system. In a nanotube, the 2D band structure is sliced or folded back on a 1D band structure between Γ and X. For ease of comparison, we use the graphite (3D) notation also for the graphene sheet and the nanotubes.

[8] A.G. Rinzler, J. Liu, H. Dai, P. Nikolaev, C.B. Huffman, F.J. Rodriguez-Macias, P.J. Boul, A.H. Lu, D. Heymann, D.T. Colbert, R.S. Lee, J.E. Fischer, A.M. Rao, P.C. Eklund, and R.E. Smalley, Appl. Phys. A **67**, 29 (1998).

[9] S. Eisebitt, A. Karl, W. Eberhardt, J. E. Fischer, C. Sathe, A. Agui and J. Nordgren, Appl. Phys. A **67**, 89 (1998).

[10] S. Eisebitt, I. Wirth, G. Kann, and W. Eberhardt, submitted.

[11] T. W. Ebbesen, H. Hiura, J. Fujita, Y. Ochiai, S. Matsui and K. Tanigaki, Chem. Phys. Lett. **209**, 83 (1993).

[12] W. Clauss, D. J. Bergeron, and A. T. Johnson, Phys. Rev. B **58**, R4266 (1998).

[13] J. Lefebvre, R. Antonow, A. T. Johnson, Appl. Phys. A **67**, 71 (1998).

[14] A. Fonseca, K. Hernadi, P. Piedigrosso, J.-F. Colomer, K. Mukhopadhyay, R. Doome, S. Lazarescu, L. P. Biro, Ph. Lambin, P. A. Thiri, D. Bernaerts, J. B. Nagy, Appl. Phys. A **67**, 11 (1998).

[15] J. A. Stroscio, R. M. Feenstra, and A. P. Fein, Phys. Rev. Lett. **57**, 2579 (1986); R. M. Feenstra, J. A. Stroscio, A. P. Fein, Surf. Sci. **181**, 295 (1987).

[16] J. W. Mintmire and C. T. White, Phys. Rev. Lett. **81**, 2506 (1998).

[17] J. Lüning, J. E. Rubensson, C. Ellmers, S. Eisebitt, and W. Eberhardt, Phys. Rev. B **56**, 13147 (1997).

Femtosecond multi-photon photoemission of small Pt_n-cluster anions

Using femtsecond pulses (Ti:S) of 3 and 1.5 eV photons, respectively, multi-photon photoionization has been observed in small Pt_n and Pd_n cluster anions [1]. Two-, three- and four-photon processes have been identified with pulse energies of 1-3 mJ. The multi-photon processes are obvious by a photoelectron signal below the electron affinity for time-to-energy conversion with 1hv, which is not observed in the photoelectron spectra taken with standard nsec-lasers (Nd:YAG). The multi-photon electron intensity distribution shows almost no fine structure which has been interpreted by a fast electron relaxation of the initially excited cluster.

Fig. 1 shows the femtosecond photo-electron spectra of Pt_3^- at different time-delays of the probe pulse (0, 400 and 1000 fs). The top curve shows the multi-photon emission spectrum taken with a single laser pulse (probe-only) of 1.5 eV. A sharp double peak appears at 2 eV. Since the electron affinity of Pt_3 is 1.8 eV, no photoelectrons from single-photon emission are detected. Two-photon processes are seen down to a binding energy of 1.8 eV. At still lower binding energies emission from three- and four-photon processes are detected. The spectrum at top should be equivalent to the result without any time delay between the pump and probe pulse (t=0fs). The intensity of the sharp peak distinctly decreases with increasing time delay: The intensity is slightly smaller at t=400 fs than in the probe-only spectrum while the signal is almost vanished at t=1ps. The decreasing intensity makes a resonant two-photon process in Pt_3^- evident in

which an excited state is detached within the lifetime of the initially excited state.
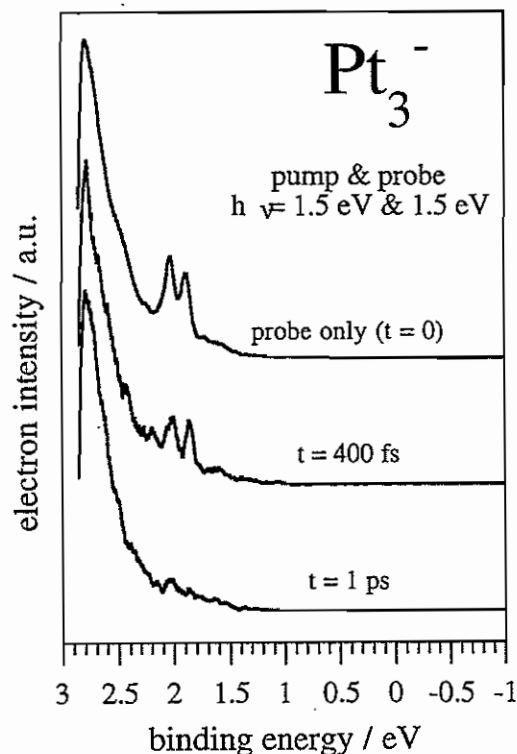
FIG. 1. The femtosecond photoelectron spectrum of Pt_3^- as a function of the time delay t between the pump and probe pulse. The photon energy is 1.5 eV. The probe-only spectrum (t=0) is equivalent to the spectrum recorded at zero time delay. Note the decreasing intensity of the peak at 2 eV from t=0 fs to t=1000 fs.

The zero-time delay between the pump and probe pulse has been determined by self-phase-modulation of the femtosecond pulse (20 GW/cm^2) behind a 5 cm long glass cell filled with water. The total intensity of the modulation frequency (Fig. 2) has been measured with an optical diode as a function of the time delay in an autocorrelation set up. The delay between the pump and probe pulse has

been varied by a movable retroreflector mounted on a linear translation stage (100fs=15μm) electrically driven by a dc motor. At zero-time delay the intensity autocorrelation signal rises strongly due to the maximum overlap of the pump and probe pulse at 11.35 mm (Fig. 3). From the width of the autocorrelation peak a temporal pulse width of ~200 fs is estimated assuming a sech-pulse shape of the femtosecond pulse.
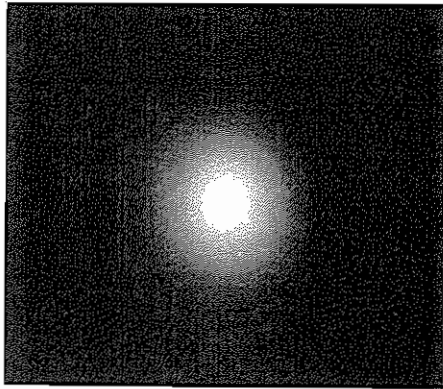
FIG. 2. The non-linear medium water gives rise to self-phase-modulation of the incoming femtosecond pulse which causes a spectral broadening as seen in the photograph. The total intensity of the emission signal has been measured by an optical diode. The fundamental wavelength of the laser pulse (820nm) has been filtered out in front of the diode detector.

shift of retroreflector
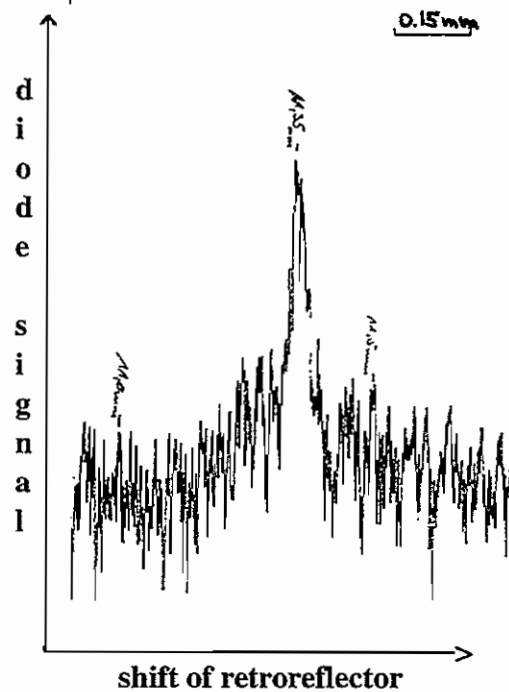
FIG. 3. The intensity autocorrelation signal measured with an optical diode as a function of the time delay t between the pump and probe pulse. The retroreflector was continuously sweept with a velocity of ~10μm/2.5sec. The sharp peak at 11.35 mm marks the zero point of time delay. A temporal pulse width of ~200 fs is approximated from the width of the peak. The measured intensity distribution of the phase modulation signal is shown in Fig. 2.

[1] N. Pontius, P.S. Bechthold, M. Neeb, W. Eberhardt; J. Electron Spectrosc. Relat. Phenom., submitted.

Niko Pontius, Paul S. Bechthold, Matthias Neeb, Wolfgang Eberhardt, Jürgen Lauer, Heinz Pfeifer

Excited state dynamics of an organic photoconductor

A basic step for laser printers or xerography devices containing organic photoconductors is the charge generation upon irradiation with visible light. Our goal is to increase the efficiency of this process by combining the organic photoconducting material with the charge accepting buckminsterfullerene C_{60} /1/. For this purpose we investigate the dynamics of the excited states, especially the lifetime of the excitons.
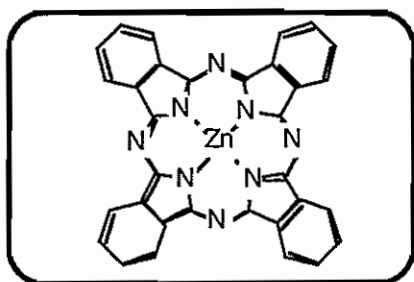
Fig.1: Model for Zn-Phthalocyanine (Zn-Pc),
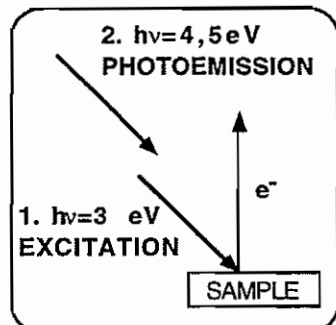
Fig.2: Principle of the 2-photon-photo-emission (2PPE),

As a typical organic photoconductor material we have chosen to study Zn-phthalocyanine (Zn-Pc) /2/. Zn-Pc builds molecular crystals from stacks of the planar molecules (see fig.1). Sublimed layers are analyzed by 2-photon photoemission (2PPE) using ultra short (fs) laser pulses (Fig.2, fig.3). An excited state is created with a first laser pulse (pump process, $h\nu = 3eV$). After a variable delay the state is probed with a second laser pulse (probe pulse, $h\nu = 4,5eV$) that

produces a photoelectron. The kinetic energy of this photoelectron is measured by a hemispherical analyzer and depends on the relaxation process: the more time the excited state has to relax the lower is the measured energy. Therefore a variation of the delay time between both laser pulses probes the lifetime of the excited and of intermediate states /3/. The time resolution is about 200fs and a repetition rate of 250kHz is used.
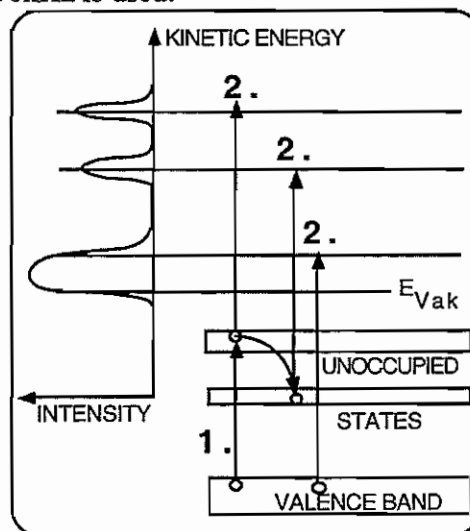
Fig.3: Energy scheme of excitation and relaxation, measured by 2PPE.

Figure 4 displays a sequence of 2PPE spectra. A background has been subtracted that corresponds to the sum of the signals from both lasers illuminating the sample separately (pump only, probe only). The bottommost spectrum (delay = -400fs) has been measured with the probe pulse arriving at the sample before the pumping process. The non zero intensity at the low-energy edge of this spectrum corresponds to long living excitations from the last pump-probe cycle and is interpreted as the triplet exciton of Zn-Pc. At higher kinetic energies the series shows changes of the structures which belong to the singlet excitons for different delay times. Additional changes at even higher kinetic

energies are only visible on an enlarged scale (not shown). The decay of the different excited states is displayed in fig.5 on a logarithmic scale of the delay times.
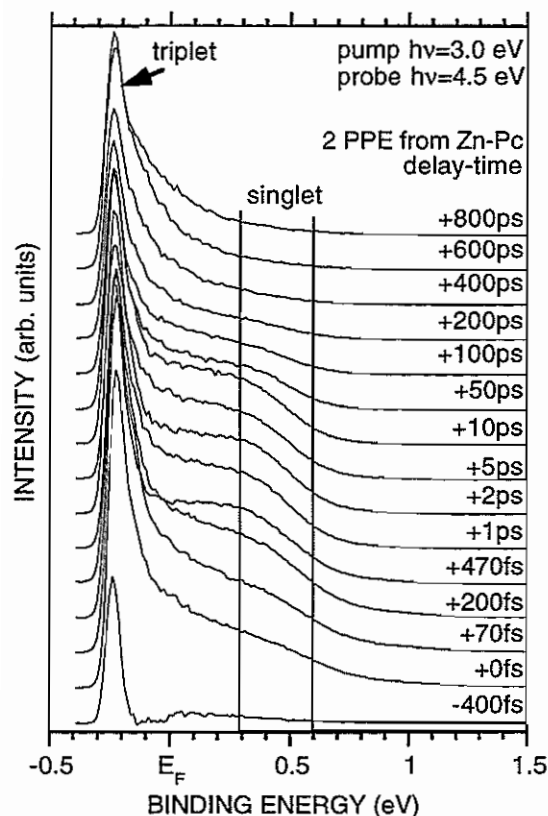
Fig.4: *2 photon photoemission spectra from Zn-Pc at different delay times (background subtracted, see text).*

These data result from the intensity of the spectra in fig.4 at specific energies, normalized to the corresponding intensity at zero delay. A fit of the curves in fig.5 assuming a simple exponential decay yields the life time of the excited states. The shortest life time with 0.2ps (which corresponds to our time resolution) belongs to the direct excitation into the LUMO+1, the second lowest unoccupied molecular orbital of Zn-Pc. At the other end of the time scale we find the triplet excitation with a life time of at least 4μs. This curve contains an additional component that has a life time of 70ps. We explain this as a contribution by

inelastically scattered electrons from higher excited singlet excitonic states with higher kinetic energies carrying their time characteristics. The singlet excitonic state at 0.6eV cannot be explained by a single lifetime only, it shows an additional component with a lifetime of 2ps. Typical error bars for the life times range between 5ps and 50ps.
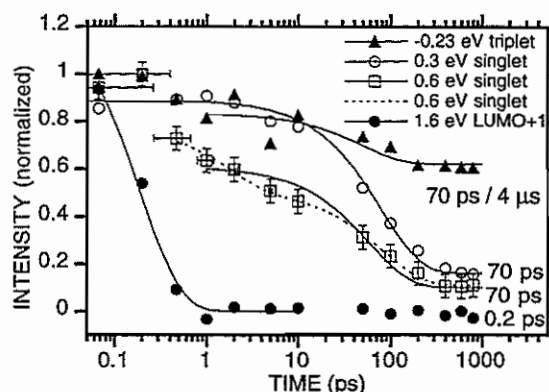
Fig.5: *Evolution of excited states in Zn-Pc as a function of the delay time (from spectra in fig.3).*

With these results we demonstrate that 2 photon-photoemission spectroscopy is a suitable tool for an investigation of the excited state dynamics of organic photoconductors. A next step will be to look for expected changes upon doping the material with C_{60} and thereby verify the benefit of the fullerenes for the charge-generation process.

/1/   B.Kessler, Appl.Phys.A 67, 125 (1998).
/2/   C.Schlebusch, Dissertation, Universität zu Köln (1998).
/3/   R.Jacquemin, S.Kraus, W.Eberhardt, Solid State Commun. 105, 449 (1998).
/4/   S.Günster, Dissertation, Universität Oldenburg (1993).

C.Schlebusch, S.Link, A.Scholl, B.Kessler, W.Eberhardt

Electric Field Induced Changes in STM Images of Metal Surfaces

Controlling and manipulating the growth of metallic ultra-thin films and nanowires is a challenging task. Growth in an electrolytic environment opens new possibilities through the extra control parameter given by the variable electrochemical potential of the electrolyte. Atomic resolution imaging by STM is used at the electrolyte-metal interface to observe structural changes, in order to do this one has to be sure that there is no other effect obscuring the image. It is well known that STM produces a real space image of the electronic and topographic structure of a conducting surface.

We present an electric field dependent change of corrugation patterns in STM images of metal surfaces. It is caused by the increase (decrease) of the potential barrier due to a positive (negative) applied electric field which in turn influences the decay behavior of electronic states into the vacuum. Under the condition of competing states with different corrugation patterns near the Fermi energy this may produce a switching from one to the other type of pattern. We explicitly demonstrated the effect for the Fe(001) surface. In this case the change corresponds to a corrugation reversal, i.e. atoms are imaged as protrusions for fields greater than a certain z-dependent field strength while they appear as dips for fields below that value. This effect is rather general and may occur for any metal surface possessing two states near the Fermi energy which produce different corrugation patterns.

The predictions are based on calculations of the electronic structure performed with the full-potential linearized augmented plane wave method (FLAPW) in film geometry and the density functional theory in the local spin-density approximation.

We analyze our *ab initio* calculations of Fe(001) with respect to STM images on the basis of the model of Tersoff and Hamann. The tunneling current I as a function of applied bias voltage V and electric field F can be written as:

$$I(\mathbf{r}_\parallel, z, V, F) \propto \int_{E_F}^{E_F + eV} n(\mathbf{r}_\parallel, z, \epsilon, F)\, d\epsilon, \qquad (1)$$

where $n(\mathbf{r}_\parallel, z, \epsilon, F)$ is the local density of states (LDOS) of the sample evaluated at the lateral $(\mathbf{r}_\parallel)$ and vertical (z) position of the tip. The electronic structure and thus the LDOS depends on the electric field F which has several sources: (i) Applied bias voltage between tip and sample $(F \leq 0.2 \text{ V/Å})$, (ii) difference between workfunctions of tip and sample $(F \leq 0.2 \text{ V/Å})$, and (iii) the charged electrolyte $(F \leq 1.0 \text{ V/Å})$. The effect on the electronic structure due to the field is twofold: (i) A Stark shift of the energetic positions of the electron states and (ii), which is important in the context of STM, a change of

the potential barrier and thereby a change in decay of wavefunctions into the vacuum. To analyze the LDOS it is convenient to expand it into symmetrized 2D plane waves (star functions) with z dependent coefficients:

$$n(\mathbf{r}_\parallel, z, \epsilon, F) = \sum_s n_s(z, \epsilon, F)\phi_s^{2D}(\mathbf{r}_\parallel). \qquad (2)$$
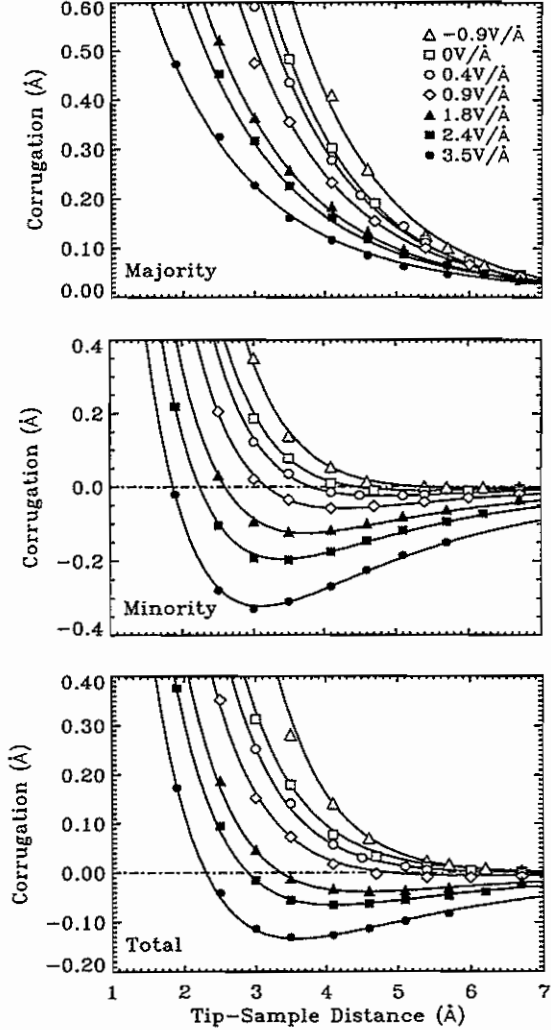
FIG. 1. Corrugation amplitude as a function of the tip-sample distance z for the Fe(001) surface at small bias voltages, i.e. states with energy $E_F \pm 30$ meV. In addition to the total corrugation, majority and minority spin contributions are shown in the upper and middle panel, respectively. Graphs are displayed at different field strength. Data points were taken from the FLAPW calculation multiplied by an enhancement factor of 6.5 accounting for a d_{z^2}-tip orbital using Chen's derivative rule. The curves have been fitted using the two-state model. Negative corrugation means atoms appear as dips instead of protrusions.

145

The first star function ϕ_1^{2D} is always a constant and its coefficient n_1 must be positive since it represents the charge when integrated over the 2D unit cell. The main contribution to the first star coefficient results from states near the $\bar{\Gamma}$ point of the 2D BZ [1]. The second star function is in the case of a (100) square lattice $\phi_2^{2D}(x,y) \propto \cos(2\pi x/a) + \cos(2\pi y/a)$ with maxima at the positions of the atoms in the square lattice and minima for the hollow positions. The coefficient value n_2 is dominated by states near the $\bar{X}$ point of the 2D BZ. n_2 can either be positive indicating a normal STM image, i.e. atom positions and maximal tunneling current coincide, or negative resulting in an anticorrugated image, where atom positions and minimal tunneling current coincide. Corrugation amplitudes, i.e. the maximal difference in vertical position of the tip within a surface unit cell as it scans the surface at constant current, were calculated by:

$$\Delta z(z, F) \propto \frac{\int n_2(z, \epsilon, F)\, d\epsilon}{\int (\partial/\partial z) n_1(z, \epsilon, F)\, d\epsilon} \qquad (3)$$

including only the first two star coefficients n_1, n_2 since higher terms were insignificant in this context (see Ref. [1] for details on neglecting higher order terms).

The total and the spin-separated corrugation amplitudes as function of the distance between tip and sample are displayed in Fig. 1. Let us focus first on the minority part. Without field the corrugation is positive for $z \leq 4.4$ Å and negative beyond this distance. If we apply a positive (negative) electric field to the surface the distance of sign reversal decreases (increases). The majority spin channel on the other hand displays a positive corrugation amplitude at all distances. At positive (negative) electric fields it decreases (increases) as a result of a higher (lower) potential barrier. Finally, we turn to the total corrugation amplitude, which is the experimentally accessible quantity. As a result of the majority contribution the characteristic curve of the minority states is weakened in the total corrugation amplitude but still clearly visible. Without field a normal STM image should even be measured at all distances.

In the case of the ferromagnetic Fe(001) surface the field dependent effect occurs in the minority spin channel and therefore we start our investigation by presenting the corresponding minority spin bandstructure without field (Fig. 2). Near the Fermi energy, which is the part of interest for STM imaging of metal surfaces usually performed at very low bias voltages ($V < 100$ meV), a surface state band ($\bullet$) is clearly visible for the even states in the $\bar{\Gamma}\bar{X}$ direction of the 2D BZ which continues in the $\bar{\Gamma}\bar{M}$ direction with odd symmetry ($\square$). Besides this surface state there are also surface resonance states found near the $\bar{X}$ point of both even d_{yz} character and possess
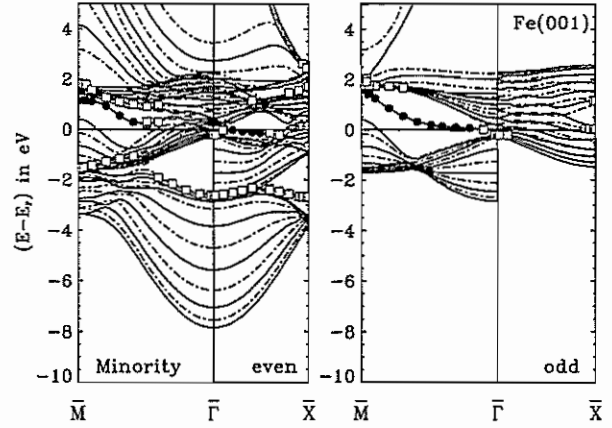
FIG. 2. Bandstructure of minority spin states for Fe(001). Surface localized states are marked according to: $\bullet$ more than 70 % localization in the surface layer and the vacuum and $\square$ more than 75 % localization in the top three surface layers and the vacuum.

charge density maxima in the vacuum on *hollow* sites of the 2D unit cell. As stated above the contribution to the different parts of the LDOS depends greatly on the location in the 2D BZ. We have therefore calculated the star coefficient contribution $n_{1,2}(\downarrow, \epsilon \in E_F \pm 30$ meV $, k_\parallel)$ for each minority spin state $|k_\parallel \nu\rangle$ in the 2D BZ. For the coefficient n_2, which controls the corrugation pattern of the STM image we found that the contribution of the discussed surface states is positive, i.e. leading to normal STM images. There is a further contribution to the second star coefficient from the surface resonance states at the $\bar{X}$ point, which is of negative value. Thus a competition of the surface and resonance states exists. Since the contribution to the second star coefficient of states near the $\bar{X}$ point decays slower with distance from the surface than that of states near $\bar{\Gamma}$ the anticorrugated image should dominate at large distances. Increasing the electric field leads to a strong decrease of the surface state contribution while the anticorrugating states at the $\bar{X}$ point remain at a relatively high value, which explains the increase of the negative corrugation amplitude for the minority states of Fe(001) with increasing field strength.

[1] S. Heinze, S. Blügel, R. Pascal, M. Bode, R. Wiesendanger, accepted in Phys. Rev. B.

S. Heinze, X. Nie, M. Weinert and S. Blügel (FE 23.20.0)

Special Group: Materials subject to high radiation doses

General Overview

Research Area

The goal of the work of the Special Group is the study and analysis of the changes in the properties of materials and the construction of models of materials subject to irradiation that is typical in fusion or in spallation. Since intensive sources of high energy neutrons are not available, the effects of bombardment are simulated using low mass ions from a cyclotron. In the case of spallation materials, information can also be gained by studying targets of existing weak sources (ISIS, LANSCE) that have been taken out of service. We have succeeded in collecting all existing available highly-dosed components from these sources in the Hot Cells of the FZJ. The results of mechanical tests yield valuable information about the servicable lifetime of targets in the High-Performance Sources ESS (European Spallation Source) and SNS (US-Spallation Neutron source) that are currently planned. In addition, theoretical models are used in an attempt to translate know-how gained via the development of materials for fission and fusion to the case of spallation. As in previous years, the group has enjoyed a close working relationship with Institute Theory II (H. Trinkhaus), which is a pre-requisite for an analysis of the experimental results that is meaningful and suggestive of further work.

Results

- Samples of the `low activation' steel F82H subject to implantation of more than 10 wt ppm hydrogen showed strong variations in their strength and ductility. This may possibly point to the creation of micro-cracks (hydrogen embrittlement).

- A model for the creation of lens-shaped helium bubbles in alpha-SiC was developed. The model also describes the growth of dislocation loops around the bubbles.

- Measurements on irradiated beta-SiC showed recovery behaviour that was only slightly different from that of alpha-SiC. The healing out of defects is shifted to slightly higher temperatures (see detailed report).

- Thermal recovery from radiation-induced dimensional changes in oxide ceramics (Al2O3, MgO, MgAl2O4) correlated with the recovery behaviour of defects observed by optical absorption and ESR.

- Segregation at grain boundaries (gb) induced in NiSi by radiation showed unusual morphologies which varied from gb to gb. For coherent and incoherent twin-boundaries, the different morphologies could be correlated with the character of the gb. In general such a correlation could not be established.

- The ductility and strength of the light metal beryllium was shown to be strongly influenced by its helium content.

- Via conclusive measurements using electron bombardment, we showed that the radiation induced electrical degradation in ceramics that has been found to follow electron- ion- and neutron-bombardment is an artefact caused by the formation of cracks and by surface contamination.

- Of the materials that were radiated by the 800MeV proton beam of the LAMPF-facility in Los Alamos, martensitic steels showed the least embrittlement in bending tests in the hot cells at FZJ. These materials are now regarded as the favoured candidate materials for the Hg-target container of ESS.

External Funding and Collaborative Projects

In 1997, the work of the special group was again an essential part of the Eurpoean Fusion Programme. This is now partly integrated within the ITER Programme. 25% of the total costs (45% for irradiation) were financed via the Association FZJ/EURATOM by the EU in Brussels. In 1998, this translated into a net income of 600,000 DM for the FZJ. The areas of work are determined in consultation with the other partners in the Programme. The group has particularly close collaborations with the Riso National Lab, the University of Ancona, the Institute for Physical Chemistry of the Russian Academy of Sciences, Moscow and the Kurchatov Institute in Moscow. The main partners in connection with the ESS-related work are the National Laboratories Los Alamos and Oak Ridge, the Paul-Scherrer Institute, Villigen and the Rutherford Appleton Laboratory, Didcot. This work is supported via an EU-TMR contract (Leading Institution FZJ; 1.6M Euro for 13 participants from 9 countries, of which 280,000 Euro devolves to FZJ as the largest partner).

A cooperative project without transfer of funding is the STIP-Cooperation (an international Radiation Programme at the Swiss 0.9 MW Spallation-Source SINQ, with follow-up examination of the samples in the Hot-Cell Laboratories in Jülich, Oak Ridge, Saclay and Villigen).

All ESS-related work is part of the HGF Strategic-Fund Project 'Research and Development related to the construction of the pulsed European Spallations Neutron Source ESS' with the Hahn-Meitner Institute as partner. (Duration mid 1998 - mid 2001).

Personnel 1998/99

1. **Regular Staff**

J. Deutz	Ion-Etching for the preparation of ceramic TEM-samples
A. Fournier	Secretary (Special Group and ESS-Office)
Dr. P. Jung	Effects of radiation in metals and ceramics, thermal desorption spectroscopy, hydrogen and helium in solids, microhardness.
Dr. W. Kesternich	Electron-Microscopy (TEM) of the microstructure of metals, conductivity changes of insulators subject to radiation, mechanical properties of beryllium
H. Klein	Instrumentation for radiation-experiments, TEM, data processing, and the measurement of mechanical and electrical properties.
W. Schmitz	Scanning-Electron-Microscopy, vacuum and electrotechnician, sample preparation.
Prof. H. Ullmaier	Group Leader, Projet Leader ESS, radiation damage in metals.

2. **Doctoral Students**

Zhi. Y. He	Effect of helium in oxide-ceramics
R. Merkes	Radiation-induced segregation at grain boundaries
F. Schliefer	Hydrogen permeation in ceramics

3. **HGS-Position**

J. Chen	Mechanical properties and TEM of spallation-target materials

4. **Guests.**

Chao Liu (NPIC, Chengdu, China)	Hydrogen embrittlement of low-activation martensitic steels.
Dr. A. Ryazonov (Kurchatov Institute, Moscow)	Models for helium embrittlement and radiation-induced amorphization.

Dimensional changes of α- and β-SiC after helium implantation and thermal annealing.

P. Jung, J. Chen and H. Klein

Sondergruppe Werkstoffe unter hoher Bestrahlungsbelastung

Production and recovery of displacement defects in α- and β-SiC were measured by surface profilometry after helium implantation and subsequent thermal annealing. Only minor differences were observed between both materials, which is a positive result with respect to the use of e.g. fiber-matrix composite materials.

Silicon-carbides, presumably in the form of fiber-composites (SiC$_f$/SiC), are candidates for structural materials in future fusion reactors. One major concern with respect to the use of these materials in nuclear environments is the possible influence of irradiation defects and of transmutation products, especially hydrogen and helium, on mechanical and thermal properties. Implantation of α-particles from accelerators is a very effective method to simulate the helium production in a fusion reactor. Similar to the situation in the reactor, displacement defects are produced in the lattice simultaneously with helium production.

A specific property of silicon-carbide is the pronounced polymorphy, i.e. the appearance of a great number of crystal structures, which differ by the stacking sequence of the close-packed SiC double layers. The most common modifications are the both hexagonal (α-SiC) structures 4H and 6H and the cubic (β-SiC) form 3C. While for example hot pressing and sintering usually give α-SiC, SiC fibers or other material, produced by chemical vapor deposition (CVD) or chemical infiltration (CVI) are mostly β-SiC. This means that, depending on production technology, composites may consist of pure β-SiC, or of a mixture of α- und β-SiC. Therefore differences of the behaviour of lattice defects and helium in both modifications is a question of basic as well as of technical interest.

Detailed investigations on α-SiC, which were recently performed at our institute [1], were now supplemented by helium implantation in β-SiC. 40x2 mm specimens of ca. 400 μm thickness were fixed by Wood's metal to water-cooled copper heat sinks and were implanted with α-particles in vacuum < 10^{-3} Pa at the Jülich compact cyclotron. The energy of the α-beam was degraded by a rotating wheel with aluminium foils of varying thicknesses, such that homogeneous implantation up to a depth of 96 μm was achieved. Volume expansion due to defect production in this region caused bending of the specimens which was recorded by profilometry.

Fig. 1 shows the linear expansion as a function of displacement dose. An average number of 60 displacements per implanted helium atom was used for calculation of displacement dose [2]. Comparison of the different measurements gives two important results:

1) The agreement of the expansions in α-SiC after transmissive proton irradiation [3] and after helium implantation [2], plotted as a function of displacement dose, indicates that expansion is mainly caused by displacement defects and not by implanted helium atoms.

2) The good agreement of the expansions in α- and β-SiC shows that lattice structure has only a minor, if any, influence on defect production.
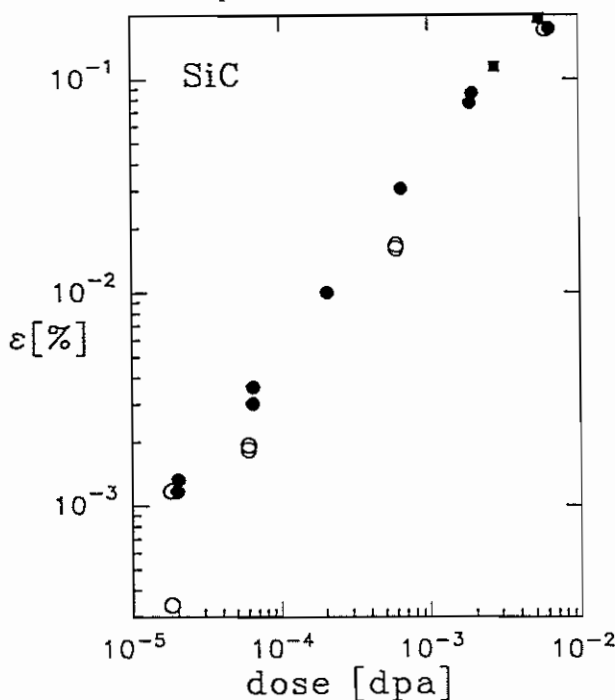
Fig. 1: Linear lattice expansion as a function of the displacement dose due to α-implantation in α- (●) and β-SiC (O). Included are uniaxial measurements of lattice expansion of α-SiC by proton irradiation (■) [3].

Fig. 2 shows the recovery of expansion of helium implanted α- and β-SiC during thermal annealing. The specimens were annealed isochronally in steps of 50°C, for ½ hour each, and subsequently analysed by profilometry. The most important results are:

1) In all specimens recovery starts already at the irradiation temperature (≈ 50°C).

2) Above about 200°C a clear dose dependence is observed.

3) A comparison of α- und β-SiC at equal dose (10 atppm He, squares in Fig. 2) shows that if at all, only between ca. 200 und 600°C recovery of β-SiC is slightly retarded. A much larger retardation of recovery was observed in a particulate composite SiC/C, the SiC content of which mainly consisted of the β-phase [1,4]. According to the results of Fig. 2 this retardation must be ascribed to the graphite content of the SiC/C.

4) Recovery of lattice defects is complete at ca.1200°C.

5) Above about 1350°C expansion increases again. This is ascribed to the growth of helium bubbles by accumulation of vacancies, as confirmed by investigations by transmission electron microscopy (TEM) [1].
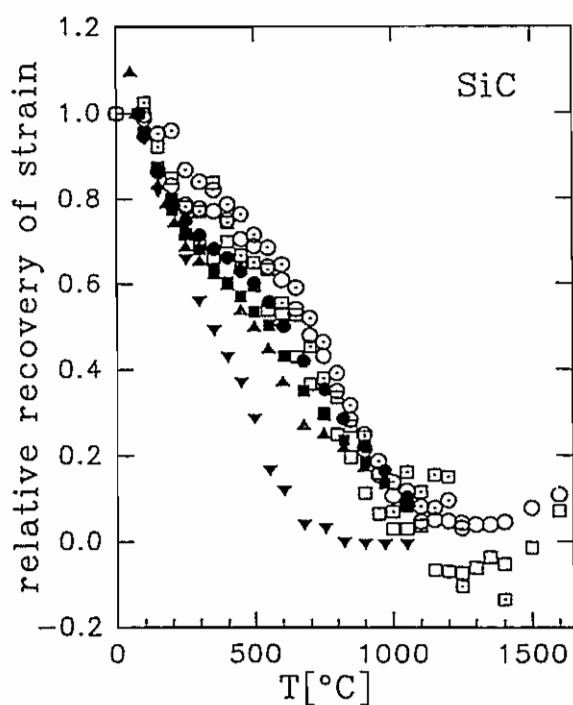
Fig. 2: Relative annealing (isochronal, $\Delta t=1/2$ h, $\Delta T=50°C$) of linear expansion in α-SiC (full symbols) and β-SiC (open symbols) after implantation of 1 (▼), 3 (▲), 10 (■,□), 30 (●) and 100 (○) atppm helium.

Therefore the present results mean that also in mixtures of α- and β-SiC no bigger problems are to be expected, e.g. from internal stresses due to differences in production or annealing of lattice defects.

On the other hand it is found that the formation of helium bubbles is not homogeneous close to grain boundaries or interfaces. Instead defect free zones of ca. 0.5 μm width are formed along boundaries, see Fig. 3. This means that for example in fibers with typical diameters of 1 μm, no helium bubbles are formed, as confirmed by experimental observation. On the other hand enhanced bubble formation is expected along the fiber-matrix interface, with possibly severe consequences on the integrity of the fiber-matrix-compound. This topic needs further investigations.

TEM investigations of the formation of helium bubbles in β-SiC and comparison to the results on α-SiC are in progress.
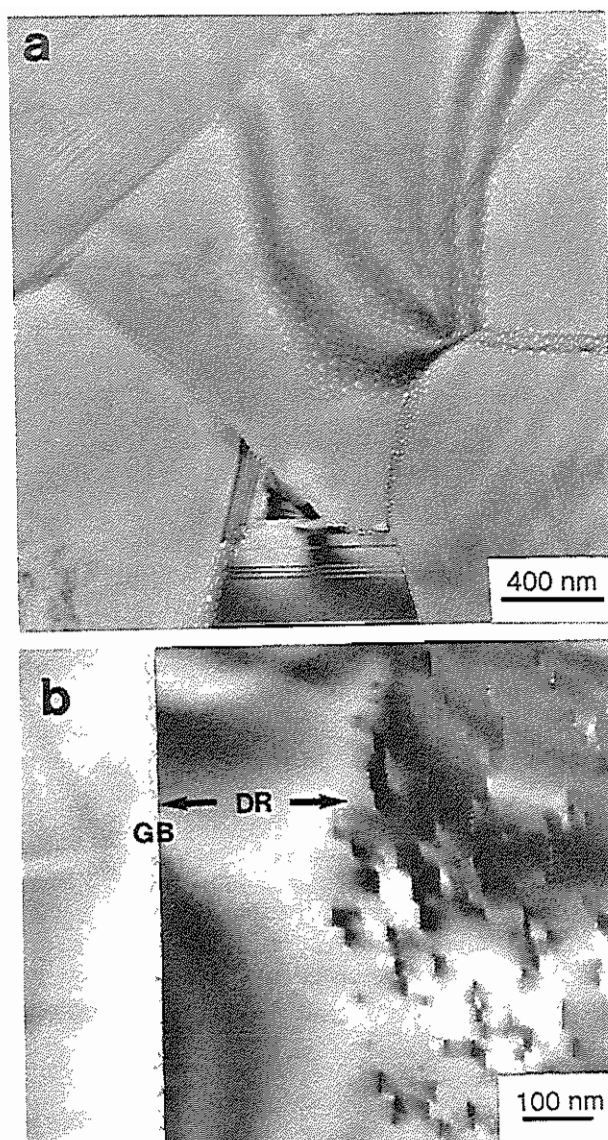
Fig. 3: Defects in α-SiC after implantation of 600 atppm helium and annealing for one hour at 1350°C.
a) Overview by kinematic, underfocus-brightfield-imaging. In the centre bubbles can be seen at a grain boundary which is oriented almost perpendicular to the beam, while the bubbles at the lower left corner are in the interior of a large grain.
b) Defects in the grain boundary (GB) and in the interior of a α-SiC (4H) grain with a clearly visible defect free zone (DR) inbetween.

[1] J. Chen, Report Forschungszentrum Jülich, Jül-3585, 1998

[2] J. Chen, P. Jung and H. Klein, J. Nucl. Mater. 258-263, 1803 (1998)

[3] P. Jung, Z. Zhu and J. Chen, J. Nucl Mater. 251, 276 (1997)

[4] J. Chen und P. Jung, Forum on New Materials, Firenze, 1998, t.b.publ.

Publications

- Publications in refereed journals
- Other publications

Publications in refereed journals

IFF-98-11-001
Abbas
Likos, C.N., Löwen, H.1, Watzlawek, M.1, Abbas, B., Jucknischke, O., Allgaier, J., Richter, D.
1Heinrich-Heine-Universität Düsseldorf
Star Polymers Viewed as Ultrasoft Colloidal Paricles
Phys.Rev.Lett. 80, 4450 (1998)
23.30.0

IFF-98-11-002
Arons
Arons, R.R.
Magnetic studies of the Ba-Tb-In-oxide, a new proton conductor with the simple perovskite-like structure
Journal of Magnetism and Magnetic Materials 177-181 (1998) 869-870
23.42.0

IFF-98-11-003
Asada
Asada, T., Blügel, S.
Prediction of magnetic structures of ultra-thin Fe films on
Cu(100): Successful understanding
of experimental findings
J. Magn. Magn. Mater. 177-181, 1233 (1998)
23.20.0

IFF-98-11-004
Biermann
Biermann, S., Hohl, D.1, Marx, D.2
1 Shell E&P Technology CO, Houston, USA
2 MPI für Festkörperforschung, Stuttgart
Proton quantum effects in high pressure hydrogen
J. Low Temp. Phys. 110, 97 (1998)
23.20.0

IFF-98-11-005

Biermann
Biermann, S., Hohl, D.1, Marx, D.2
1 Shell E&P Technology CO, Houston, USA
2 MPI für Festkörperforschung, Stuttgart
Quantum effects in solid hydrogen at ultra-high pressure
Solid State Com. 108, 337 (1998)
23.20.0

IFF-98-11-006
Brener
Abel, T., Brener, E. and Müller-Krumbhaar, H.
Three-Dimensional Growth-Morphologies
in Diffusion-Controlled Channel Growth
Phys. Rev. E 55 (1997) 7789-7792
23.15.0

IFF-98-11-007
Brener
Brener, E., Marchenko, V.I.1
1P.L. Kapitza Institute for Physical Problems, RAS, 117334, Kosygin Str.2, Moscow, Russia
Surface Instabilities in Cracks
Phys. Rev. Lett. 81 (1998) 5141-5144
23.15.0

IFF-98-11-008
Brener
Feng, X., Brener, E., Temkin, D., Saito Y.1 and Müller-Krumbhaar, H.
1KEIO University, Japan
Solidification in the one-dimensional model for a disordered binary alloy under diffusion
The European Physical Journal B 5 (1998) 663-669
23.15.0

IFF-98-11-009
Brückel
Chattopadhyay, T.a,b, Liss, K.D.c, Brückel, T.d
a Institut Max von Laue-Paul Langevin (ILL), BP 1 56, F-38042 Grenoble Cedex 9
b Max-Planck-Institut für Physik Komplexer Systeme, D-Dresden
c European Synchrotron Radiation Facility (ESRF), BP 2 20, F-38043 Grenoble Cedex
d Forschungszentrum Jülich GmbH, Institut für Festkörperforschung, D-52425 Jülich
Incommensurate-commensurate lock-in phase transition in EuAs3
Journal of Magnetism and Magnetic Materials 177 - 181 (198) 1058 - 1060
23.89.1

IFF-98-11-010
Brückel
Perry, S.C.1, Costa, M.M.R.2, Stirling, W.G.3, Longfield, M.J.3, Mannix, D.3, Brückel, T.4
1 Physics Department, School of Physical Science and Engineering, Keele University, Staffordshire ST5 5BG, UK
2 Physics Department, Universidade do Coimbra, 3000 Coimbra, Portugal
3 Department of Physics, Oliver Lodge Laboratory, University of Liverpool, Liverpool L69 7ZE, UK
4 Forschungszentrum Jülich GmbH, Institut für Festkörperforschung, D-52425 Jülich
Energy-dependent polarization study of the x-ray magnetic scattering in terbium metal
J. Phys.: Condens. Matter 10 (1998) 1951 - 1964
23.89.1

IFF-98-11-011
Buchenau
Ramos, M.A.1, Buchenau, U.
1Universidad Autonoma, Madrid
Beyond the Standard Tunneling Model: The Soft-Potential Model in Tunneling Systems in Amorphous and Crystalline Solids, ed. P. Esquinazi (Springer, Berlin 1998), p. 527ff
23.30.0

IFF-98-11-012
Caliebe
Caliebe, W. A.1,2, Kao, C.-C.2, Hastings, J. B.2, Taguchi, M.3, Kotani, A.3, Uozumi, T.4, de Groot, F. M. F.5
1 Forschungszentrum Jülich GmbH, Institut für Festkörperforschung, D-52425 Jülich
2 National Synchrotron Light Source, Brookhaven National Laboratory, Upton, New York, 11973, USA
3 Institute for Solid State Physics, University of Tokyo, Roppongi, Minato-ku, Tokyo 106, Japan
4 College of Engineering, University of Osaka Prefecture, Gakuen-cho, Sakai 593, Japan
5 Solid State Physics Laboratory, University of Groningen, Nijenborgh 4, 9747 AG Groningen, The Netherlands
1s2p resonant inelastic x-ray scattering in (-Fe2O3
Physical Review B, Volume 58 (20) 13452 - 13458 (1998)
23.20.0

IFF-98-11-013
Caliebe
Hill, J.P.1, Kao, C.-C.2, Caliebe, W.A.L.2,3, Matsubara, M.4, Kotani, A.4, Peng, J.L.5, Greene, R.L.5
1 Department of Physics, Brookhaven National Laboratory, Upton, New York 11973, USA
2 National Synchrotron Light Source, Brookhaven National Laboratory, Upton, New York,

11973, USA
3 Forschungszentrum Jülich GmbH, Institut für Festkörperforschung, D-52425 Jülich
4 Institute for Solid State Physics, University of Tokyo, Roppongi, Minato-ku, Tokyo 106, Japan
5 Center for Superconductivity Research, Department of Physics and Astronomy, University of Maryland, College Park, Maryland 20742, USA
Resonant Inelastic X-Ray Scattering in Nd2CuO4
Phys. Rev. Lett. 22, 4967 - 4970 (1998)
23.20.0

IFF-98-11-014
Chen
Chen, J., Jung, P., Klein, H.
Production and recovery of defects in SiC after Irradiation and
Deformation
J. Nucl. Mater. 258-263 (1998) 1803
23.80.5

IFF-98-11-015
Conrad
Gawronski, M., Conrad, H., Springer, T.
Forschungszentrum Jülich GmbH, Institut für Festkörperforschung, D-52425 Jülich
Proton-Deuteron and H2O-D2O Exchange in Polysaccharides by X-ray and Small-Angle Neutron Scattering
Macromolecules, Vol. 31, No. 8, 1998
23.30.0

IFF-98-11-016
Conrad
Conrad, H.
Forschungszentrum Jülich GmbH, Institut für Festkörperforschung, D-52425 Jülich
Es muß nicht immer Spaltung sein
Physik in unserer Zeit / 29. Jahrg. 1998 / Nr. 2
23.60.0

IFF-98-11-017
Dederichs
Asato, M.1, Hoshino, T.1, Asada, T.1, Zeller, R. and Dederichs, P. H.
1Department of Applied Physics, Faculty of Engineering, Shizuoka University, Japan
Vacancy formation energies in FCC metals: non-local effect beyond the LSDA
J. Mag. Mag. Mat. 177-181 (1998) 1403-1404
23.20.0

IFF-98-11-018
Dederichs
Binder, J.1, Zahn, P.1, Mertig, I.1, Zeller, R., Dederichs, P.H.
1Institut für Theoretische Physik, Technische Universität Dresden, 01062 Dresden
Magnetic properties of impurities and impurity pairs in magnetic multilayers
Phil. Mag. B 78 (1998) 537-544
23.20.0

IFF-98-11-019
Dederichs
Dederichs, P.H., Wildberger, K., Zeller, R.
Interlayer exchange coupling and interface reflectivities in Fe/Cu, Co/Cu and Ni/Cu(001) layers
Physica B 237-238 (1997) 239-243
23.20.0

IFF-98-11-020
Dederichs
Eisebitt, S., Lüning, J., Rubensson, J.-E., Settels, A., Dederichs, P.H., Eberhardt, W., Patitsas, S.N.1, Tiedje, T.2
1Department of Physics, University of British Columbia, Vancouver, B.C., V6T 1Z1, Canada
2Department of Electrical Engineering, University of British Columbia, Vancouver, Canada
Resonant inelastic soft X-ray scattering at the Si L3 edge: experiment and theory
J. El. Spectr. Rel. Phen. 93 (1998) 245-250
23.20.0

IFF-98-11-021
Dederichs
Hoshino, T.1, Asato, M.1, Asada, T.1, Zeller, R. and Dederichs, P. H.
1Department of Applied Physics, Faculty of Engineering, Shizuoka University, Japan
Non-self-consistent first-principles calculations for total-energy differences
J. Mag. Mag. Mat. 177-181 (1998) 1411-1412
23.20.0

IFF-98-11-022
Dederichs
Hoshino, T.1, Zeller, R., Dederichs, P. H., Asada, T.1
1Dept. of Applied Physics, Faculty of Engineering, Shizuoka University, Japan
Interaction energies of point defects in metals: Non-local effect beyond the LSDA
Physica B 237-238 (1997) 361-362
23.20.0

IFF-98-11-023
Dederichs
Huhne, T.1, Zecha, C.1, Ebert, H.1, Dederichs, P.H., Zeller, R.
1Institut für Physikalische Chemie, Universität München, 80333 München
Full-potential spin-polarized relativistic Korringa-Kohn-Rostoker method implemented and applied to bcc Fe, fcc Co, and fcc Ni
Phys. Rev. B 58 (1998)
23.20.0

IFF-98-11-024
Dederichs
Kläsges, R., Schmitz, D., Carbone, C., Eberhardt, W., Lang, P., Zeller, R., Dederichs, P. H.
Short-period oscillations in photoemission from Cu films on Co(100)
Phys. Rev. B 57 (1998)
23.20.0

IFF-98-11-025
Dederichs
Korhonen, T., Papanikolaou, N., Zeller, R., Dederichs, P.H.
Ab initio calculation of forces and lattice relaxations in metallic alloys
Phil. Mag. B 78 (1998) 429-433
23.20.0

IFF-98-11-026
Dederichs
Mavropoulos, P.H.1, Stefanou, N.1, Nonas, B., Zeller, R., Dederichs, P.H.
1Section of Solid State Physics, University of Athens, Panepistimioupolis, GR-157 84 Athens, Greece
Hyperfine fields of probe atoms on the (001) surface of Ni
Philosophical Magazine B 78 (1998) 435-440
23.20.0

IFF-98-11-027
Dederichs
Nayak, S. K.1, Weber, S. E.1, Jena, P.1, Wildberger, K., Zeller, R., Dederichs, P. H., Stepanyuk, V. S.2, Hergert, W.2
1 Physics Dept., Virginia Commonwealth University, Richmond, USA
2 Fachbereich Physik, Martin-Luther-Universität Halle
Relationship between magnetism, topology and reactivity of Rh clusters
Phys. Rev. B 56 (1997) 8849

23.20.0

IFF-98-11-028
Dederichs
Nonas, B., Wildberger, K., Zeller, R. and Dederichs, P. H.
Energetics of 3d Impurities on the (001) Surface of Iron
Phys. Rev. Lett. 80 (1998) 4574
23.20.0

IFF-98-11-029
Dederichs
Nonas, B., Wildberger, K., Zeller, R., Dederichs, P. H. and Gyorffy, B. L.1
1H.H. Wills Physics Lab., University of Bristol, UK
Magnetic properties of 4d impurities on the (001) surfaces of nickel and iron
Phys. Rev. B 57 (1998) 84
23.20.0

IFF-98-11-030
Dederichs
Papanikolaou, N.1, Zeller, R., Dederichs, P. H., Stefanou, N.1
1University of Athens, Section of Solid State Physics, Athens, Greece
Ab initio study of structural distortion and its influence on the magnetic properties of metallic dilute alloys
Comp. Mat. Sci. 8 (1997) 131-135
23.20.0

IFF-98-11-031
Dederichs
Stefanou, N.1, Mavropoulos, Ph.1, Nonas, B., Zeller, R. Dederichs, P.H.
1Section of Solid State Physics, University of Athens, Panepistimioupolis, GR-157 84 Athens, Greece
Hyperfine Fields of sp Impurities on Ni and Fe Surfaces
Phys. Rev. Lett. 81 (1998) 1505
23.20.0

IFF-98-11-032
Dederichs
Stepanyuk, V. S.1, Hergert, W.2, Rennert, P.2, Wildberger, K., Zeller, R. and Dederichs, P. H.
1MPI für Mikrostrukturphysik, Halle
2Martin-Luther-Universität Halle-Wittenberg, FB Physik, Halle

Transition metal magnetic nanostructures on metal surfaces
Surf. Sci. 377-379 (1997) 495-498
23.20.0

IFF-98-11-033
Dederichs
Tatarchenko, A. F.1, Stepanyuk, V. S.2, Hergert, W.2, Rennert, P.3, Zeller, R. and Dederichs, P. H.
1Institute of High Pressure Physics, Troitsk, Moscow region 142092, Russia
2Fachbereich Physik, Martin-Luther-Universität, 06099 Halle
Total energy and magnetic moments in disordered Fe_xCu_{1-x} alloys
Phys. Rev. B 57 (1998) 5213
23.20.0

IFF-98-11-034
Dederichs
Weber, S. E.1, Rao, B. K.1, Jena, P.1, Stepanyuk, V. S.2, Hergert, W.3, Wildberger, K., Zeller, R. and Dederichs, P. H.
1Physics Department, Virginia Commonwealth University, Richmond, USA
2MPI für Mikrostrukturphysik, Halle
3Fachbereich Physik, Martin-Luther-Universität, Halle
Magnetism of free and supported vanadium clusters
J. Phys.: Condens. Matter 9 (1997) 10739-10748
23.20.0

IFF-98-11-035
Dederichs
Wildberger, K., Zeller, R., Dederichs, P.H., Kudrnovsky, J.1, Weinberger, P.2
1Institute of Physics AS CR, C2-18040 Praha, Czech Republic and Center for Materials Science, Technical University, A-1060 Vienna, Austria
2Center of Materials Science, Technical University, A-1060 Vienna, Austria
Interface reflectivities and quantum-well states in magnetic multilayers
Phys. Rev. B 58 (1998) 13721
23.20.0

IFF-98-11-036
Dederichs
Zahn, P.1, Mertig, I.1, Zeller, R. and Dederichs P.H.
1Institut für Theoretische Physik, Technische Universität Dresden, 01062 Dresden
Screened KKR with hard-core potentials
Phil. Mag. B 78 (1998) 411-415
23.20.0

IFF-98-11-037
Dederichs
Zahn, P.1, Binder, J.1, Mertig, I.1, Zeller, R. and Dederichs, P. H.
1Institut für Theoretische Physik, TU Dresden, Dresden
Origin of Giant Magnetoresistance: Bulk or Interface Scattering
Phys. Rev. Lett. 80 (1998) 4309
23.20.0

IFF-98-11-038
Dederichs
Zeller, R., Asato, M.1, Hoshino, T.1, Zabloudil, J.2, Weinberger, P.2, Dederichs, P.H.
1Department of Applied Physics, Faculty of Engineering, Shizuoka University, Hamamatsu 432, Japan
2Institut für Technische Elektrochemie, Technische Universität Wien, A-1060 Wien, Austria
Total-energy calculations with the full-potential KKR method
Phil. Mag.B 78 (1998) 417-422
23.20.0

IFF-98-11-039
Denton
Denton, A.R.;Löwen, H.:
Stability of colloidal quasicrystals
Physical Review Letters 81 (1998), 469-472
23.30.0

IFF-98-11-040
Domke
Domke, C., Ebert, Ph. and Urban, K.
Changes of defect and active dopant concentrations induced by annealing of highly Si-doped GaAs
Phys. Rev. B 57, 4482-4485 (1998).
23.42.0
3.55.0

IFF-98-11-041
Domke
Domke, C., Ebert, Ph. and Urban, K.
Atomic-scale properties of the amphoteric dopant Si in GaAs(110) surfaces
Surf. Sci. 415, 285-298 (1998).
23.42.0
3.55.0

IFF-98-11-042
Domke
Domke, C., Heinrich, M., Ebert, Ph. and Urban, K.
Oscillating contrast in room-temperature STM images of localized charges in III-V semiconductor cleavage surfaces
J. Vac. Sci. Technol. B 16, 2825-2832 (1998).
23.42.0

IFF-98-11-043
Dreja
Dreja, M.1, Pyckhout-Hintzen, W., Tieke, B.1 1Universität Köln
Copolymerization behavior and structure of styrene and polymerizable surfactants in three-components cationic microemulsions
Macromolecules, 32, 272-280 (1998)
23.30.0

IFF-98-11-044
Ebert
Ebert, Ph., Yue, F. and Urban, K.
Surface structures of cleaved icosahedral Al-Pd-Mn single-quasicrystals after heat treatment
Phys. Rev. B 57, 2821-2825 (1998).
23.55.0

IFF-98-11-045
Ebert
Ebert, Ph. and Urban, K.
Electronic properties of the Ga vacancy in GaP(110) surfaces determined by scanning tunneling microscopy
Phys. Rev. B 58,1401-1404 (1998).
23.42.0

IFF-98-11-046
Eilenberger
Schmidt, K.1, Eilenberger, G.
1 EDS, Rüsselsheim
Poincaré maps of Duffing-type oscillators and their reduction to circle maps: II. Methods and numerical results
J. Phys. A31 (1998) 3903
23.15.0

IFF-98-11-047
Eisebitt
Eisebitt, S., Lüning, J., Rubensson, J.-E., Settels, A., Dederichs, P.H., Eberhardt, W., Patitsas, S.N.1, Tiedje, T.1
1 University of British Columbia, Vancouver, Canada
Resonant Inelastic Soft X-ray Scattering at the SiL3 Edge: Experiment and Theory
J. of Electron Spectroscopy and Related Phenomena 93, 245 (1998)
Proceedings of the Fourth International Workshop on Auger Spectroscopy and Electronic Structure Jülich 1997
23.20.0/23.89.1

IFF-98-11-048
Eisebitt
Eisebitt, S., Karl, A., Eberhardt, W., Fischer, J.E.1, Sathe, C.2, Agui, A.2, Nordgren, J.2
1 LSRM, University of Pennsylvania, Philadelphia, USA
2. Department of Physics, Uppsala University, Sweden
Electronic Structure of Single-wall Carbon Nanotubes studied by Resonant Inelastic X-ray Scattering
Applied Physics A 67, 89 (1998)
23.89.1

IFF-98-11-049
Eisebitt
Eisebitt, S., Karl, A., Scherer, R., Eberhardt, W.
Speckle with soft X-rays: A Demonstration
Synchrotron Radiation News 11, 15 (1998)
23.89.1

IFF-98-11-050
Eisebitt
Eisebitt, S., Lüning, J., Rubensson, J.-E., Settels, A., Dederichs, P.H., Eberhardt, W., Patitsas, S.N.1, Tiedje, T.1
1 Department of Physics. British University of Columbia, Vancouver, Canada
Resonant Inelastic Soft X-ray Scattering at the SiL3 Edge: Experiment and Theory
J. of Electron Spectroscopy and Related Phenomena 93, 245 (1998)
Proceedings of the Fourth International Workshop on Auger Spectroscopy and Electronic Structure Jülich 1997
23.20.0

IFF-98-11-051
Eisenhower

Eisenhower, R., Colella, R., and Grushko, B.
Multiple X-ray diffraction study of decagonal quasicrystals
Phys. Rev. B57 (1998) 8218.
23.55.0

IFF-98-11-052
Eisenriegler
Hanke, A.1, Schlesener, F.1, Eisenriegler, E., Dietrich, S.1
1 FB Physik, Universität Wuppertal
Critical Casimir forces between spherical particles in fluids
Phys. Rev. Lett. 81, 1885 (1998)
23.30.0

IFF-98-11-053
Engels
Engels, B., Richard, P., Schroeder, K., Blügel, S., Ebert, Ph. and Urban, K.
Comparison between ab initio theory and scanning tunneling microscopy for (110) surfaces of III-V semiconductors
Phys. Rev. B 58, 7799-7815 (1998).
23.42.0

IFF-98-11-054
Englich
Englich, J.1, Novak, P.2, Lütgemeier, H.
1 Faculty of Mathematics and Physics, Charles University, Prague
2 Institute of Physics. Academy of Sciences, Prague
Defects in Ferrites studied by 57Fe NMR
Int. J. of Modern Physics B 12, 609 (1998)
23.42.0

IFF-98-11-055
Franz
Franz, V., Feuerbacher, M., Wollgarten, M. and Urban, K.
Electron diffraction analysis of plastically deformed icosahedral Al-Pd-Mn single-quasicrystals.
Phil. Mag. Lett. in press.
23.42.0

IFF-98-11-056
Frielinghaus
Frielinghaus, H., Schwahn, D., Willner, L., Springer, T.

Thermal Composition Fluctuations in Binary Homopolymer Mixtures as a Function of
Pressure and Temperature
Physica B 241-243 (1998) 1022-1024
23.30.0

IFF-98-11-057
Frielinghaus
Frielinghaus, H., Abbas, B., Schwahn, D., Willner, L.
Temperature and Pressure dependent Composition Fluctuations in a
Polybutadiene/Polystyrene Polymer Blend and Diblock Colpolymer
Europhys. Lett. 44(5) (1998) 606-612
23.30.0

IFF-98-11-058
Ganteför
Ganteför, G., Kraus, S., Eberhardt, W.
Femtosecond Photoelectron Spectroscopy of the Photodissociation of Au3-
J. of Electron Spectroscopy and Related Phenomena 88-91, 35 (1998)
23.20.0

IFF-98-11-059
Goerigk
Benedetti, A.*, Polizzi, S.*, Riello, P.*, Pinna, F.**, Goerigk, G.***
* Dipartimento di Chimica Fisica, Università di Venezia, Dorsoduro 2137, I-30123 Venice
** Dipartimento di Chimica, Università di Venezia, Dorsoduro 2137, I-30123 Venice
*** Forschungszentrum Jülich GmbH, Institut für Festkörperforschung, D-52425 Jülich
Note ASAXS Investigation of a Au/C Catalyst
Journal of Catalysis 171, 345 - 348 (1997) Article No. CA971787
23.89.1

IFF-98-11-060
Goerigk
Goerigk, G., Haubold, H.-G., Schilling. W.
Forschungszentrum Jülich GmbH, Institut für Festkörperforschung, D-52425 Jülich
Kinetics of Decomposition in Copper-Cobalt: a Time-Resolved ASAXS Study
J. Appl. Cryst. (1997). 30, 1041 - 1047
23.89.1

IFF-98-11-061
Goerigk
Goerigk, G.a, Williamson, D. L.b

a Forschungszentrum Jülich GmbH, Institut für Festkörperforschung, D-52425 Jülich
b Department of Physics, Colorado School of Mines, Golden, Colorado 80401, USA
Nanostructured Ge Distribution in (-SiGe: H Alloys from Anomalous Small-Angle X-Ray
Scattering Studies
23.89.1

IFF-98-11-062
Grimm
Shotton, M.W.1, Pope, L.H.1, Forsyth, V.T.1, Langan, P.2, Grimm, H., Rupprecht, A.3,
Denny, R.C.4, Fuller, W.1
1University Keele, United Kingdom
2Institut Laue-Langevin, Grenoble
3University Stockholm, Sweden
4Blackett Laboratory, Imperial College, United Kingdom
A high-angle neutron fibre diffraction study of the hydration of B-DNA
23.15.0

IFF-98-11-063
Grossmann
Grossmann, M.1, Hoffmann, S., Gusowski, S.1, Waser, R.
1 Institut für Werkstoffe der Elektrotechnik, RWTH Aachen
Resistance Degradation Behavior of Ba0,7 Sr0,3TiO3 Thin Films compared to Mechanisms
found in Titanate Ceramics and Single Crystals
23.42.0

IFF-98-11-064
Grossmann
Grossmann, M.1, Lohse, O.1, Bolten, D. 1 and Waser, R., Hartner, W. 2, Schindler, G. 2,
Dehm, C. 2, Nagel, N. 2, Joshi, V. 3, Solayappan, 3, Derbenwick, G. 3
1 Institut für Werkstoffe der Elektrotechnik, RWTH Aachen
2 Siemens AG, Semiconductor Group, Dept. HL MP E TF, München
3 Symetrix Corporation, 5055 Mark Dabling Boulevard, Colorado Springs, CO
Imprint in Ferroelectric Sr2 Bi2 Ta9O Capacitors for Non-Volatile Memory Applications"
23.42.0

IFF-98-11-065
Grushko
Grushko, B., Holland-Moritz, D.1, Wittmann, R2. and Wilde, G.3
1 DLR, Köln

2 Laboratorium für Elektronenmikroskopie, Universität Karlsruhe, D-76128 Karlsruhe
3 Department of Materials Science and Engineering, University of Wisconsin/Madison, 53706 Madison WI, USA
Transition between periodic and quasiperiodic structures in Al-Ni-Co.
J. Alloys Comp. 280 (1998) 215-230
23.42.0

IFF-98-11-066
Gui
Gui, J.1,2, Jia, C.L.1, Hoffmann, S.3, Waser, R.
2 Department of Physics, Wuhan Univ., Wuhan, 430072, PR China
3 Institut für Werkstoffe der Elektrotechnik, RWTH Aachen
The effect of Zr on the microstructure of Ba(Ti1-yZry)O3 thin films prepared by chemical-solution deposition
Materials Letters 35 (1998) 375-379
23.42.0

IFF-98-11-067
Gui
Gui, Jianian1, Jia, C.L., Hoffmann, S.2, Waser, R.2
1Department of Physics, Wuhan University, Wuhan, 430072, People´s Republic of China
2Institut für Werkstoffe der Elektrotechnik, Rheinisch-Westfälische Technische Hochschule Aachen
The effect of Zr on the microstructure of Ba(Ti1-yZry)O3 thin films prepared by chemical-solution deposition
Materials Letters 35 (1998) 375
23.42.0

IFF-98-11-068
Göcking
Göcking, K.D., Monkenbusch, M.
Neutron scattering investigation of a macroscopic single crystal of a lyotropic L(phase
Europhys. Lett. 43 (1998), p.135
23.30.0

IFF-98-11-069
Göcking
Göcking, K. D., Monkenbusch, M.
Forschungszentrum Jülich GmbH, Institut für Festkörperforschung, D-52425 Jülich
Neutron scattering investigation of a macroscopic single crystal of a lyotropic L(phase
Europhys. Lett., 43 (2), pp. 135-140 (1998)
23.30.0

IFF-98-11-070
Hagenbeck
Hagenbeck, R. 1, Waser, R.
1 Institut für Werkstoffe der Elektrotechnik der RWTH Aachen
Influence of temperature and interface charge on the grain-boundary conductivity in acceptor-doped SrTiO3 ceramics
J. Appl. Phys. 83, No. 4 (1998) 2083
23.42.0

IFF-98-11-071
Haider
Haider, M., Uhlemann, S., Schwan, E., Rose, H., Kabius, B., Urban, K.
Electron microscopy image inhanced
Nature, 392, 768 (1998)
23.55.0

IFF-98-11-072
Haider
Haider, M., Rose, H., Uhlemann, S., Schwan, E., Kabius, B., Urban, K.
A spherical-aberration-corrected 200kV transmission electron microscope
Ultramicroscopy, 74, 53-60 (1998)
23.55.0

IFF-98-11-073
Handschuh
Handschuh, S., Blügel, S.
Magnetic Exchange Coupling of 3d Metal Monolayers on
Fe(001)
Solid State Comm. 105, 633 (1998)
23.20.0

IFF-98-11-074
Hasenkox
Hasenkox, U. 1, Hoffmann, S., Waser, R.
1 Institut für Werkstoffe der Elektrotechnik, RWTH Aachen
Influence of precursor chemistry on the formation of MTiO3 (M=Ba,Sr) ceramic thin films
Journal of Sol-Gel Science and Technology 12 (1998) 1-13
23.42.0

IFF-98-11-075
Haubold
Haubold, H.-G., Wang, X.H., Goerigk, G., Schilling, W.
Forschungszentrum Jülich GmbH, Institut für Festkörperforschung, D-52425 Jülich
In Situ Anomalous Small-Angle X-ray Scattering Investigation of Carbon-Supported
Electrocatalysts
J. Appl. Cryst. (1997). 30, 653-658
23.89.1

IFF-98-11-076
Hauck
Hauck, J., Bickmann, K., Mika, K.
Pseudobinary phase diagrams of RBa2Cu3Ox, R = La, Ce, Pr, Nd and Y
Supercond. Sci. Technol. 11 (1998) 63-67
23.55.0

IFF-98-11-077
Hauck
Hauck J., Mika, K.
Structure families of superconducting oxides and interstitial alloys
Supercond. Sci. Technol. 11 (1998)
23.55.0

IFF-98-11-078
Hauck
Hauck, J., Mika, K.
Ordering of Metal Atoms in Wurtzite and Sphalerite Structures
Journal of Solid State Chemistry 138 (1998)
23.55.0

IFF-98-11-079
Heinen
Heinen, B.1, Waser, R.
1 Institut für Werkstoffe der Elektrotechnik, RWTH Aachen)
Influence of the Thickness and Area of NiCr/AG-Electrodes on the Characteristics of BaTiO3
Ceramic Based PTC Thermistors
Journal of Materials Science 33, No. 18 (1998) 4603-4608
23.42.0

IFF-98-11-080
Heinze

Heinze, S., Blügel, S., Pascal, R.1, Bode, M.1, Wiesendanger, R.1
1 Zentrum für Mikrostrukturforschung, Universität Hamburg
Prediction of bias-voltage-dependent corrugation reversal for STM images of bcc (110) surfaces: W(110), Ta(110), and Fe(110)
Phys. Rev. B 58, 16432 (1998)
23.20.0

IFF-98-11-081
Hintermaier
Hintermaier, F.1, Hendrix, B.2, Desrochers, D.2, Roeder, J.2, Baum, G.2, van Buskirk, P.2, Bolten, D.3, Grossmann, M.3, Lohse, O.3 , Schumacher, M.3, Waser, R., Cerva, H.1, Dehm, D.1, Fritsch, E.1, Hönlein, W.1, Mazuré, C.1, Nagel, N.1, Thwaite, P.1, Wendt, H.1,
1 Siemens AG, Semiconductor Devision, München
2 Advanced Technology Materials Inc., Danbury, USA
3 Institut für Werkstoffe der Elektrotechnik, RWTH Aachen
Properties of SrBi2Ta2O9 Thin Films Grown by MOCVD for High Density FeRAM Applications
Integrated Ferroelectrics 21 (1998) 27-40
23.42.0

IFF-98-11-082
Hoffmann
Hoffmann, S.1, Waser, R.
1 Institut für Werkstoffe der Elektrotechnik, RWTH Aachen
"Curie-Weiss Law of (Ba1-xSrx)TiO3 Thin Films Prepared By Chemical Solution Deposition",
J. Phys. IV 8 (1998) 221-224
23.42.0

IFF-98-11-083
Holland-Moritz
Holland-Moritz, D., Schroers, J., Herlach, D.M., Grushko, B., and Urban, K.
Undercooling and solidification behaviour of melts of the quasicrystal-forming alloys Al-Cu-Fe and Al-Cu-Co
Acta Mater., 46 (1998) 1601.
23.42.0

IFF-98-11-084
Houben
Houben, L.1, Luysberg, M., Hapke, P.1, Vetterl, O.1, Finger, F.1, Carius, R.1, Wagner, H.1
1Institut für Schicht-und Ionentechnik, Forschungszentrum Jülich, 52425 Jülich, Germany
Morphological and crystallographic defect characteristics in plasma chemical-vapour-deposition grown microcrysalline silicon: A comparison between different growth modes

J. Non-Cryst.Solids 227-230, 896 (1998)
23.42.0

IFF-98-11-085
Houben
Houben, L.1, Luysberg, M., Hapke, P.1, Carius, R.1, Finger, F.1, Wagner, H.1
1Institut für Schicht-und Ionentechnik, Forschungszentrum Jülich, 52425 Jülich, Germany
Structural properties of microcrystalline silicon in the transition from highly crystalline to amorphous growth
Phil. Mag. A, 77, 1447 (1998)
23.42.0

IFF-98-11-086
Jacquemin
Jacquemin, R., Kraus S., Eberhardt W.
Direct Observation of the Dynamic of Excited Electronic States in Solids: F-sec Time resolved Photoemission of C60
Solid State Comm. 105, 449 (1998)
23.20.0

IFF-98-11-087
Jia
Jia, C.L., Urban, K., Hoffmann, S., Waser, R.
Microstructure of columnar-grained SrTiO3 and BaTiO3 thin films prepared by chemical solution deposition
J. Mater. Res. 13, No. 8 (1998) 2206
23.42.0

IFF-98-11-088
Jia
Jia, C.L., Urban, K., Mertin, M. 1, Hoffmann, S. 2, Waser, R.
1 Fraunhofer-Institut für Lasertechnik, Aachen
2 Institut für Werkstoffe der Elektrotechnik der RWTH Aachen
The structure and formation of nanotwins in BaTiO3 thin films
Phil. Mag. A77, 4 (1998) 923-939
23.42.0

IFF-98-11-089
Jia
Jia, C.L., Urban, K., Hoffmann, S.1, Waser, R.1
1Institut für Werkstoffe der Elektrotechnik, Rheinisch-Westfälische Technische Hochschule

Aachen
Microstructure of columnar-grained SrTiO3 and BaTiO3 thin films prepared by chemical solution deposition
J. Mater. Res.13 (1998) 2206
23.42.0

IFF-98-11-090
Jia
Jia, C.L., Urban, K., Mertin, M.1, K., Hoffmann, S.2, Waser, R.2
1Fraunhofer-Institut für Lasertechnik,
2Institut für Werkstoffe der Elektrotechnik, Rheinisch-Westfälische Technische Hochschule Aachen
The structure and formation of nanotwins in BaTiO3 thin films
Phil. Mag. A 77 (1998) 923
23.42.0

IFF-98-11-091
Jiang
%Jiang Jiang, X.1, Schiffmann, K. 1, Klages, C.-P. 1, Wittorf, D., Jia, C.L., Urban, K., Jäger, W.2 1Fraunhofer-Institut für Schicht- und Oberflächentechnik (FhG-IST), Braunschweig 2Mikrostrukturanalytik, Technische Fakultät, Universität Kiel
Improved diamond heteroepitaxy on silicon (001) by coalescence and overgrowth of grains
J. Appl. Phys. 83 (1998) 2511
23.42.0

IFF-98-11-092
Jung
Hirsch, S., Jung, P.
Dimensional changes and creep of glassy carbon under proton
Irradiation
Carbon, 36 (1998) 153
23.80.5

IFF-98-11-093
Jung
Jung, P.
Hydrogen inventory and embrittlement in low activation steels
J. Nucl. Mater. 258-263 (1998) 124
23.80.5

IFF-98-11-094

Jung
Jung, P.
A hydrogen problem in fusion material technology
Fusion Technology 33 (1998) 63
23.80.5

IFF-98-11-095
Jung
Zhu, Z., Jung, P.
Effect of stress and point defect retention on straining of
Refractories under irradiation
Radiat. Effects & Defects in Solids 144 (1998) 85
23.80.5

IFF-98-11-096
Kehr
Kehr, K.W.; Murthy, K.P.N.1; Ambaye, H.:
1 IGCAR, Kalpakkam, India
Connection between dispersive transport and statistics of extreme events
Physica A 253 (1998), 9-22
23.15.0

IFF-98-11-097
Kehr
Kehr, K.W.:
First-passage time distributions for linear chain segments with general site-dependent waiting-time distributions
Czechoslovak Journal of Physics, 48 (1998), 449 - 456
23.15.0

IFF-98-11-098
Kehr
Kehr; K.W., Mussawisade, K.; Wichmann, T; Dieterich, W.1:
1 Univ. Konstanz
Nonlinear Mobility of Particles in Nonsymmetric Potentials under Strong Bias Conditions
phys. stat. sol. (b) 205 (1998), 73-76
23.15.0

IFF-98-11-099
Kessler
Kessler, B.

Phthalocyanine-C60 composites as improved photoreceptor materials?
Appl. Phys. A 67, 125 (1998)
23.20.0

IFF-98-11-100
Kesternich
Garcia-Borquez, A., Kesternich, W.
Radiation-Induced Segregation and Precipitation in a N6-Stabilized Stainless Steel
Proc. 14th Int. Conf. On Electron Microscopy, Cancun, Mexico (1998) vol 2, 617
23.80.5

IFF-98-11-101
Kesternich
Kesternich, W.
Nucleation and Growth Instabilities of Precipitates Induced under Irradiation
Phil. Mag. A 77 (1998) 129
23.80.5

IFF-98-11-102
Kesternich
Kesternich, W.
Radiation-Induced Electrical Degradation : an Effect of Surface Conductance and
Microcracking
J. Nucl. Mater. 253 (1998) 167
23.80.5

IFF-98-11-103
Kesternich
Kesternich, W.
Energy Dispersive X-ray Spectroscopy with High Spatial Resolution and High Quantitative
Accuracy
Proc. Asian Science Seminar on New Direction in Transmission Electron Microscopy and
Nano-Characterization of Materials, Fukuoka, Japan (1998) 223
23.80.5

IFF-98-11-104
Kietzmann
Kietzmann, H., Rochow, R., Ganteför, G., Eberhardt, W., Vietze, K., Seifert, G., Fowler,
P.W.
Electronic Structure of Small Fullerenes: Evidence for the High Stability of C32
Phys. Rev. Lett. 81, 5378 (1998)

23.20.0

IFF-98-11-105
Kietzmann
Kietzmann, H., Morenzin, J., Bechthold, P.S., Ganteför, G., Eberhardt, W.
Photoelectron Spectra of Nbn-clusters: Correlation between Electronic Structure and Hydrogen Chemisorption
J. of Chemical Physics 109, 2275 (1998)
23.20.0

IFF-98-11-106
Kläsges
Kläsges, R., Schmitz, D., Carbone, C., Eberhardt, W., Lang P., Zeller R., Dederichs, P.H.
Short Period Oscillations in Photoemission from Cu Films on Co(100)
Phys. Rev. B 57, R696 (1998)
23.42.0

IFF-98-11-107
Kläsges
Kläsges R., Schmitz D., Carbone, C., Eberhardt W., Kachel.T1
1 Bessy GmbH Berlin
Surface Magnetism and Electronic Structure of Ultrathin fcc Fe Films
Solid State Comm. 107, 13 (1998)
23.42.0

IFF-98-11-108
Kordos
Kordos, P.1, Marso, M.1, Luysberg, M.
1Institut für Schicht-und Ionentechnik, Forschungszentrum Jülich, 52425 Jülich, Germany
Conduction in nonstoichiometric molecular-beam epitaxial GaAs grown above the critical thickness
Appl. Phys. Lett., 72, 1851 (1998)
23.42.0

IFF-98-11-109
Krenzlin
Krenzlin, H.M.; Budczies; J.1, Kehr, K.W.:
1 Univ. Köln
Wave packet tunneling
Ann. Phys. (Leipzig) 7, (1998), 732-736
23.15.0

IFF-98-11-110
Köbler
Köbler, U.a, Mueller, R. M.a, Schnelle, W.b, Fischer, K.a
a Forschungszentrum Jülich GmbH, Institut für Festkörperforschung, D-52425 Jülich
b Max-Planck Institut für Festkörperforschung, D-70506 Stuttgart
Critical magnetic behaviour of a ferromagnet with antiferromagnetic fourth-order exchange interactions: GdMg
Journal of Magnetism and Magnetic Materials 188 (1998) 333 - 345
23.15.0

IFF-98-11-111
Lichtensstein
Lichtenstein, A.I., Katsnelson, M.I.1
1 Institute of Metal Physics, Ekaterinburg
Ab initio calculations of quasiparticle band structure in correlated systems: LDA++ approach
Phys. Rev. B57 (1998) 6884-6895
23.20.0

IFF-98-11-112
Lichtenstein
Lichtenstein, A.I., Jones, R.O., Xu, H.1, Heaney, P.J.,1
1 Department of Geosciences, Princeton University
Anisotropic thermal expansion in the silicate (-eucryptite - a neuron diffraction and density functional study
Phys. Rev. B58, 6219 (1998)
23.20.0

IFF-98-11-113
Lichtenstein
Fleck, M.1, Lichtenstein, A.I., Oles, A.M.2, Hedin, L.1, Anisimov, V.I.3
1 MPI Festkörperforschung, Stuttgart
2 Jagellonian University, Kraków
3 Institute of Metal Physics, Ekaterinburg
Dynamical mean-field theory for doped antiferromagnets
Phys. Rev. Lett. 80 (1998) 2393-2396
23.20.0

IFF-98-11-114
Lichtenstein
Solovyev, I.V.1, Lichtenstein, A.I., Terakura, K.1

1 JRCAT-NAIR, Ibaraki, Japan
Is Hund's second rule responsible for the orbital magnetism in solids?
Phys. Rev. Lett. 26 (1998) 5758-5761
23.20.0

IFF-98-11-115
Lichtenstein
Solovyev, I.V.1, Lichtenstein, A.I., Terakura, K.2
1 JRCAT-ATP, Ibaraki, Japan
2 JRCAT-NAIR, Ibaraki, Japan
Orbital magnetism in FeO
3.20.0

IFF-98-11-116
Lichtenstein
Schick, A.B.1, Freeman, A.J.1, Lichtenstein, A.I.
1 Dept of Physics and Astronomy, Northwestern University, Evanston, USA
Orbital magnetic moment enhancement at surfaces and interfaces within the framework of the local density approximation+U method
23.20.0

IFF-98-11-117
Liebsch
Liebsch, A.
Prediction of a Ag multipole surface plasmon
Phys. Rev. B57, 3803 (1998)
23.20.0

IFF-98-11-118
Liebsch
Ishida, H.1, Liebsch, A.
1 Nihon University, okyo
Electronic excitation in alkali-metal overlayers. I. Unreconstructed low-temperature phase of Li/Al
Phys. Rev. B57, 12550 (1998)
23.20.0

IFF-98-11-119
Liebsch
Ishida, H.1, Liebsch, A.
1 Nihon University, Tokyo

Electronic excitations in alkali-metal overlayers. II. Effects of substitutional adsorption of Na/Al(001).
Phys. Rev. B57, 12558 (1998)
23.20.0

IFF-98-11-120
Liebsch
Barman, S.R.1, Horn, K.1, Häberle, P.2, Ishida, H.3, Liebsch, A.
1 Fritz-Haber-Institut der MPG, Berlin
2 Universidad Tecnica, Valparaiso, Chile
3 Nihon University, Tokyo
Photoinduced plasmon excitation in alkali-metal overlayers
Phys. Rev. 57, 6662 (1998)
23.20.0

IFF-98-11-121
Likos
Likos, C.N.; Löwen, H.; Poppe, A.; Willner, L.; Roovers, J.; Cubitt, B.; Richter, D.:
Ordering phenomena of star polymer solutions approaching the theta state
Phys. Rev. E 58 (1998), 6299-6307
23.30.0

IFF-98-11-122
Likos
Likos, C.N.; Löwen, H.; Watzlawek, M.; Abbas, B.; Jucknischke, O.; Allgaier, J; Richter, D.:
Star Polymers Viewed as Unltrasoft Colloidal Particles
Phys. Rev. Lett. 80 (1998) 4450
23.30.0

IFF-98-11-123
Likos
Likos, C.N., Löwen, H.1, Poppe, A., Willner, L., Roovers, J.2, Cubitt, B.3, Richter, D.
1Universität Düsseldorf
2National Research Council of Canada, Ottawa
3Institut Laue-Langevin, Grenoble
Ordering phenomena of star polymer solutions approaching the theta state
Physical Review E, 58 (1998), 6299
23.30.0

IFF-98-11-124
Lohse

Lohse, O.1, Tiedke, S.1, Grossmann, M., Waser, R.
1 Institut für Werkstoffe der Elektrotechnik, RWTH Aachen
Externally Determined and Intrinsic Contributions to the Polarization Switching Currents in SrBi2 Ta2O9 Thin Films
Integrated Ferroelectrics 22 (1998) 123-131 (1998)
23.42.0

IFF-98-11-125
Luysberg
Luysberg, M., Sohn, H.1, Prasad, A.1, Specht, P.1, Liliental-Weber, Z.2, Weber, E.R.1, Gebauer, J.3, Krause-Rehberg, R.3
1Department of Materials Science, University of California Berkeley, CA 94720, USA
2Materials Science Devision, Lawrence Berkeley National Laboratory, CA 94720, USA
3Fachbereich Physik, Universität Halle, D-06108 Halle, Germany
Effects of the growth temperature and As/Ga flux ratio on the incorporation of excess As into low-temperature-grown GaAs
J. Appl. Phys. 83, 561 (1998)
23.42.0

IFF-98-11-126
Löwen
Allahyarov, E.; D'Amico, I.; Löwen, H.:
Attraction between like-charged macroions by Coulomb depletion
Physical Review Letters 81 (1998) , 1334-1337
23.30.0

IFF-98-11-127
Löwen
Watzlawek, M.; Löwen, H.; Likos, C.N.:
Anomalous structure factor of dense star polymer solutions
Journal of Physics (Condensed Matter) 10 (1998), 8189-8205
23.30.0

IFF-98-11-128
Ma
Ma, X.L., Köster, U., and Grushko,
Al13Co4-type monoclinic phase and its orthorhombic variant in the Al-Co alloy system
Z. Kristallogr. 213 (1998) 75
23.55.0

IFF-98-11-129

Messerschmidt
Messerschmidt, U., Baither, D., Bartsch, M., Baufeld, B., Guder, S., Wasilkowska, A., Czyrska-Filemonowicz, A., Yamaguchi, M., Feuerbacher, M. and Urban, K.
High-Temperature in situ Straining Experiments in the High-Voltage Electron microscope.
Microscopy and Microanalysis 4, (1998), 226.
23.42.0

IFF-98-11-130
Messerschmidt
Messerschmidt, U., Bartsch, M., Feuerbacher, M., Geyer, B. and Urban, K.
Friction Mechanism of Dislocation Motion in Icosahedral Al-Pd-Mn Quasicrystals.
Phil. Mag. A, in press.
23.42.0

IFF-98-11-131
Mitze
Mitze, C.1, Hasenkox, U.1, Arons, R.R., Waser, R.
1 Institut für Werkstoffe der Elektrotechnik, RWTH Aachen
Granularity effects on the magnetic and electrical properties of La(Ca,Sr)MnO3 thin films
J. Phys. IV, Vol. 8 (1998) 273-275
23.42.0

IFF-98-11-132
Monkenbusch
Arbe, A.1, Colmenero, J.1, Monkenbusch, M., Richter, D.
1Universidad del Pais Vasco, San Sebastian
Departamento de Fisica de Materiales, San Sebastian, Spain
Dynamics of Glass-Forming Polymers: "Homogeneous" versus "Heterogeneous" Scenario
Phys.Rev.Lett., 0031-9007 (1998)
23.30.0

IFF-98-11-133
Monkenbusch
Arbe, A.1, Colmenero, J.1, Frick, B.2 Monkenbusch, M., Richter, D.
1Universidad del Pais Vasco, San Sebastian
2Institut Laue-Langevin, Grenoble
Investigation of the dielectric ?-process in polyisobutylene by incoherent quasielastic neutron scattering
Macromolecules, 31, 4926 (1998)
23.30.0

IFF-98-11-134
Montanari
Montanari, B., Ballone, P., Jones, R.O.
Density functional study of molecular crystals: Polyethylene and a crystalline analog of bisphenol-A polycarbonate
J. Chem. Phys. 108 (1998) 6947-6951
23.20.0

IFF-98-11-135
Mussawisade
Mussawisade, K.; Santos, J.E.1; Schütz, G.M.:
1 Univ. Oxford,
Branching-annihilating random walks in one dimension: Some exact results
J. Phys. A 31 (1998) 4381 - 4394
23.15.0

IFF-98-11-136
Mussawisade
Mussawisade, K.; Wichmann, T.; Kehr, K.W.:
Single-Particle Diffusion Coefficient on Surfaces with Ehrlich-Schwoebel-Barriers
Surface Science 412/413 (1998) 55-60
23.15.0

IFF-98-11-137
Müller-Krumbhaar
Brener, E., Müller-Krumbhaar, H., Temkin, D. and Abel, T.
Morphology diagram of possible structures in diffusional growth
Physica A 249 (1998) 73-81
23.15.0

IFF-98-11-138
Müller-Krumbhaar
Kassner, K.1, Misbah, C.2, Durand, I.2, Müller-Krumbhaar, H.
1Institut für Theoretische Physik, Otto-von-Guericke-Universität Magdeburg
2Laboratoire de Spectrometrie Physique, Universite Joseph Fourier (CNRS), Grenoble, Frankreich
Directional solidification under stress
Phys. Rev. E 58, 6027 (1998).
23.15.0

IFF-98-11-139

Nemeth
Németh, Z.T.; Löwen, H.:
Freezing in finite systems: hard discs in circular cavities
J. Phys. Condensed Matter 10 (1998), 6189-6204
23.30.0

IFF-98-11-140
Neuhold
Neuhold, G.1, Barman, S.B1, Horn, K.1, Theis, W.2, Ebert, Ph. and Urban, K.
1Fritz-Haber-Institut der Max-Planck-Gesellschaft, 14195 Berlin, Germany
2Fachbereich Physik der Freien Universitèt Berlin, D14195 Berlin, Germany
Enhanced Surface Metallic Density of States in Icosahedral Quasicrystals
Phys. Rev. B 58, 734-738 (1998).
23.55.0

IFF-98-11-141
Oates
Oates, W.A., Wenzl, H.
Foreign atom thermodynamics in liquid gallium arsenide
Journal of Crystal Growth 191 (1998)
23.42.0

IFF-98-11-142
Osthöver
Osthöver, C., Grünberg, P., Arons, R.R.
Magnetic properties of doped {La0.67Ba0.33}{Mn1-yAy}O3, A=Fe,Cr
J. Magn. And Magn. Mat. 177-181 (1998) 854-855
23.42.0

IFF-98-11-143
Osthöver
Osthöver, C., Sauer, C., Arons, R.R.
57Fe Mössbauer experiments of doped (La0.67Ba0.33)(Mn0.9Fe0.1)O3
Aust. J. Phys. 51 (1998) 379-84
23.42.0

IFF-98-11-144
Osthöver
Osthöver, C., Grünberg, P., Arons, R.R.
Magnetic Properties of doped {La0.67Ba0.33}{Mn1-?A?},
O3, A = Fe, Cr

J. of Magnetism and Magnetic Materials 177-181, 854
(1998)
23.42.0

IFF-98-11-145
Partyka
Partyka, P. 1, Averback, R.S. 1, Forbes, D.V. 1, Coleman, J.J. and Ehrhart, P.
1 Frederick Seitz Materials Research Laboratory, University of Illinois, Urbana, IL 61801
X-ray diffraction and Channeling-Rutherford Backscattering Spectroscopy studies of ion implantation damage in AlxGa1-xAs
J. Appl. Phys. 83 (1998) 1265-69
23.55.0

IFF-98-11-146
Persson
Persson, B.N.J., Zhang, Z.1
1 Solid State Division, ORNL, Oak Ridge, & University of Tennessee, Knoxville, USA
Theory of friction: Coulomb drag between two closely spaced solids
Phys. Rev. B 57, 7327 (1998)
23.20.0

IFF-98-11-147
Persson
Lamoen, D.1, Persson, B.N.J.
1 University of Antwerp, Wilrijk, Belgium
Adsorption of potassium and oxygen on graphite: A theoretical study
J. Chem. Phys. 108, 3332 (1998)
23.20.0

IFF-98-11-148
Persson
Persson, B.N.J.
On the theory of rubber friction
Surface Science 401, 445 (1998)
23.20.0

IFF-98-11-149
Persson
Persson, B.N.J., Gadzuk, J.W.1
1 NIST, Gaithersburg, USA
Comments on vibrational dynamics of low-frequency adsorbate motion

Surface Science 410, L779 (1998)
23.20.0

IFF-98-11-150
Persson
Persson, B.N.J., Tosatti, E.1
1 ASICTP & SISSA, Trieste, Italy
The puzzling collapse of electronic sliding friction on a superconductor surface
Surface Science 411, L855 (1998)
23.20.0

IFF-98-11-151
Pertsev
Pertsev, N.A.1,2, Zembilgotov, A.G.2,3, Waser, R.
1 A.F. Ioffe Physicotechnical Institute, St. Petersburg
2 Institut für Werkstoffe der Elektrotechnik, RWTH Aachen
3 St. Petersburg State Techn. Univ.
Effective dielectric and piezoelectric constants of polycrystalline ferroelectric thin films
Physics of Solid State 12 (1998) 2206-2212
23.42.0

IFF-98-11-152
Pertsev
Pertsev, N.A.1, Zembilgotov, A.G.1, Waser, R.
1 Institut für Werkstoffe der Elektrotechnik, RWTH Aachen
Aggregate linear properties of ferroelectric ceramics and polycrystalline thin films:
Calculation by the method of effective piezoelectric medium
J. Appl. Phys. 84, 3 (1998) 1524
23.42.0

IFF-98-11-153
Poppe
Nakano, M.1, Matsuoka, H.1, Yamaoka, H.1, Poppe, A., Richter, D.
1Kyoto University, Japan
Micellization of vinyl ether amphiphilic block copolymers by small angle neutron scattering
Physica B, 241-243 (1998)1038
23.30.0

IFF-98-11-154
Poppe
Nakano, M.1, Matsuoka, H.1, Yamaoka, H.1, Poppe, A., Richter, D.

1University Kyoto, Japan
Mizellization of vinyl ether amphiphilic block copolymers by small-angle neutron scattering
Physica B 241-243 (1998) 1038-1040
23.30.0

IFF-98-11-155
Prager
Prager, M., Havighorst, M., Büttner, H.1, Langel, W.2
1Institut Laue-Langevin, Grenoble
2GKSS, Geesthacht
Multi-dimensional tunnelling: Spectroscopy, modelling and isotope effects of ammonia adsorbed on the MgO{100} surface
Physica B 241-253, 262-268 (1998)
23.15.0

IFF-98-11-156
Prager
Schiebel, P.1, Amoretti, G.2, Ferrero, C.3, Paci, B.4, Prager, M., Caciuffo, R.4
1Institut Laue-Langevin, Grenoble
2Università di Parma, Italy
3ESRF, Grenoble
4Università di Ancona, Italy
Coherent internal and centre of mass quantum rotation of methyl groups in the p-tert-butyl-calix[4]arene(2:1)p-xylene supramolecular complex
J.Phys.: Condens.Matter 10 (1998) 2221-2231
23.15.0

IFF-98-11-157
Prager
Prager, M., Heidmann, A.1
1Institut Laue-Langevin, Grenoble
Rotational Tunneling and Neutron Spectroscopy: A Compilation
Chemical Reviews, reprinted from Vol.97, No.8, Pages 2933-2966

IFF-98-11-158
Prager
Ramzi, A1, Prager, M., Richter, D., Efstratiadis, V2, Hadjichristidis, N.2, Young, R.N.3, Allgaier, J.B.3
1DSM Research, Geleen
2University of Athens, Greece
3University of Sheffield, United Kingdom
Influence of Polymer Architecture on the Formation of Micelles of Miktoarm Star Copolymers Polytethylene/Poly(ethlenepropylen) in the Selective Solvent Decane

Macromolecules 30 (1997) 7171-7182
23.30.0

IFF-98-11-159
Rathgeber
Paul, W.1, Smith, G.D.2, Yoon, D.Y.3, Farago, B.4, Rathgeber, S., Zirkel, A., Willner, L., Richter, D.
1Johannes-Gutenberg-Universität, Mainz
2University of Utah, USA
3IBM Almaden Research Center, USA
4Institut Laue-Langevin, Grenoble
Chain Motion in an Unentangled Polyethylene Melt: A Critical Test of the Rouse Model by Molecular Dynamics Simulations and Neutron Spin Echo Spectroscopy
Phys.Rev.Lett., Vol. 80, No, 11 (1998)
23.30.0

IFF-98-11-160
Richter
Stellbrink, J.; Abbas, B.; Allgaier, J.; Monkenbusch, M.; Richter, D.; Likos, C.N.; Löwen, H.; Watzlawek, M.:
Structure and dynamics of star polymers,\/
Prog. Colloid Polym. Sci. 110 (1998), 25-28
23.30.0

IFF-98-11-161
Richter
Hauer, B.1, Hempelmann, R.2, Udovic, T.J.3, Rush, J.J.3, Jansen, E.4, Kockelmann, W., Schäfer, W.4, Richter, D.
1Verein Deutscher Zementwerke, Düsseldorf
2Universität des Saarlandes, Saarbrücken
3National Institute of Standards and Technology, Gaithersburg
4Institut für Mineralogie der Universität Bonn
Neutron-scattering studies on the vibrational excitations and the structure of ordered niobium hydrides: The (phase
Phys.Rev.B, Vol. 57, 18, 115 (1998)
23.15.0

IFF-98-11-162
Richter
Richter, D., Monkenbusch, M., Arbe, A.1, Colmenero, J.1, Farago, B.2
1Universidad del Pais, Vasco, San Sebastian
2Institut Laue-Langevin, Grenoble
Dynamic structure factors due to relaxation processes in glass-forming polymers

Physica B, 1997, Vol. 241, p.1005
23.30.0

IFF-98-11-163
Richter
Richter, D., Arbe, A.1, Colmenero, J.1, Monkenbusch, M., Farago, B.2, Faust, R.3
1Universidad del Pais Vasco, San Sebastian
2Institut Laue-Langevin, Grenoble
3University of Massachusetts, USA
Molecular Motions in Polyisobutylene - A Neutron Spin-Echo and Dielectric Investigation
Macromolecules 1998, 31, 1133-1143
23.30.0

IFF-98-11-164
Richter
Richter, D.
Viscoelasticity and Microscopic Motion in Dense Polymer Systems
Buch: "Diffusion in Condensed Matter" von J. Kärger, P. Heitjans, R. Haberlandt
23.30.0

IFF-98-11-165
Richter
Richter, D., Monkenbusch, M., Arbe, A.1, Colmenero, J.1, Farago, B.2
1Universidad del Pais Vasco, San Sebastian
2Institut Laue-Langevin, Grenoble
Dynamic structure factors due to relaxation processes in glass-forming polymers
Physica B 000 (1997) 000-000
23.30.0

IFF-98-11-166
Rosenfeld
Rosenfeld, R., Thust, A., Yang, W., Feuerbacher, M. and Urban, K.
Investigation of the cluster substructure of icosahedral Al-Pd-Mn quasicrystals by means of exit plane wave reconstruction in high-resolution electron microscopy.
Phil. Mag. Lett. 78, (1998), 127.
23.42.0

IFF-98-11-167
Ross
Ross, Ch.1, Wuttig, M., Gauthier1, Y., Bihlmayer, G., Blügel, S.
1 Laboratoire de Cristallographie, CNRS, Grenoble, France

Structure, Growth and Magnetism of Mn on Cu (110)
Phys. Rev. B 57, 2607 (1998)
23.20.0

IFF-98-11-168
Sarma
Sarma, D.D.1, Barman, S.R.1, Carbone, C., Cimino, R.2, Eberhardt, W., Gudat, W.3
1 Indian Institute of Science,. Bangalore, India
2 Laboratori Nazionali di Frascati, Frascati, Italy
3 Bessy GmbH Berlin
Comparative Study of the L23-M45M45 Auger Decay in CuO and Cu using Synchrotron Radiation
J. of Electron Spectroscopy and Related Phenomena 93, 181 (1998)
23.20.0

IFF-98-11-169
Sarma
Sarma, D.D1., Chainani, A.1, Krishnakumar, S.R.1, Vescovo, E., Carbone, C., Eberhardt, W., Rader, O.2, Jung, Ch.2, Hellwig, Ch.2, Gudat W.2, Srikanth, H.1, Raychaudhuri, A.K.1
1 Indian Institute of Science, Bangalore, India
2. Bessy GmbH Berlin
Disorder Effects in Electronic Structure of Substituted Transition Metal Compounds
Phys. Rev. Lett. 80, 18, 4004 (1998)
23.20.0

IFF-98-11-170
Schlebusch
Schlebusch, C., Kessler, B., Hilger, A.1, Fröba, C.1, Kreibig, U.1
1 I. Physikalisches Institut der RWTH Aachen
Photoemission from Ag-clusters in a C60 matrix
Solid State Comm 107, 277 (1998)
23.20.0

IFF-98-11-171
Schmidt
Schmidt, R.1, van der Ahe, M.1, Dieker, Ch.1, Gauer, D.1, Hauck, T.1, Hardtdegen, H.1, Luysberg, M., Meertens, D., Schmitz, D.2
1Institut für Schicht-und Ionentechnik, Forschungszentrum Jülich, 52425 Jülich, Germany
2AIXTRON AG, Kackertstraße 15-17, D-52072 Aachen, Germany
Contributions to understanding the optical properties of partially ordered (Al0.3Ga0.7)0.52In0.48P deposited by MOVPE using N2 or H2 as the carrier gas
J. Cryst. Growth 195 124 (1998)
23.42.0

IFF-98-11-172
Schober
Dattagupta, S. and Schober, H.R.
Phonon-assisted asymmetric tunneling in a double-well potential: Consequences for neutron scattering and diffusion
Phys. Rev. B 57 (1998) 7606
23.30.0

IFF-98-11-173
Schober
Gaukel, C. and Schober, H.R.
Diffusion Mechanisms in Under-cooled Binary Metal Liquids of Zr67Cu33
Solid State Commun. 107 (1998) 1
23.30.0

IFF-98-11-174
Schober
Gurevich, V. L.[1], Schober, H.R.
[1]A.F. Ioffe Institute, 194021 St. Petersburg, Russia
Decay of mesoscopically localized vibrations in porous materials
JETP Lett. 67 (1998) 55
23.30.0

IFF-98-11-175
Schober
Gurevich, V. L.[1] and Schober, H. R.
[1]A.F.Ioffe Institute, Solid State Physics Division, 194021 Saint Petersburg, Russia
Decay of mesoscopically localized vibrational eigenstates in porous materials
Phys. Rev. B 57 (1998) 11295
23.30.0

IFF-98-11-176
Schober
Parshin, D. A.[1] and Schober, H.R.
[1]State Technical University, 195251 St. Petersburg, Russia
Multifractal structure of eigenstates in the Anderson model with long-range off-diagonal disorder
Phys. Rev. B57 (1998) 10232
23.30.0

IFF-98-11-177
Schroeder
Engels, B., Richard, P., Schroeder, K., Blügel, S., Ebert, Ph. and Urban, K. Comparison of ab initio theory and scanning tunneling microscopy of (110) surfaces of III-V semiconductorsPhys. Rev. B 58 (1998) 7799
23.42.0

IFF-98-11-178
Schroeder
Schroeder, K., Engels, B., Richard, P. and Blügel, S.
Re-exchange controlled Diffusion in Surfactant-mediated Epitaxial Growth: Si on As-terminated Si(111)
Phys. Rev. Lett. 80, 2873 (1998)
23.42.0
rinkaus, H.
Dynamics of viscoelastic flow in ion tracks: origin of plastic deformation of amorphous materials
Nucl. Instr. and Meth. in Phys. Res. B 146 (1998) 204
23.15.0

IFF-98-11-179
Schroeder
Schroeder, K., Engels, B., Richard, P., Blügel., S.
Re-exchange controlled Diffusion in Surfactant-mediated
epitaxial Growth: Si on As
terminated Si(111)
Phys. Rev. Lett. 80, 2873 (1998)
23.20.0

IFF-98-11-180
Schumacher
Schumacher, M.1, Manetta, S.1, Waser, R.
1 Institut für Werkstoffe der Elektrotechnik, RWTH Aachen
Dielectric Relaxation Phenomena in Superparaelectric and Ferrolectric Ceramic Thin Films and the Relevance with respect to High Density DRAM and FRAM Applications"
Journal de Physique IV, 8 (1998) 117-120
23.42.0

IFF-98-11-181
Schwahn
Schwahn, D., Müller, G., Frielinghaus, H.

The Effect of Thermal Composition Fluctuations on Phase Decomposition in Polymer Blends
- An Experimental Study
Recent Research Developments in Macromolecules Research 2 (1997) 107-119
23.30.0

IFF-98-11-182
Schwahn
Schwahn, D., Frielinghaus, H., Mortensen, K.1, Almdal, K.1
1Ris(National Laboratory, Denmark
Pressure Dependence of the Order-Disorder Transition in several Diblock Copolymers studied
with SANS
Physica B 241-243 (1998) 1029-1031
23.30.0

IFF-98-11-183
Schwahn
Waibel, B.1, Schwahn, D., Magerl, A.1
1Institut Laue-Langevin, Grenoble
Reflectivity of sound-excited crystals measured on a double crystal diffractometer
Physic B 241-243 (1998) 183-185
23.30.0

IFF-98-11-184
Schwahn
Dux, Ch.1, Musa, S.1, Reus, V.1, Versmold, H.1, Schwahn, D., Lindner, P.2
1RWTH Aachen
2Institut Laue-Langevin, Grenoble
Small Angle Neutron Scattering Experiments from Colloidal Dispersions at Rest and under
Sheared Conditions
J.Chem.Phys. 109 (1998) 2556-2561
23.30.0

IFF-98-11-185
Schütz
Schütz, G.M.; Mussawisade, K.:
Annihilating random walks in one-dimensional disordered media
Phys. Rev. E 57 (1998), 1388 - 1396
23.15.0

IFF-98-11-186
Schütz

Murthy, K.P.N.1; Schütz, G.M.:
1 permanent address: IGCAR, Kalpakkam, India
Aging in two- and three-particle annihilation processes
Phys. Rev. E 57 (1998). 1388 - 1396
23.15.0

IFF-98-11-187
Schütz
Antal, T.1; Racz, Z.1,2; Rakos, A.1; Schütz, G.M.:
1 Eötvös Univ., Budapest, Hungary
2 Univ. of Oxford, United Kingdom
Isotropic Transverse XY Chain with Energy- and Magnetization Currents
Phys. Rev. E 57 (1998), 5184 - 5190
23.15.0

IFF-98-11-188
Schütz
Schütz, G.M.:
Dynamic Matrix Ansatz for Integrable Reaction-Diffusion Processes
Eur. Phys. J. B 5 (1998), 589-597
23.30.0

IFF-98-11-189
Schütz
Kolomeisky, A.B., Schütz, G.M., Kolomeisky, E.B. and Straley, J.P.
Phase diagram of one-dimensional driven lattice gases with open boundaries
J. Phys. A 31 (1998), 6911-6919
23.30.0

IFF-98-11-190
Stellbrink
Stellbrink, J., Abbas, B., Allgaier, J., Monkenbusch, M., Richter, D., Likos, C.N., Löwen,
H.1, Watzlawek, M.1
1Heinrich-Heine-Universität Düsseldorf
Structure and Dynamics of Star Polymers
Progr.Colloid Polym.Sci, 110, 25-28 (1998)
23.30.0

IFF-98-11-191
Stellbrink
Stellbrink, J., Willner, L., Jucknischke, O., Richter, D., Lindner, P.1, Fetters, L.J.2, Huang,

J.S.2
1Institut Laue-Langevin, Grenoble
2Exxon Research and Engineering Company, USA
Self-Assembling Behaviour of Living Polymers
23.30.0

IFF-98-11-192
Stepankova
Stepankova,, H.1, Kohout, J.1, Novak, P.2, Englich, J.1, Lütgemeier, H., Trhlik, M.1
1 Faculty of Mathematics and Physics, Charles University, Prague
2 Institute of Physics. Academy of Sciences, Prague
Hyperfine field Anisotropy in YIG with diamagnetic Impurities
23.42.0

IFF-98-11-193
Stepankova
Stepankova, H.1, Englich, J.1, Caspary, E.G., Lütgemeier, H.
Hyperfine Field Anisotropy on iron nuclei in barium Hexaferrite
23.42.0

IFF-98-11-194
Stepankova
Stepankova, H.1, Caspary, E.G.1, Englich, J.1, Kohout, J.1 Kucera M.1, Novak, P.2, Nitsch, K.2. Savosta, M.M.3, Lütgemeier, H., de Gronckel, H.A.M.
1 Faculty of Mathematics and Physics, Charles University, Prague
2 Institute of Physics. Academy of Sciences, Prague
3 Institute of Technical Physics, Doneck, Ukraine
Charged substitutions in yttrium iron garnets
23.42.0

IFF-98-11-195
Stepankova
Stepankova, H.1, Kohout, J.1, Novak, P.2, Englich, J.1, Caspary, E.G., Lütgemeier, H.
1 Faculty of Mathematics and Physics, Charles University, Prague
2 Institute of Physics. Academy of Sciences, Prague
Dependence of 57Fe hyperfine field in yttrium iron garnet on ionic radius of diamagnetic defects: NMR study
23.42.0

IFF-98-11-196
Stockmeyer
Stockmeyer, R.
Diffusive Motion of Water Molecules in Harmotome Studied by Neutron Scattering
Ber.Bunsenges. Phys.Chem. 102, 623-628 (1998)
23.15.0

IFF-98-11-197
Teitelbaum
Teitel'baum, G.B.1, Vavilova, E.L.1, Büchner, B.2, Lütgemeier, H.
1 Physicotechnical Institute, Russian Academy of Sciences, Kazan, Russia
2 Universität zu Köln
Electronic Phase Separation in a Low-temperature Tetragonal Phase of Ianthanum-strontium
Cuprates according to 139La NQR Data
JETP Letters 67, 363 (1998)
23.42.0

IFF-98-11-198
Trinkaus
Fichtner, P.F.P1, Kaschny, J.R.2, Kling, A.3, Trinkaus, H., Yankov, R.A.2, Mücklich, A.2,
Skorupa, W.2, Zawislak, F.C.4, Amaral, L.4, da Silva, M.F.3, Soares, J.C.3
1Departamento de Metalurgica, Universidade Federal do Rio Grande do Sul,
Nucleation and growth of platelet bubble structures in He implanted silicon
Nucl. Instr. and Meth. in Phys. Res. B 136-138 (1998) 460-464
23.42.0

IFF-98-11-199
Trinkaus
Tillmann, K.1, Rahmati, B., Trinkaus, H., Jäger, W.1, Hartmann, A.2, Loo, R.2 Vescan, L.2,
Urban, K.
1Mikrostrukturanalytik, Technische Fakultät, Christian-Albrechts-Universität zu Kiel, D-
24143 Kiel
2Institut für Schicht- und Ionentechnik, Forschungszentrum Jülich
Strain-induced vertical ordering effects of islands in LPCVD-grown Si1-xGex/Si-bilayer
structures on Si(001)
Inst. Phys. Conf. Ser. No. 157 (1998)
23.42.0

IFF-98-11-200
Trinkaus

Trinkaus, H. and Schober H.R.
Strained ion tracks in amorphous solids: origin of plastic deformation
Mat. Res. Soc. Symp. Proc. Vol. 481 (1998) 359
23.15.0

IFF-98-11-201
Trinkaus
Almazouzi, A.*, Diaz de la Rubia, T.*, Ishino, S.*, Lam, N.Q.*, Singh, B.N.*, Trinkaus, H.,
Victoria, M.*, Zinkle, S.*
Defect production, accumulation, and materials performance in an irradiation environment
J. Nucl. Mater. 291-294 (1998) 251
23.80.5

IFF-98-11-202
Trinkaus
Singh, B.N.*, Golubov, S.I.*, Trinkaus, H., Serra, A.*, Osetsky, Yu.N.*, Barashev, A.V.*
Aspects of microstructure evolution under cascade damage conditions
J. Nucl. Mater. 107-122 (1998) 251
23.80.5

IFF-98-11-203
Trinkaus
Trinkaus, H., Singh, B.N.*, Foreman, A.J.E.*
Segregation of cascade induced interstitial loops at dislocations: possible effect on initiation
of plastic deformation
J. Nucl. Mater. 172-187 (1998) 251
23.80.5

IFF-98-11-204
Turek
Turek, I1, Blügel, S, Kudrnovsky, J.2
1 Institute of Physics of Materials, ASCR, CZ-61662 Brno
2 Institute of Physics, ASCR, CZ-1804 Praha
Magnetic Nature of (100) Surfaces of bcc RuV, RhV, and PdV Binary Alloys
Phys. Rev. B 57 (1998)
23.20.0

IFF-98-11-205
Ullmaier
Chernikov, V.N.*, Zakharov, A.P.*, Ullmaier, H.
Gas Bubbles in Beryllium Implanted with Helium Ions

at Temperatures (700 K and after Post-Implantation
Annealing
J. Nucl. Mater. 258-263 (1998) 694
23.80.5

IFF-98-11-206
Vetterl
Vetterl, O.1, Hapke, P.1, Finger, F.1, Houben, L.1, Luysberg, M. and Wagner, H.1
1Institut für Schicht-und Ionentechnik, Forschungszentrum Jülich, 52425 Jülich, Germany
Growth of microcrystalline silicon using the layer-by-layer technique at various plasma
excitation frequencies
J. Non-Cryst. Solids 227-230, 866 (1998)
23.42.0

IFF-98-11-207
Wang
Wang, R., Feuerbacher, M., Wollgarten, M. and Urban, K.
Dislocation reactions in Al-Pd-Mn icosahedral quasicrystals.
Phil. Mag. A. 77, (1998), 523.
23.42.0

IFF-98-11-208
Wang
Wang, R., Feuerbacher, M., Yang, W., and Urban, K.
Stacking faults in high-temperature deformed Al-Pd-Mn icosahedral quasicrystal.
Phil. Mag. A. 78, (1998), 273.
23.42.0

IFF-98-11-209
Waser
Waser, R., Lohse, O.1
1 Institut für Werkstoffe der Elektrotechnik, RWTH Aachen
Electrical Characterization of Ferroelectric, Paraelectric, and Superparaelectric Thin Films
Integrated Ferroelectrics 21 (1998) 27-40
23.42.0

IFF-98-11-210
Waser
Waser, R., Hoffmann, Su.1
1 Institut für Werkstoffe der Elektrotechnik, RWTH Aachen
Microstructure-property relationsships of (Ba,Sr)TiO3 films

J. Korean Phys. Soc. 32 (1998) 1340
23.42.0

IFF-98-11-211
Westermann
Westermann, S., Urban, V.1, Pyckhout-Hintzen, W., Richter, D., Straube, E.2
1IPNS Argonne, USA
2Universität Halle
Comment on Lozenge contour plots in scattering from polymer networks
Phys.Rev.Lett., 80, 5449 (1998)
23.30.0

IFF-98-11-212
Wischnewski
Wischnewski, A., Buchenau, U., Dianoux, A.J.1, Kamitakahara, W.A.2, Zarestky, J.L.3
1Institut Laue-Langevin, Grenoble
2National Institute of Standards and Technology, USA
3Iowa State University, Ames, USA
Neutron scattering analysis of low-frequency modes in silica
Phil.Mag. B77, 579 (1998)
23.30.0

IFF-98-11-213
Wischnewski
Wischnewski, A., Buchenau, U., Dianoux, A.J.1, Kamitakahara, W.A.2, Zarestky, J.L3.
1Institut Laue-Langevin, Grenoble
2National Institute of Standards and Technology, USA
3Iowa State University, Ames, USA
Sound wave scattering in silica
Phys.Rev. B57, 2663 (1998)
23.30.0

IFF-98-11-214
Wischnewski
Engberg, D.1, Wischnewski, A., Buchenau, U., Börjesson, L.2, Dianoux, A.J.3, Sokolov, A.P., Torell, L.M.1
1Department of Physics, Chalmers University of Technology, Göteborg, Sweden
2Department of Applied Physics, Chalmers University of Technology, Göteborg, Sweden
3Institut Laue-Langevin, Grenoble
Sound waves and other modes in the strong glass former B2O3
Phys.Rev. B58, 9087 (1998)
23.30.0

IFF-98-11-215
Yang
Yang, W., Feuerbacher, M., Tamura, N., Ding, D., Wang, R. and Urban, K.
Atomic model of dislocations in Al-Pd-Mn icosahedral quasicrystals.
Phil. Mag. A 77, (1998), 1481.
23.42.0

IFF-98-11-216
Zeller
Zeller, R. Conceptual and computational advances in multiple-scattering electronic-structure calculations
Comp. Mat. Sci. 10 (1998) 373-380
23.20.0

IFF-98-11-217
Zimmermann
Mueller, H.W. and Zimmermann, W.
Faraday instability in a linear viscoelastic fluid
Europhys. Lett. 38 (1998)
23.30.0

IFF-98-11-218
Zimmermann
Pleiner, W., Stannarius, R. and Zimmermann, W.
Electrically Driven Instabilities in Smectic Liquid Crystal Films
in "Evolution of Spontaneous Structures in Dissipative Systems", Lecture Notes in Physics, (Springer, Berlin, 1998)
23.30.0

IFF-98-11-219
Zimmermann
Zimmermann, W., Painter, B.1, Behringer, R.1
1Department of Physics and Center of Nonlinear Science and Complex Systems Duke University, Durham NC, 27708-0305, USA
Pattern formation in an inhomogeneous environment
Eur. Phys. J. B 5 (1998) 757-770
23.30.0

IFF-98-11-220

Zimmermann

Zimmermann, W., Painter, B.1 and Behringer, R.1
1Department of Physics and Center of Nonlinear Science and Complex Systems Duke University, Durham NC, 27708-0305, USA
Pattern Formation in an inhomogeneous environment
in "Evolution of Spontaneous Structures in Dissipative Systems", Lecture Notes in Physics, (Springer, Berlin, 1998)
23.30.0

IFF-98-11-221
Zorn
Zorn, R., Alegria, A.1, Arbe, A.1, Colmenero, J.1, Richter, D., Frick, B.2
1Universidad del Pais Vasco, San Sebastian
2Institut Laue-Langevin, Grenoble
Fast-dynamics in plasticized poly(vinyl chloride).
J.Non-Cryst.Solids 235-237 169-172 (1998)
23.15.0

IFF-98-11-222
Zorn
Zorn, R. Frick, B.1
1Institut Laue-Langevin, Grenoble
Absence of annealing effect in the vibrational density of states in a glassforming polymer
J. Chem. Phys. 108, 3327-3331 (1998)
23.15.0

IFF-98-11-223
Zorn
Kanaya, T.1, Zorn, R., Tsukushi, I.1, Murakami, S.1, Kaji, K.1, Richter, D.
1Kyoto University, Japan
Orientational Effects on Low Energy Modes in Amorphous Poly(ethylene terephthalate Fiber
J. Chem. Phys. 109, 10456-10463 (1998)
23.15.0

Other publications

IFF-98-12-001
Basceri
Basceri, C., Lash, S.E., Parker, C.B., Streiffer, S.K., Kingon, A.I., Grossmann, M., Hoffmann, S., Schumacher, M., Waser, R., Bilodeau, S., Carl, R., van Buskirk, P.C., Summerfelt, S.R:
1 Institut für Werkstoffe der Elektrotechnik, RWTH Aachen
An Important Failure Mechanism in MOCVD (Ba,SR)TiO3 Thin Films: Resistance Degradation

Mat. Res. Soc. Symp. Proc. 493 (1998) 9 -14
23.42.0

IFF-98-12-002
Caliebe
Caliebe, W.A.a,b, Kao, C.-C.a, Krisch, M.c, Oversluizen, T.a, Montanez, P.a, Hastings, J.B.a
a National Synchrotron Light Source, Brookhaven National Laboratory, Upton, New York 11973, USA
b Forschungszentrum Jülich GmbH, Institut für Festkörperforschung, D-52425 Jülich
c European Synchrotron Radiation Facility, F-38043 Grenoble Cedex
Optical Design and Performance of the Phase II Inelastic Scattering Beamline at the National Synchrotron Light Source
1-56396-742-1 288 pages illustrated cloth (AIP Conference Proceedings #417)
23.89.1

IFF-98-12-003
Chen
Chen, J., Jung, P.
Effect of helium on radiation damage in a SiC/C composite
Proceedings of the Forum on New Materials, Firenze, 1998
23.80.5

IFF-98-12-004
Chernikov
Chernikov, M.A., Felder, E., Bianchi, A.D., Wälti, C., Kenzelmann, M., Ott, H.R., Edagawa, K., De Boissieu, M., Janot, C., Feuerbacher, M., Tamura, N., and Urban, K.
Low-Temperature Lattice Excitations and Dynamics of Quasicrystals from Specific Heat and Thermal Conductivity.
Invited contribution. Proc. 6.th Int. Conf. on Quasicrystals, Tokyo, World Scientific, Singapore, (1998), 451
23.42.0

IFF-98-12-005
Conrad
Conrad, H.
Forschungszentrum Jülich GmbH, Institut für Festkörperforschung, D-52425 Jülich
The European Spallation Source (ESS) Technical Study
AccApp`98, American Nuclear Society, Inc., La Grange Park, Illinois 60526 USA
23.60.0

IFF-98-12-006

Dekorsy
Dekorsy, T.1, Segschneider, G.1, Nagel, M.1, Heiliger, H.-M.1, Kurz, H.1, Hey, R.2, Ploog, K.2, Luysberg, M.

1Institut für Halbleitertechnik II, RWTH Aachen, D-52056 Aachen, Germany
2Paul Drude Institut für Festkörperphysik, Hausvogteiplatz 5-7, D-10117 Berlin Germany

Characterization and applications of low temperature grown GaAs based on femtosecond lasers
Proc of the Symposium on non-stoichiometric III-V compounds, Erlangen (1998) in: Physik mikrostrukturierter Halbleiter Vol 6 ed.: T. Marek, S. Malzer, and P. Kiesel, Verlag: Lehrstuhl für Mikrocharakterisierung, Universität Erlangen 1998 p.85
23.42.0

IFF-98-12-007
Divin
Divin, Y.Y. , Volkov, O.Y.1, Shirotov, V.V.1, Poppe, U. , Schmueser, P. 2, Tonutti, P. 3, Hanke, K.2 , Geitz, M. 2

1 Institute of Radioengineering and Electronics of RAS, Moscow, Russia
2 DESY, Hamburg
3 III Physikalisches Institut der RWTH Aachen

Terahertz Hilbert-Transform Spectral Analysis with High-Tc Josephson Junctions: First Applications.
Proceedings SPIE 3465 (1998) 309-317
23.42.0

IFF-98-12-008
Eisenriegler
Eisenriegler, E.
Random walks in polymer physics
Lecture Notes in Physics 508 (1998) 1-23
23.30.0

IFF-98-12-009
Feuerbacher
Feuerbacher, M., Urban, K. and Weller, M.
Mechanical spectroscopy of Al-Pd-Mn single-quasicrystals.
Proc. 6.th Int. Conf. on Quasicrystals, Tokyo, World Scientific, Singapore, (1998), 521
23.42.0

IFF-98-12-010
Frey
Frey, F., Hradil, K., Grushko, B., and McIntyre, G.
Disorder of decagonal AlCoNi, AlNiFe and AlCoCu phases studied by diffuse x-ray and neutron diffraction

6-th Int. Conf. on Quasicrystals. Tokyo, Japan 1997. (Ed. by S. Takeuchi
and T. Fujiwara) World Sci. 1998, p. 379
23.42.0

IFF-98-12-011
Geitz
Geitz, M.1, Hanke, K.1, Schmueser, P.1, Divin,Y.Y., Poppe, U., Pavlovskii, V.V.2, Shirotov
,V.V.2, Volkov, O.Y.2, Tonutti, M.3
1 DESY, Hamburg
2 Institute of Radioengineering and Electronics of RAS, Moscow, Russia
3 III Physikalisches Institut der RWTH Aachen
A Hilbert Transform Junction Spectrometer Using a High-Tc Josephson Junction for Bunch
Length Measurements at the TTF Linac.
DESY-TESLA Reports, 98-10 (1998) 1-18
23.42.0

IFF-98-12-012
Grushko
Grushko, B., and Holland-Moritz, D.
Transformation features of the stable decagonal phases in Al-Cu(Ni)-Co(Fe)
6-th Int. Conf. on Quasicrystals. Tokyo, Japan 1997 (Ed. by S. Takeuchi and T. Fujiwara)
World Sci. 1998, p. 297
23.42.0

IFF-98-12-013
Haiml
Haiml, M.1, Siegner, U.1, Morier-Genoud, F.1, Keller, U.1, Luysberg, M., Specht, P.2,
Weber, E.R.2
1Institute of Quantum Electronics, ETH Hönggerberg, CH-8093 Zürich, Switzerland
2Department of Materials Science, University of California Berkeley, CA 94720, USA
Defect engineering of low-temperature grown GaAs for applications in ultrafast optics
Proc of the Symposium on non-stoichiometric III-V compounds, Erlangen (1998) in: Physik
mikrostrukturierter Halbleiter Vol 6 ed.: T. Marek, S. Malzer, and P. Kiesel, Verlag:
Lehrstuhl für Mikrocharakterisierung, Universität Erlangen 1998 p.79
23.42.0

IFF-98-12-014
Heinen
Heinen, D., Schroeder, H. and Schilling, W.
"In-situ TEM-investigations of mass transport in "near-bamboo" Al-interconnects due to
electromigration"
Proc. of Forth Int. Workshop on "Stress-induced Phenomena in Metallization",
Tokyo (Japan), June 1997,

AIP Conf. Proc. 418, 195 (1998)
23.42.0

IFF-98-12-015
Houben
Houben, L.1, Luysberg, M., Lundszien, D.1, Carius, R.1, Wagner, H.1
1Institut für Schicht- und Ionentechnik, Forschungszentrum Jülichz, 52425 Jülich, Germany
Structural and compositional properties of SixGe1-x grown by plasma-enhanced chemical vapor deposition
Proc. of the ICEM14, Cancun Mexico ed.:H. A. Calderon Benavides and M. J. Yacaman
Institute of Physics Publishing, Bristol (1998) Vol. III, p. 39
23.42.0

IFF-98-12-016
Jones
Jones, R.O.
Density functional calculations for molecules and clusters - Lin, LinO, Cn
in Electronic Density Functional Theory: Recent Progress and New Directions, eds. Dobson et al., Plenum Press, New York (1998) 349-360
23.20.0

IFF-98-12-017
Kehr
Kehr, K.W.; Mussawisade, K.; Wichmann, T.:
Diffusion of Particles on Lattices
in "Diffusion in Condensed Matter", Eds. J. Kärger, P. Heitjans, and R. Haberlandt, Vieweg, Braunschweig (1998) 265-305
23.15.0

IFF-98-12-018
Lentzen
Lentzen, M., Urban K.
Reconstruction of the Projected Crystal Potential by means of a Maximum-Likehood Refinement Algorithm
Proc. Of the ICEM 14, Cancun Mexico, 1998 ed.: H.A. Calderon Benavides and M.J. Yacaman, Institute of Physics Publishing, Bristol (1998) Vol. I, p. 135
23.42.0

IFF-98-12-019
Lohse
Lohse, O.1, Bolten, D.1, Grossmann, M.1 , Waser, R., Hartner. W.2, Schindler, G.2

1 Institut für Werkstoffe der Elektrotechnik, RWTH Aachen
2 Siemens AG, Semiconductor Group, München
Reversible and irreversible contributions to the polarization in SBT Ferroelectric Capacitors
Materials Research Society Symp. Proceed, Vol 493 (1998) 267
Ferroelectric Thin Films VI (1998) 267-278
23.42.0

IFF-98-12-020
Lustfeld
Lustfeld, H.
Instabilities of pollutant concentrations in the troposphere due to chemical reactions
Perspective Look at Nonlinear Media in Physics, Chemistry and Biology, eds. J. Parisi, S.C.
Müller, W. Zimmermann, Springer Verlag (1998)
23.15.0

IFF-98-12-021
Luysberg
Luysberg, M., Specht, P.1, Sohn, H.1, Weber, E.R.1
1Department of Materials Science, University of California Berkeley, CA 94720, USA
Transition from epitaxial to columnar growth of non-stoichiometric GaAs deposited at low
temperatures
Proc. of the ICEM14, Cancun Mexico ed.:H. A. Calderon Benavides and M. J. Yacaman
Institute of Physics Publishing, Bristol (1998) Vol. III, p. 455
23.42.0

IFF-98-12-022
Luysberg
Luysberg, M., Thul, K., Specht, P.1, Weber, E.R.1
1Department of Materials Science, University of California Berkeley, CA 94720, USA
Formation of As precipitates in Be doped non-stoichiometric GaAs and their influence on the
electrical properties
Proc of the Symposium on non-stoichiometric III-V compounds, Erlangen (1998) in: Physik
mikrostrukturierter Halbleiter Vol 6 ed.: T. Marek, S. Malzer, and P. Kiesel, Verlag:
Lehrstuhl für Mikrocharakterisierung, Universität Erlangen 1998 p.23
23.42.0

IFF-98-12-023
Messerschmidt
Messerschmidt, U., Geyer, B., Bartsch, M., Feuerbacher, M. and Urban, K.
Dislocation motion in Al-Pd-Mn single quasicrystals.
Proc. 6.th Int. Conf. on Quasicrystals, Tokyo, World Scientific, Singapore, (1998), 509
23.42.0

IFF-98-12-024
Schober
Schober, T.
Protonic conduction in BaIn0.5Sn0.5O2.75
Solid State Ionics 109 (1998) 1-11
23.90.0

IFF-98-12-025
Schroeder
Schroeder, H. and Heinen, D.
In-situ TEM-investigations of stress-and electromigration-induced void formation growth in passivated Al-interconnects
Proc. of Forth Int. Workshop on "Stress-induced Phenomena in Metallization",
Tokyo (Japan), June 1997,
AIP Conf. Proc. 418, 183 (1998)
23.42.0

IFF-98-12-026
Schweika
Schweika, W., Pionke, M.
Forschungszentrum Jülich GmbH, Institut für Festkörperforschung, D-52425 Jülich
Neutron Scattering and Monte Carlo Studies of Disorder in Oxides and Hydrides
in: Local Structure from Diffraction, M.F. Thorpe and S. Billinge (Eds.), Fundamental
Materials Science Series, Plenum Press, New York, 85 - 100 (1998)
23.55.0, 23.89.1, 23.90.0

IFF-98-12-027
Schweika
Schweika, W.
Forschungszentrum Jülich GmbH, Institut für Festkörperforschung, D-52425 Jülich
Disordered Alloys, Diffuse Scattering and Monte Carlo Simulations
Springer Tracts in Modern Physics Vol. 141, G. Höhler (Ed.), Springer, Heidelberg (1998)
23.89.1, 23.55.0, 23.15.0

IFF-98-12-028
Schütz
Schütz, G.M.:
Reaction-Diffusion Mechanisms and Quantum Spin Systems
ed. H. Meyer-Ortmanns and A. Klümper, Lecture Notes in Physics 508 (Springer, Berlin,
1998)
23.30.0

IFF-98-12-029
Stadnik
Stadnik, Z.M., Grushko, B., and Tsai, A.-P.
Mössbauer spectroscopy study of Al-Ni-Fe decagonal alloys
6-th Int. Conf. on Quasicrystals. Tokyo, Japan 1997. (Ed. by S. Takeuchi and T. Fujiwara)
World Sci. 1998, 708
23.42.0

IFF-98-12-030
Thust
Thust, A. and Rosenfeld, R.
State of the art of focal-series reconstruction in HRTEM
Proc. 14th ICEM, Cancun Mexico ed.: H. A. Calderon Benavides
and M. J. Yacaman, Institute of Physics Publishing, Bristol (1998)
Vol 1, p. 119.
23.42.0

IFF-98-12-031
Ullmaier
Rauh, H.*, Ullmaier, H.
Hydrogen Concentrations Around Cracks in Target Materials
for Spallation Neutron Sources
ESS-Report 98-97T, FZ Jülich (Nov.1998)
23.60.0

IFF-98-12-032
Urban
Urban, K., Ebert, P., Feuerbacher, M., Franz, V., Wollgarten, M., Baufeld, B., Bartsch, M., and Messerschmidt, U.
Mechanical properties of Quasicrystals. Invited contribution.
Proc. 6.th Int. Conf. on Quasicrystals, Tokyo, World Scientific, Singapore, (1998), 493
23.42.0

IFF-98-12-033
Yang
Yang, W., Tamura, N., Feuerbacher, M., Ding, D., Wang, R., and Urban, K.
Elastic displacement fields and computer simulation of dislocations in Al-Pd-Mn icosahedral quasicrystals.
Proc. 6.th Int. Conf. on Quasicrystals, Tokyo, World Scientific, Singapore, (1998), 433
23.42.0

Patents

IFF-98-31-001
Allgaier, J., Richter, D., Willner, L., Strey, R., Jakobs, B., Sottmann, T.
Verfahren zur Effizienzsteigerung von Tensiden und Verfahren zur Unterdrückung lamellarer Mesophasen in Mikroemulsionen sowie ein Tensid, welchem ein Additiv beigemischt ist.
German Patent Application
DE19839054.8-41
PT 1.1605
23.30.0

IFF-98-31-002
Althaus, M. Küssel, E., Sonnenberg, K.
Verfahren und Vorrichtung zur Gewinnung rißfreier Kristalle
US: 5.833, 748 (10.11.98)
PT 1.1209
23.42.0

IFF-98-31-003
Conrad, H.
Target-Moderator-Reflektor-Anordnung für eine gepulste Hochleistungs-Spallationsquelle
DE: P 43 04 667.3-33 (08.05.1998)
PT 1.1153
23.60.1

IFF-98-31-004
Kormany, K.
Verfahren zur Bestimmung der Energie des gepulsten Teilchenstrahls eines Beschleunigers
DE: 42 35 476 (03.11.1998)
PT 1.1147
23.05.0

IFF-98-31-005
Sauenbach, F., Fuß, A.
Verfahren zur Rastersondenmikroskop und Rastersondenmikroskop mit Detektorsonde"
DE: 43 44 499 (27.04.98)
PT 1.1188
23.42.0

IFF-98-31-006

Saurenbach, A., Fuß, A.
Halterung für eine Tastspitze eines Rasterkraft-o der Rastertunnelmikroskops
EP: 0728294 (08.07.1998)
PT 1.1177
23.15.0

IFF-98-31-007
Speen, R., Bausch, St.
Preßwerkzeug zum uniaxialen Kaltpressen von Pulverproben
DE: 197 28 767 (15.06.1998)
PT 1.1474
23.90.0

Patent applications

IFF-98-32-001
Baldus, O. 1, Hoffmann, S.1, Waser, R.
1 Institut für Werkstoffe der Elektrotechnik
Verfahren zur Herstellung einer oder mehrerer kristallisierter keramischer Dünnschichten sowie Bauelement mit einer solchen Schicht
PT 1.557
Deutsche Patentanmeldung 198 06 013.0
23.42.0

IFF-98-32-002
Baldus, O.1, Schuster, A.1, Waser, R.
1 Institut für Werkstoffe der Elektrotechnik
Erweiterung: Verfahren zur Herstellung einer oder mehrerer kristallisierter keramischer Dünnschichten durch Kombination von Vorheizung mit Licht und Bauelement mit einer solchen Schicht
(Erfindungsmeldung PT 0.1747 "Kristallisation keramischer Dünnschichten")
Deutsche Patentanmeldung 198 06 013.0-45
23.42.0

IFF-98-32-003
Blügel, St., Nie, X.
Elektrisches Feld für Umagnetisierung eines dünnen Films
DE: 198 41 034.4-53 (09.09.1998)
PT 1.1610
23.20.0

IFF-98-32-004
Eberhardt, W., Morenzin, J.
Markierungseinrichtung
DE: 198 52 368.8 (13.11.1998)
PT 1.1633
23.42.0

IFF-98-32-005
Ghosh, I., Klein, N., Poppe, U.
Abstimmbarer Hohlraumresonator
DE: 198 41 078.6-35 (09.09.1998)
PT 1.1617
23.42.0

IFF-98-32-006
Waser, R. Hoffmann, S.1, Slowak, R.1, Grossmann, M.1.
Keramischer Mehrlagen-Dünnschichtkondensator
PT 1.1560
Deutsche Patentanmeldung 198 06 002.5
23.42.0

IFF-98-32-007
Mantl, S., Zhao, Q.T., Kappius, L., Antons, A.
Verfahren zur Herstellung von Nanostrukturen in dünnen Filmen
DE: 198 53 023.4 (18.11.1998)
PT 1.1625
23.42.0

IFF-98-32-008
Mussawisade, K., Kehr, K.W., Wichmann, T., Poppe, U
Bauelement mit Gleichrichtungsfunktion mit Hilfe von Ladungstransport durch Ionen
PCT:/DE 98/02292 (05.05.1998
PT 1.1477
23.15.0

IFF-98-32-009
Nie, X., Blügel, S.
Elektrisches Feld zur Ummagnetisierung eines dünnen Films
Patentamt München, Amtl. Az. 19841034.4
23.20.0

IFF-98-32-010
Schornstein, St., Klein, N., Ghosh, I.
Mehrpol-Bandpaßfilter mit elliptischer Filtercharakteristik
DE: 198 24 997.7 (05.06.1998)
PT 1.1596
23.42.0

IFF-98-32-011
Speier, W., Szot, K.
AVO3-Perowskit mit Stufe,
PT 0.1762/1.1563
Deutsche Patentanmeldung 198 08 778
23.42.0

IFF-98-32-012
Waser, R., Hoffmann, S., Baldus, O., Schuster, A.
Verfahren zur Herstellung einer oder mehrerer kristallierter keramischer Dünnschichten sowie
Bauelement mit einer solchen Schicht
DE: 298 15 601.6 (01.09.1998)
PT 1.1557A
23.42.0

IFF-98-32-013
Waser,R., Großmann, M., Hoffmann, S. Slowak, R.,
Keramischer Mehrlagen-Dünnschichtkondensator
DE: 198 06 002.5 (16.02.1998)
PT 1.1560
23.42.0

Guest Scientists

M. Abdel-Goad El	Minia University, El-Minia, Egypt
S. Abdullaev	Bilkent University, Ankara, Turkey
R. Abt	University Graz, Austria
H. Ambaye	Alemaye University, Ethiopia
T. Antal	Eötvös University Budapest, Hungary
M. Arbe	Universidad Pais Vasco, St. Sebastian, Spain
A. Baranov	Moscow State University, Russia
J. Bene	Eötvös University Budapest, Hungary
G. Bihlmayer	University Vienna, Austria
Fr. C. Blaas	Technical University Vienna, Austria
F. Bobba	University Salerno, Italy
S. Borbely	Hungarian Academy of Sciences, Budapest
C. Byloss	University Ferrara, Italy
D. Caprion	University Montpellier II, France
F. Carsughi	University Ancona, Italy
I. Cendoya	University San Sebastian, Spain
S. Clarke	University of Wales, UK
J. Colmenero	University San Sebastian, Spain
Y. Dai	Paul-Scherrer-Institute, Villigen, Switzerland
A.R. Denton	Technical University Vienna, Austria
Y. Divin	Inst. of Radioeng. & Electr., Moscow, Russia
V. Drchal	Czech Academy of Sciences, Prague
H. Endo	Kyoto University, Japan
A. Gordon	Haifa University, Israel
H. Hasegawa	Kyoto University, Japan
Fr. M. Heinrich	Louis Pasteur University, Straßbourg, France
T. Hoshino	Shizouka University, Japan
St. C. Hwang	University of California, Santa Barbara, USA
T. Kanaya	Kyoto University, Japan
Z. Kaufmann	Eötvös University Budapest, Hungary
M. Kawasaki	Kyushu University, Japan
E. Kentzinger	Louis Pasteur University Straßbourg, France
A. Kisliuk	Free University, Berlin, Germany
S. Koizumi	Japan Atomic Energy Resarch Institute, Tokai, Japan
T. Korhonen	Helsinki Institute of Technology, Otaniemi, Finland
J. Kudrnovsky	Czech Academy of Sciences, Prague
Fr. U. Kühn	IFW, Dresden, Germany
C. Lei	Academy of Science, Beijing, China
J. Lüning	University Cologne, Germany
K. Maiti	IISC Bangalore, India

V. Marchenko	Academy of Sciences, Chernogolovka, Russia
K. Marton	University Miscolc, Hungary
H. Matsouka	Kyoto University, Japan
P. Mavropoulos	University Athens, Greece
J.A. Maytorena Cordova	University Cuernavaca Mexico
Fr. H. Montes	University Paris, France
Z. Nemeth	University Veszprem, Hungary
X. Nie	Massachusetts Inst. of Technology, Cambridge, USA
Y. Ozaki	Nagoya Technical University, Japan
N. Papanikolaou	University Athens, Greece
L. Petit	Daresbury Laboratory, England
P. Peyla	University Grenoble, France
V. Podgursky	Tallinn Technical University, Estland
W. Pohle	University Jena, Germany
V. Popkov	Center for Theoretical Physis, Korea, Seoul
A. Prodan	Kharkov State University, Ukraine
A. Rakos	Eötvös University Budapest, Hungary
A. Rupprecht	University Stockholm, Sweden
A.I. Ryazanov	Kurchatov Institute, Moscow, Russia
Y. Saito	Keio University, Yokohama, Japan
A. Schmets	University Delft, Netherlands
J.F. Scott	University of New South Wales, Sydney, Australia
H. Seto	Hiroshima University, Japan
T. Sintes	University Palma, Spain
A. Skripov	Institute for Metal Physics, Jekaterinburg, Russia
A. Sokolov	Max-Planck-Institute for Polymer Research, Mainz, Germany
N. Stefanou	University Athens, Greece
V. Stepanyuk	Moscow State University, Russia
E. Straube	University Merseburg, Germany
K. Szot	University Katowice, Poland
G. Teitelbaum	Kazan State University, Russia
D. Temkin	I.P. Bardin Inst. Moskau, GUS
N.N. Ukhansky	Institute of Terrestrial Magnetism, Troitsk, Russia
V. Verhoeven	University Delft, Netherlands
Ke. Xia	University Enschede, Netherlands
L.B. Xu	Zhejiang University, China
S. Yan	Shandong University, Jinan, China
J. Zabloudil	Technical University Vienna, Austria

IFF Scientists on leave 1998

Dr.W. Caliebe	HASYLAB at DESY, Hamburg, Germany
Prof. P. Grünberg	Tohoku University Sendai, Japan
Dr. J. Harris	MSI Inc. (formerly Biosym Technologies Inc), San Diego, USA
Dr. L. Heller	ESRF Grenoble, France
Dr. R. Lässer	Forschungszentrum Karlsruhe, Germany
Dr. A. Liebsch	Universidad Technica Guernavaca, Valparasio, Chile
Dr. W. Schmidt	ILL Grenoble, France
Dr. A. Scholl	Lawrence Berkeley Laboratory, USA

IFF-Scientists Teaching at Universities

Lecturer:	University:
Dr. A. Baumgärtner	Duisburg
Dr. P.S. Bechthold	Köln
Dr. S. Blügel	Aachen
Prof. U. Buchenau	Düsseldorf
Prof. P. Dederichs	Aachen
Prof. W. Eberhardt	Köln
Dr. P. Ehrhart	Aachen
Prof. G. Eilenberger	Köln
Prof. E. Eisenriegler	Düsseldorf
Prof. P. Grünberg	Köln
Prof. K. Kehr	Köln
Dr. N. Klein	Aachen
Dr. H. Lustfeld	Duisburg
Prof. H. Müller-Krumbhaar	Aachen
Prof. D. Richter	Münster
Dr. H. Schober	Aachen
Prof. T. Schober	Aachen
Dr. H. Schroeder	Aachen
Prof. K. Schroeder	Aachen
Dr. G. Schütz	Bonn
Dr. W. Schweika	Aachen
Prof. K. Sturm	Düsseldorf
Prof. H. Ullmaier	Aachen
Prof. K. Urban	Aachen
Prof. R. Waser	Aachen
Prof. H. Wenzl	Aachen
Dr. W. Zimmermann	Aachen
Dr. R. Zorn	Münster

Spring Schools of the IFF

Beginning in 1970, our institute has organized an annual two-week Spring School on modern topics in solid state physics.

The topics of the Spring Schools over the past 10 years were:

1990	Solid State research for Information Technology
1991	Physics of Polymers
1992	Synchrotron Radiation for investigating Condensed Matter
1993	Magnetism of Solids and Boundaries
1994	Complex Systems between Atoms and Solids
1995	Electroceramics – Basics and Applications
1996	Scattering Methods for investigating Condensed Matter
1997	Dynamics and Pattern Formation in Condensed Matter
1998	Physics of Nanostructures
1999	Magnetic Layer Structures

Spring School 1998 on „Physics of Nanostructures"

This event took place from 9th to 24th March 1998. As usual, it was organized in collaboration with the universities at Aachen, Köln and Münster. About 300 participants, most of them graduate students and post docs from university and research institutions, came to Jülich.

The following lecture were presented (in chronological order):

A. Thust	Basis and advanced methods of highly resolved electron microscopy
Ph. Ebert	Scanning probe microscopy
S. Blügel	Theory of scanning tunnel microscopy
P. Ehrhart	X-ray scattering and EXAFS
D. Richter	Starpolymers in ultrasoft colloids
R. Zorn	Lightscattering (colloids)
S. Eisebitt	Spectromicroscopy
S. Mantl	Structuring procedures
V. Saile	LIGA-techniques with synchrotron radiaton
B. Lengeler	Mesoscopic electron transport
Th. Schäpers	Ballistic electrons in semiconductor-heterostructures
L.W. Mohlenkamp and H. Buhmann	Single-electron-transistor in a quantum circuit
K. Schroeder	Electrons in quantum dots (Theory)
H. Wenzl	Porous silicon
Th. Schäpers	Metallic nanostructures, quantum wires
K. Sturm	Photonic band structure
Ch. Buchal	Optical investigations of nanocrystals
M. Wuttig	New technologies in optical data storage
L.Risch	Nanoelectronics
B. Voigtländer	Selforganisation in the growth of islands
M. Grunze	Selforganisation of organic molecules on surfaces
R. Berud	Scanning-tunnel-microscopy: The example of surface states
R. Hempelmann	Nanocrystalline metals and oxides with controlled particle sizes: Synthesis and Characterization
M. Neeb	Cluster: Introduction, Synthesis and shell models
G. Gantefőr	Photo electron spectroscopy on mass separated clusters
P.H. Dederichs	Magnetic clusters
G. Seifert	Computer simulation of structure, electronic structure and dynamics of clusters
W. Andreoni	Fullerenes and Silicon clusters: Structures, electronic properties and dynamics
P.S. Bechthold	Chemical reactions on free clusters
S. Krummacher	Clusters from the shelf: C_{60} the new form of carbon

J. Pink	Intercalated and endohedral fullerenes. Heterofullerenes
C. Schlebusch	Organic photoconductor and C_{60}: Increased photo-conduction by light-induced charge transfer
B. Kessler	Carbon nanotubes
H. Weller	Colloid chemistry of semiconductor-clusters
J.S. Bradley	Catalysis by nanoclusters
U. Kreibis	Optical spectroscopy on cluster-matter
H. Haberland	Thin layers of fast and slow clsuters

Spring School 1999 on „Magnetic Layer Systems"

This event was the 30th spring school offered by the IFF. It took place from 1st to 12th March 1999 and included the latest developments in the fields of giant magnetoresistance (GMR) and tunneling magnetoresistance (TMR).

The following lectures were presented (in chronological order):

P.H. Dederichs, P. Grünberg and R. Hölzle	Magnetic layer systems
K. Schroeder	Atomic magnetism and exchange interaction
K. Sturm	Basic elements of electron theory
R. Zeller	Band magnetism
P. Ehrhart	Preparation of thin layers: Molecular beam epitaxy
W. Schweika	Preparing layers by sputtering
R. Zorn	Magnetometry
D. Richter	Atoms as solid state probes
L. Baumgarten	Angular resolved photoemission for investigating band Structures in solids
G. Güntherodt, U. Rüdiger	Magnetic solids: An overview
A. Lichtenstein	Electronic structure of magnetic oxides
H.-J. Elmers	Magnetism of thin films
C. Carbone	Photoemission from magnetic films
T. Brückel, E. Kentzinger	Scattering methods for investigating thin layer systems
D. Stoeffler	Spin structure in metallic multilayers: Theoretical aspects
H. Zabel	Chromium as single and intermediate layer
R. Schäfer	Magnetic microstructure
U. Hartmann	Magnetically imaging scanning probe methods
P. Bruno	Theory of interlayer exchange coupling
P. Grünberg	Intermediate layer exchange coupling: Phenomenological Description, material dependence
D.E. Bürgler	Intermediate layer exchange coupling: Dependence on layer Formation and boundary quality
B. Hillebrands	Spin dynamics in magnetic layers and multilayers
S. Blügel	Magnetic anisotropy and magnetostriction
R. Koch	Magnetoelastic coupling in thin epitatic layers
R. Allenspach	Anisotropy of boundaries
E. Quandt	Magnetostrictive layers for application in microsystem technologies
H. Ebert, Ya. Perlov	Magnetooptical effects (theory)
S. Eisebitt	Magnetic circular dichroism (MCD)

Scientific Advisory Board 1999

The 1999 meeting of the Scientific Advisory Board will take place on the 22th/23th April. Currently, the board consists of the following members:

Dr. C. **Carlile**, ISIS Rutherford Laboratory, UK

Prof. R. **Dronskowski**, RWTH Aachen

Prof. H. **Eschrig**, IFW Dresden

Prof. W.M. **Finnis**, Queen's University of Belfast, UK

Prof. U. **Gösele**, MPI Halle/Saale

Prof. S. **Hess**, TU Berlin

Dr. J. **Joosten**, DSM Research, Geleen, NL

Prof. H. **Lüth**, Forschungszentrum Jülich, ISI

Prof. H. **Micklitz**, Universität zu Köln

Prof. W. **Press**, Universität Kiel

Dr. I. **Rieger**, BASF, Ludwigsburg

Prof. U.W. **Suter**, ETH Zürich

Prof. L. **Singheiser**, FZJ-IWV2

Prof. H. **Thomann**, Siemens AG München

Prof. J. **Schnakenberg**, RWTH Aachen, **Chairman**

Prof. E. **Umbach**, Universität Würzburg

Prof. P. **Wyder**, CNRS-MPI, Grenoble

List of IFF-Scientists

(G: Guests; GS: Graduate students)

Abbas, B.	(Neutron Scattering, GS)
Abt, R.	(Electronic Properties)
Alaga-Bogdanovic, M.	(Theory III,GS)
Alefeld, B.	(Scattering Methods)
Allgaier, J.	(Neutron Scattering)
Ambaye, H.	(Theory II, GS)
Antons, A.	(Theory III, GS)
Arbe, A.	(Neutron Scattering, G)
Arons, R.R.	(Electroceramic Materials)
Baldus, O.	(Electroceramic Materials, GS)
Ballone, P.	(Theory I, G)
Barton, M.	(Electroceramic Materials, GS)
Baumgarten, L.	(Electronic Properties)
Baumgärtner, ,A.	(Theory II)
Bechthold, P.S.	(Electronic Properties)
Bellini, V.	(Theory III, GS)
Bene, J.	(Theory I, G)
Berger, R.	(Theory III, GS)
Biermann, S.	(Theory I, GS)
Bihlmayer, G.	(Electronic Properties)
Blügel, S.	(Electronic Properties)
Bohn, H.G.	(Electroceramic Materials)
Borbely, S.	(Neutron Scatteirng, G)
Botti, A.	(Neutron Scattering, GS)
Brener, E.	(Theory III)
Bringer, A.	(Theory I)
Brückel. Th.	(Scattering Methods)
Buchenau, U.	(Neutron Scattering)
Byloss, C.	(Scattering Methods, G)
Caliebe, W.	(Scattering Methods, GS)
Carbone, C.	(Electronic Properties)
Chen, J.	(Microstructure Research, G)
Chen, J.	(Special Group)
Chirotov, V.	(Microstructure Research, GS)
Clarke, S.	(Electronic Properties)
Colmenero, J.	(Neutron Scattering, G)
Conrad, H.	(Scattering Methods)
Cramm, S.	(Electronic Properties)

|	
Dallmeyer, A.	(Electronic Properties; GS)
de Gronckel, H.	(Electronic Properties)
Dederichs, P.H.	(Theory III)
Denton, A.	(Theory II, G)
Divin, Y.	(Microstructure Research, G)
Eberhardt, W.	(Electronic Properties)
Ebert, Ph.	(Microstructure Research, GS)
Ehrhart, P.	(Electroceramic Materials)
Eilenberger, G.	(Theory I)
Eisebit, S.	(Electronic Properties)
Eisenriegler, E.	(Theory I)
Endo, H.	(Neutron Scattering, GS)
Evers, W.	(Microstructure Research)
Faley, M.	(Microstructure Research, G)
Feng, X.	(Theory III, GS)
Fetters, L.-J.	(Neutron Scattering, G)
Feuerbacher, M.	(Microstructure Research ,GS)
Fischer, K.H.	(Theory I, G)
Fitsilis, F.	(Electroceramic Materials, GS)
Frielinghaus, H.	(Neutron Scattering, GS)
Goad, M.	(Neutron Scattering, GS)
Göcking, K.-D.	(Scattering Methods, GS)
Goerigk, G.	(Scattering Methods)
Graf, K.-H.	(Microstructure Research)
Grimm, H.	(Neutron Scattering)
Grünberg, P.	(Electronic Properties)
Grushko, B.	(Microstructure Research)
Harris, J.	(Theory I)
Haubold, H.-G.	(Scattering Methods)
Hauck, J.	(Materials Development)
He, Zhi.Y.	(Special Group, GS)
Heinrich, M.	(Neutron Scattering)
Hoffmann, S.	(Electroceramic Materials)
Hoffmann, S.	(Neutron Scattering, GS)
Huck, H.	(Electroceramic Materials, GS)
Hwang, St.	(Electroceramic Materials, G)
Jahnen, B.	(Microstructure Research, GS)
Jia, C.L.	(Microstructure Research)
Jones, R.O.	(Theory I)
Jung, P.	(Special Group)
Kabius, B.	(Microstructure Research)

Kahle, St.	(Neutron Scattering)
Kann, G.	(Electronic Properties, GS)
Karibiants, N.	(Neutron Scattering)
Karl, A.	(Electronic Properties, GS)
Kaschner, R.	(Theory I, G)
Kaya, H.	(Neutron Scattering, GS)
Kehr, K.	(Theory II)
Kentzinger, E.	(Scattering Methods, G)
Kessler, B.	(Electronic Properties)
Kesternich, W.	(Special Group)
Kienle, D.	(Theory III, GS)
Kirstein, O.	(Neutron Scattering)
Klein, H.	(Microstructure Research, GS)
Klein, H.	(Special Group)
Klein, N.	(Microstructure Research)
Klingeler, R.	(Electronic Properties, GS)
Kluge, F.	(Microstructure Research, GS)
Kluge, M.	(Theory III, GS)
Köbler, U.	(Scattering Methods)
Kohlstedt, H.H.	(Electroceramic Materials)
Koizumi, S.	(Neutron Scatteirng, G)
Kollmar, A.	(Scattering Methods)
Krasser, W.	(Electroceramic Materials)
Kreitschmann, M.	(Neutron Scattering, GS)
Krenzlin, M.	(Theory II, GS)
Kromen, Wi.	(Theory III, GS)
Kümmerle, E.	(Scattering Methods, GS)
Kurz, P.	(Electronic Properties, GS)
Lei, Ch.	(Microstructure Research, GS)
Lentzen, M.	(Microstructure Research, GS)
Leube, W.	(Neutron Scattering)
Lichtenstein, A.	(Theory I, G)
Liebsch, A.	(Theory I)
Likos, C.N.	(Theory II, G)
Lin, J.-H.	(Theory II, GS)
Link, S.	(Electronic Properties, GS)
Liu, C.	(Special Group, G)
Lustfeld, H.	(Theory I)
Lüttgens, G.	(Electronic Properties, GS)
Luysberg, M.	(Microstructure Research, GS)
Ma, W.	(Electroceramic Materials, G)

Maiti, K.	(Electronic Properties)
Malagoli, M.	(Electronic Properties, GS)
Marton, K.	(Neutron Scattering, G)
Merkes, R.	(Special Group, GS)
Metz, A.	(Scattering Methods)
Meuffels, P.	(Electroceramic Materials)
Mihailescu, M.	(Neutron Scattering, GS)
Monkenbusch, M.	(Neutron Scattering)
Montanari, B.	(Theory I, GS)
Montes, H.	(Neutron Scattering, G)
Morenzin, J.	(Electronic Properties)
Mueller, R.	(Scattering Methods)
Müller-Krumbhaar, H.	(Theory III)
Mussawisade, K.	(Theory II, GS)
Neeb, M.	(Electronic Properties)
Nemeth, Z.	(Theory II, G)
Nie, X.	(Electronic Properties)
Noack, M.	(Materials Development)
Nonas, B.	(Theory III, GS)
Olligs, D.	(Electronic Properties, GS)
Otterstedt, R.	(Electroceramic Materials)
Persson, B.N.J.	(Theory I)
Pontius, N.	(Electronic Properties, GS)
Popkov, V.	(Theory II, G)
Poppe, A.	(Neutron Scattering, GS)
Poppe, U.	(Microstructure Research)
Prager, M.	(Neutron Scattering)
Pyckhout-Hintzen, W.	(Neutron Scattering)
Reif, Th.	(Scattering Methods, GS)
Richter, D.	(Neutron Scattering)
Rickes, J.	(Electroceramic Materials, GS)
Rosenfeld, R.	(Microstructure Research, GS)
Rottländer, P.	(Electronic Properties, GS)
Rücker, U.	(Scattering Methods, GS)
Rupprecht, A.	(Neutron Scattering, G)
Ryazonov, A.	(Special Group, G)
Rzehak, R.	(Theory III, GS)
Sänger, J.	(Neutron Scattering)
Sauer, C.	(Electronic Properties)
Schäfer, P.	(Electroceramic Materials, GS)
Schall, P.	(Microstructure Research, GS)

Schemion, D.	(Microstructure Research, GS)
Scherer, R.	(Electronic Properties, GS)
Schlebusch, C.	(Electronic Properties)
Schliefer, F.	(Special Group, GS)
Schmidt, W.	(Neutron Scattering)
Schmitz, R.	(Electroceramic Materials, GS)
Schmitz, S.	(Electroceramic Materials, GS)
Schneider, St.	(Electroceramic Materials, GS)
Schober, H.	(Theory III)
Schober, T.	(Materials Development)
Schornstein, St.	(Microstructure Research, GS)
Schroeder, H.	(Electroceramic Materials)
Schroeder, K.	(Theory III)
Schütz, G.	(Theory II)
Schwahn, D.	(Neutron Scattering)
Schweika, W.	(Scattering Methods)
Scott, J.	(Electroceramic Materials, G)
Settels, A.	(Theory III, GS)
Sokolov, A.	(Neutron Scattering, G)
Sonnenberg, K.	(Materials Development)
Stellbrink, J.	(Neutron Scattering)
Stockmeyer, R.	(Neutron Scattering)
Straube, E.	(Neutron Scattering, G)
Sturm, K.	(Theory I)
Szot, K.	(Electroceramic Materials, G)
Temkin, D.	(Theory III, GS)
Thust, A.	(Microstructure Research)
Trinkaus, H.	(Theory III)
Ullmaier, H.	(Special Group)
Urban, K.	(Microstructure Research)
Vad, Th.	(Scattering Methods, GS)
Voges, F.	(Electronic Properties, GS)
Volokitin, A.	(Theory I, G)
Waser, R.	(Electroceramic Materials)
Westermann, A.	(Neutron Scattering, GS)
Willner, L.	(Neutron Scattering)
Wingbermühle, J.	(Electronic Properties, GS)
Winter, M.	(Microstructure Research, GS)
Wischnewski, A.	(Neutron Scattering)
Yan, S.-S.	(Electronic Properties)
Yi, H.	(Microstructure Research, GS)

Yurechko, M.	(Microstructure Research, GS)
Zeiske, Th.	(Scattering Methods, G)
Zeller, R.	(Theory III)
Zorn, R.	(Neutron Scattering)
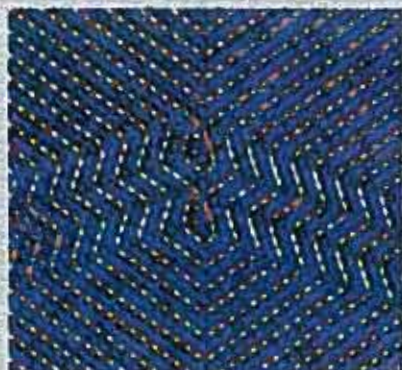
Atomic view of a complex arrangement of twin boundaries in the electroceramic material barium titanate ($BaTiO_3$). The pseudocolour image shows the phase of a quantum mechanical electron wave function which was reconstructed numerically from a series of high-resolution transmission electron microscopy (HRTEM) images. In contrast to an image, the interpretation of the quantum mechanical phase is straight forward, because the latter is free from the severe imaging artefacts introduced by the observation instrument. Since electrons (particle description) traverse the object faster near atomic cores than in the surrounding areas, the corresponding phase (wave description) is peaked at atomic positions. The prominent bright coloured peaks reveal titanium positions, whereas the darker coloured peaks reveal barium positions.

Forschungszentrum Jülich